HIGH RESOLUTION MULTINUCLEAR NUCLEAR MAGNETIC RESONANCE STUDIES OF OXIDE GLASSES

Martin William Geoffrey Lockyer

A thesis submitted to the University of Warwick for admission to the degree of Doctor of Philosophy.

Department of Physics

September 1993

This thesis is dedicated to Elizabeth, for being there.

"Then the fun started— and went on and on for years and years. The correspondence files grew even faster than the piles of manuscripts, and many were the bribes, threats, promises, and shared jokes (which were especially effective and mutually rewarding), which were vital stimuli for action— but now lie silent in the dark, their work done."

R.L. Gregory, "The Oxford Companion to the Mind", O.U.P. 1987.

List of Contents

List of Tables.

List of Figures.

Acknowledgements

I would formally like to thank the S.E.R.C. for their provision of financial assistance, and the Department of Physics for providing the research facilities that made this work possible. I also thank the S.E.R.C, for the provision of time on the 600 MHz spectrometer in the Chemistry Department of the University of Edinburgh.

I extend a great deal of gratitude to my supervisors, Dr. Diane Holland and Professor Ray Dupree, who developed and encouraged my interest in the study of glass structure and its investigation via Magic Angle Spinning nuclear magnetic resonance. My thanks also to Dr. Mark E. Smith and Dr. Golam Mortuza for passing on their experience and expertise on the MSL spectrometer. Advice on other technical, and not so technical, matters was patiently given by Bob Lamb and Harold Mathers and was particularly invaluable.

A great many people have been influential in providing welcome distractions during the period that this work was undertaken, including all those members of the Glass-Ceramics coffee club, both past and present. If anyone feels neglected for not receiving a personal mention, my sincere apologies, but the list of names would have been enormous.

Declaration

The work for this thesis was executed in the Department of Physics of the University of Warwick from October 1988 to September 1991. It is the result of all my own independent research except where specifically referenced and has not been previously submitted in any form for any other degree.

Some parts of this thesis have been published, or accepted for publication as follows :

(1) "MAS NMR Applied to Potassium Phosphosilicate Glasses"
M.W.G. Lockyer, R. Dupree & D. Holland
(*Trans. Am. Crystallogr. Ass. 1991* to be published)

(2) "Structure of some Lead Aluminophosphate Glasses"
M.W.G. Lockyer & D. Holland
(*Topical Issues in Glass* 1, 53, (1992))

It is anticipated that other portions of this thesis will be submitted for publication at a later date.

Martin W. G. Lockyer.

Abstract

Multinuclear Magic Angle Spinning nuclear resonance has been used as the main technique in the investigation of the structure of glasses from three different systems.

A series of K_2O . $4SiO_2$ based glasses with P_2O_5 addition have been investigated via natural abundance ^{29}Si, ^{31}P and ^{27}Al (present as an impurity) MAS NMR. The ^{29}Si spectra reveal the occurrence of octahedrally coordinated silicon in addition to the normal tetrahedrally coordinated silicon for glasses with analysed P_2O_5 contents in excess of 28 mol%. Increasing the P_2O_5 concentration increases the relative proportion of the higher coordination species. IRAS also detected the presence of Si^{vi}, but only for concentrations >10% of the total Si content. ^{27}Al MAS NMR has shown the presence only of four coordinated aluminium for 5 mol% P_2O_5, whereas for 10 and 15 mol% small amounts of six and possibly five coordinated aluminium species occur. Higher concentrations of P_2O_5 also increase the amount of higher coordinated aluminium until 28 mol% when practically all the aluminium is octahedrally coordinated with phosphorus in the next nearest shell. The ^{31}P MAS NMR spectra show the formation of metaphosphate chains for P_2O_5 concentrations greater than 10 mol%, which increase in length and become more disordered as the P_2O_5 content rises. The relative concentration of octahedral silicon has been found to be a function of fictive temperature, with the proportion of Si^{vi} higher for higher T_f. An estimated energy for the conversion Si^{iv} to Si^{vi} was obtained, of 9.98 kJ/mol, indicating the reaction is exothermic. The relative proportions of Si^{iv} and Si^{vi} also affect the measured density of the glasses, density increasing as the proportion of Si^{vi} increases. Potassium phosphosilicate and silicon phosphate xerogels were also prepared, but it did not prove possible to prepare amorphous samples free from water or organic residue. MAS NMR indicates that no Si - O - P bonding was formed below 500°C and XRD shows the presence of both SiP_2O_7 and $Si_5O(PO_4)_6$ as crystal phases in the heated potassium phosphosilicate xerogel and $Si_3(PO_4)_4$ in the silicon phosphate xerogel.

Multinuclear MAS NMR investigations of Na_2O . CaO . SiO_2 . P_2O_5 glasses has indicated a preferential association of Na^+ ions with the Q^3 species and Ca^{2+} with Q^2 units. The glasses are believed to consist of a mixture of two amorphous silicate environments similar to calcium metasilicate and sodium disilicate, which has been interpreted in terms of a possible model for the structural requirements for bioactivity. The glasses were subsequently converted into glass-ceramics via a controlled heat treatment process and the resulting structures investigated via MAS NMR and XRD. It has been established that all compositions prepared from within the bioactive region of the phase diagram contain $Na_2CaSi_3O_8$ as the major crystalline phase. Certain crystal phases that went undetected by XRD were observed via MAS NMR.

Glasses prepared from the PbO . P_2O_5 . Al_2O_3 system have shown some interesting structural species. Compositions with >10 mol% Al_2O_3 contained Al in 4,5 and 6 coordination with a variety of next nearest neighbours. It is supposed that this multiple coordination stabilises longer metaphosphate chains than previously observed in glasses. In PbO . P_2O_5 glasses with >46.6 mol% PbO the network contains (PbO_4) tetrahedra which act in an apparent intermediate-like role in a similar manner to that observed in PbO . SiO_2 glasses.

This study has emphasised that multinuclear MAS NMR is an ideal technique for the investigation of completely or partially amorphous inorganic materials, particularly when employed in conjunction with other techniques such as thermal analysis, IRAS and XRD.

CHAPTER 1.

INTRODUCTION.

1.1 DEFINITION OF 'GLASS'.

The simplest description of a 'glass' is as a non-crystalline, or amorphous, solid that lacks long range periodicity of atomic arrangement. The majority of glasses encountered are composed of certain metal oxides melted together and subsequently cooled. Thus the American Society for Testing of Materials defined a glass as " an inorganic product of fusion which has cooled to a rigid condition without crystallizing." However this definition excludes organic glasses such as polystyrene, it also ignores the vast collection of amorphous materials prepared by techniques other than melting such as sol-gel, chemical vapour deposition etc. The final drawback with this definition is that no exact definition is given regarding the crystallization.

Therefore a more precise answer to 'What is a glass?' would be, "A glass is a material that exhibits the glass transition phenomenon." Having said that however, the term 'glass' when used in this study is generally going to imply an amorphous silicate or phosphate based solid material.

1.2 DIFFERENT MODELS OF GLASS STRUCTURE.

Practically all glasses encountered in everyday applications, with the exception of quartz, are multicomponent in nature. Consequently the resulting

structures can become extremely complicated. Attempts to envisage the structure of these materials has produced a variety of models. The general belief is that some rigid backbone or skeleton exists and that, in the immediate vicinity of particular atoms, the bonding arrangement in not too dissimilar to the crystalline equivalent. In relation to oxide glasses, the most widely accepted model is the Random Network Model originally proposed by Zachariasen [1]. This model, along with its major modifications, and alternative models derived independently are discussed in the following sections.

1.2.1. RANDOM NETWORK MODEL.

The paper presented by Zachariasen is perhaps the seminal work in attempts to interpret and model oxide glass structure. He began by assuming that the standard rules of crystal bonding also applied to glasses, i.e. the SiO_4 tetrahedron, which is the basic structural unit of crystalline silicates, is also the basis of silicate glasses. However instead of this regular geometric pattern repeating ad infinitum as in crystals, the silicate glass tetrahedra have a distribution of inter polyhedra bond angles and lengths varying by as much as 10% [2]. The resulting lack of long range atomic order produces the diffuse, liquid-like x-ray diffraction pattern. Zachariasen thus derived some empirical restrictions on glass formation.

(i) The oxygen anion should not be coordinated to more than two cations,

(ii) The coordination of the cation should be small, (4 or less),

(iii) The cation-oxygen polyhedra should share only corners and not edges or faces, and

(iv) the structure should form a continuous three dimensional network, which necessitates that three corners of each polyhedron be shared.

From these postulates , the dominant type of polyhedra would be the tetrahedron as octahedra would tend to share edges and faces with neighbouring polyhedra.

Subsequently Warren and his co-workers [3-7] confirmed Zachariasen's hypothesis via x-ray diffraction. Intensity variations in the diffuse x-ray pattern were analysed by Fourier transformation and converted into radial distribution functions. The maxima of these distributions were compared with interatomic distances calculated from ionic radii and structural data from crystalline polymorphs and found to correspond. The experimental distribution curves levelled out after distances of 5-6Å, reflecting the rapid onset of disorder of the glass's atomic arrangement.

Zachariasen also proposed a system of categorization for various oxides;

Network formers - oxides that readily form glasses, e.g. SiO_2, B_2O_3, GeO_2 and P_2O_5.

Intermediate oxides - oxides that cannot independently form glasses, but can readily substitute for a network former, e.g. Al_2O_3 and TiO_2.

Modifier oxides - oxides that disrupt the network by breaking dihedral bonds, e.g. alkali-metal and alkaline-earth oxides. These broken dihedral bonds were termed 'non-bridging oxygens'. A schematic representation of the role of these types of oxides is given in figure 1.1.

As can be seen, the introduction of modifier oxide depolymerises the silicate network, so reducing the stability of the glass, via the production of the non-bridging oxygens. The schematic diagram suggests that the introduction of one mol of Na_2O to SiO_2 will produce 2 mols of non-bridging oxygens. The fact that the number of non-bridging oxygens in an alkali silicate glass is equivalent to the concentration of alkali metal ions was established conclusively via XPS by Jen and Kalinowski [8]. Consequently there is a limit to the amount of modifier and hence the number of non-bridging oxygens that can be accommodated whilst still forming

(a)

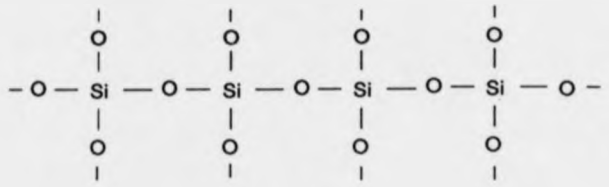

(b)

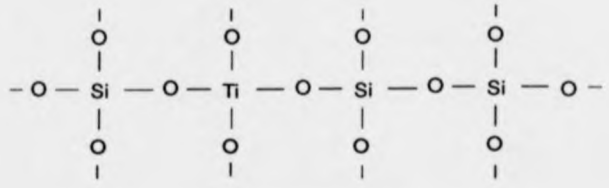

(c)

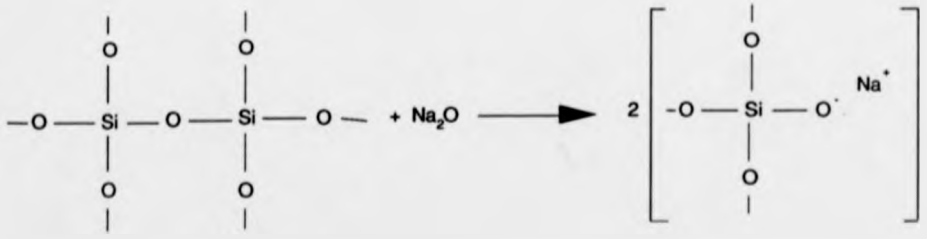

Figure 1.1. Schematic representation of the roles of the various categories of oxides. (a) A continous network formed by network forming oxides. (b) The incorporation of intermediate oxides into a glass forming oxide network. (c) The production of non-bridging oxygens via the introduction of typical network modifying oxide.

a stable glass. Simple empirical calculations reveal that the glass forming limit of a binary alkali silicate has a stoichiometry of $Na_2O.SiO_2$ where the average SiO_4 tetrahedron has 2 each of bridging and non-bridging oxygens. Further addition of alkali oxide will further disrupt the network leading to the formation of silicate dimers. This results in a significant decrease in stability and in the ability to form a continuous silicate skeleton, thus making glass formation extremely difficult.

We now consider how the non-bridging oxygens are distributed through the glass. There are two descriptions; the binary model and the statistical model. However, before detailing these models it is pertinent to define a system of nomenclature to enable differentiation of the various SiO_4 tetrahedron with varying numbers of bridging and non-bridging oxygens. The most widely accepted description employed in discussing the connectivity of a silicate glass structure is that proposed by Lippmaa et al [9]. The SiO_4 tetrahedra is represented by Q with a superscript representing the number of bridging oxygens to neighbouring SiO_4 tetrahedra, i.e. Q^n where n is between 0 and 4. Figure 1.2 details the various Q^n species schematically.

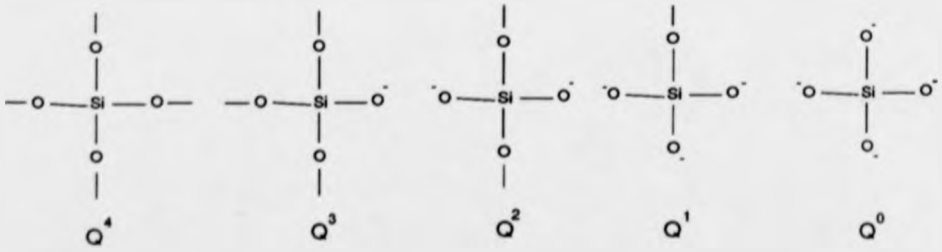

Figure 1.2. A schemetic representation of the different Q^n SiO_4 species as defined by Lippmaa et al [9].

The binary model of non-bridging oxygen distribution, as its name implies, limits the number of different Q^n species to two in any single composition. This would suggest that the non-bridging oxygens repel each other producing a

maximum dispersion. Thus in binary alkali silicate glasses the variation in concentration of Q^n species with glass composition is shown in figure 1.3.

The statistical distribution model has no limit upon the number of Q^n species present for any one composition. In this case the distribution is determined solely by composition and statistics such that the distribution for a given composition is also given by figure 1.3.

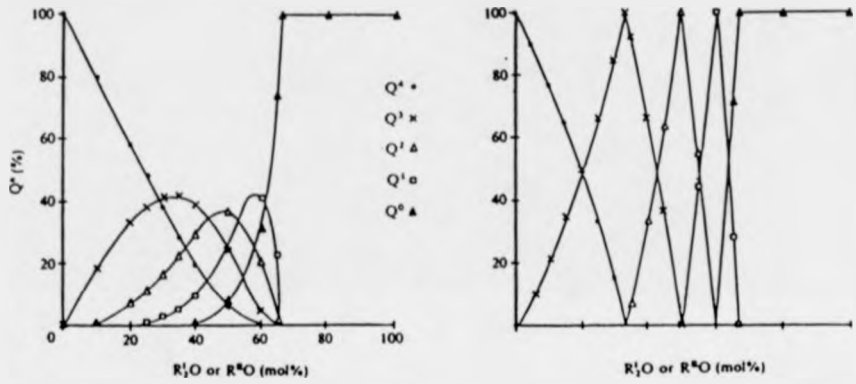

Figure 1.3. The distribution of the various Q^n species as predicted by the binary (righthand) and statistical (lefthand) distribution models.

Disagreements continue as to which of these two models best describes the non-bridging oxygen distribution; for example a ^{29}Si MAS NMR investigation of glasses in the $Li_2O.SiO_2$ system by Schramm et al [10] was interpreted as following the statistical distribution. However, Gladden et al [11] and Grimmer et al [12] obtained data via the same technique on the same glass system that was best fitted to the binary distribution model. Notably however, both studies made no mention, or allowance, of the thermal histories of these glasses. It appears that modifier ions with either large or small charge to ionic size ratios, e.g. Li, Cs and Rb, are best fitted to a statistical distribution, whilst intermediate ions such as Na or K follow a binary distribution.

Therefore it appears that the true distribution of non-bridging oxygens for a given composition lies somewhere between these two models [13], with factors such as fictive temperature, total modifier concentration, ionic size and charge density being influential [14].

The structural role of certain intermediate oxides, e.g. Al_2O_3, has the opposite effect to that of the modifying oxides, namely the removal of non-bridging oxygens. The mechanism is shown schematically in figure 1.4.

Figure 1.4. A representative illustration of the 'network repolymerising' role undertaken by intermediate oxides. For charge neutrality purposes the sodium ion is located close to the AlO_4 tetrahedron, which has a delocalised single negative charge.

This enables the network as a whole to repolymerise, albeit with Si - O - Al linkages, and so produce a glass of greater stability. It is also worth noting here that lead, amongst others, can act as either a modifier or intermediate oxide depending upon concentration [15]. Thus 'invert' glasses can be stabilised in the $PbO.SiO_2$ system with PbO concentrations of up to 70 mol%. This would obviously be impossible if Pb^{2+} were acting solely in a network modifying capacity, and so it is believed that in these high concentrations PbO_4 square pyramid polyhedra are formed, similar to those found in crystalline polymorphs of PbO, and are distributed among the SiO_4 tetrahedra. A ^{29}Si MAS NMR study of the lead silicate system [15] produced the following observations:

(i) *PbO concentration <30 mol%* - Pb^{2+} acts as a typical modifier following the binary model of non-bridging oxygen distribution.

(ii) *PbO concentration between 30 to 40 mol%* - the distribution of non-bridging oxygens is more accurately described by the statistical model as aQ^4

resonance is still distinguishable in the ^{29}Si spectrum. There also exists the possibility of Si - O - Pb bonding.

(iii) *PbO concentration between 40 and 65 mol%* - the statistical model is consistent with the Q^n species detected by ^{29}Si NMR.

(iv) *PbO concentration >70 mol%* - the SiO_4 tetrahedra are isolated species contained within a PbO matrix.

Other invert glasses are prepared with a mixture of modifying oxides, the common conception being that mixing modifiers increases the activation energy for crystallization by hindering diffusion of the crystal phase components [16].

The question regarding the random network model is its applicability. Wright [17] states that, as it was developed solely to describe glasses quenched from metastable melts at relatively low cooling rates, its application to glasses prepared via alternative techniques such as chemical vapour deposition is limited. However MacKenzie [18] published a set of tentative conclusions regarding all known non-crystalline oxides and stated that " Zachariasen's rules ..... are applicable to all types of non-crystalline oxide."

1.2.2 THE MODIFIED RANDOM NETWORK MODEL.

This model, as its name suggests, has been derived from Zachariasen's postulates, but was developed to encompass the findings of EXAFS and neutron diffraction data which was interpreted as showing evidence of a well defined first coordination sphere surrounding alkali/alkali-earth modifier cations. Both Greaves [19] and Eckersley [20] raise the idea that cations, and consequently the non-bridging oxygens, play a significant role in determining glass structure. In the standard random network model the cation occupies interstitials within the silicate network with an irregular and poorly defined bonding arrangement to ensure local

charge neutrality. Thus Greaves proposed the modified random network hypothesis where the overall structure of a glass comprises two interlaced sublattices; those of the network former and those of the modifier. Figure 1.5 illustrates this idea in two dimensions. It can be seen from this figure that an "archeopelago" structure exists where clusters of network former lattice are interspersed by regions of modifier lattice. In the figure these modifier lattice regions coalesce to form channels or rivers, although, as Greaves points out, the extent of these channels is dependent upon the concentration of modifying oxide in the glass.

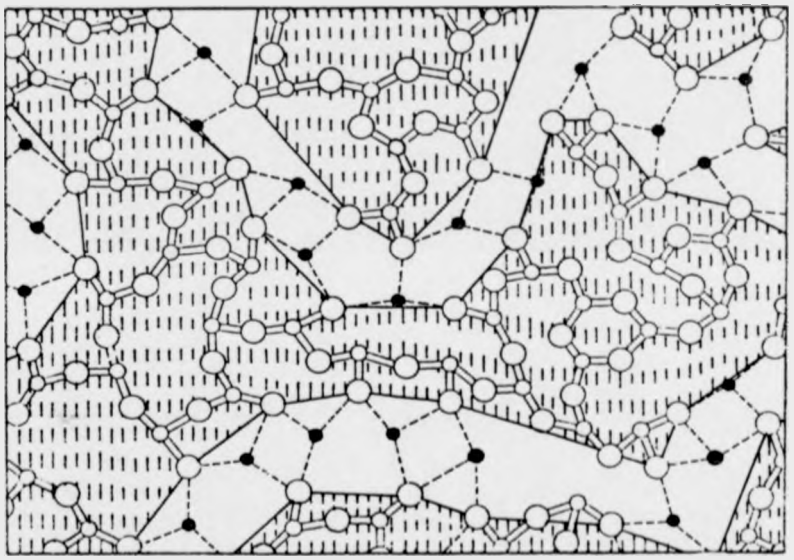

Figure 1.5. A modified random network for a two dimensional oxide glass; $M_2O_3(G_2O_3)_2$, where M are modifier cations and G network forming cations. Covalent bonds are represented by solid lines, ionic bonds by dotted lines. Illustration taken from [19].

The modified random network model successfully describes the decrease in viscosity of the melt as the concentration of modifier oxide is increased as well as the ionic conductivity of glasses where the current flow can proceed via the percolation channels. In the standard random network model ionic conduction is achieved via ions undergoing interstitial hopping. However the modified model does appear to be restricted to describing regular mineral type glasses as opposed to

alternatively prepared compositions. One further point worth stressing regarding the modified random network hypothesis is that, although the coordination sphere surrounding the cation is well defined, there is no implication of the formation of any microcrystalline regions. Eckersley and Gaskell [20] are adamant that there are pronounced differences between the calcium coordination sphere in crystalline and amorphous calcium silicates for distances in excess of 0.5 nm from the cation.

1.2.3 CRYSTALLITE THEORY

The basis of the crystallite theory or hypothesis of glass structure is the formation of minute coherent crystallites of any number of several polymorphs of the melt composition, or compounds from the extremes of the phase diagram, during cooling of the melt, i.e. a form of microsegregation. For example, in a sodium silicate glass, discrete crystalline regions of SiO_2 and $Na_2O.SiO_2$ would be formed within a chemically disordered transition region. However no evidence has been found of these discontinuous silicon species within homogeneous glasses.

According to Porai-Koshits [21] the origin of the crystallite theory predates Zachariasen by around 10 years when Lebedev is credited with its initial proposal, although the phrase 'crystallite hypothesis' was not reported until 1937 [22]. Lebedev observed changes in the thermal expansion of silicate glasses within the temperature range of the reversible $\alpha - \beta$ transition of quartz. Lebedev interpreted this as indicating that minute quartz crystals were present within the glass, although highly dispersed. Interestingly this phenomena has not been observed in vitreous quartz. Porai-Koshits [21] also notes a publication by Nemilov [23] who has uncovered work by Frankenheim [24] published in 1835 that also suggested glasses were composed of minute crystals. Notably both Lebedev and Frankenheim were attempting to explain observed changes in macroscopic

properties of glasses. The crystallite hypothesis was later developed by Randall, Rooksby and Cooper [25-28] who established a correspondence between the diffuse x-ray pattern maxima of particular glasses and the most intense lines in x-ray photographs of the equivalent crystalline phase. They estimated the crystallite size to be around 15-20 Å. More accurate x-ray techniques revised this figure to 10-12 Å [29,30] although interestingly Warren and his various co-workers [4,7,31,32] estimated the maximum size from their x-ray photographs to be only 8 Å. This figure is hardly dissimilar to the dimension of a single cristobalite unit cell, 7.1 Å, and so to talk of crystallites rather than considering the second coordination sphere surrounding particular atoms seems futile.

The crystallite model has undergone numerous periods of being in vogue and subsequently dismissed since the 1930's. Porai-Koshits [21] details these various periods up to the present day, including the paper from Phillips [33] who proposed that vitreous silica was composed of crystallite clusters, or granules, of β-cristobalite around 66 Å in diameter. Subsequently Galeener and Wright [34] convincingly refuted this via Raman spectroscopy and neutron diffraction. In addition Porai-Koshits [21] mentions some unpublished work by Golubkov who observed that the medium x-ray scattering, at an angle of 300 minutes, from vitreous silica and quartz monocrystals exhibited intensity variations around the quartz $\alpha - \beta$ transition temperature. He concluded that this was evidence of structural rearrangement of quartz crystallites within the vitreous material. However even Porai-Koshits doubts if this is sufficient to confirm the crystallite hypothesis.

Hence the crystallite hypothesis remains unsubstantiated even after the numerous x-ray, electron and neutron diffraction studies, although the later experimental results do indicate the existence of a greater degree of orderliness within glasses than predicted by the random network model.

1.2.4 STRAINED CLUSTER MODEL.

This model was proposed by Goodman [35] as a viable alternative to the random network model. It is essentially based on a phase diagram approach with consideration given to variations in free energy. Goodman notes that glass forming materials show polymorphism in their crystalline forms with very little difference in their respective free energies. The model proposes that, as the melt is cooled, small clusters form with structures corresponding to the different polymorphs. Of these polymorphs, the phase with the lowest free energy will be of a larger size. Thus the supercooled liquid will contain a mixture of types and sizes of clusters which will collide with similar and dissimilar clusters due to Brownian motion. Consequently, as the liquid cools,the mixed clusters will experience a strained interface when they encounter other, randomly orientated, clusters. This lack of epitaxy between clusters will increase the free energy. As these clusters are below the critical size required for nucleation, crystallization will not occur, but the overall viscosity will increase as the concentration of the mixed phase, strained clusters increase. The remaining liquid matrix phase eventually cools to form a space filling solid matrix (-35 vol%) surrounding the mixed strained clusters. This corresponds to the glass transition temperature, where Goodman states that the variation in glass transition temperature with respect to cooling rate can be explained by this model; slow cooling leaves more time for structural adjustments in regard of minimising cluster interfacial strain, hence a close fitting of mixed clusters, whereas rapid cooling would produce higher interfacial strain, less efficient cluster packing, a higher concentration of space filling liquid phase and therefore a higher temperature for the glass transition. Figure 1.6, taken from Goodman's paper [35], illustrates the structural representation of the model.

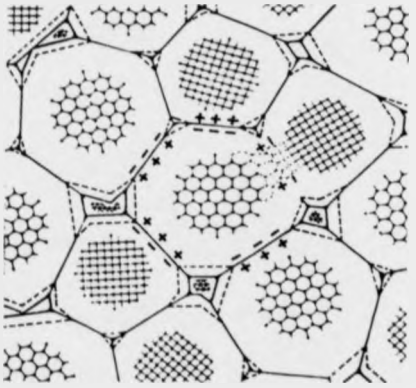

Figure 1.6. Goodman's illustration of a two-polymorph mixed cluster random network glass at temperature below T_g. Interfacial strain is indicated by + and - symbols [35].

In the final glass, the model proposes that each cluster is surrounded by close packing of other clusters whereupon half of the interfaces will be under tension and half under compression. Therefore the outer regions of each and every cluster, estimated to be 3 nm or more in diameter, will be significantly distorted in comparison to the 'ideal' core region. Hence x-ray, or other diffraction techniques will only detect regions of 1 nm or less in size.

Goodman also states that as this model is independent of bonding type it can explain how glass forming ability is present in such a wide range of materials where the bonding is highly ionic, mixed ionic-covalent, highly covalent or metallic in nature.

1.2.5 STEREO-CHEMICALLY DEFINED MODEL.

This is a recently proposed model [36,37], developed in the main to account for the significant correlation between neutron diffraction data obtained from calcium silicate glasses and their crystalline counterparts in respect of the local and medium range environment surrounding the calcium atoms [38,39]. This model

concerns certain structure-forming principles or limitations that are common to both the glass and crystalline materials, i.e. "many of the principles that rationalise periodic structures apply to aperiodic structures too." [37]. For example consider the case of silica. The common structural principle relating crystalline and amorphous forms is that the basic structural species is a SiO_4 tetrahedron, which is connected to neighbouring tetrahedra via the oxygen atoms. Additional limits are then applied relating to macroscopic properties and atomic characteristics which eventually produces a three dimensional disordered network. If the additional restriction that the SiO_4 tetrahedra form six member rings is applied, the resulting topography is crystalline.

As Gaskell states [36,37], this model differs from typical random network type models by assuming the medium range atomic arrangement surrounding particular atoms is well ordered, i.e. that the extent of similarity between atoms in crystalline and amorphous compounds extends beyond the first coordination sphere. It is an attempt to move away from the proposition that a glass is a completely disordered material and towards one where certain structure defining principles are applicable to the glass form as well as the crystalline. Indeed in the random network model the arrangement of atoms is not completely random as no Si - Si or O - O bonding is permitted.

However as Gaskell reports certain questions regarding this model require answers, namely what does the model predict for the structures of glasses that have no direct crystalline analogue either through composition or via phase separation.

1.2.6 SUMMARY.

This is not an extensive classification of models of glass structure, but

only of those most applicable to silicate or phosphate glasses. Other models exist, but are generally only applicable to specific types of glasses, e.g. Krogh-Moe molecular grouping theory for borate glasses [40], or Bernal sphere packing for amorphous metals [41].

All the models described above do have some general concord; (i) multicomponent glasses are extremely complex compounds that may encompass different types of bonding within the whole solid, and (ii), out to the second coordination sphere of the glass forming atom the atomic arrangement is very similar to that of the corresponding crystalline compound.

1.3 AIMS OF THE THESIS.

The fact that Magic Angle Spinning nuclear magnetic resonance (MAS NMR) is a technique well suited to the analysis of the intermediate range of glass structure is well established [14,42]. Hence this study is concerned with the application of multinuclear MAS NMR to the study of various oxide glass systems, each of which maybe considered 'novel'. The use of the description 'novel' is my suggestion as all the chosen glass systems may show some curious or interesting atomic environments.

$K_2Si_4O_9$ (Wadeite) [43] is one of an interesting set of crystalline silicates, including Stishovite [44,45], SiP_2O_7 [46] and ξ - $Na_2Si_2O_5$ [47], that exhibit silicon in an octahedral coordination. Predominantly these materials are high pressure crystalline polymorphs. Interestingly it has been found that sodium disilicate glasses prepared with high concentration of P_2O_5 (>40 mol%) also contain octahedral silicon species [48]. Consequently part of this study will examine the effect upon $K_2O.4SiO_2$ based glasses of increasing additions of P_2O_5. The effect of fictive temperature upon glass structure and possible correlations between the final structures of glasses prepared via melt-fusion and sol-gel techniques are also to be examined briefly.

Glasses that exhibit the property of bioactivity are also well documented [49,50]. However in spite of numerous detailed investigations of their surface reaction and subsequent bonding mechanics when situated in vivo or in vitro, little is known of their structure. Therefore the $Na_2O.CaO.SiO_2.P_2O_5$ system, which contains the original bioactive composition Bioglass 45S5 [51] and is the basis of practically all subsequent bioactive materials, will also be examined. The structure of the chosen compositions after conversion to glass-ceramics via controlled heat treatment is also undertaken.

Phosphate glasses, like bioactive glasses, are under represented in

terms of structural investigation. However they are coming to the fore in various fields of glass technology where additions of Al_2O_3 has increased their chemical durability [52]. The effect and structural role of lead within phosphate/ aluminophosphate glasses may be curious. Lead oxide has been found to fulfil various structural roles as either modifier or intermediate oxide within silicate glasses depending upon composition. Hence the final glass system studied in this thesis is $PbO.Al_2O_3.P_2O_5$.

Overall the aim of this thesis is to illustrate the applicability of multinuclear MAS NMR towards the attempt to develop a greater understanding of the intermediate atomic structure of oxide glasses.

1.4. REFERENCES.

[1] W. Zachariasen, *J. Am. Chem. Soc.* 54, 3841, (1932)

[2] P.W. McMillan, "Glass Ceramics", 2ed,Academic Press, 1979

[3] H. Krutter, O. Morningstar & B.E. Warren, *J. Am. Ceram. Soc.* 19, 202, (1936)

[4] B.E. Warren & J. Biscoe, *J. Am. Ceram. Soc.* 21, 49, (1938)

[5] J. Biscoe & B.E. Warren, *J. Am. Ceram. Soc.* 21, 259, (1938)

[6] J. Biscoe & B.E. Warren, *J. Am. Ceram. Soc.* 21, 287, (1938)

[7] B.E. Warren, B.S. Robinson & J. Biscoe, *J. Am. Ceram. Soc.* 22, 180, (1939)

[8] J.S. Jen & M.R. Kalinowski, *J. Non-Cryst. Solids* 38/9. 21, (1980)

[9] E. Lippmaa, M. Magi, A. Samoson, G. Engelhardt &A-R. Grimmer, *J. Am. Chem. Soc.* 102. 4889, (1980)

[10] C.M. Schramm, B.H.W.S. de Jong & V.E. Parziale, *J. Am. Chem. Soc.* 106, 4396, (1984)

[11] L.F. Gladden, T.A. Carpenter & S.R. Elliot, *Phil. Mag. B*53. L81, (1986)

[12] A.R. Grimmer, M. Magi, M. Hahnert, H. Stade, A. Samoson, W. Wieker & E. Lippmaa, *Phys. Chem. Glasses* 25, 105, (1984)

[13] W.R. Taylor, *Proc. Ind. Acad. Sci.* 99, 99, (1990)

[14] R. Dupree & D. Holland, in " Glasses and Glass-Ceramics", ed. M.H. Lewis, Chapman Hall, London, 1989

[15] R. Dupree, N. Ford & D. Holland, *Phys. Chem. Glasses* 28, 78, (1987)

[16] H. Rawson, "Inorganic Glass Forming Systems", Academic Press, 1967

[17] A.C. Wright, *J. Non-Cryst. Solids* 123, 129, (1990)

[18] J.D. MacKenzie, *J. Non-Cryst. Solids* 95/6, 441, (1987)

[19] G.N. Greaves, *J. Non-Cryst. Solids* 71. 203, (1985)

[20] M.C. Eckersley, P.H. Gaskell, A.C. Barnes & P. Chieux, *Nature* 335. 525, (1988)

[21] E.A. Porai-Koshits, *J. Non-Cryst. Solids* 123. 1, (1990)

[22] A.A. Lebedev, *Izv. Akad. Nauk SSR, Otd. Mat. Estestv. Nauk, Ser. Fiz.* (3) 381 (1937)

[23] S.V. Nemilov & A.I. Stozharov, *Trudy Goz. Opt. Inst.* 58, (N192) (1985) 2. p. 148

[24] M.L. Frankenheim, "Die Lehre von der Cohäsion", Breslau (1835)

[25] J.T. Randall, H.P. Rooksby & B.S. Cooper, *J. Soc. Glass Tech.* 14, 219, (1930)

[26] J.T. Randall, H.P. Rooksby & B.S. Cooper, *J. Soc. Glass Tech.* 15. 54, (1931)

[27] J.T. Randall, H.P. Rooksby & B.S. Cooper, *J. Soc. Glass Tech.* 17, 287, (1933)

[28] J.T. Randall, H.P. Rooksby & B.S. Cooper, *Z. Krist.* 75, 196 (1930)

[29] N. Valenkov & E.A. Porai-Koshits, *Z. Krist.* 95, 195, (1936)

[30] N. Valenkov & E.A. Porai-Koshits, *Nature* 137. 273, (1936)

[31] B.E. Warren, *Phys. Rev.* 46, 368, (1934)
[32] B.E. Warren, *J. Amer. Ceram. Soc.* 18, 269, (1935)
[33] J.C. Phillips, *Physics Today* 35, (2), 27, (Feb. 1982)
[34] F.L. Galeener & A.C. Wright, *Solid State Comm.* 57, 677, (1986)
[35] C.H.L. Goodman, *Phys. Chem. Glasses* 26, 1, (1985)
[36] P.H. Gaskell, *Trans. Am. Crystallogr. Ass.* 1991 to be published
[37] P.H. Gaskell, *Bol. Soc. Esp. Ceram. Vid.* 31-C1, 25, (1992)
[38] M.C. Eckersley, P.H. Gaskell, A.C. Barnes & P. Chieux, *J. Non-Cryst. Solids*, 106, 132, (1988)
[39] R.W. Cahn, *Nature* 335, 493 (1988)
[40] J. Krogh-Moe, *Phys. Chem. Glasses* 1, 26, (1960)
[41] J.D. Bernal & J. Mason, *Nature* 188, 910, (1960)
[42] H. Eckert, *Prog. in NMR Spectroscopy* 24, 159, (1992)
[43] S. Schweinsberg & F. Liebau, *Z. Anorg. Allgem. Chem.* 387, 241 (1972)
[44] S.M. Stishov & S.V. Popova, *Geokhimiya* 10, 837 (1961)
[45] Chao et al, *J. Geophys. Res.* 67, 419, (1962)
[46] Makart, *Helv. Chim. Acta* 50, 399, (1967)
[47] B.D. Santarsiero, X. Xue & M. Kanzaki, *Trans. Am. Crystallogr. Ass.* 1991 to be published
[48] R. Dupree, D. Holland & M.G. Mortuza, *Nature* 328 , 416 (1987)
[49] L.L. Hench & J. Wilson, *Science* 226, 630 (1984)
[50] L.L. Hench, *J. Am. Ceram. Soc.* 74, 1487 (1991)
[51] Bioglass 45S5 is a registered trade mark of the University of Florida, Gainesville, FL, U.S.A.
[52] J.A. Wilder & J.E. Shelby, *J. Am. Ceram. Soc.* 67, 438 (1984)

CHAPTER 2.

NUCLEAR MAGNETIC RESONANCE.

2.1 INTRODUCTION.

Nuclear magnetic resonance (NMR) spectroscopy is a form of spectroscopy concerned solely with the absorption of electromagnetic energy by the inducement of quantum transitions from lower to higher nuclear energy levels. However, as the separation of these nuclear energy levels is rather small, the corresponding net energy absorption is also small, ~ 0.1 J/mol, hence NMR is a low energy (low frequency) spectroscopic technique with the inducing electromagnetic radiation in the radio frequency band.

The first recorded observations of nuclear magnetic resonance were reported independently by two groups of workers in 1945 [1,2]. Purcell and his colleagues detected a loss in the electrical circuit, constituting one arm of a balanced bridge arrangement, that supplied r.f. power to a sample of solid paraffin when the frequency corresponded to the resonating frequency for the protons. Bloch et al however, whilst also investigating protons, noted that the reorientation of the magnetisation due to resonance induced an e.m.f. in a coil wound around a phial of water, a process of NMR detection he called 'nuclear induction'. NMR would not have continued to develop as a technique if the resonating frequency of a particular nucleus was invariant in respect to its environment. The discovery that a different environment does indeed alter the resonating frequency slightly was first observed in metals in 1949 [3] and subsequently, in 1951, the different proton resonances due to the different functional groups in alcohol molecules were also detected [4]. This

frequency difference due to local environment of the nuclide was termed the Knight shift in metals and the chemical shift in the non-metal liquid state, whereupon NMR became an important technique employed mainly in the field of liquid (solution state) structure. A further discussion of cause of this shift is given in section 2.2.2.

Extension of nuclear magnetic resonance to the solid state was complicated because, whereas in liquids the random motion of the surrounding molecules averaged away any anisotropic local fields, in solids the neighbouring molecules are fixed in position and therefore interact with each other resulting in anisotropic distortions of the applied field (see sections 2.2.2-4), and the resulting broad spectral lines can completely mask the small frequency differences in the isotropic chemical shift. Subsequently it was proposed that, by imposing a rapid macroscopic motion on the molecules, any anisotropic interaction in solid samples could be averaged to its isotropic value. The actual degree of averaging depends upon the details of the interaction along with both the speed and angle of inclination from the static field of the rotation. This method was both proposed and demonstrated independently by Andrew [5] and Lowe [6] whose main objective was the reduction of dipolar broadened resonant linewidths. Subsequent combination of sample spinning and other techniques such as cross-polarisation [7] and decoupling [8,9], which became available as vast improvements were made in the spectrometer hardware, enabled reductions in linewidths of around two orders of magnitude for crystalline compounds. Thus high resolution solid-state spectra could be obtained which were 'liquid-like' in that slightly different environments were easily discernible where previously only broad, largely featureless, spectra were obtained, figure 2.1.

Further improvements and enhancements to high resolution solid-state NMR such as the development of the multinuclear approach [10,11,12], as well as 2-dimensional NMR [13,14] have greatly increased its area of applicability; from the structure of organic solids, consisting mainly of protons and carbon-13, to structural

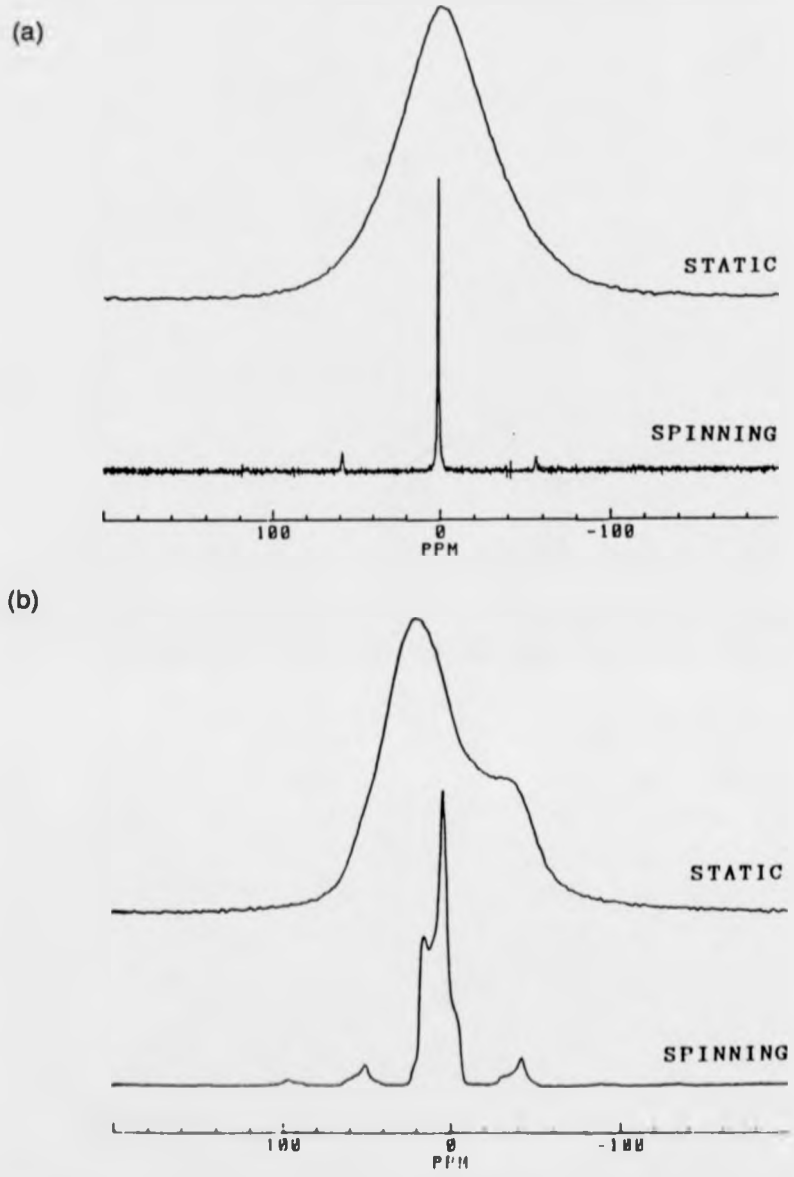

Figure 2.1 *Two illustrations of the improvement in resolution that is achievable in solid state NMR with Magic Angle Spinning. (a) The static and spinning ^{29}Si spectra of crystalline $Li_2Si_2O_5$. The majority of the broadening in the static spectrum is due to chemical shift anisotropy, which is averaged away by rapid spinning of the sample. (b) The static and spinning ^{31}P spectra of Li_3PO_4. The majority of the broadening in the static spectrum is due to dipole-dipole interaction, which is also averaged away by rapid spinning of the sample at the magic angle. All spectra taken from reference [44].*

studies of minerals [15,16], glasses [17] and ceramics [18]. NMR has many advantages over other diffraction based structure determining techniques, eg electrons and x-rays, in that NMR is atom-type specific; sensitive to symmetry and coordination; site selective and sensitive to dilute components [19].

2.2. NMR THEORY.

This section provides a basic introduction to some relevant NMR theory. In particular, it explains how the various characteristics of the resulting spectra relate to the environment of the resonating nuclei, the type and distance of the neighbouring atoms and the chemical bonds formed between these atoms.

2.2.1. BASIC PRINCIPLES.

If we consider a single isolated nucleus, with a non-zero nuclear spin I, then in a magnetic field the nucleus will act as a dipole as it possesses a magnetic moment given by

$$\mu = \gamma \hbar \mathbf{I} \qquad (2.1)$$

where γ is the gyromagnetic ratio and is characteristic of the nucleus.

If the nucleus is now placed in a static magnetic field B_o, applied in the z direction, the magnetic moment couples to the field such that

$$H = -\mu \cdot \underline{B} \qquad (2.2)$$

which in terms of cartesian components can be expressed as

$$H = - \gamma \hbar I_z B_o \qquad \{ 2.3 \}$$

Now as I is a quantum number, from basic quantum mechanical theory, its z component m_z may take any of a number of values specified by the series

$$m_z = I, (I-1), \ldots\ldots , -I \qquad \{ 2.4 \}$$

and the energy of the system will correspondingly depend upon this series as

$$E_m = - \gamma \hbar B_o m_z. \qquad \{ 2.5 \}$$

i.e. the energy levels are not identical but separated by an energy gap $\Delta E = \gamma h B_o$. This is the nuclear Zeeman interaction and has lifted the degeneracy of the nuclear spin energy levels.

If we consider the simple case of $I = ½$, then m_z can take values of either ½ or -½, figure 2.2 (a), and therefore if an amount of excitation energy equivalent to the energy gap is applied then transition between the two levels will be stimulated. Hence if an oscillating magnetic field is applied perpendicular to the static field B_o with a frequency of ν, such that $h\nu = \Delta E$, then

$$h \nu = \gamma \hbar B_o \qquad \{ 2.6 \}$$

or rearranging

$$\omega = \gamma B_o \qquad \{ 2.7 \}$$

where ω is known as the Larmor frequency, such that a radiofrequency field of that

frequency will produce resonance.

In real experiments it is not practical to consider a single isolated

Figure 2.2. (a) Energy level diagram for a I=½ nucleus experiencing a static magnetic field. (b) Resulting 'spectrum' from such a nucleus experiencing only the Zeeman interaction.

nucleus but a collection of similar nuclear dipoles giving rise to bulk magnetization M. Now, considering the same two level system, I = ½, each of the dipoles can either align itself with (m_z=½) or against (m_z=-½) the static field B_o. The actual occupancy of the two levels is governed by Boltzmann statistics and, in order to establish a thermal equilibrium between the two levels, results in a small excess in the lower state; around 1 in a 100000 for ^{29}Si at room temperature with B_o = 8.45T. Thus with the Zeeman interaction lifting the degeneracy of the nuclear energy levels the small population difference existing between these levels makes NMR a viable spectroscopic technique. However if the Zeeman interaction were the only interaction experienced by a collection of nuclei with I ≥ ½ then any sample under investigation would only absorb energy at the exact Larmor frequency and the resulting spectrum would not be very informative, figure 2.2 (b). This is very much not the case though as certain "internal" interactions are present, which although small compared to the Zeeman effect, are still significant enough to be considered perturbations in relation to the lifting of degeneracy. The major interactions under consideration here are the dipole-dipole, the chemical shift and, for nuclei with I > ½, the quadrupole interaction. These individual interactions will be discussed

briefly in the following sections, whilst a more rigorous and mathematical approach to the theory of NMR maybe found in numerous texts, notably those by Abragam, Slichter, Mehring and Haeberlen [20-24].

2.2.2 CHEMICAL SHIFT INTERACTION.

The chemical shift interaction is perhaps the most significant "internal" interaction as it is experienced by all nuclei regardless of the size of the spin quantum number. It is in effect the perturbation of the applied magnetic field by the surrounding (bonding) electrons and so provides much information regarding the local structure surrounding a particular type of nucleus.

Thus the actual magnetic field experienced by a particular nucleus in a sample is not equal to the applied field $\underline{B}_o$, but is modified by the interaction of the field with the surrounding electron cloud. This interaction induces a polarisation of the electron shells which can produce either diamagnetic shielding, (reducing $\underline{B}_o$), or generate a second order paramagnetic effect, which will enhance $\underline{B}_o$ at the nucleus [25,26]. Thus

$$\underline{B}_{loc} = \underline{B}_o (1 - \sigma) \qquad [2.8]$$

where $\underline{B}_{loc}$ is the field local to the nucleus and σ is the shielding factor. σ is generally a second rank tensor due to the three dimensional nature of the electron cloud distribution, and as such is a function of the bond angle, bond length, bond strength, type of nearest neighbour atom and the type of next nearest neighbour atom as well as the electron distribution.

In the simplest case, spherical symmetry, σ is a scalar quantity, thus from equation 2.7

$$\omega = \gamma \, . \, \underline{B}_{loc} \qquad \{ 2.9 \}$$

or

$$\nu = \gamma/2\pi \, . \, (1 - \sigma) \, . \, \underline{B}_{o} \qquad \{ 2.10 \}$$

hence the resonating frequency has been shifted from ω_o to ω. Thus each crystallographically distinct site will undergo a different amount of 'chemical shift' from the Larmor frequency where the bonding arrangement differs in either bond angles, bond lengths or coordination number of neighbouring atoms. Therefore a great deal of structural information can be directly obtained from the chemical shift of a resonance, for example the range of shifts experienced by ^{29}Si when tetrahedrally coordinated by oxygen in silicates is ~ -60 to -128 ppm [17] as compared to the range -191 to -221 ppm when octahedrally coordinated by the same type of atom in similar materials [27], figure 2.3.

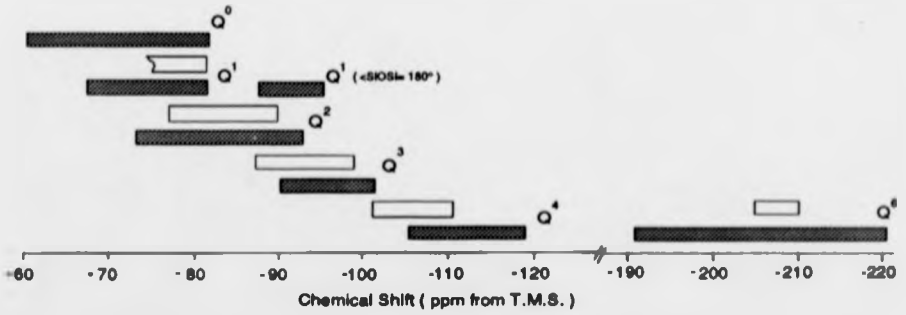

Figure 2.3. The reported shift ranges for silicate polyhedra with different degrees of polymerization, (white ranges are for glasses from reference [17] and dark ranges are for 'solid' silicates from references [27] and [57]).

This can be broken down further with respect to the type of neighbouring atom where the ^{29}Si shift for (SiN_4) in β-Si_3N_4 is -49 ppm as opposed to -63 ppm when one of the nitrogen atoms is replaced by an oxygen atom [17], or even further where the occurrence of aluminium atoms, rather than silicon, as next nearest neighbours alters the shift of ^{29}Si in SiO_4 by approximately 5 ppm [28]. Thus it can be seen that there is a hierarchical order concerning the effect these factors have on the chemical shift [29];

change in coordination number > nearest neighbour substitution > next nearest neighbour substitution

^{29}Si NMR can also detect subtle environment changes between two polymorphs of the same material, e.g. the α- and β- forms of Si_3N_4 where the α– form has alternate Si-N layers inverted and offset to produce two distinct silicon sites and so two separate resonances as opposed to the regular β- form which has only one resonance, figure 2.4.

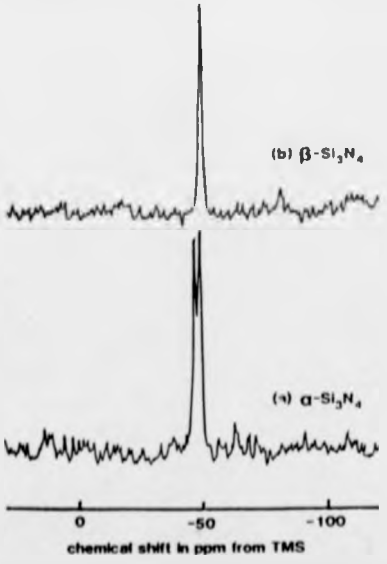

Figure 2.4 ^{29}Si MAS NMR spectra obtained from the two forms of silicon nitride, (a) α–Si_3N_4 and (b) β–Si_3N_4 [30]

The equation for the local field becomes somewhat more complicated when cubic symmetry is broken, and for axial symmetry the local effective field becomes

$$B = B_o [(1-\sigma_\perp)^2 \sin^2 \theta + (1-\sigma_{//})^2 \cos^2 \theta]^{½} \qquad \{ 2.11 \}$$

where $\sigma_\perp$ and $\sigma_{//}$ are the values of the shielding parameter with the field either perpendicular or parallel to the axis of symmetry, and θ is the angle between the applied field and the symmetry axis. However in the case of a polycrystalline sample all values of θ are equally valid, so an envelope or 'powder pattern' results. With the additional range of environments found in vitreous materials, a spread of chemical shifts is also encountered which, when convoluted with the powder pattern, can mask the majority of structural information contained within the spectrum. Therefore some method of recovering this information is required. This is achieved via the imposition of 'liquid-like' random molecular motion by rapidly spinning the sample at the so-called 'Magic Angle' from the static magnetic field. The rapid sample spinning effectively adds an additional time dependent Hamiltonian for the interaction which itself can be decomposed into both static and time dependent components [30], the time dependent part then averaging to zero. The static component remains however but it is now dependent upon the angle between the z axes of the laboratory and rotating frames of reference, β, such that ($3\cos^2 \beta - 1$). Hence if this factor is made to equal zero, i.e. β is 54° 44' 8" then this component also vanishes and the remaining Hamiltonian is identical to the isotropic case [30]. This is then the technique of Magic Angle Spinning NMR. It is worth noting that the actual speed of sample rotation should be greater than the non-spinning linewidth produced by each spin, due to the dipole-dipole interaction (section 2.2.3) which is typically less than 1kHz provided no strongly dipolar nuclei such as ^1H or ^{19}F are present. This approach however does introduce new features to the resulting

spectrum because, as the macroscopic magnetization decays after the pulse, the rotation of the sample produces a sort of coherence effect. For each complete rotation the magnetization 'reforms' and again decays rapidly once more, only to reconverge after another complete rotation. This does not continue indefinitely but the amplitude of these rotational echoes decays within the envelope described by the isotropic case, figures 2.5(a). Figure 2.5(b) shows that the resulting spectrum now contains a series of identically shaped lines, separated by the spinning speed. In order to deduce which of these lines is the actual isotropic peak, it is easiest to

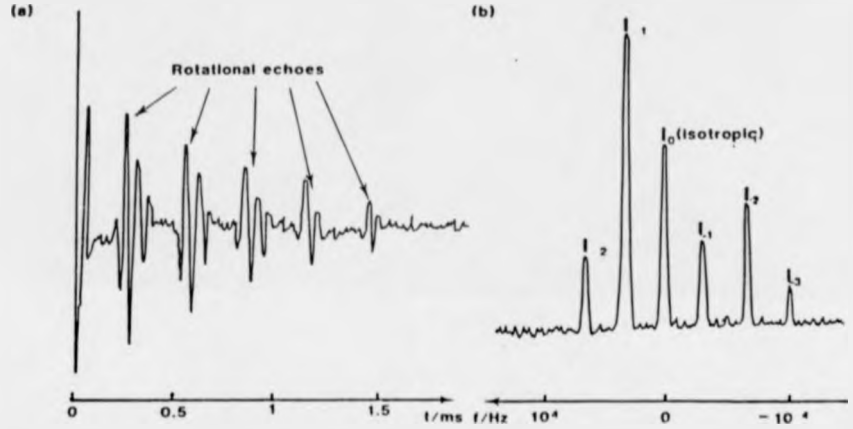

Figure 2.5. (a) The time domain signal recorded from ^{119}Sn in SnO_2 with the accompanying rotational echos. (b) The resulting spectrum after Fourier transform complete with the associated spinning sidebands. Illustration taken from reference [30]

collect another spectrum accumulated with a different sample spinning speed as the position of the isotropic peak is not dependent upon the speed of rotation whereas the positions of the sidebands are.

The chemical shift itself (δ_i)is dimensionless and defined with respect to some arbitrary reference compound, normally a liquid, such that

$$\delta_i = \sigma_{ref} - \sigma_i = (\nu_i - \nu_{ref}) / \nu_{ref} \qquad [\ 2.12\ ]$$

and is expressed in parts per million, ppm.

2.2.3 DIPOLE - DIPOLE INTERACTION.

This is a form of spin-spin coupling, ie an interaction between neighbouring spins directed through space and so depending upon the internuclear distance. Another form of spin-spin coupling exists, known as indirect or J-coupling, directed through the bonding electrons although in the solid-state case this is so small in comparison to the linewidth as to be effectively negligible [29].

If we consider two nuclei with magnetic moments placed in a large static field separated by a distance r_{ij}, then as each moment precesses around the direction of the field it generates an additional small field, in respect of the static field, at the site of the other nucleus with two components; one parallel and one rotating perpendicular to the large static field.

Obviously, in a many nuclei system this becomes a many body problem and is not easy to calculate quantitatively, however it is possible to illustrate qualitatively how the static parallel component produces broadening of the lineshape. Any single nucleus experiences an additional field due to the sum of all the fields produced by the other nuclei, where the field will depend upon the orientation of the spin; either aligned with or against the large field. Thus there will be a range of values for the magnitude of the additional field from all the spins aligned with $\underline{B}_o$ to all the spins aligned opposing $\underline{B}_o$ which will correspondingly produce a range of resonant frequencies.

The rotating component induces more subtle changes. If the spins involved have identical resonant frequencies then the rotating local field will induce mutual energy conserving 'flip-flop' transitions. This form of spin diffusion can lead to extremely rapid relaxation of the spin system. Obviously for non-identical nuclei the rotating field will not be able to induce these transitions as their rotating frequency will not be equivalent to the resonating frequency. However for unlike

spins the interaction has an angular dependence of the form $(1 - 3 \cos^2 \theta_{ij})$ [29].

In conclusion the main characteristics of the dipole-dipole interaction are that it occurs between all magnetically active particles in the sample, is a second rank tensor (and as such is anisotropic), and for spin ½ nuclei is usually the dominant interaction in terms of broadening the spectral lines. Magic angle spinning of the sample can average away the anisotropy, although this is only strictly true to the first order. Subsequently, for higher orders and in cases where the interaction is between identical spins, MAS will have no line narrowing effect [30].

2.2.4 QUADRUPOLE INTERACTION.

Nuclei with a spin number greater than ½ possess a quadrupole moment due to the non-spherical charge distribution within the nucleus. Such nuclei therefore experience a coupling or interaction between this moment and the surrounding electron charge distribution, (provided the electronic symmetry is not cubic) [29], which is known as the nuclear quadrupole interaction. Qualitatively, the magnetic moment of the nucleus wishes to to align itself with the magnetic field, whereas the quadrupole moment attempts to reorientate along the direction of the electric field gradient. As in the previous interactions, sections 2.2.2 and 3, the energy levels of the spin system are affected, although to a larger extent. This is because the quadrupolar interaction is generally of greater magnitude than either the dipole-dipole or chemical shift interaction [31]. For example consider the case of two identical dipoles, magnetic moment μ, separated by a distance r, then the energy of interaction would be of the order of μ^2/r^3. For quadrupoles the energy of interaction is a product of the nuclear quadrupole moment, eQ, and the electric field gradient created by the distribution of the electronic charge surrounding the nucleus, which we can assume for simplicity to be a point charge, and to be approximately

e/r^3. Hence the ratio between these two examples is of the order of $e^2Q:\mu^2$, which generally is between 10 to 1000 [31]. Therefore in cases where the quadrupolar interaction is present it tends to dominate over other interactions.

It is still possible though to treat the quadrupole interaction as simply a perturbation of the Zeeman interaction provided the applied static field $\underline{B}_o$ is sufficiently large, and therefore predict, via quantum mechanics, the effect upon the energy levels [20-24] which form a series :

$$E_m = \sum_{k\geq 0} E_m^{(k)} \qquad \{ 2.13 \}$$

Now expanding this series yields for the zeroth order (k=0) the simple Zeeman interaction viz;

$$E_m^{(0)} = - \gamma h_b B_o m \qquad \{ 2.14 \}$$

for the first order

$$E_m^{(1)} = {}^3/_2 \; A \; (3 \cos^2 \theta - 1) \; (m^2 - {}^1/_3 \; I(I+1)) \qquad \{ 2.15 \}$$

and for the second order

$$E_m^{(2)} \; \alpha^{al} \text{ to } A \; [\cos^2 \theta \; (1 - \cos^2 \theta)] \text{ and } A[\; (1 - \cos^2 \theta)^2 \;] \qquad \{ 2.16 \}$$

where

$$A = e^2 \, q \, Q \, / \, 4 \, I \, (2 \, I - 1) \qquad \{ 2.17 \}$$

From these equations it is possible to establish that there is no quadrupolar interaction for I=½ nuclei as in this instance A vanishes. Also notice that the first order expression contains an angular dependance of the form ($3\cos^2\theta - 1$). Hence by spinning at the 'magic angle' of 54° 44' 8" this term should disappear. However the setting of the angle is crucial [30]. The problem arises from the third term in the expansion, $E_m^{(2)}$, where the angular dependence is not of the form where spinning at the magic angle would eliminate this term. However it has been established that MAS does reduce the second order broadening by an approximate factor around 3 - 4 [32]. Further reduction of this second order can be achieved via a process of dynamic angle spinning (DAS) or double rotation (DOR) [33-35] although this obviously increases the line broadening effects due to both the dipolar and chemical shift interactions.

2.2.5 PARAMAGNETIC IMPURITIES.

A common problem encountered in high resolution solid state NMR is the long spin-lattice relaxation times of certain nuclei, specifically, in the study of glasses, ^{29}Si where it can take tens of minutes or even hours before the spin system reaches its equilibrium distribution [18,28,30]. This can be overcome by doping the samples with paramagnetic impurities, usually transition metal ions, which act as "spin-sinks" with the unpaired electron spins rapidly removing the Zeeman energy from the resonating nuclei so enabling the delay between pulses to be drastically reduced.

The excess nuclear Zeeman energy diffuses by a spin exchange process towards the large electronic moments due to the unpaired d electrons, which then transfer this energy to the lattice via their fluctuating magnetic field [31]. Thus the effectiveness of this approach depends upon the rate of diffusion from nuclear to

electron spins and the spin-lattice relaxation time of the paramagnetic ion, which is generally very much less than T_1 for the nuclei. Hence we are mainly concerned with the speed of the initial diffusion. If we consider a simple crystal lattice, cell parameter *a*, with a paramagnetic impurity concentration of *N* ions per unit volume then each nucleus within a certain sphere of radius *b* will experience a very distorted local field such that their relaxation times will be very short and their resonating frequencies so different to the Larmor frequency as to be unobservable [20]. Blumberg [36] defined this radius length *b* as the diffusion barrier radius where *b* is both a function of the impurity and nuclear moments and should lie in the range $a << b >> N^{-1/3}$. If *b* were greater than $N^{-1/3}$ all the nuclei would experience broadening so as to render them undetectable.

The question remains though as to what degree does the incorporation of paramagnetic impurities affect the resulting lineshapes and positions. Van Vleck [37] proposed that even the incorporation of as little as 1 ppm of paramagnetic impurity would increase the linewidth, although Bloembergen [38] states that the interaction between the nuclei and spins would only become significant for impurity concentrations greater than 1000ppm. Kittel and Abrahams [39] showed that, for a randomly distributed concentration of approximately 1000 ppm paramagnetic ions, the dipolar broadening would produce a Lorentzian lineshape. Numerous studies have shown the experimental advantages of the reduction in relaxation times produced by low levels of doping. The intensity of the resonant line, even in multi-line spectra, is not affected by the paramagnetic ions [40-44] provided their concentration is < 3 mol% as above this significant spectral features can be masked, but there does appear to be a change in the position and width of the line. Mortuza [45] prepared a series of nominally identical glasses with varying amounts of Mn^{3+} ions, 0 to 0.8 mol%, and observed an increase in linewidth and a slight shift in peak position of the ^{29}Si peak. The increase in full width at half maximum was from 10.5 to 15.0 ($\pm$ 0.5) ppm and the shift in position from -88.8 to - 89.5 ($\pm$ 0.5) between

mol%, no discernible movement in the chemical shift could be detected above the experimental error. Conversely the spin-lattice relaxation time was reduced by a factor of approximately 60 to less than 2 seconds (0.8 mol% MnO) or, for 0.2 mol%, to approximately 8 seconds. Therefore the slight increase in line width and possible small shift in position seems a worthwhile price to pay for the ability to employ natural abundance ^{29}Si NMR and the achievable reduction in the spectrum accumulation time.

2.3. BRUKER MSL 360 NMR SPECTROMETER.

2.3.1. INTRODUCTION TO PULSE FOURIER TRANSFORM NMR.

With the introduction, in 1951 by Hahn [46], of pulse NMR the original continuous wave approach was largely overshadowed. It was shown by Lowe and Norberg [47] that the response of the spin system to a radio frequency pulse, a decaying signal with respect to time known as the free induction decay, formed a Fourier pair with the frequency domain. Experimentally verified by Clark [48] and later by Ernst and Anderson [49] pulsed Fourier transform NMR flourished as a technique as computers reduced in physical size and cost whilst increasing in speed along with the development of fast Fourier transform algorithms.

Not only is the FID half of a Fourier pair, the pulse train also has a comparable half in the frequency domain. This is the radiation packet or frequency range envelope. If we consider a rectangular pulse of period t_p and frequency ω, figure 2.6, this will produce an oscillating field, B_1, orthogonal to the static field and acting on the magnetization vector $\underline{M}$. From classical angular momentum considerations the result will be a torque on $\underline{M}$ shifting or 'tipping' it away from its

equilibrium position, $\underline{M}_o$, parallel to $\underline{B}_o$ by an angle θ_p given by

$$\theta_p = \gamma B_1 t_p \qquad \{ 2.18 \}$$

However if the sample under investigation contains nuclei with differing resonant frequencies, due to a variety of reasons possibly including differing coordination or

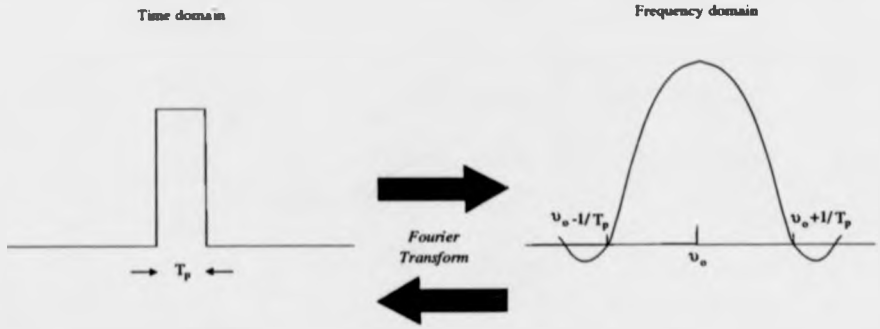

Figure 2.6. The relationship between the time and frequency domains of a square rectangular pulse of frequency ν *and duration* T_p

bonding arrangements etc., then in order to ensure that all the resonances are tipped through the same angle, i.e. all are irradiated equally, the frequency envelope should be of a sufficient width to cover all these possible frequencies. By performing a fourier transform on an ideal rectangular pulse the result is a sinc function centred on the pulse frequency, figure 2.6. This is of particular importance to solid state spectroscopy where linewidths of the order of 100 ppm are not uncommon. Hence to produce a wide frequency envelope, short sharp pulses are necessary.

The basic requirements for pulsed FT NMR are;

(i) *a magnet* - to provide the net macroscopic magnetization required. Generally speaking the larger the field the better, as it will increase the effective magnetization of the system so increasing the small population difference between the energy levels. It is also necessary for the field to be both stable and homogeneous across the whole of the sample and throughout the duration

of a measurement. Problems associated with increasing the field strength mainly concern the broadening mechanisms. If the chemical shift anisotropy is the dominating interaction then this will produce even wider lines, although conversely if quadrupolar broadening is the major broadening mechanism then this will reduce as a function of B_o.

(ii) *a radio frequency oscillator* - necessary for the production of the rf signal. Not only should the oscillator produce a stable signal but it should also be flexible and able to tune to a wide range of frequencies because the field strength is fixed.

(iii) *a pulse programmer*, which, along with the gate, should not only have very short rise and fall times but have the capability to construct complicated pulse trains with variations in both time and phase.

(iv) *a transmitter* - capable of transferring the pulse train, with the necessary amplification (~ 1KW), to the probe and hence the sample.

(v) *the probe* - essentially a tunable LCR circuit containing the coil within which is the sample. Furthermore for MAS experiments the sample needs to be rotated within the coil at speeds in order of 1 - 18 KHz achieved via gas bearings. However the coil must be able to not only receive the pulse, where the voltage could be in the kilovolt range, and convert it into the oscillating field B_1,but also detect the resulting nuclear magnetization, with a signal strength of perhaps only a few microvolts. According to Smith [30] this is most often accomplished via a Lowe and Tarr circuit [50].

(vi) *the receiver* - detects the signal from the coil. The receiver must be able to recover quickly from any spurious signal due to the rf pulse such as 'ringing' due to mechanical resonances in either the probe or the rf filters induced by the pulse [11]. The quick recovery is necessary as broad resonance lines rapidly decay in the time domain.

(vii) *the detector* - usually 2 phase sensitive detectors operating in quadrature in most modern spectrometers which increases the signal to noise ratio (S/N) by 1.414 [11]. The S/N can be further improved by coherent addition of a number of FIDs, n, which, according to Poisson statistics, improves S/N by $n^{½}$. This does create a problem in that sufficient time must elapse between pulses to enable the spin system to reattain the equilibrium Boltzmann population distribution otherwise saturation will occur. Convention states that for short spin-lattice relaxation times (T_1) 90° pulses followed by a delay of $4T_1$ is satisfactory for the production of quantitative spectra [30]. However when this is not practical, i.e. if the relaxation time approaches a few hours as opposed to a few seconds, then it is necessary to optimize the acquisition parameters such that quantitative spectra can be obtained with both adequate S/N and within a reasonable time period [51]. However, in systems where relaxation rates are markedly different, this approach leads to the loss of real quantitative data [30].

(viii) *the computer* - where finally the signal is digitized and stored prior to manipulation, i.e. fourier transforming and phase correction.

2.3.2 THE MSL 360 SYSTEM.

The MSL 360 spectrometer (Multipurpose Solid and Liquid; proton frequency of 360 MHz) was obtained from Bruker Spectrospin and operated in conjunction with an 8.45 T superconducting Oxford magnet. An Aspect 3000 computer complete with Winchester drive system was used both for spectrometer control and data accumulation, storage and manipulation. A schematic diagram is shown in figure 2.7.

Shim coils within the magnet were able to produce small local field

gradients ($B_{shim} << B_o$) such that the field immediately surrounding the sample was

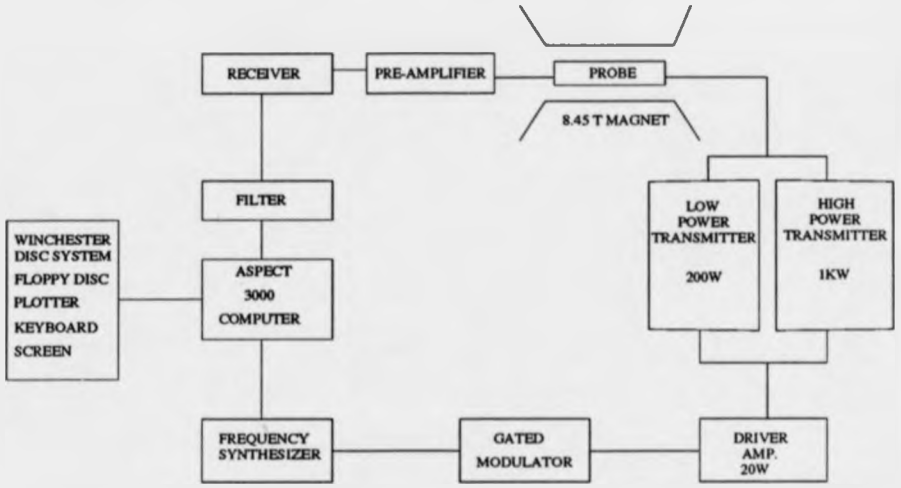

Figure 2.7. A schemetic representation of the main components comprising the Bruker MSL 360 spectrometer.

sufficiently homogenous to obtain proton linewidths of ~ 30 Hz [52].

The radiofrequency pulse at the sample was generated by collection of electronic hardware, The basic frequency of the radiofrequency pulse was provided by the PTS 200 synthesizer which was subsequently gated by the modulating pulse programmer. The resulting pulse train was then amplified before being transmitted to the sample via the coil, which also acted as the receiver for the resulting sample magnetization (see section 2.3.1). This signal was then amplified by a linear broad band amplifier before finally passing through a Bessel filter designed to produce a final signal of the optimum bandwidth without any phase distortion.

The whole process is controlled by the Aspect 3000 computer system, operating under a high level machine language known as DISMSL, including the driving of the other peripherals such as the floppy drives,VDU, plotter and printer. Further descriptions of these components may again be found in the relevant Bruker

manuals and handbooks [52-55].

The MSL is compatible with a variety of probes; static and both single and double bearing sample spinning, provided they fit the bore of the magnet.

The static probe, Bruker Z33vHP, came with a set of interchangeable coils to cover different frequency ranges. The sample was in the horizontal plane enclosed in sealed nylon tubes. In order to change sample it was necessary to remove the whole probe from the magnet and detach part of the probe outer casing.

For spinning spectra the sample was contained in one of two types and sizes of cylindrical ceramic spinner depending upon which of the two types of spinning probe was being used, figure 2.8. The Doty Scientific 360 MHz double bearing probe [56] utilises 5 mm outer diameter spinners with two fluted end caps. The caps were made of either vespel or Kel-F the choice between which depended upon the desired spinning rate; Kel-F upto 14 KHz compared to vespel maximum of 10.5 KHz. The spinners themselves were either silicon nitride, alumina or zirconia. These types of spinners were also used in a homemade probe which was based around a Doty Scientific stator assembly. In order to change samples in either of these probes the whole unit had to removed from the magnet.

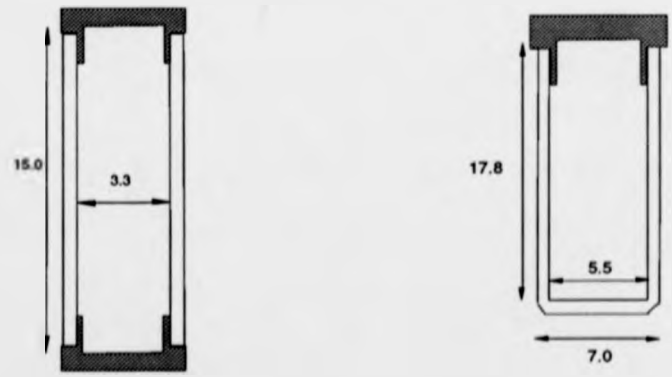

Figure 2.8. Different types of spinner employed in the NMR experiments. (a) A Doty spinner used in probes equipped with a Doty rotor assembly. (b) A Bruker double bearing spinner used in the Bruker probes. All dimensions given in mm.

However it was not necessary to remove the Bruker Z 33.6 DR-MAS-7DB double bearing probes to change samples as this could be achieved via a separate compressed air powered insert/eject system incorporated in the top of the magnet. The Bruker spinners had an external diameter of 7mm and were made of either zirconia, silicon nitride or alumina. Their larger diameter restricts the maximum spinning speed to ~ 5 KHz, although the larger sample volume is an asset in terms of the S/N. The sample spinning rate was measured by an optical ratemeter. For MAS experiments the packing of the spinner is critical. If the spinner is not balanced then smooth fast spinning is not possible and repacking is necessary.

All the spinning probes had the coils nominally aligned at the magic angle in respect of B_o with a manually adjusted range of movement restricted to a few degrees either side. The magic angle was set using the ^{79}Br resonance from KBr [57]. ^{79}Br is a quadrupolar nucleus, spin $^3/_2$, and occupies a symmetric cubic environment in this compound. The resulting resonance is large and consists of a central line with an envelope of symmetric sidebands. The intensity of these sidebands is maximised when the magic angle is achieved. For lower frequency nuclei the magic angle is better set via the ^{85}Rb resonance fron RbCl [30].

Operation of the spectrometer is a relatively simple procedure provided that an appropriate reference file for the nucleus under investigation already exists. Once this file is recalled the spectrometer is immediately set with the appropriate parameters including the operating frequency, see table 2.1. The operator has only to choose the appropriate frequency restricted preamplifier and probe. Throughout this study only the low power broad band transmitter was employed. The probe was impedance matched to the preamplifier via the tune and match components of the probe circuitry. Before each series of spectra for a particular nucleus was recorded the relevant shim file was recalled and a reference spectrum accumulated. The reference material is generally a liquid, see table 2.1, and enables the spectrometer to set the zero of the chemical shift for that particular

nucleus. This has to be performed before each experiment as the field does vary slightly over a period of time.

PARAMETER	NUCLEUS				
	^{29}Si	^{27}Al	^{31}P	^{23}Na	^{1}H
Spectrometer Frequency (MHz)	71.5	93.6	145.8	95.3	360.0
Pulse Length (μ sec.)	2	1	4	1	1
Delay between pulses (sec.)	60	1	1	1	1
Reference Standard	T.M.S.	1 molar $AlCl_3$ soln.	85% H_3PO_4	1 molar NaCl soln.	T.M.S.

Table 2.1. A list of the spectral acquisition parameters and reference materials employed in the study of various nuclei in this work.

All the data were acquired via quadrature PSD with a simple single pulse phase cycled pulse train. By cycling the pulse through the 4 directions, +x, -y, -x, +y, any artefact due to detection in one phase is removed. Short intense pulses, typically less than 4 μs, were used so as to excite a sufficiently large frequency range (section 2.3.1) to encompass all possible resonant frequencies for a particular nucleus, table 2.1.

Once the data has been collected in the form of the FID various processing techniques are employed before the frequency domain spectrum is interpreted. However care must be taken during processing to ensure that the final spectrum is indeed a true reflection of the time domain signal. Firstly the FID is generally 'smoothed', or more correctly truncated, by multiplying with an exponential. This is carried out to increase the S/N although it does increase the resonance linewidth, hence 'smoothing' is usually called linebroadening. The resulting linebroadened FID is then Fourier transformed and phased before any baseline correction is applied. As the phasing is performed by eye again attention

must be paid to not distorting the data, a particular problem in glasses where the lines tend to be rather broad. Computerised algorithms allow the superimposition of different spectra as well as integration and other data manipulation techniques in order that the maximum amount of information is retrievable from each spectrum.

For further details on the spectrometer, its operation, computer control and how to create a reference file for a new nucleus the reader is referred to references [30,45,52-55].

2.4. REFERENCES.

[1] E.M. Purcell, H.C. Torrey & R.V. Pound, *Phys. Rev.* 69, 37, (1946)

[2] F. Bloch, W.W. Hansen & M.E. Packard, *Phys. Rev.* 69, 127, (1946)

[3] W.D. Knight, *Phys. Rev.* 76, 1259, (1949)

[4] J.T. Arnold, S.S. Dharmati & M.E. Packard, *J. Chem. Phys.* 19, 507, (1951)

[5] E.R. Andrew, A. Bradbury & R.G. Eades, *Arch. Sci. (Geneva)*, 11, Fasc. Spec. 223, (1958) and also *Nature (London)* 182, 1659, (1958)

[6] I.J. Lowe, *Phys. Rev. Lett.* 2, 285, (1959)

[7] S.R. Hartman & E.L. Hahn, *Phys. Rev.* 128, 2042, (1962)

[8] A.N. Garancy, D.L. van der Hart & W.L. Earl, *Phil. Trans. Royal Soc. Lond.* A229, 609, (1981)

[9] A. Pines, M.G. Gibby & J.S. Waugh, *J. Chem. Phys.* 59, 569, (1973)

[10] Proceedings of the NATO Advanced Study Institute, Stirling 1982, "The Multinuclear Approach to NMR Spectroscopy"

[11] Vols. I & II of "NMR of Newly Accessible Nuclei", ed. by P. Laszlo, Academic Press 1983

[12] E. Fukushima & S.B.W. Roeder, "Experimental Pulse NMR", Addison Wesley 1981

[13] C.T.G. Knight, R.J. Kirkpatrick & E. Oldfield, *J. Non-Cryst. Solids* 116, 140, (1990)

[14] I. Farnan & J.F. Stebbin, *J. Non-Cryst. Solids* 124, 207, (1990)

[15] R.J. Kirkpatrick in "Spectroscopic Methods in Mineralogy & Geology" ed. F.C. Hawthorn, Mineral Soc. of America 1988

[16] J.F. Stebbins in "Spectroscopic Methods in Mineralogy & Geology" ed. F.C. Hawthorn, Mineral Soc. of America 1988

[17] R. Dupree & D. Holland in "Glasses and Glass-Ceramics", ed. M.H. Lewis, Chapman Hall, 1990

[18] G.R. Hatfield & K.R. Cardunner, *J. Mater. Sci.* 24, 4209, (1989)

[19] S.R. Elliot, *J. Non-Cryst. Solids* 123, 149, (1990)

[20] A. Abragam, "Principles of Nuclear Magnetism", Oxford, 1985

[21] C.P. Slichter, "Principles of Magnetic Resonance", 2nd ed., Springer-Verlag, 1980

[22] M. Mehring, "Principles of High Resolution NMR in Solids", 2nd ed., Springer-Verlag, 1983

[23] U. Haeberlin, "Principles of High Resolution NMR in Solids", Academic Press, 1976

[24] C.A. Fyfe, "Solid State NMR for Chemist", CRC Press, 1984

[25] W. Lamb, *Phys. Rev.* 60, 817, (1941)

[26] N.F. Ramsey, *Phys. Rev.* 78, 699, (1950)

[27] A.-R. Grimmer, F. Von Lampe & M. Mägi, *Chem. Phys. Lett.* 132, 549, (1986)

[28] B. Coleman, p.223 in "NMR of Newly Accessible Nuclei: Vol.2", ed.

P. Laszlo, Academic Press, 1983
[29] H. Eckert, *Progress in NMR Spectroscopy*, 24, 159, (1992)
[30] M.E. Smith, PhD Thesis, University of Warwick, 1989
[31] E.R. Andrew, "Magnetic Resonance", Cambridge Press, 1958
[32] D.Freude, J. Hasse, J. Klinowski, T.A. Carpenter & G. Ronikier, *Chem. Phys. Lett.* 119, 365, (1985)
[33] S. Ganapathy, S. Schramm & E. Oldfield, *J. Chem. Phys.* 77, 4360, (1982)
[34] A. Samoson, E. Lippmaa & A. Pines, *Mol. Physics* 65, 1013, (1988)
[35] B.F. Chmelka, K.T. Mueller, A. Pines, J.F. Stebbins, Y. Wu & J.W. Zwanziger, *Nature* 339, 42, (1989)
[36] W.E. Blumberg, *Phys. Rev.* 119, 79, (1960)
[37] J.H. Van Vleck, *Phys. Rev.* 74, 1168, (1948)
[38] N. Bloembergen, *Physica* 15, 386, (1949)
[39] C. Kittel & Abrahams, *Phys. Rev.* 90, 238, (1953)
[40] R. Dupree, D. Holland, P.W. McMillan & R.F. Pettifer, *J. Non-Cryst. Solids* 68, 399, (1984)
[41] R. Dupree, N. Ford & D. Holland, *Phys. Chem. Glasses* 28, 78, (1987)
[42] R. Dupree, D. Holland & D.S. Williams, *J. Non-Cryst. Solids* 81, 185, (1986)
[43] R. Dupree, D. Holland & M.G. Mortuza, *Phys. Chem Glasses* 29, 18, (1988)
[44] R. Dupree, D. Holland & M.G. Mortuza, *Nature* 328, 416, (1987)
[45] M.G. Mortuza, PhD Thesis, University of Warwick, 1989
[46] E.L. Hahn, *Phys. Rev.* 80, 580, (1950)
[47] I.J. Lowe & R.E. Norberg, *Phys. Rev.* 107, 46, (1957)
[48] W.G. Clark, *Rev. Sci. Instr.* 35, 316, (1964)
[49] R.R. Ernst & W.A. Anderson, *Rev. Sci. Instr.* 37, 93, (1966)
[50] I.J. Lowe & C.E. Tarr, *J. Phys. E* 1, 320, (1968)
[51] R. Dupree & M.E. Smith, *J. Magn. Res.* 75, 153, (1987)
[52] "MSL System Description", Bruker Spectrospin Manual, Ref. #431001 (1986)
[53] Aspect 3000 Software Manual, Bruker Spectrospin Manual (1986)
[54] NMR Probehead Manual: Series MAS-DB, Bruker Spectrospin Manual (1985)
[55] Users Manual: MSL Series, Bruker Spectrospin, 1985
[56] Users Manual for Solid State Probes, Doty Scientific Instruments, Columbia U.S.A., 1986
[57] J.S. Frye & G.E. Maciel, *J. Magn. Reson.*, 48, 125, (1982)
[58] G. Engelhardt & D. Michel, "High Resolution Solid State NMR of Silicates and Zeolites", Wiley, 1987

CHAPTER 3.

OTHER EXPERIMENTAL TECHNIQUES.

3.1 INTRODUCTION.

Although Magic Angle Spinning Nuclear Magnetic Resonance (MAS NMR) is the main experimental technique of this study, the information regarding glass structure obtained from this, or any other single technique, will always be limited. Consequently a variety of other techniques have been applied in order to complement the MAS NMR data and so provide a better understanding of the structural components within these glass systems.

Not all the techniques were employed in the investigation of every system, therefore the aim of this chapter is to collate these methods and the equipment used into one section. The descriptions are brief and are intended to convey the procedures specific to this work.

3.2 THERMAL TECHNIQUES.

Thermal analysis covers a variety of techniques which are concerned with the measurement of a physical property of a material as a function of temperature whilst undergoing controlled heating or cooling. Of the thermal methods applied in this study Differential Thermal Analysis (DTA) and Differential Scanning Calorimetry (DSC) are concerned with changes in enthalpy, heat capacity and thermal diffusivity due to phase transitions and reactions and Dilatometry evaluates the variation in physical size, specifically length, of a material

with respect to temperature. Obviously the accuracy of thermal analysis and the reliability in comparing results requires consistency in all the contributing properties excluding the one under measurement. These extraneous factors include pressure, sample condition and other experimental parameters.

3.2.1 DIFFERENTIAL THERMAL ANALYSIS.

This is usually employed as a dynamic temperature technique where the difference in temperature between a sample and a reference material is recorded during either controlled heating or cooling and can be used to determine whether the sample undergoes any transformation, or reaction, that necessitates either the absorption or evolution of energy in the form of heat. Consequently any transformation can be categorized as being either endothermic or exothermic in nature. A typical DTA trace is illustrated in figure 3.1 where endo- and exothermic phenomena are present. According to Pope [1] the main factors influencing DTA experiments are; sample weight, sample particle size, sample packing, heating rate and atmospheric conditions. Therefore all these factors were maintained as constant as possible at least within experiments on the same glass system. Throughout, the reference material was fine ground Limoges quartz, except in cases where it was believed that the $\alpha - \beta$ quartz transition around 570 °C masked transformations within the sample. When this was the case the experiment was re-run with a fresh sample and analytical grade alumina as a reference.

The equipment used was a Stanton Redcroft S-R DTA 673-4 unit which was operated under standard atmospheric conditions. Typical heating rate was 6 °C/min except for particular cases detailed in the relevant chapters. Around 0.2 to 0.6 g of fine ground sample and a similar mass of reference material were heated in platinum crucibles. The temperature of the two materials was measured via PtRh

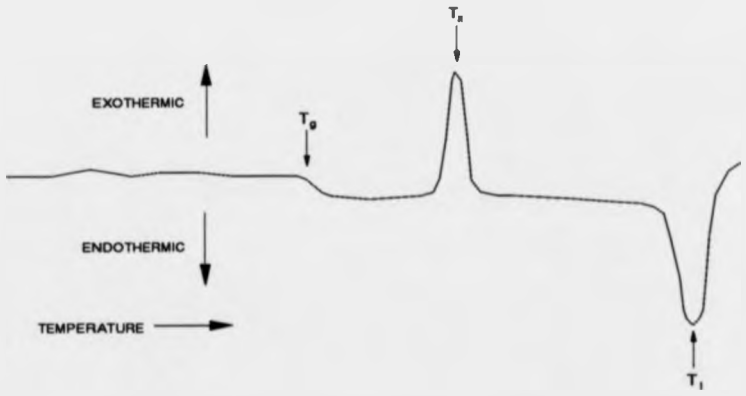

Figure 3.1. A representation of a typical DTA trace. The various transformations corresponding to glass transition, crystallization and melting are shown.

thermocouples located in recesses in the crucibles. The resulting temperatures of the glass transition, onset of crystallization and softening/liquidus points, where appropriate, can be found in the relevant tables of chapters 4 and 5.

More detail regarding the experimental and theoretical background of DTA can be found in the book by Pope [1].

3.2.2 DIFFERENTIAL SCANNING CALORIMETRY.

Normally differential scanning calorimetry is concerned with the energy necessary to maintain the sample and reference materials at the same temperature during heating and cooling. However the equipment used in this study, a Netzsch high temperature DSC 404, measures the difference in temperature between the sample and reference. Thus the specific heat capacity can be determined over a wide range of temperatures if the system is calibrated using known enthalpy changes [2].

The specific heat capacity can subsequently be used to evaluate the

fictive temperature of a glass via the approach of Moynihan et al [3]. The fictive temperature is a function of quench rate and can be expressed in terms of enthalpy [3-7];

$$H(T) = H_e(T_f) - \int_{T}^{T_f} C_{pg}\, dT' \qquad \text{.....(3.1)}$$

where H is enthalpy, T temperature and the subscripts e and g refer to the glass itself and the material in equilibrium respectively. Thus, via differentiation and integration;

$$\int_{T^*}^{T_f'} (C_{pe} - C_{pg})\, dT_f = \int_{T^*}^{T'} (C_p - C_{pg})\, dT \qquad \text{.....(3.2)}$$

where T* is a temperature above the glass transition, where the specific heat, C_p, is equivalent to the specific heat of equilibrium, C_{pe}, and T' is a temperature below the glass transition. Consequently the fictive temperature, T_f, can be estimated graphically from the DSC trace by equating integrated areas as shown in figure 3.2.

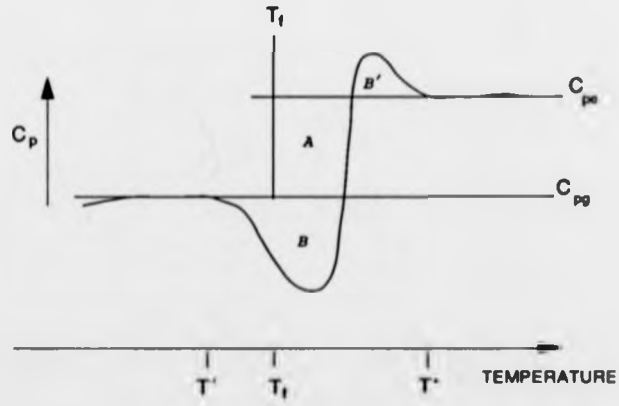

Figure 3.2. An illustration of the graphical method of fictive temperature determination of Moynihan et al [3]. The area A is eqivalent to the sum of areas B and B'.

Approximately 0.1g of powdered glass, along with an identical mass of alumina as a reference were heated in platinum crucibles through the glass transition range. Heating rate was controlled by a Netzsch 410 microprocessor unit. The results obtained via this technique are detailed in chapter 4.

3.2.3. DILATOMETRY.

Thermal expansion can frequently be a critical factor in the adhesion of dissimilar materials across an interface. If the degree of mismatch between the coefficients of thermal expansion is large, then heating or cooling could induce critical strains across the interface leading to catastrophic failure of the adhesion.

The thermal coefficients of expansion of the glasses prepared in chapter 5, Bioglasses [8], were investigated because of their possible potential as bioactive coatings on metallic substrates. A homemade vertical fused quartz [9] dilatometer was used calibrated by a platinum standard. Extension of the material was monitored by a linear variable differential transducer and recorded on chart paper. Typical heating rate was 6 °C/min with the temperature rising until the dilatometric softening point was reached. The coefficient of thermal expansion, α, was calculated according to the equation,

$$\alpha = \Delta L / L.\Delta T \qquad \text{.....\{eqn. 3.3\}}$$

where L is the original length, ΔL the consequential change in length and ΔT the temperature range.

3.2.4. X-RAY DIFFRACTION.

X-Ray Diffraction (XRD) is a long established technique [10]. Regular spacing of interatomic planes within a material can diffract electromagnetic radiation of a similar wavelength to the spacing of the planes, see figure 3.3, according to Braggs law.

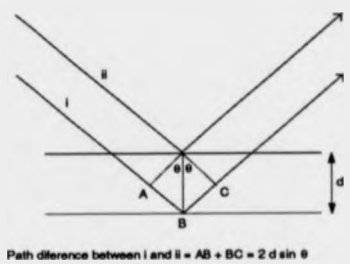

Figure 3.3. An illustration of Bragg's Law and the requirements for it to be satisfied.

Of the many XRD methods the one employed in this study is that of the rotating sample method [9]. The angle of incidence of the monochromatic x-rays upon the crystal, or glass, powder is varied and the diffracted intensity recorded by a counter. Figure 3.4 illustrates this schematically.

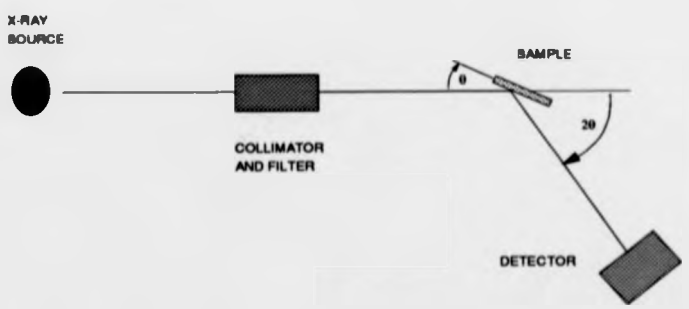

Figure 3.4. A schemetic illustration of the equipment set-up employed in XRD investigations in this study. Finely powdered samples were firmly pressed into aluminium holders with a glass microscope slide.

Consequently the variation in diffracted x-ray intensity will produce a diffraction pattern that is particular to one specific crystalline material as the spacing of the interatomic planes and atomic scattering factors is different for each material. Therefore evaluation of an unknown material can be achieved via cross referencing the experimental pattern with the standard J.C.P.D.S. diffraction files [11].

More detail on the theory and practice of this technique and other XRD methods is available from references [10,12-14].

XRD was performed on all samples investigated in this study to ascertain their degree of amorphicity. Glasses, having no long range periodicity in their atomic arrangement, produce diffuse x-ray patterns with no intense reflections. Figure 3.5 illustrates the XRD powder patterns of crystalline quartz and a glass (BG7) for comparison. The technique was also employed to establish the crystal phases formed after devitrification according to a specified heat treatment in chapter 5.

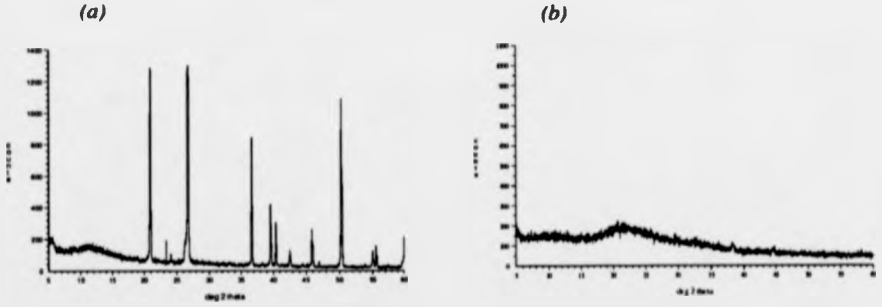

Figure 3.5. Powder X-ray diffraction patterns obtained from a crystalline material, quartz, (a) and glass, BG7 of chapter 5, (b). The lack of long range ordering of atomic planes in the glass, which is present in the crystalline material, producing the diffuse diffraction pattern. Note that 'hump' around 12 ° 2Θ in (a) is a due to the diffractometer and not an amorphous phase within the quartz.

Samples were crushed to a fine powder in an agate mortar and pestle and then mounted in aluminium sample holders. The sample and holder were then placed in the x-ray beam on the rotational axis. Copper K_α was used, a nickel filter eliminating the K_β radiation. The angles of incidence at the sample and the counter

were controlled by a Philips goniometer, the sample at Θ °/min and the counter at 2 Θ °/min. The output of the counter was recorded on a chart recorder. From this diffraction pattern the numerous reflections can be indexed to the relevant d_{hkl} spacing, which was then referenced with the J.C.P.D.S file [11]. The limit of detection of the equipment is approximately 5% volume fraction.

3.4 INFRA RED ABSORPTION SPECTROSCOPY.

Interatomic bonds within a material have vibrational modes at frequencies within the infra red wavelength range of electromagnetic radiation. Different molecular functional groups have characteristic vibrational frequencies. Consequently the particular wavelengths within the range of 2 -1000 microns that induce these vibrations will provide information on the structural species present in the material. Obviously in crystalline materials where the interatomic bonds are regular and well defined, illuminating the material over a range of infra red wavelengths will produce a set of sharp absorption peaks. Conversely in amorphous materials the lack of definite bond lengths and angles will lead to an absorption spectrum with broader peaks, hence interpretation is achieved via correlation with the absorption spectra of crystalline analogues.

Glasses prepared in chapter 4 were examined by Infra-Red Absorption Spectroscopy (IRAS) as a complementary technique to multinuclear MAS NMR. Samples for examination were prepared via the potassium bromide technique; small quantities of finely powdered glass and dry analar KBr in the ratio of 1:15 by weight were ground together in an agate pestle and mortar before being pressed into translucent discs of approximately 0.3 mm thickness. The discs were then mounted in a Perkin Elmer PE 983 infra red spectrometer controlled by a computer workstation and the absorption measured over the range of 4000 to 180 cm^{-1}.

Further aspects of IRAS as an experimental technique can be obtained elsewhere [15,16].

3.5 ATOMIC ABSORPTION SPECTROSCOPY.

This technique was employed solely as a tool for analysis of the potassium concentration in the $K_2O.4SiO_2.xP_2O_5$ glasses (chapter 4). A Varian Techtrons AA-6 absorption spectrophotometer with Hilger Analytical potassium hollow cathode lamp was used according to the manufacturers instructions [17]. Calibration solutions were prepared by diluting a standard solution prepared from 1.907g of potassium chloride in 1 litre of distilled water [17]. Calibration curves were plotted of the absorbed intensity against potassium ion concentration.

Sample solutions were prepared by dissolving approximately 1.5g of finely powdered glass in 10 ml of HF acid, heating to leave a dry residue, dissolving in 10 ml of HCl acid, drying again before dissolving again in 1:1 diluted HCl and subsequently diluting to 100 ml with distilled water. The concentration of potassium ions in the sample solutions was then determined from the calibration curves.

3.6 WET CHEMICAL ANALYSIS.

It is well established that the composition of a glass can vary during the melting process. Therefore the only way to discuss the possible structure of a glass in relation to its composition is via knowledge of the final composition.

Consequently the final concentration of silica in certain melt prepared glasses in the $K_2O.4SiO_2.xP_2O_5$ system and silica, sodium oxide and calcium oxide in one composition in the Bioglass system (BG4) were determined via wet chemical

analysis following the approach of the relevant sections of British Standard B.S. 2649 Part 1, Glasses of the soda-lime-magnesia-silica type : 1988, [18]. The concentrations of the remaining components were determined via quantitative NMR (P_2O_5 and Al_2O_3 in the potassium phosphosilicate glasses) or by difference (some SiO_2 and P_2O_5). Final analysed compositions for the potassium phosphosilicate glasses and the one Bioglass [8] can be found in tables 4.2 and 5.1 respectively.

The final concentrations of lead oxide and aluminium oxide in the $PbO.Al_2O_3.P_2O_5$ glasses (chapter 6) were determined by following the procedure outlined by method 1.8, "Rapid determination of PbO and Al_2O_3 in full lead crystal glasses", in the British Glass Industry Research Analysis handbook [19]. Essentially the procedure involves decomposition of a known mass of sample via hydrofluoric/ perchloric acids with lead and aluminium oxides complexed by ethylene di-nitrilo tetra acetic acid (EDTA). The resulting solution is then back titrated with zinc acetate solution and ammonium fluoride, using xylenol orange as an indicator, to determine values for the PbO and Al_2O_3 concentrations. Subsequently the P_2O_5 content was calculated by difference. The analysed compositions are given alongside the nominal in table 6.1.

3.7 DENSITY MEASUREMENTS.

The density of melt prepared glasses in the potassium phosphosilicate system was determined via Archimedes' Principle using a Sartorius IAC digital balance and integrated densitometer. Ethandiol (ethylene glycol) was the suspending medium. Pieces of splat cooled glass were placed on the tray and their mass recorded in and out of the ethandiol enabling the density to be calculated from

$$\rho = \frac{W_A}{W_A - W_G} \cdot \rho_E \qquad \text{.....(3.3)}$$

3.8. REFERENCES.

[1] M.I. Pope, "Differential Thermal Analysis", Heyden, 1977

[2] Netzch High Temperature DSC 404 Operating Instructions, Issue I, 09-88

[3] C.T. Moynihan, A.J. Easteal, M.A. DeBolt & J. Tucker, *J. Am. Ceram. Soc.* 59, 12, (1976)

[4] M.A. DeBolt, A.J. Easteal, P.B. Macedo & C.T. Moynihan, *J. Am. Ceram. Soc.* 59,16, (1976)

[5] R.O. Davies & G.O. Jones, *Adv. Phys.* 2, 370, (1957)

[6] R. Gordon & O.S. Narayanaswamy, *J. Am. Ceram. Soc.* 53, 380, (1970)

[7] O.S. Narayanaswamy, *J. Am. Ceram. Soc.* 54, 491, (1971)

[8] Bioglass is a registered trade mark of the University of Florida, Gainesville, Fl, USA.

[9] Details on the dilatometer can be found in D.R. Bridges, PhD. Thesis, University of Warwick, 1986.

[10] W.P. Binnie & I.G. Geils in "Methods of Experimental Physics: vol. 6A", eds. K. Lark-Horovitz & V.A. Johnson, Academic Press, 1959

[11] J.C.P.D.S. Powder Diffraction Files, Alphabetical and Search Indexes, J.C.P.D.S., 1984

[12] H.P. Klug & L.E. Alexander, "X-Ray Diffraction Procedures for Polycrystalline and Amorphous Materials", 2nd ed., Wiley, 1974

[13] H.S. Lipson, "Crystals and X-rays", Springer-Verlag, 1970

[14] B.E. Warren, "X-Ray Diffraction", Addison Wesley, 1969

[15] W.R. Taylor, *Proc. Indian Acad. Sci. (Earth Planet. Sci.)* 99, 99, (1990)

[16] J.E. Stewart, "Infra-Red Spectroscopy; Experimental Methods and Techniques", Dekker, 1970

[17] Varian Techtrons, Atomic Absorption spectrophotometer AA-6, instruction manual.

[18] British Standard Methods for Analysis of Glass, Part 1, "Glasses of the soda-lime-magnesia-silica type", B.S. 2649:part 1:1988, British Standards Institution.

[19] "BGIRA Handbook, Part 1 - Analysis of Glass", The British Glass Industry Research Association, Northumberland Road, Sheffield, U.K.

CHAPTER 4.

K_2O . SiO_2 . P_2O_5 SYSTEM.

4.1. INTRODUCTION.

4.1.1. GENERAL INTRODUCTION.

Establishing the relationship between composition and glass structure or connectivity is a major goal for glass scientists. In efforts to evaluate this relationship numerous and varied techniques have been used including XRD, IR, Raman, XPS, EXAFS, neutron scattering and NMR, and of these it is perhaps high resolution solid state NMR, both static and magic angle spinning, that has become one of the most powerful and widely used technique in the determination of the local structure of inorganic solids.

Lippmaa et al [1] first established that MAS NMR was able to discriminate between different Q^n types in the structural determination of a crystalline zeolite. Earlier low field static NMR had provided some structural information but resolution problems associated with line broadening effects hindered attempts to quantify the concentration and presence of the different Q^n units. That is not to say that static NMR is redundant. Indeed static studies with the latest stable high fields have been shown to provide more information than MAS in instances where the resolution of Q^n types partially depends upon the bonding anisotropies [2,3]

Numerous independent studies of binary alkali silicate systems

other than Li_2O-SiO_2 exhibit a distribution of non-bridging oxygens and Q^n types close to that predicted by the constrained binary model for most conditions and compositions. It is generally believed that it is the high charge density surrounding the relatively small Li^+ nucleus that causes the discrepancy. Indeed several contradictory MAS NMR investigations of the local structure of Li_2O-SiO_2 have been published [4-6]. Stebbins [2] has also provided evidence that in a $Na_2Si_2O_5$ glass a small amount of Q^4 species was present even though not required by the simple stoichiometric conditions of the binary model and contrary to an XRD study of the same composition which had indicated the presence of only one type of Q^n species; Q^3 [7,8].

In the K_2O-SiO_2 system Emerson et al [9] applied both static and MAS NMR to compare the resolutions of the species present. In the disilicate glass they observed a single symmetric peak in the MAS spectra as opposed to a static spectrum which evidently contained two overlapping resonances; the computerised fitting of this spectrum showed the pattern was composed of three resonances due to three separate Q^n units viz; 89% Q^3 axial, 5.5% Q^4 isotropic and 5.5% Q^2 anisotropic. For the tetrasilicate composition two resonances were recorded in both static and MAS experiments, although Emerson claims that the chemical shift is more readily obtained from the static spectrum. An ideal stoichiometric tetrasilicate would consist of 50% Q^4 and 50% Q^3. However the computerised fit performed by Emerson on his static spectra generated concentrations of 57%, 35% and 8% for the Q^4, Q^3 and Q^2 species respectively.

It is noticeable from all of these studies that there is a variation in the ^{29}Si chemical shift for each particular Q^n species, in addition to the spread of shift values due to immediate network bonding conditions. The type of network modifier ion also alters the ^{29}Si shift; eg in alkali tetrasilicate glasses the Q^4 resonance position changes from -111 to -109 to -103 for the alkali ions Li^+, Na^+ and K^+[9]. This is because, as is well known , the chemical shift becomes more negative

when the resonating nucleus experiences greater shielding [10,11], hence when the metal cation is less electronegative. In the case of the larger alkali ions , Rb^+ and Cs^+, the binary model predictions for Q^n species distribution initially is in very good agreement with measured spectra,however it breaks down for high concentrations (>45 mol%) [12]. These ^{29}Si spectra could only be fitted to a combination of 3 gaussians suggesting a partial disproportionation of the type

$$2x\ Q^2 \text{ -----> } x\ Q^3 + x\ Q^1.$$

Thus the ratio of $Q^3:Q^2:Q^1$ is given by

$$I_3 + x : (I_2 - 2x) : x$$

for concentrations of less than 50 mol% R_2O, where I_3 and I_2 are the expected intensities of the Q^3 and Q^2 species predicted by the binary model. For compositions with > 50 mol% by

$$x : (I_2 - 2x) : I_1 + x.$$

The amount of disproportionation increases therefore with increasing R_2O concentration indicating that these larger ions prefer the arrangement of a mixture of sheet (Q^3) and dimer (Q^1) species over the ring/chain arrangement of Q^2. It is believed that this particular network configuration may provide a greater interstitial volume enabling the accommodation of the greater steric and coulombic requirements of Rb^+ and Cs^+.

Further reviews of the application of NMR both to silicate and borate glasses include those by Elliott [13,14], Kirkpatrick [15,16], Bray [17,18], Stebbins and Farnan [19], Stallworth and Bray [20] and Eckert [21].

4.1.2. OCTAHEDRAL SILICON IN GLASSES.

The occurrence of higher coordinations of silicon is rare, observed in some metallorganic and even fewer crystalline inorganic compounds. The latter are usually high pressure polymorphs of regular tetrahedral silicates viz; stishovite (SiO_2) [22], ξ–$Na_2Si_2O_5$ [23] and wadeite ($K_2Si_4O_9$) [24]. Regular SiP_2O_7, and some of its polymorphs, also exhibit silicon in an octahedral environment, although both ^{29}Si MAS NMR [25] and IR [26] investigations of $SiO_2.P_2O_5$ glasses found no evidence of any [SiO_6] species until the glasses were devitrified. The occurrence of octahedral silicon in glasses is contrary to one of Zachariasen's observations [27] that formed the basis of the random network theory of glass structure, namely that the coordination of the cation should be small; silicon 4 and boron either 3 or 4 coordinated to oxygen. However workers investigating silicate melts and geologists examining the coordination state of magmas, (the assumption being that the structure of rapidly quenched glasses is similar to that of the equilibrium liquid at its fictive temperature), have often suggested that, at sufficiently high pressures, silicate melts should contain higher Si coordination states. Ion dynamics simulations of molten SiO_2, its analogue BeF_2 and alkali silicates [28-33] have repeatedly shown that 5 coordinated silicon should exist in the melts albeit as rapidly relaxing intermediary products during oxygen exchanges from one [SiO_4] tetrahedra to another. Therefore the total number of this species at any instance is likely to be very small, although it is argued that they play an important role in the viscous flow of these melts. Density studies of crystalline silicates under high pressure [34,35] claim that, for pressures in the range 8 to 24 GPa, Si^{vi} should predominate over Si^{iv}. Theoretically Si^{vi} is not only stable at high pressures. Gibbs [36] has determined that Si^{vi} is not thermodynamically unstable at standard temperature and pressure, whilst Geisinger [37], using solution calorimetry, has shown that mixed Si^{vi} and Si^{iv} potassium tetrasilicate ($K_2Si^{vi}Si^{iv}_3O_9$) is more stable in terms of enthalpy than the

phase containing only Si^{iv}.

Hard evidence of the existence of higher silicon coordinations has proved difficult to come by, although evidence for the existence of higher aluminium coordinations in silicate glasses has been presented. Raman and ^{27}Al MAS NMR have been employed in examining $Al_2O_3.SiO_2$ roller quenched glasses [38,39] but each have only suggested higher Al coordination along with Si^{iv}. Other attempts to observe higher Al or Si coordinations in glasses quenched from pressures up to 3 GPa have also proved fruitless [40-42]. Ohtani did report Al^{vi} via ^{27}Al MAS NMR from an albite glass quenched from 6 GPa [43], and Dickinson [44] has suggested that his Raman spectra obtained from a 2.4GPa quenched $K_2Si_4O_9$ glass was consistent with octahedral [SiO_6] species.

The first direct spectroscopic evidence concerning the existence of octahedral silicon in a glass was reported by Dupree, Holland and Mortuza [45].Whilst investigating the structure of a series of $Na_2O.2SiO_2$ based glasses containing large amounts of P_2O_5 (20-60 mol%) with MAS NMR, they observed a second separate resonance with a chemical shift of -213 ppm in the ^{29}Si spectrum of the 40 mol% sample, figure 4.1(a). Previous NMR data collated on Si^{vi} crystalline compounds confirmed that octahedral silicon has a shift range of -194 to -214 ppm [25,46,47]. The relative intensity of this second environment then increased with further increases in the P_2O_5 concentration. Earlier and subsequent work on the same system [48] has shown that for low P_2O_5 content (0-6 mol%) the modifier ions are removed from the silicate network and become associated with the phosphate groups. This permits the silicate network to repolymerise, resulting in the formation of Q^4 species from Q^3. Examination of the local environment of phosphorus with ^{31}P MAS NMR revealed the presence of either ortho- or pyro-phosphate units depending upon the actual P_2O_5 concentration, the type of alkali ion and thermal history. Further additions of P_2O_5 (up to 12 mol%) produced a change in the ^{29}Si and ^{31}P spectra; the ^{29}Si spectrum contained a broad asymmetric peak centred on

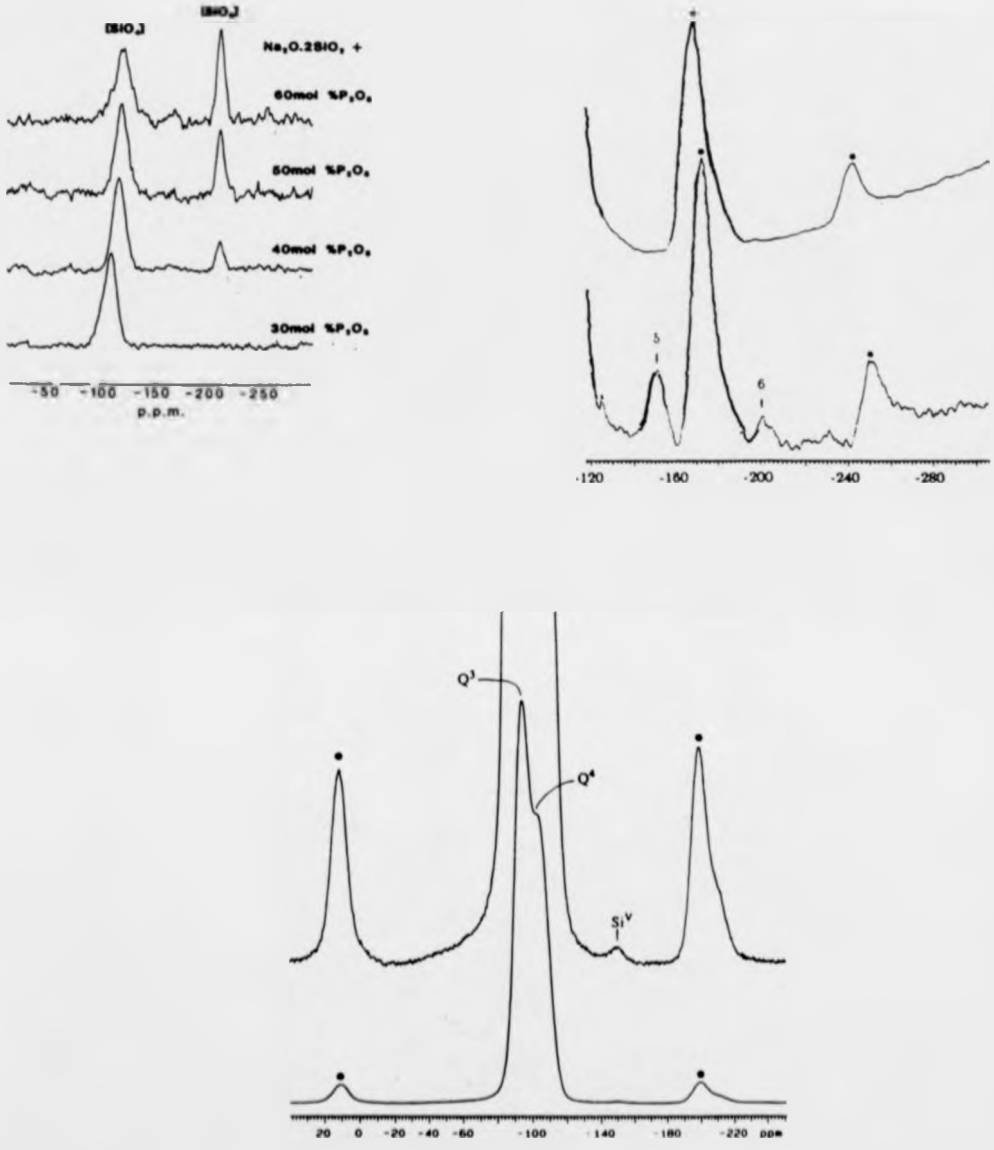

Figure 4.1. Published ^{29}Si MAS NMR spectra of higher silicon coordination in glasses. (a) Spectra from Dupree et al [45], sodium disilicate glasses containing 30,40,50 and 60 mol% P_2O_5. (b) Spectrum from Stebbins and M^{c}Millan [51], $K_2Si_4O_9$ glass quenched from 1 bar (upper) and 1.9GPa (lower). Spinning sidebands, denoted by dots, from tetrahedral resonance and feature at -125 ppm is a machine artifact (c) Spectrum from Stebbins [52], fast quenched ($2x10^4$ - $5x10^5$ Ks^{-1}) $K_2Si_4O_9$. Upper trace is x10 lower trace.

- 99 ppm and the ^{31}P became mainly metaphosphate from being predominantly ortho-phosphate. Dupree et al argue that this is due to incorporation of phosphorus into the silicate network also releasing alkali to reintroduce non-bridging oxygens once more. However these Q^3 species now have P as next nearest neighbours which, due to higher electronegativity of P, moves the Q^3 resonance to a more negative shift. This resonance then overlaps with that of the remaining Q^4 so resulting in the broad asymmetric ^{29}Si resonance. From 12 to 25 mol% P_2O_5 the ^{29}Si peak reverts back to -109 ppm, typical of Q^4 species observed in SiO_2, whereas the ^{31}P spectrum changes only slightly as the width of the peaks increases. This was believed to indicate that once more the additional phosphorus is removing alkali from the silicate network and into the metaphosphate $(PO_3)_n^{n-}$ regions where the greater widths of the peaks implies a larger range of n, ie chains of various lengths.

At a P_2O_5 concentration of 40 mol% new features were observed in both the ^{29}Si and ^{31}P spectra. The position of the Q^4 resonance has shifted to -117 ppm indicating that Si-O-P bonding is the norm rather than Si-O-Si but, more dramatically, a new resonance was observed at -213 ppm, close to the shift for six coordinated silicon in SiP_2O_7. Similarly the ^{31}P spectra contained an extra peak at -33 ppm consistent with the P environment in SiP_2O_7 also. The relative proportions of these "SiP_2O_7-like" resonances then continued to increase for increased P_2O_5 concentrations.

Dupree et al [49] also suggested that the presence of alkali ions was essential to the formation of $[SiO_6]$. Gradual reduction in the Na_2O content of a series of glasses initially containing the octahedral silicon species produced a rapid reduction in the percentage of $[SiO_6]$ observed for Na_2O concentrations below 6 mol%. Complete absence of soda produced no observed -213 ppm resonance in the ^{29}Si spectra.

The substitution of Al_2O_3 for P_2O_5 in the glasses containing six coordinated silicon leads to a decrease in the $[SiO_6]$ resonance until, at a nominal

composition of 16.7 Na_2O - 33.3 SiO_2 - 43.3 P_2O_5 - 6.7 Al_2O_3, it disappears completely. Thus it appears that aluminium will occupy any octahedrally coordinated sites in preference to silicon. The Q^4 resonance remained at -118 ppm, the position of silicon tetrahedrally bonded to 4 phosphorus atoms via oxygen, until the P_2O_5:Al_2O_3 ratio was 3:2 whereupon it became -113 ppm, more typical of silicon with 4 Si-O-Si bonds. The corresponding ^{27}Al MAS spectra showed a change from octahedral aluminium with phosphorus as next nearest neighbour, to tetrahedral aluminium with next nearest neighbour phosphorus as the amount of Al_2O_3 for P_2O_5 substitution increased. No evidence of aluminium either 4 or 6 coordinated via oxygen to silicon was detected, although apparently some [AlO_6] with aluminium in the next nearest shell was detected at intermediate stages of the substitution. It was concluded that the structure of the Na_2O-$2SiO_2$-$3P_2O_5$ glass converted from a "SiP_2O_7 + SiO_2 + sodium metaphosphate"-like structure to that of an "$AlPO_4$ + sodium disilicate"-like glass when half of the P_2O_5 is substituted by Al_2O_3.

The fictive temperature of the glass also contributed to the relative concentration of [SiO_6] species in the high phosphate (60 mol%) glasses. There was a steady increase in the amount of octahedral silicon as the fictive temperature was reduced by means of slow cooling. However in the case of glasses with a lower concentration of P_2O_5 but still containing [SiO_6] the trend seemed to be the reverse. No explanation was given for this.

Subsequently octahedral silicon has been observed by several other teams of workers. Sekiya et al [50] examined a number of SiO_2.P_2O_5 compositions with ^{29}Si MAS NMR. Their spectra for crystalline SiP_2O_7 showed 3 sharp peaks centred around -215 ppm, due to the three distinct crystallographic silicon sites present, and for crystalline $Si_5O(PO_4)_6$, the same separation of peaks around -215 ppm as well as a broader peak at -120 ppm. They propose that $Si_5(PO_4)_6$ has the same structure as $Ge_5(PO_4)_6$, i.e. both six and four coordinated silicon where the tetrahedral silicon, in a Si_2O_7 unit, connects the vertices of an SiO_6 octahedron and a

PO_4 tetrahedron. The two amorphous samples they studied were 83.7 SiO_2 . 16.3 P_2O_5 and 66.7 SiO_2 . 33.3 P_2O_5. They were prepared with fine silica powder and an excess of P_2O_5, in the form of H_3PO_4, in a sealed silica ampoule and melted at temperatures 1550-1800 °C for 1-2 hours. The first composition contained only a tetrahedral resonance but, in the higher P_2O_5 composition, a resonance at -215 ppm was detected. The amount of octahedral silicon is estimated from their published spectra to be approximately 10%, although with a peak to peak separation of around 90-95 ppm, sample spinning speeds of 3-3.5KHz and a spectral frequency of 39.66 MHz there is a possibility that the nominated octahedral resonance is a spinning sideband. There is no mention of additional experiments performed at different spinning speeds which would clarify the situation.

Stebbins and McMillan have reported both six and five coordinated silicon in a rapidly quenched, high pressure (1.9GPa) melt of $K_2Si_4O_9$ [51]. The main feature of these ^{29}Si MAS NMR spectra is an asymmetric, broad tetrahedral resonance, due to Q^3 and Q^4 species but there are some small but obvious features detectable at -150 and -200 ppm, figure 4.1(b). The use of highly enriched (95%) ^{29}Si silica made it possible to observe these peaks which have areas of 0.4 and 0.2% of the total. The widths of these peaks indicate that they are not due to strange crystalline phases and it can be assumed that the resonance at -200 ppm is from silicon in octahedral environment. However Stebbins states that a shift near -150 ppm, previously unobserved in silicates, is from five coordinated silicon by analogy with the progression of 4 to 5 to 6 coordinated aluminium which shows a systematic increase in chemical shielding. They postulate that the mechanism of formation of these higher silicon coordinations is through a pressure induced disproportionation reaction where Q^4 sites are destabilised with respect to 5 coordinated silicon units.

More recently Stebbins has provided evidence of five coordinated silicon [52] in the same composition although prepared at 1 atmosphere. Noticeably though, no evidence of any octahedral silicon was detected. Two samples of the

$K_2Si_4O_9$ glass were prepared with different cooling rates; with a controlled cooling of 1K/min from 1300 to 300 °C and also by an extremely rapid quench estimated to be approximately 20000 to 500000 K/sec. The rapidly quenched sample was subsequently annealed by reheating to 1050 °C and then cooled at 1K/min. In all cases the major spectral features were two overlapping peaks with shifts within the tetrahedrally coordinated silicon range, assigned to silicon sites with 3 and 4 bridging oxygen neighbours. Stebbins noted that the rapidly quenched sample had a slightly broader resonance, which he attributed to the greater structural disorder indicative of a higher fictive temperature. Also present in the ^{29}Si MAS NMR spectra were small peaks around -150 ppm, figure 4.1(c), previously assigned to five coordinated silicon [51]. The relative abundance of this environment was given as 0.06 ±0.02 % in the slow cooled example and 0.10 ±0.02 % in the raid quenched material. This subsequently reverted to 0.06 ±0.02 % after annealing, implying that the change in structure is a reversible one.

MAS NMR has also been employed in the investigation of longer range structure in silicate glasses, ie the actual connectivity between individual types of silicon sites [53]. This is achieved via a process initially used in the study of the resonating protons in non-crystallizable proteins in solution [54], ie two-dimensional shift correlated (COSY) NMR spectroscopy. The technique is not solely limited to protons though as 'shift correlated NMR spectroscopy may be used whenever sites with different chemical environments, and consequently different chemical shifts , interact with each other' [54]. This interaction may take either of two forms; via the chemical bonds themselves (so called scalar or 'J' coupling), or through physical space (simple dipolar coupling). However in the case of silicon, where only 4.7% of nuclei are magnetically active, a substantial amount of isotropic enrichment is necessary, in order to provide for any possible scalar coupling signal indicating the direct connectivity of two types of silicon site. Knight et al [53] prepared 3 glasses of nominal compositions $Na_2O.SiO_2$, $Na_2O.4SiO_2$ and $Na_2O.SiO_2.3P_2O_5$ and examined

them with COSY 2-D MAS NMR. They reported cross peaks in both the soda silicate compositions confirming that there is some direct interconnection between the different types of nearest neighbour silicon tetrahedra. However, although the 1-D ^{29}Si MAS spectra of the soda phosphosilicate glass contained an octahedral resonance, the COSY spectra showed no evidence of any cross peak between the octahedral and tetrahedral environments. Knight interprets this observation as implying that the two types of coordination are not substantially interconnected on a nearest neighbour level but concludes, both from their observations and the data presented by Dupree et al [45,49], that the structure of the glass is composed of silicate tetrahedra and octahedra cross-linked by phosphorus tetrahedra with the sodium ions neutralizing the excess charge on the PO_4^{3-} unit.

In this study, natural abundance ^{29}Si, ^{31}P and ^{27}Al MAS NMR has been applied to the study of a series of glasses based on $K_2O.4SiO_2$ with P_2O_5 addition, (the aluminium is present due to contamination from alumina crucibles used during glass preparation). The thermal properties of the glasses were investigated by both differential scanning calorimetry and differential thermal analysis, and some infra red absorption spectroscopy has also been performed. As an additional study two compositions; $K_2O.4SiO_2$ with 40 mol% P_2O_5 and SiP_2O_7 were prepared via a sol-gel route and their respective structures analysed by ^{29}Si, ^{31}P and ^{1}H MAS NMR as well as powder XRD.

4.2. CONVENTIONAL MELT GLASSES.

4.2.1. PREPARATION.

The nominal compositions of the samples prepared in this study are given in table 4.1 along with melting temperatures and the exact method of cooling.

The starting materials were Limoges quartz (SiO_2) and analytical grade K_2CO_3 and $NH_4H_2PO_4$, which decompose upon heating to evolve gases and the required composition constituents thus,

$$K_2CO_3 \text{ ----------> } K_2O + CO_2$$

$$2\ NH_4H_2PO_4 \text{ ----------> } P_2O_5 + 3\,H_2O + 2\,NH_3$$

In addition, 20mg of $MnCO_3$ was added to each 50g batch (0.1mol%) as a paramagnetic impurity. This was necessary as the ^{29}Si NMR relaxation times are typically tens of minutes to a few hours. Previous control experiments on undoped lithium and sodium phosphosilicate glasses showed that there was no observable effect upon the relative intensities of ^{29}Si signals recorded [45,48,49,55] at this level of concentration.

Each batch was weighed and then milled for 16 hours prior to melting so as to homogenize the mixture of powders. Melting took place in two stages; a pre-melt to release the gases evolved in the above reactions, and a final melting at a high temperature to produce a homogeneous melt capable of pouring. Due to the high concentration of P_2O_5 (known to attack Pt) present in some of the compositions, alumina crucibles were used in all batches for consistency, although this lead to a significant amount of Al_2O_3 contamination, contrary to Tallant and Nelson [56], in the final composition of all glasses containing P_2O_5. The pre-melt took place at 400 °C and the batch was added in 3 portions. Subsequently the temperature was increased to the melting temperature and held there for 1 ½ hours once the pre-melt was completed. Usually the melt was splat cooled between two graphite coated steel plates at room temperature, although for compositions with between 10 to 25 mol% P_2O_5, glass making is difficult because of high liquidus temperatures and low melt viscosities. Therefore in the compositions KSP2 and

SAMPLE	NOMINAL COMPOSITION (MOL%)			MELT TEMP. (°C)	METHOD OF COOLING
	K_2O	SiO_2	P_2O_5		
KSP0	20.0	80.0	-----	1500	SPLAT
KSP1	19.0	76.0	5.0	1550	SPLAT
KSP2	18.0	72.0	10.0	1550	CRUCIBLE
KSP3	17.0	68.0	15.0	1650	CRUCIBLE
KSP4	15.0	60.0	25.0	1700	SPLAT
KSP5	14.0	56.0	30.0	1570	SPLAT
KSP6	12.0	48.0	40.0	1300	SPLAT
KSP7	10.0	40.0	50.0	1390	SPLAT
KSP8	8.0	32.0	60.0	1300	SPLAT

Table 4.1. Nominal composition, melt temperature and method of cooling of the potassium tetra-silicate phosphate glasses.

SAMPLE	ANALYSED COMPOSITION (MOL%)			
	K_2O ¶	SiO_2	P_2O_5 ‡	Al_2O_3 ‡
KSP0	19.7	80.3 †	----	----
KSP1	18.8	76.1 •	4.8	0.3
KSP2	18.0	71.7 †	9.2	1.1
KSP3	16.2	68.5 †	13.9	1.4
KSP4	14.4	61.0 •	23.0	1.6
KSP5	13.3	56.8 †	28.7	1.2
KSP6	11.7	48.8 •	38.1	1.4
KSP7	9.6	42.2 †	46.8	1.4
KSP8	7.9	35.2 †	55.1	1.8

† Determined via wet chemical analysis. (± 2%)

• Determined via difference. (± 6%)

‡ Determined by quantitative NMR. (± 3%)

¶ Determined via Atomic Absorption Spectroscopy (± 1%)

Table 4.2. Actual final compositions of the potassium tetra-silicate phosphate glass as determined from a number of techniques.

KSP3 the glasses were formed by placing the crucible directly onto the steel plates. X-ray diffraction established that all the samples prepared were amorphous, and all were optically clear except KSP2. Glasses were kept under vacuum in desiccators to prevent any reaction with atmospheric moisture, which was readily observable for the compositions containing 40 mol% or more P_2O_5.

4.2.2. CHEMICAL ANALYSIS.

It is well established that the composition of a glass can vary during the melting process. Hence the only way to discuss the structure of a glass is via the knowledge of its final composition. This information can be obtained by a variety of methods, including gravimetric and spectroscopic means. For the glasses in this chapter several methods were used; the amount of SiO_2 was determined via wet chemical analysis as set out in the British standard B.S. 2469 [57] as well as by deduction; the K_2O content via K^+ atomic absorption spectroscopy; and finally the P_2O_5 and Al_2O_3 concentration via quantitative MAS NMR. It has been assumed that the amount of MnO is invariant, an assumption borne out by previous work on similar systems [55]. The results of the chemical analysis are shown in table 4.2.

4.2.3. NUCLEAR MAGNETIC RESONANCE.

4.2.3.1. ^{29}Si MAS NMR.

The ^{29}Si spectra were all acquired on the Bruker MSL 360 spectrometer operating under the conditions given in table 2.1 and the Bruker double bearing Z33.6 DR-MAS-7DB probe (section 2.3.2). Samples were powdered in an

KSP3 the glasses were formed by placing the crucible directly onto the steel plates. X-ray diffraction established that all the samples prepared were amorphous, and all were optically clear except KSP2. Glasses were kept under vacuum in desiccators to prevent any reaction with atmospheric moisture, which was readily observable for the compositions containing 40 mol% or more P_2O_5.

4.2.2. CHEMICAL ANALYSIS.

It is well established that the composition of a glass can vary during the melting process. Hence the only way to discuss the structure of a glass is via the knowledge of its final composition. This information can be obtained by a variety of methods, including gravimetric and spectroscopic means. For the glasses in this chapter several methods were used; the amount of SiO_2 was determined via wet chemical analysis as set out in the British standard B.S. 2469 [57] as well as by deduction; the K_2O content via K^+ atomic absorption spectroscopy; and finally the P_2O_5 and Al_2O_3 concentration via quantitative MAS NMR. It has been assumed that the amount of MnO is invariant, an assumption borne out by previous work on similar systems [55]. The results of the chemical analysis are shown in table 4.2.

4.2.3. NUCLEAR MAGNETIC RESONANCE.

4.2.3.1. ^{29}Si MAS NMR.

The ^{29}Si spectra were all acquired on the Bruker MSL 360 spectrometer operating under the conditions given in table 2.1 and the Bruker double bearing Z33.6 DR-MAS-7DB probe (section 2.3.2). Samples were powdered in an

agate pestle and mortar and carefully packed into 7mm diameter zirconia spinners (see figure 2.8). Typical spinning speeds were 3.3 to 3.6 KHz.

The ^{29}Si MAS NMR spectra of the potassium tetra¬silicate glasses, KSP0 to KSP8, are shown in figure 4.2., with table 4.3 containing the chemical shifts, full widths at half maximum and estimated relative intensities of the resonances.

It is easy to distinguish the two resonances present in the KSP0 spectrum, even though they overlap by a considerable amount, and the presence of the single pair of spinning sidebands implies that one of these resonating environments is not completely isotropic in its bonding. By varying the sample spinning speed it has been determined that the sidebands are associated with the resonance centred on -96.1ppm rather than the resonance at -103.5ppm. The shifts recorded in this study are within experimental error of those reported by Stebbins [51] and earlier non-enriched glasses [58,3].

Addition of 5 mol% P_2O_5 (KSP1), significantly alters the relative amount of the low field resonance in comparison to the spectrum of the KSP0 sample, confirmed by the reduction in the amplitudes of the spinning sidebands. Further additions of P_2O_5, 10 to 25 mol%, in the glasses KSP2 to KSP4, produced only one observable ^{29}Si resonance for each sample, although the chemical shift of that resonance steadily becomes more negative from -104.7 to -116.8 ppm. As stated in table 4.3, throughout this part of the series the full width half maxima of these resonances are also reasonably constant at approximately 15 ppm. However the ^{29}Si spectrum obtained from the KSP5 glass contains a second resonance, but at a significantly much more negative shift position of -211.1ppm. At the same time the previous resonance has now shifted to a less negative position in comparison to the trend set by the series KSP2 to KSP4 at -114.3ppm.

Further additions of P_2O_5, up to 60 mol%, continue to increase the relative intensity of this new resonance as well as making the shift of the other

SAMPLE	SPECTRAL PARAMETERS								
	^{29}Si			^{31}P			^{27}Al		
	SHIFT (±0.2 PPM)	FWHM (±0.2 PPM)	RELATIVE INTENSITY (±0.1)	SHIFT (±0.2 PPM)	FWHM (±0.2 PPM)	RELATIVE INTENSITY (±0.1)	PEAK POSITION (±0.5 PPM)	FWHM (±0.2 PPM)	RELATIVE INTENSITY (±0.1)
KSP0	-96.1 -103.5	15.8 13.4	0.50 0.50	-------	-------	-------	-------	-------	-------
KSP1	-97.4 -107.6	12.1 14.3	0.35 0.65	11.6 0.0	4.1 4.3	0.10 0.90	49.0	14.8	1.00
KSP2	-104.7	19.8	1.00	-9.0	17.2	1.00	47.9 15.4 -13.0	18.2 n.m. n.m.	0.88 0.07 0.05
KSP3	-109.0	16.6	1.00	-16.5	15.6	1.00	45.0 12.9 -13.5	17.8 15.2 n.m.	0.75 0.17 0.08
KSP4	-116.8	14.3	1.00	-22.8	15.4	1.00	44.0 17.0 -17.2	18.2 15.6 12.7	0.21 0.18 0.61
KSP5	-114.3 -211.0	13.6 9.9	0.87 0.13	-26.6	20.1	1.00	10.4 -17.5	n.m. 11.8	0.10 0.90
KSP6	-116.5 -211.2	14.4 8.7	0.76 0.24	0.7 -11.0 -34.9	2.7 3.0 18.9	0.02 0.03 0.95	7.1 -19.7	n.m. 12.1	0.12 0.88
KSP7	-118.4 -212.1	15.0 9.7	0.72 0.28	-6.4 -17.0 -44.2	n.m. n.m. 17.8	0.03 0.06 0.91	-17.0	14.3	1.00
KSP8	-118.4 -212.0	16.0 8.5	0.65 0.35	-1.5 -11.5 -40.1	n.m. n.m. 18.3	0.02 0.02 0.96	-19.4	16.4	1.00

Table 4.3. The deduced spectral parameters for glasses prepared in the K_2O - SiO_2 - P_2O_5 system.

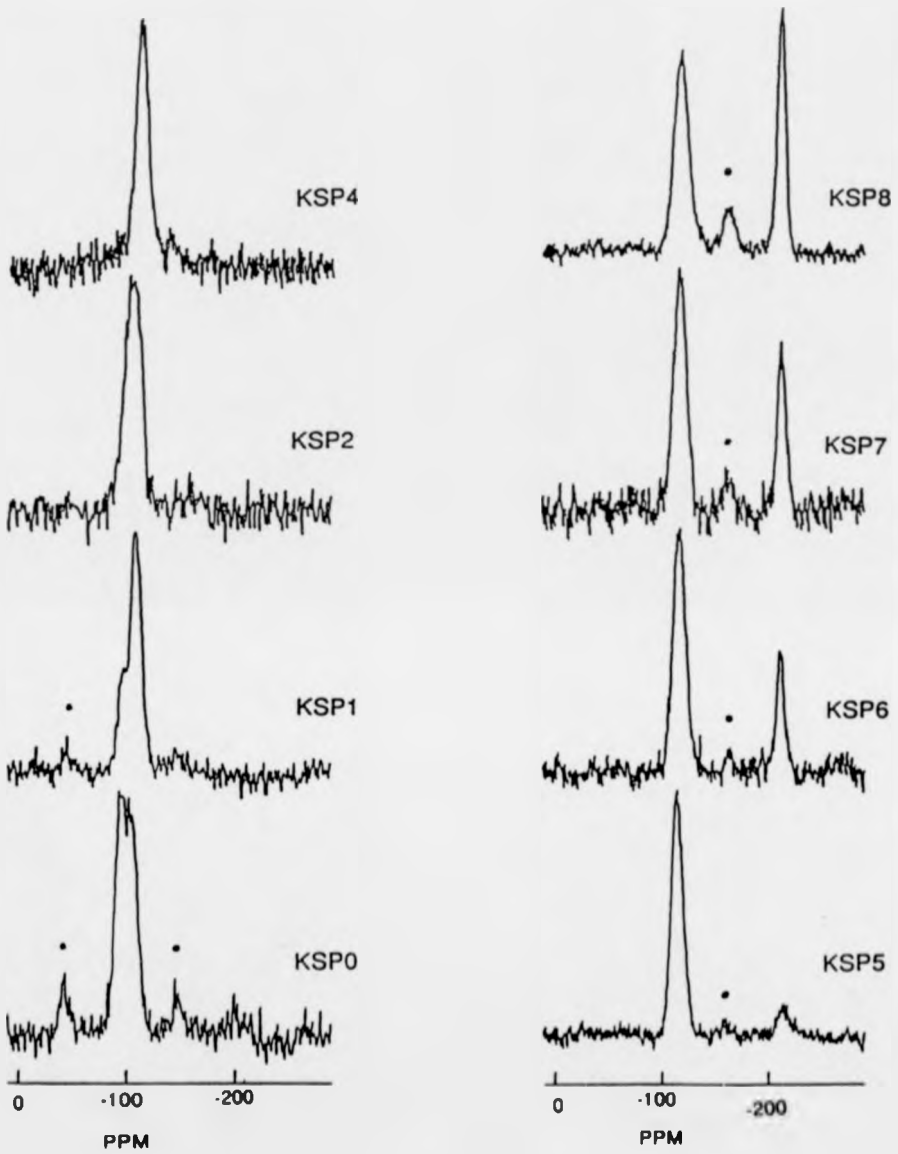

Figure 4.2. A selection of the ^{29}Si MAS NMR spectra recorded from glasses within this investigation. Typical number of sweeps accumulated for each spectrum is between 1000 and 1700. Exponential broadening of 50Hz was applied to each time domain signal prior to Fourier transform. Spinning sidebands, where present are denoted •

environment slightly more negative; -118.4ppm for the KSP9 glass.

These high P_2O_5 glasses also appear to have yet another resonance situated inbetween the two resonances, but in a series of spectra obtained at a number of sample spinning speeds it has been established that this 'middle resonance' is in fact a single spinning sideband associated with the -118ppm resonance. No evidence was found of a corresponding low field sideband to partner this sideband.

4.2.3.2. ^{31}P MAS NMR.

All ^{31}P MAS NMR spectra were recorded using 5mm diameter Si_3N_4 spinners fitted with vespel caps (figure 2.8). Spectrometer acquisition parameters and reference material data can be found in 2.3.2. Spinning speeds were varied in order to determine the isotropic chemical shift(s). The ^{31}P MAS NMR spectra recorded for this series of glasses are illustrated in figure 4.3..

The spectrum from KSP1 may look complicated but actually contains just two separate resonances with shifts of 11.6 and 0.0ppm which have 1 and 3 pairs of spinning sidebands respectively. The isotropic peak is established by varying the spinning speed as the separation of the sideband peaks is dependent upon the sample spinning speed.The situation becomes a little clearer in the spectrum obtained from KSP2 in which only 1 environment is present, plus sidebands, at -9.0 ppm. As the P_2O_5 content increases, the position of the isotropic ^{31}P peak becomes more negative, up to -44.2ppm for KSP7. Also observed in the spectra of all the high P_2O_5 glasses are two very narrow resonances either side of 0.0ppm. They are due to the absorption of atmospheric moisture by the powdered glasses which, when containing such large concentrations of P_2O_5, are very hygroscopic. Controlled deliberate exposure of powdered samples to the atmosphere increased the size of these resonances and so they are therefore ignored when considering the bulk structure of these glasses.

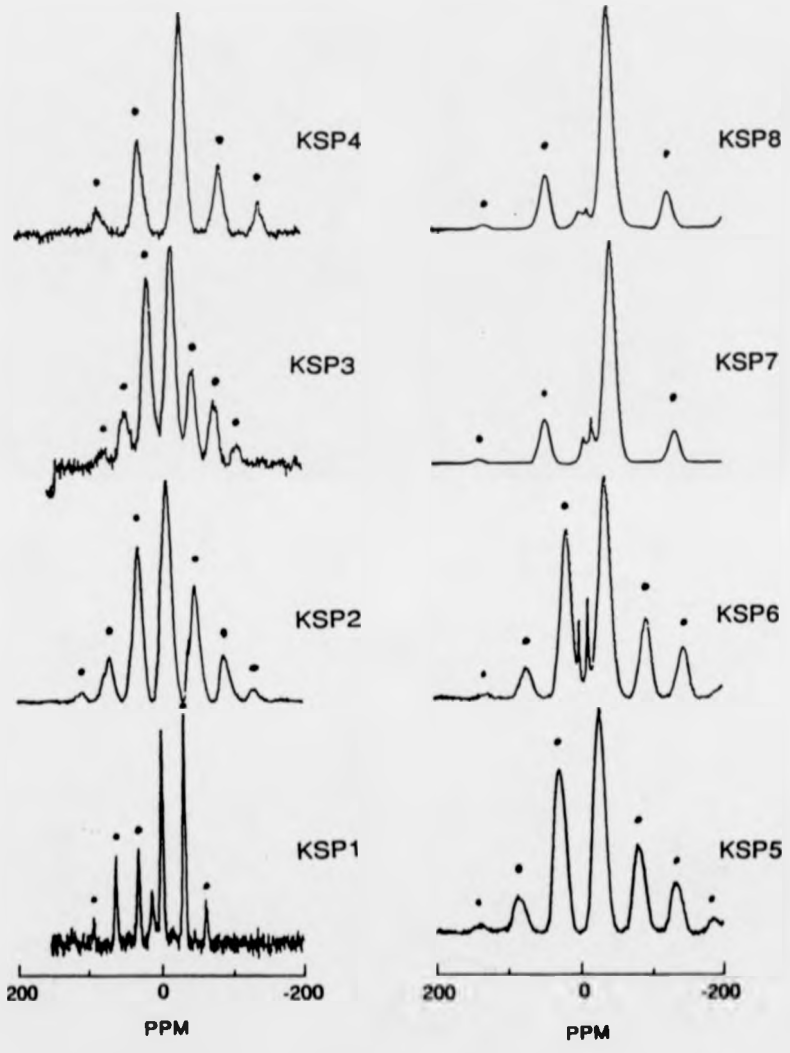

Figure 4.3. The ^{31}P MAS NMR spectra recorded from compositions containing P_2O_5. Typical spinning speeds of these spectra is >10kHz, with approximately 1600 sweeps in each accumulation. Exponential broadening of 50Hz was applied to the time domain signal prior to Fourier transform. Spinning sidebands are denoted ●.

4.2.3.3. ^{27}Al MAS NMR.

The ^{27}Al spectra of three samples, (KSP1,KSP2 and KSP3), were recorded on a Varian 600MHz spectrometer (14.1T) at Edinburgh in addition to the Bruker 360MHz (8.45T) spectrometer at Warwick. Full details of pulse times, delays etc. can be found in sections 2.3.2.

Figure 4.4 shows the 8.45T spectra and figure 4.5 two of the 14.1T spectra. The reason for examining these particular compositions at the higher field was that although there appeared to be 3 possible resonances contained within the 8.45T spectra it was not possible to be absolutely certain about either their presence or position. As ^{27}Al is a quadrupolar nucleus (I=3/2) any resonance is substantially broadened by the nuclear quadrupole interaction, which when present tends to dominate. However this interaction is dependent upon the field strength and therefore the effect of this broadening can be reduced by the application of higher magnetic fields.

There was no detectable ^{27}Al signal obtained from samples of the KSP0 composition, whereas the signal from KSP1 was only just visible above the background with a peak position of 49.0ppm. The 3 sites present in the spectra of KSP2 and KSP3 are most easily seen in the high field spectra, figure 4.5. The peak positions for KSP2 are 47.9,15.4 and -13.0ppm, and for KSP3 at 43.0,12.4 and -13.5ppm. The three resonances found in KSP4 are easily determinable from the lower field spectra, and it is noticeable that the -15.2ppm resonance now begins to dominate, such that in subsequent compositions there is no ^{27}Al peak at or near 40ppm.

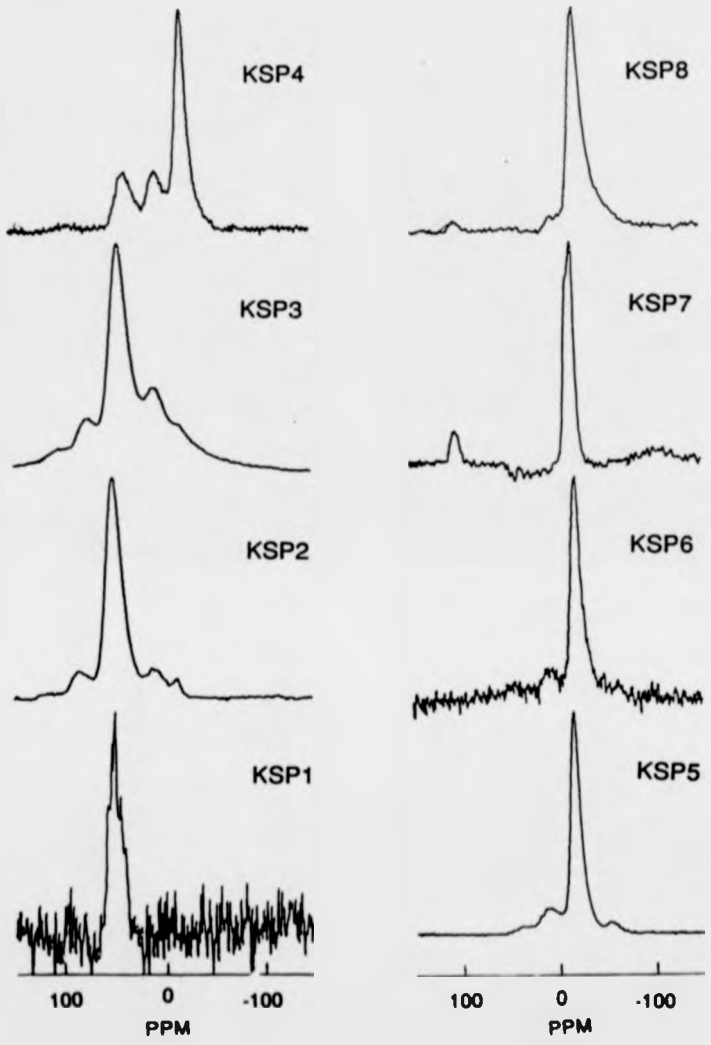

Figure 4.4. *^{27}Al MAS NMR spectra of compositions KSP1 to KSP8. Al_2O_3 was present as an impurity at levels between 1 - 2 mol%. Each spectra has 1600 accumulated sweeps and exponential broadening of 50Hz applied prior to Fourier transformation. Note that feature at -110 ppm is a machine artifact.*

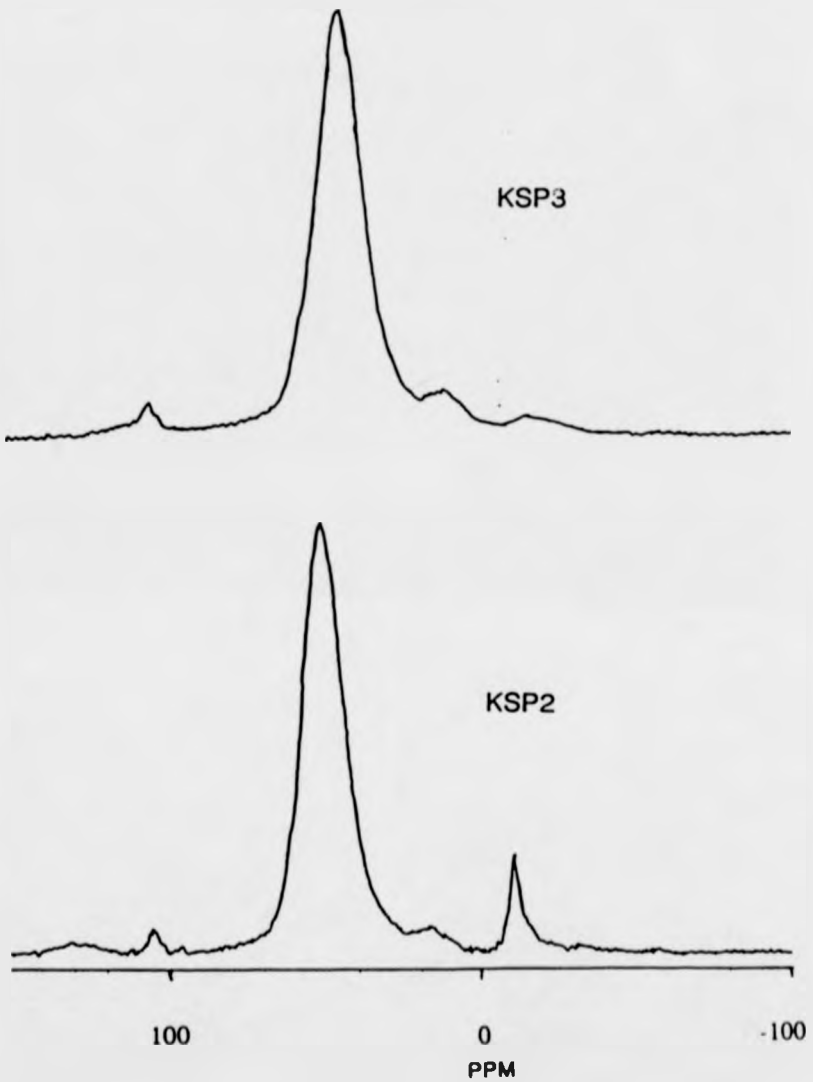

Figure 4.5. *^{27}Al MAS NMR spectra of KSP2 and KSP3 recorded at a field of 14.1T. Each spectrum is composed of 1984 sweeps with 100Hz of exponential broadening prior to Fourier transformation. Similarly to figure 4.4 the features at 105ppm are a machine artifact.*

4.2.3.4. DISCUSSION OF NMR RESULTS.

The two overlapping ^{29}Si resonances, with shifts of -96.1 and -103.5 ppm respectively, found in the base tetrasilicate glass (zero mol% P_2O_5) can be assigned unambiguously to Q^3 and Q^4 tetrahedral units respectively. The non-bridging oxygen in the Q^3 unit, obviously breaks the isotropic bonding environment, thus produces the spinning sidebands seen either side of the resonances. The relative concentrations of the two resonances were determined via computerised gaussian fitting and showed a 1:1 ratio. This is what was expected from the simple molecular calculation assuming a constrained binary distribution model for the alkali ions. The relatively poor signal to noise ratio of the spectra, compared to other isotopically enriched spectra which detailed small but measurable amounts of Q^2, made the determination of any less shielded environments impossible. The lack of any signal whatsoever in the ^{27}Al MAS NMR spectra from this composition indicates that it is the presence of P_2O_5 in the melt that leads to chemical attack of the crucible thus causing the Al_2O_3 contamination.

The concentration of the Q^3 site is reduced significantly in the silicon spectrum of KSP1, as is the intensity of the associated spinning sidebands. This suggests that the silicate network in the glass is repolymerising, ie formation of isotropically bonded Q^4 units at the expense of Q^3 type units with non-bridging oxygens. However, even with the addition of 5 mol% P_2O_5, the nominal ratio of alkali K^+ ions to network Si^{4+} ions remains 1:2. Therefore some of the alkali ions must have been removed from their network modifying role. This would be consistent with the earlier work on low P_2O_5 concentration glasses mentioned in the introduction [48] where alkali ions were 'scavenged' from the silicate network upon the addition of P_2O_5 to become closely associated with the phosphorus ions. Dupree at al [48] also observed the presence of two phosphorus environments in sodium and potassium disilicate glasses containing less than 5 mol% P_2O_5. This was attributed to

steric hindrance impeding the formation of completely isolated PO_4 tetrahedra. Examination of the ^{31}P MAS spectrum from KSP1, figure 4.3, does indeed show the two types of phosphorus units present in the glass; pyro-phosphate at 11.9 ppm and ortho-phosphate at 0.0 ppm. It is also apparent from figure 4.3 that these resonances are relatively narrow, due to fact that the pyro and ortho are isolated species and the range of bond angles and lengths is rather restricted. The shift values are close to those quoted for crystalline $K_4P_2O_7$ and K_3PO_4 [59] and suggest that not all the potassium ions have been removed from the silicate network. An estimation of the K^+:Si^{4+} ratio can be deduced from the relative intensities of the Q^3 and Q^4 resonances. Computerized gaussian fitting gave 1:5. The sample of KSP1 examined by ^{27}Al MAS NMR at both 14.1T and 8.45T contained just a single broad resonance centred on 49.0 ppm, indicating aluminium in a tetrahedral environment with silicon as the next nearest neighbour .

The ^{29}Si MAS NMR spectrum from KSP2 contains only a single resonance at -104.7 ppm, slightly less negative than in the KSP1 case. This is consistent with silicon coordinated via oxygen to other silicon atoms, ie the silicate network in this composition has completely repolymerised. There appears to be very little bonding of phosphorus into the silicate network, as the greater electronegativity of phosphorus would shift the ^{29}Si resonance position to the high field. Upon further additions of P_2O_5 though, compositions KSP3 and KSP4, the ^{29}Si chemical shift does become more negative; -109.0 and -116.8 ppm respectively because of the presence of first one and then more phosphorus atoms in the second coordination sphere providing greater shielding of the silicon nucleus. The corresponding ^{31}P MAS NMR spectra of these compositions also show that phosphorus is playing a larger part within the glass network. Rather than the spectra showing isolated phosphate groups such as pyro- or ortho-phosphate units they illustrate the polymerisation of the phosphorus in forming meta-phosphate chains, figure 4.3. As the concentration of P_2O_5 increases the ^{31}P isotropic peak position becomes more

negative, -9.0 to -28.2 ppm, consistent with an increase in the length in the metaphosphate chains [60]. Therefore with the ^{29}Si shift indicating phosphorus in the second coordination sphere, it appears that the metaphosphate chains are terminated by Si - O -P units.

Previous work on the occurrence of octahedral silicon in similar glass systems [49] has proposed that the appearance of octahedral aluminium is a precursor to the formation of six coordinated silicon environments. Hence particular attention was paid to the aluminium environment as the addition of P_2O_5 continued. The ^{27}Al MAS NMR spectra from KSP2 and KSP3 collected at a magnetic field strength of 8.45T (figure 4.4) , show not only a significantly stronger signal, due to the larger concentration of Al_2O_3 impurity, but additional resonances. However it was not possible from these spectra to ascertain accurately either their peak position or relative abundance. Therefore spectra from these two compositions were also obtained using the 600 MHz spectrometer in Edinburgh. These spectra are shown in figure 4.5. From these spectra it is possible to confirm that both compositions contain aluminium in 3 separate environments; tetrahedral aluminium centred around 45 to 50 ppm, octahedral aluminium centred around -12 to -19 ppm and another environment in the range 16 to 12 ppm. This latter range of shifts is difficult to assign as the occurrence of phosphorus in the second coordination sphere has a marked effect upon the peak position of an AlO_x unit; a shift from 65 to 38 ppm for $Al[OAl]_4$ to $Al[OP]_4$ and from +10 to -20 ppm for $Al[OAl]_6$ to $Al[OP]_6$ [12,61,62]. Hence the expected shift range for $Al[OP]_5$ is likely to be close to that for $Al[OAl]_6$ [61,62].

In the 14.1T ^{27}Al spectrum of KSP2 the predominant resonance has a peak position of 50.0 ppm which corresponds to aluminium four coordinated with silicon; $Al[OSi]_4$, whilst the -13.0 ppm peak can be assigned to octahedral aluminium with some phosphorus as next nearest neighbour, the remainder being either Si or Al. Statistically though any Al-O-Al bonding would be highly unlikely

for such low concentrations of Al_2O_3, but would be feasible provided there were a phase separated Al rich region in the glass. Now, as KSP2 was the sole partially opaque sample prepared, some degree of phase separation into Al-rich and Al-poor phases is a possibility, hence the possibility of a mixed P,Si and Al second coordination shell for octahedral aluminium is reasonable. The final ^{27}Al resonance, peak position 15.4 ppm, although it could arise from $Al[OP]_5$, is believed to be more likely due to $Al[OAl]_6$.

The small shifts to 45.1 ppm and -13.5 ppm for the tetrahedral and octahedral aluminium sites in KSP3 may indicate the replacement of some, but not all, of the silicon next nearest neighbours by phosphorus atoms. The peak at 12.9 ppm is believed to be due to $Al[OP]_5$ in this instance because of both the slightly more negative position in comparison to KSP2 and the lack of any visible phase separation.

Returning to the ^{27}Al MAS NMR spectra obtained at 8.45T, figure 4.4, the spectrum obtained from KSP4 most definitely contains the 5 coordinated aluminium resonance as well as both the 4 and 6 although the octahedral resonance is now the most dominant. The slight shift to more negative position is consistent with further substitution of phosphorus for silicon in the next nearest shell.

The first observation of any silicon resonance corresponding to silicon in an octahedral environment was in the ^{29}Si MAS NMR spectrum of KSP5, figure 4.2. The shift recorded was -211.0 ppm, which is substantially more negative than the quoted shifts for octahedral silicon in stishovite [46] at -194 ppm and for $K_2Si_4O_9$ (1.9 GPa) glass [51] at -200 ppm. However in materials where silicon is six coordinated via oxygen to phosphorus the reported shifts are much more similar; cubic SiP_2O_7 at -214 ppm [46], $Si_5O(PO_4)_6$ at -217 ppm [46,50] and in a sodium disilicate glass with 40 to 60 mol% P_2O_5 at -213 ppm [45,49,55]. Therefore it appears that the octahedral silicon units are largely isolated from the rest of the silicate network by Si-O-P bonding, which still exists as shown by the continued

presence of the (SiO_4) resonance. Interestingly the sudden appearance of this new environment coincides with changes in both the chemical shift and width of the [SiO_4] peak. The new position is -114.3 ppm and suggests that the average number of phosphorus atoms surrounding the [SiO_4] unit has decreased. The full width at half maximum also decreases from around 17 ppm to 13.6 ppm. The implication is that the general environment of the lower coordinated silicon has become less disordered, possibly because of the apparent reduction in the amount of Si-O-P bonding. The width of the octahedral resonance, 9.9 ppm, is also less than would be expected from a glass, although this was also observed in the sodium disilicate case [45,49,55], again indicating a more ordered structure than in the normal vitreous case, possibly because of an increase in the steric constraints of an octahedral coordination. Interestingly the composition has a Si:P ratio of 1, therefore further additions of P_2O_5 would make phosphorus the major network former.

The intensity of the [SiO_6] resonance increases with the addition of more P_2O_5, compositions KSP6 through KSP8, although the width of the resonance remains at around 9 ppm. Over the same compositions the position of the [SiO_4] resonance again becomes more negative which is indicative of the reappearance of more Si-O-P linkages, whilst the width shows a gradual increase to approximately 16 ppm signifying a return to a more disordered average arrangement. A new feature is also present in the shape of another possible resonance centred on -155 ppm. Initially it was thought that this may arise from five coordinated silicon as Stebbins reported that the position for this environment is -150 ppm. However a series of additional spectra accumulated from KSP7 at different sample spinning speeds from 1.8 to 4 KHz showed that the position of this 'resonance' is not invariant but it is actually a spinning sideband associated with the [SiO_4] peak. The fact that the [SiO_4] resonance now has an associated spinning sideband is characteristic of a non-isotropic bonding arrangement, and therefore, even though the more negative peak position of [SiO_4] implies more phosphorus in the second coordination sphere, the

spinning sideband confirms that not all the next nearest atoms are phosphorus. However no matching low field sideband was observed, which can be interpreted as suggesting that the symmetry of the [SiO_4] unit is probably axial. Indeed molar composition based calculations regarding the average number of phosphorus next nearest neighbouring atoms for tetrahedral silicon still give an Si^{iv}:P of 1:2.3, and as the shift is typical of Q^4 it is suggested that these silicon atoms constitute chains or rings of $Si(OSi)_2(OP)_2$, being essentially axial in symmetry.

From the ^{31}P MAS spectra of these high P_2O_5 compositions the continued shift to more negative positions for the isotropic metaphosphate peak illustrates a lengthening of these chain-like structures, whereas the ^{27}Al MAS spectra show the dominance of the [AlO_6] resonance, although there is the possibility that a small amount of 5 coordinated aluminium remains. The peak position of the [AlO_6] resonance, -19.3 ppm, suggests that the aluminium is now totally coordinated with phosphorus as the next nearest neighbour.

4.2.3.5. SUMMARY OF NMR RESULTS.

As far as it is possible to ascertain, the base $K_2O.4SiO_2$ glass is consistent with the binary model of non-bridging oxygen distribution. Additions of small amounts of P_2O_5, up to 10 mol%, have produced a repolymerization of the silicate network as K^+ modifying ions are removed by the P_2O_5 to form phosphorus environments similar to those of crystalline potassium phosphates , and subsequently metaphosphate chains. The appearance of Al_2O_3 as an impurity is due to chemical attack by P_2O_5 in the melt upon the crucible.

For KSP1 the aluminium is in tetrahedral coordination with silicon as the next nearest neighbour. KSP2 and KSP3 show multiple aluminium resonances. However KSP2 is strongly believed to be partially phase separated into Al-deficient and Al-rich regions; the resonances probably due to $Al[OSi]_4$, $Al[OAl]_6$

and $Al[OAl]_i[OSi]_j[OP]_k$ where (i+j+k=6). ^{27}Al MAS NMR spectra accumulated at 14.1T show KSP3 resonances which are attributed to tetrahedral aluminium coordinated by silicon, octahedral aluminium with a mixed silicon/phosphorus second coordination sphere and penta coordinated aluminium with 5 next nearest neighbour phosphorus atoms. The octahedral environment dominates thereafter for higher concentrations of P_2O_5.

Octahedral silicon was first observed in KSP5, with a ^{29}Si shift consistent with phosphorus as the next nearest neighbour atom. Increasing the P_2O_5 content was shown to increase the relative amount of octahedral silicon species. An additional feature in these ^{29}Si MAS NMR spectra was initially thought to suggest penta coordinated silicon, but was subsequently found to be a single spinning sideband associated with the tetrahedral silicon species.

4.2.4. INFRA RED ABSORPTION SPECTROSCOPY.

Spectra from all compositions were recorded over the wavenumber range of 4000 to 180 cm^{-1} as described in section 3.5. Figure 4.6 illustrates the resulting spectra for each composition over the wavenumber range of 1500 to 400 cm^{-1}.

According to Chakraborty and Condrate, who examined a series of $SiO_2.P_2O_5$ glasses with additions of Na_2O via both Raman and infra red absorption spectroscopies [26], the i-r spectrum of cubic SiP_2O_7 (which contains only octahedrally coordinated silicon atoms) has a fundamental mode at 650 cm^{-1}. In this system the compositions shown by ^{29}Si MAS NMR to contain a relatively large concentration of silicon in an octahedral environment have an absorption centred on 660 cm^{-1}, the intensity of which increases for the higher P_2O_5 glasses. Thus it is believed that this absorption arises from the $[SiO_6]$ units in the glass. The slight jump from Chakraborty and Condrate's calculated position [26] may be due to the

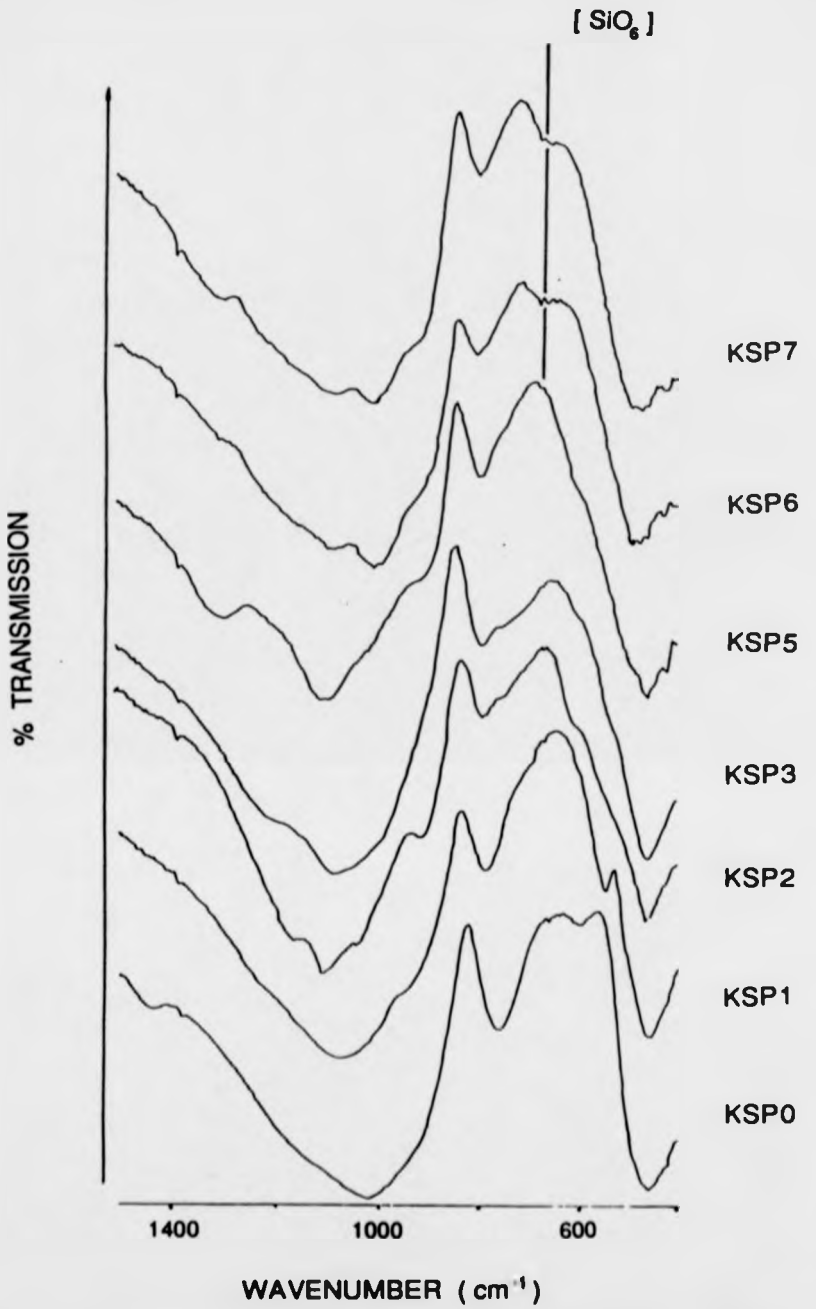

Figure 4.6. A selection of the Infra-Red absorption spectra recored. This also contains evidence of octahedrally coordinated silicon species in compositions with nominally 30 mol% or more P_2O_5.

distorted bond angles and lengths found in vitreous materials.

The lack of any definite absorption in this region of the spectrum for KSP5, which was shown by MAS NMR to contain around 10% of the silicon in the octahedral arrangement, serves to illustrate that the latter technique is far more sensitive when it comes to investigating the local structure of glasses.

Other absorption bands can also be assigned similarly [26,63]; absorption around 1330 cm^{-1} could arise from a P=O stretching vibration, absorption around 1100 cm^{-1} by P-O stretching in P-O-P and P-O-Si linkages, Si-O stretching vibrations have an absorption band centred on 1040 cm^{-1}, bending motions of Si-O-P, P-O-P and O-P-O are centred around 800 cm^{-1}, and absorptions between 500 and 400 cm^{-1} due to combinations of the bending modes of Si-O-P, P-O-P and O-P-O.

4.2.5. DIFFERENTIAL THERMAL ANALYSIS.

Differential thermal analysis, DTA, was performed on all samples as detailed in section 3.2.1. The determined glass transition temperatures, peak crystallisation temperatures and softening/liquidus points, where appropriate, are given in table 4.4.

SAMPLE	GLASS TRANSITION TEMPERATURE (°C)	PEAK CRYSTALLIZATION TEMPERATURE (°C)	LIQUIDUS / SOFTENING TEMPERATURE (°C)
KSP0	380 ± 20	--------	> 1250
KSP1	570 ± 10	--------	1210 ± 5
KSP2	690 ± 2	730 ± 2	> 1250
KSP3	770 ± 5	870 ± 4	> 1250
KSP4	830 ± 2	925 ± 5	1160 ± 5
KSP5	395 ± 5	--------	790 ± 2
KSP6	456 ± 4	903 ± 5	990 ± 5
KSP7	490 ± 5	700 ± 8	1100 ± 2
KSP8	506 ± 5	715 ± 4	960 ± 10

Table 4.4. Thermal parameters of the K_2O - SiO_2 - P_2O_5 compositions as determined via DTA.

The most striking feature concerning the thermal analysis of this series of glasses is the dramatic discontinuity in the T_g once the octahedral silicon environment appears, figure 4.7. Initially T_g rises in an almost linear fashion from 380 °C for KSP0 to 820 °C for KSP4. This is consistent with the assessment of the glass structures via the MAS NMR data, (section 4.2.3.4), where the addition of P_2O_5 allowed repolymerization of the silicate network by removing modifier ions to form phosphate species related to potassium phosphates.Therefore as non-bridging oxygens are also removed in this process the 'strength' of the network is increased, so increasing the transition temperature range. However, for compositions KSP5 to KSP9, T_g is within the range 450 to 510 °C. No evidence of the existence of two different T_g's were found which would indicate possible phase separation, although in these compositions we are dealing with glasses that have P_2O_5 as the major glass forming oxide. Therefore this 'anomaly' can be explained, since phosphate glasses are known to have relatively low T_g's [64]. However it would be of interest to investigate the possibility of other physical properties undergoing a similar discontinuity.

It was also interesting that no crystallisation was detected in either

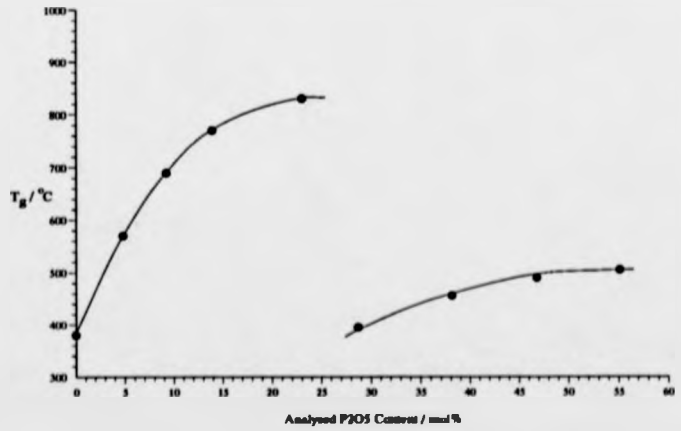

Figure 4.7. An illustration of the relationship between the glass transition temperature (T_g) and P_2O_5 content. Note that errors are insignificant on this scale.

of the KSP0 and KSP1 compositions despite varying the heating rate from 4C/min up to 14C/min. A crystalline form of the base composition is known to exist, Wadeite, with an octahedral silicon environment, therefore it would appear that in order to enable these glasses to crystallize successfully to this phase pressures higher than atmospheric are required.

4.2.6. DENSITY VARIATION AS A FUNCTION OF COMPOSITION.

The specific density of all the compositions was determined via Archimedes principle outlined in section 3.7. An average of ten separate readings was taken and the results tabulated in table 4.5 and shown graphically in figure 4.8.

SAMPLE	MEAN DENSITY (g / cm ^{3}) (± 0.005)
KSP0	2.369
KSP1	2.328
KSP2	2.308
KSP3	2.312
KSP4	2.322
KSP5	2.355
KSP6	2.417
KSP7	2.471
KSP8	2.489

Table 4.5. A table of the measured density of each composition investigated in this study.

The density measurements obtained from these glasses show an interesting trend, figure 4.8, which may be interpreted in terms of changes within the glass structure as the series progresses.

The measured density of KSP0 is 2.369 g/cm^3 and is as expected lower that the corresponding crystalline potassium tetrasilicate figure of 2.417 g/ cm^3[65]. Upon addition of P_2O_5 the change in glass structure, repolymerization of

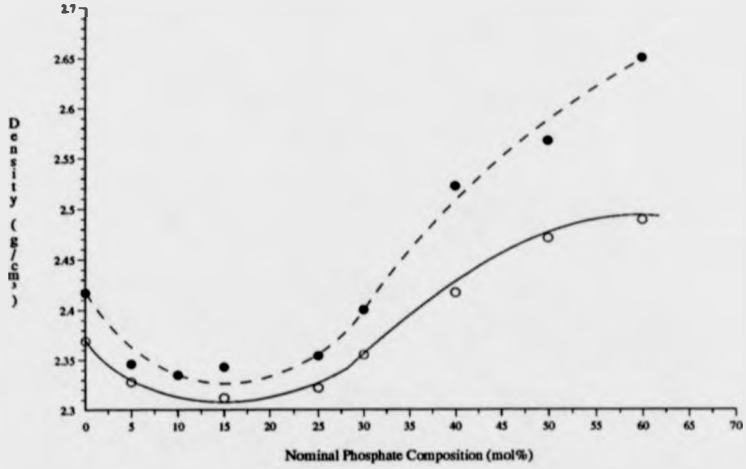

Figure 4.8. A graphical illustration of the dependence of the measured density (o) with P_2O_5 content. The estimated density of the "corresponding crystal" is also shown (o). Errors are negligible on this scale.

the silicate network as potassium ions are 'scavenged' by phosphate species, leads to a density decrease. The density of KSP3 is lower still, 2.312 g/cm^3, where the structural species of the glass are a fully bonded silicate network with some Si-O-P bonding and metaphosphate chains, as interpreted from the MAS NMR data. The density figures first show a significant rise for KSP5, the composition where six coordinated silicon species were observed for the first time. The density of the compositions then show a continual increase for further additions of P_2O_5 with there being some evidence of a possible tailing off to a plateau of approximately 2.5 g/ cm^3.

It is also possible to provide an estimate of the density of the "corresponding" crystalline material. Obviously no compositionally equivalent crystalline compounds exist apart from the base glass, KSP0, which has nominal composition $K_2Si_4O_9$. However it is possible to estimate a figure from the analysed glass compositions and the concentration of the various structural species determined from the MAS NMR data. The "corresponding crystal" density is obtained via the weighted averaging of the densities of cristobalite (2.32 g/cm^3) [65], KPO_3 (2.258

g/cm^3) [66], $K_4P_2O_7$ (2.33 g/cm^3) [65], K_3PO_4 (2.564 g/cm^3) [65] and SiP_2O_7 (3.22 g/cm^3) [67]. The weighting given to each 'phase' is determined from the ratios of resonating linewidths (including sidebands) and the silicon, phosphorus and potassium ions from the analysed compositions. For the sake of simplicity all tetrahedral silicon species were accorded the density of cristobalite, and all octahedral silicon the density of SiP_2O_7. These calculated "corresponding crystal" densities are shown in figure 4.8 along with the experimental data. Note that the structural role of the aluminium impurity is disregarded in these calculations because of its low concentration.

There is a good degree of correlation between the trend of the measured glass density and the pattern 'calculated' for the "corresponding crystal" densities, especially for compositions with less than 40 mol% P_2O_5. The two plots then appear to diverge for higher levels of P_2O_5, the measured data appearing to head towards a plateau whilst the estimated "corresponding crystal" data continues to rise.

Thus it can be seen that macroscopic properties of this type of phosphosilicate glass, such as density, are related to the concentration of intermediate structural species and do change discontinuously upon the introduction of 'novel' structural species; i.e. octahedrally coordinated silicon. Consequently it may be of interest to determine how the presence of octahedrally coordinated silicon affects other macroscopic properties. What would be the effect upon the refractive index and the other optical and infra-red transition characteristics? Would an Si^{vi} containing material make a good laser host for rare earth ions? What is the effect upon cation mobility, i.e. would the material be a good or poor ionic conductor? How will the dielectric response to high frequency A.C. fields vary? These are all physical properties that may, or may not be greatly effected not only by the presence of octahedral silicon species but also by their concentration.

4.2.7. CONCLUSION.

MAS NMR has found that silicon in an octahedral coordination is present in potassium tetrasilicate glasses containing 28 mol% or more P_2O_5, a lower concentration than that reported for the stabilisation of this species in the sodium disilicate - phosphate system [45,55]. Increasing the P_2O_5 content increases the proportion of silicon that is octahedrally coordinated as previously, however the thermal history of the glass, notably the fictive temperature, is also believed to be a determining factor.

Multinuclear MAS NMR has shown that the addition of small concentrations of P_2O_5 results in the removal of network modifying potassium ions allowing a degree of repolymerisation of the silicate network. This 'strengthening' has also been indirectly observed by an increase in the glass transition temperature measured by DTA. Additions of further amounts of P_2O_5 (>25 mol%) produced a phosphate network of metaphosphate chains of increasing length and Si - O - P bonding, eventually forming an octahedral silicon environment, similar to that found in SiP_2O_7, with phosphorus as the next nearest neighbour. The appearance of the octahedral silicon corresponds to a discontinuity in the glass transition temperatures. However this is attributed to the fact that P_2O_5 is now the major glass former and phosphate glasses have relatively low T_g's [64]. Infra-Red absorption spectroscopy also detected the presence of [SiO_6], although only for concentrations greater than 10%. ^{27}Al MAS NMR, aluminium was present at levels of 1-2 mol% as an impurity, has also indicated a progression of higher cordinations; from tetrahedral to mixed tetra-, penta- and octahedral species to solely octahedral with increasing concentrations of P_2O_5.

The density of the glasses has been found to be related to the intemediate range structural species; initially falling with the addition of P_2O_5 before increasing, and possibly tending towards a plateau value, in compositions shown by ^{29}Si MAS NMR to contain six coordinated silicon.

4.3. RELATIONSHIP BETWEEN FICTIVE TEMPERATURE AND STRUCTURE.

4.3.1. INTRODUCTION.

Fictive, or configurational, temperature defines a temperature at which the given glass would be in thermodynamic equilibrium. It has been shown [68] that T_f is related to the rate of cooling through the glass transition temperature range thus,

$$\frac{d \ln |q|}{d(1/T_f)} = \frac{-\Delta h^*}{R} \qquad [4.1]$$

where R is the molar gas constant, q the quench rate through the T_g range and Δh^* the activation energy of structural relaxation.

If the relative concentration of octahedral silicon species to tetrahedral is proportional to the rate of cooling then

$$\frac{d \ln [Si^{iv}/Si^{vi}]}{d(1/T_f)} = \frac{-\Delta h^*}{R} \qquad [4.2]$$

Now T_f can be determined by the method described by Moynihan et al [68] where the variation in specific heat capacity with respect to temperature is obtained via differential scanning calorimetry, DSC, and the Si^{iv} to Si^{vi} ratio estimated from the ^{29}Si MAS NMR spectral intensities. With R constant it is possible to deduce a figure for the energy required to convert 1 mol of Si^{iv} species to 1 mol of Si^{vi}.

The physical properties of a particular glass are known to be

dependent upon the quench rate [69] and as such this dependence must also be apparent in the glass structure. MAS NMR should be able to ascertain whether this structural difference is simply a variation in polyhedra free volume or due to differences in the type or relative amounts of polyhedra species present.

4.3.2. SAMPLE PREPARATION AND EXAMINATION.

Composition KSP7 was chosen for investigation as the normally quenched glass contained a significant amount of octahedral silicon. A larger 100g batch was prepared as before (section 4.2.1) except the melt was splat quenched at four different temperatures; between two graphite coated steel plates at 260 °C, similar pairs of plates heated to 110 °C and at room temperature (25 °C) and also between two copper plates cooled to an assumed -77°C by liquid nitrogen.

The glasses were kept under vacuum in a desiccator until required. Samples for NMR were prepared under dry N_2 and the spectra accumulated as before (4.2.3.1). The ratio Si^{vi} / Si^{iv} was estimated from the relevant peak intensities in the ^{29}Si spectra, figure 4.9. Examples of the ^{27}Al and ^{31}P MAS NMR spectra are illustrated in figures 4.10 and 4.11 respectively

Fictive temperatures were obtained graphically from the DSC traces. Approximately 0.1g of sample, along with an identical mass of Al_2O_3 as a reference, were heated in platinum crucibles through the transition range in a Netzsch High Temperature DSC 404, see section 3.2.2. Table 4.6 contains the

SPLAT TEMP. (°C)	FICTIVE TEMP. (°K)	SiO_6 / SiO_4 (± 10%)	ln (SiO_6 / SiO_4)
260	580 ± 10	0.36	-1.02
100	606 ± 10	0.34	-1.08
25	700 ± 20	0.43	-0.84
-77	760 ± 20	0.57	-0.56

Table 4.6. A table of the data deduced from DSC and ^{29}Si MAS NMR for KSP7 quenched at different temperatures.

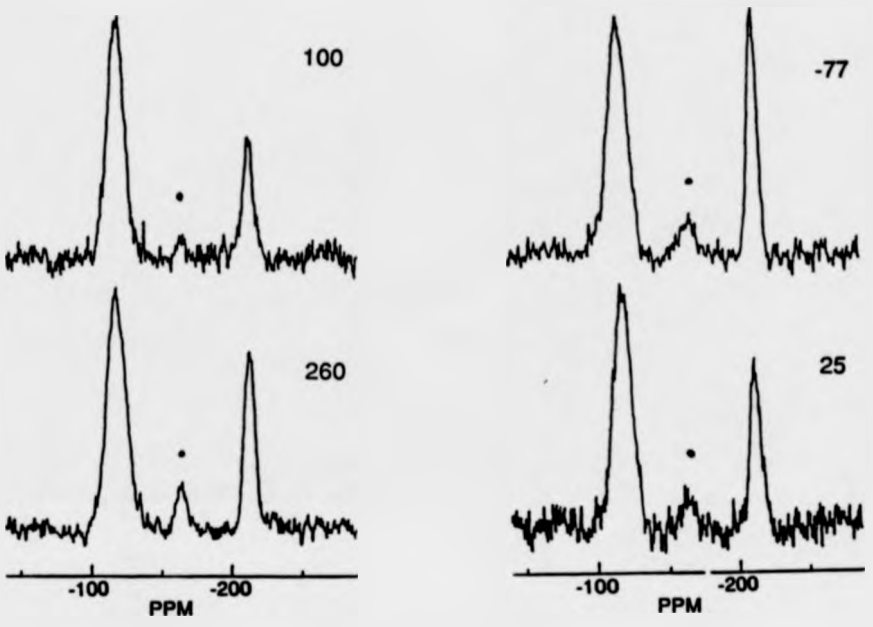

Figure 4.9. The ^{29}Si MAS NMR spectra recorded for KSP7 splat quenched at different temperatures. Each spectrum contains approximately 1600 sweeps with 50Hz of broadening.

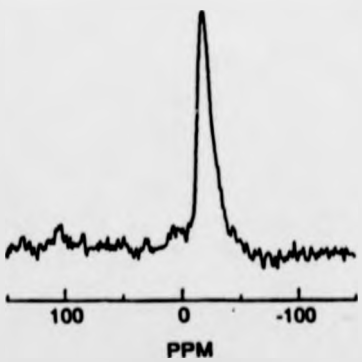

Figure 4.10. ^{27}Al MAS NMR spectrum from KSP7 quenched at 100°C.

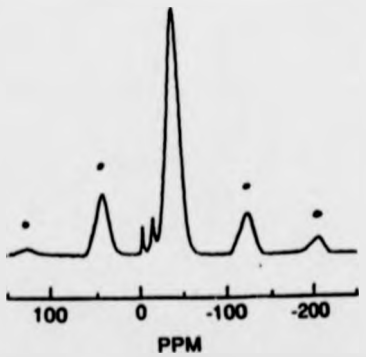

Figure 4.11. ^{31}P MAS NMR spectrum KSP7 quenched at -77°C.

extracted data.

The density of these compositions was also estimated via the Archimedean principle (section 3.2.6).

4.3.3. DISCUSSION.

The ^{29}Si MAS spectra of figure 4.9 clearly illustrate that varying the quench rate, and hence T_f, results in modification of the relative concentration of tetrahedral and octahedral silicon species. Variation in free volume could also be a factor although from this study it appears to be a minor one. The ^{27}Al and ^{31}P MAS spectra, figures 4.10 and 4.11, of all glasses were identical for each sample. The ^{27}Al spectra contained a single resonance typical of octahedral aluminium with phosphorus as the next nearest neighbour, consistent with the samples containing high levels of P_2O_5 studied previously in this chapter. The ^{31}P MAS NMR spectra were also consistent with the earlier samples where the major environment is of long metaphosphate chains and two small resonances due to moisture absorption from the atmosphere.

The data in table 4.6 is best displayed graphically, figure 4.12, where $-\ln [Si^{vi} / Si^{iv}]$ is plotted against $10^3 / T_f$. The gradient will then provide an estimate of the energy necessary to transform tetrahedral silicon species to octahedral species in this composition according to equation 4.2. From this data a figure of 9.98 $KJmol^{-1}$ is deduced. The positive value implies that this transformation is an exothermic reaction. This is significantly different from the figure obtained in the case of sodium disilicate with 60 mol% P_2O_5, -22.37 $KJmol^{-1}$ [55], although opposite trends have been seen in other compositions within similar glass systems [69]. Hence it appears that the fictive temperature - structure relationship is dependent upon a number of factors including composition, i.e. Si / P ratio, the viscosity - temperature relationship of the melt as well as the actual rate of

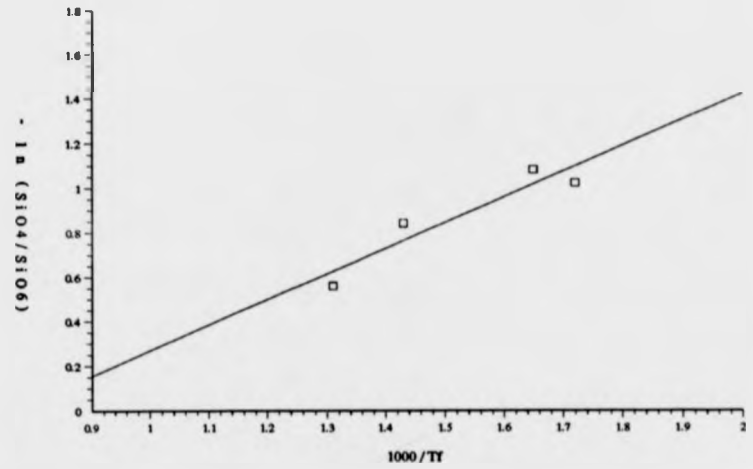

Figure 4.12. A graphical representation of the data in table 4.6 in order to determine an estimate for Δh° for the reaction $[SiO_4] \rightarrow [SiO_6]$. The straight line is plotted using a least squares linear regression.

cooling through the transition temperature range.

In order to ascertain if there is a relationship between the measured density and the structure within glasses containing differing concentrations of octahedral silicon the graph shown in figure 4.13 was plotted. As well as the 4 samples of KSP7 specially prepared for this section the density data of glasses within the main series found to contain Si^{vi} are also included.

As can be seen there is a definite increase in the measured density with an increase in the level of concentration of octahedral silicon. This is not necessarily unexpected as the density of stishovite is higher than that of any of the tetrahedrally coordinated silica polymorphs. However it is interesting that this increase in the measured density is not linear but the trend appears to suggest a tailing off to a maximum density of approximately 2.5 g/cm^3, in a similar manner to figure 4.8.

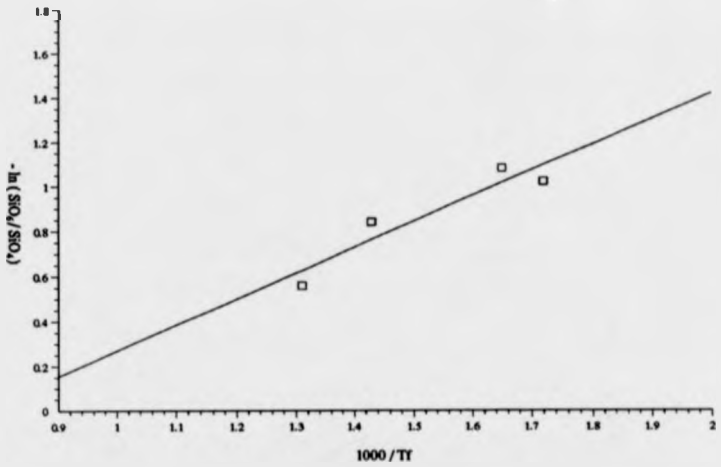

Figure 4.13. An illustration of the relationship between measured density and the relative proportions of octahedral and tetrahedral silicon species.

4.3.4. CONCLUSION.

This small examination of the variation in fictive temperature has shown that the level of concentration of octahedrally coordinated silicon is a function of T_f. The samples were prepared in such a manner as to provide glasses with identical composition with the only variable being the quench temperature, and hence the fictive temperature. These glasses were then found, via ^{29}Si MAS NMR, to contain varying concentrations of octahedral silicon species, the concentration increasing for glasses with higher fictive temperatures. An estimate of the activation energy required for the conversion of tetrahedral silicon to octahedral silicon was obtained, 9.98 $Kjmol^{-1}$, the positive value implying that the reaction is exothermic in nature.

In addition it has been established that the measured density of samples containing octahedrally coordinated silicon species is a function of the relative proportions of Si^{vi} and Si^{iv}, and thus fictive temperature, with the density appearing to tend towards a plateau value of approximately 2.5 gcm^{-3}.

4.4. SOL-GEL PREPARED GLASSES.

4.4.1. INTRODUCTION.

Sol-gel is a technique of glass production that has come to prominence in the last two decades, although the principles were laid down in the nineteenth century [70-73].

In general the sol-gel process consists of the controlled hydrolysation of metal alkoxide precursors followed by polymerization and condensation reactions resulting in the formation of metal oxides in the form of gels, monoliths, submicron powders and thin films. Roy [74] introduced the term "sol-gel" with the first demonstration of the process for the production of ceramics. The sol-gel method has a number of distinct advantages as a preparation technique; (1) resulting oxides are of extremely high purity, i.e. no fusion impurities, because of the high degree of purity available from the precursor organic alkoxides. (2) A high level of homogeneity is possible because of the intimate mixing within the sol. (3) Catalysis can be employed to control the rate of sol-gel transition enabling the production of either bulk monoliths, ultrafine, submicron powders or thin films. The extremely fine powders can consequently be sintered at a significantly reduced temperature in comparison to the temperature required for fusion of the component oxides/carbonates.

Zarzycki [75] described the gel to glass transition as the formation of a continuous glass network prepared by chemical polymerization, via subsequent elimination of unwanted organic or aqueous residues. In this study the sol to gel transition has been achieved via a hydrolysis and condensation reaction, i.e. initial hydrolysis of the precursor materials followed by polymerization of the monomers e.g. $Si(OH)_4$, into dimers and higher species. These then condense to form primary particles which increase in size before forming linkages or chains and ultimately a

3-d network.

The general consensus is that sol-gel is an ideal technique for the production of highly homogenous and pure glasses, particularly glasses that are notoriously difficult to fabricate via traditional melt/fusion techniques. MacKenzie examined sol-gel and fused oxide glasses of similar compositions and concluded that the structure, and hence physical properties of the glasses were similar [76]. This opened the way for sol-gel as a production route for glasses, although normally only for the more exotic or specialised compositions because the high cost of the organic precursors leads to relatively high production costs.

A more comprehensive review of the sol-gel process can be found in numerous review articles [77-80].

One particular application is that of phosphosilicate gel-produced glass as host materials for fast ionic conductors [81,82]. Other studies of phosphosilicate gels are reported by Perison and White [83], Szu et al [84], Prabakar et al [85], Douglass et al [86,87] and Tian et al [88].

This study has involved the production and analysis via MAS NMR and XRD of two phosphosilicate gel prepared compositions; SiP_2O_7 and K_2O - 4.SiO_2 with 40 mol% P_2O_5. Time did not permit a full evaluation of the hydrolysis or sol-gel transformation, hence this study is concerned solely with an investigation of the structure of these compositions after various heat treatments.

4.4.2. SAMPLE PREPARATION.

Two compositions were prepared; KSP7SG, identical to the nominal composition of KSP7 (12 K_2O - 48 SiO_2 - 40 P_2O_5), and SiP_2O_7. Flow diagrams, figure 4.14 and 4.15 illustrate the exact preparation routes taken for each sample. Temperatures for the various thermal treatments were obtained from

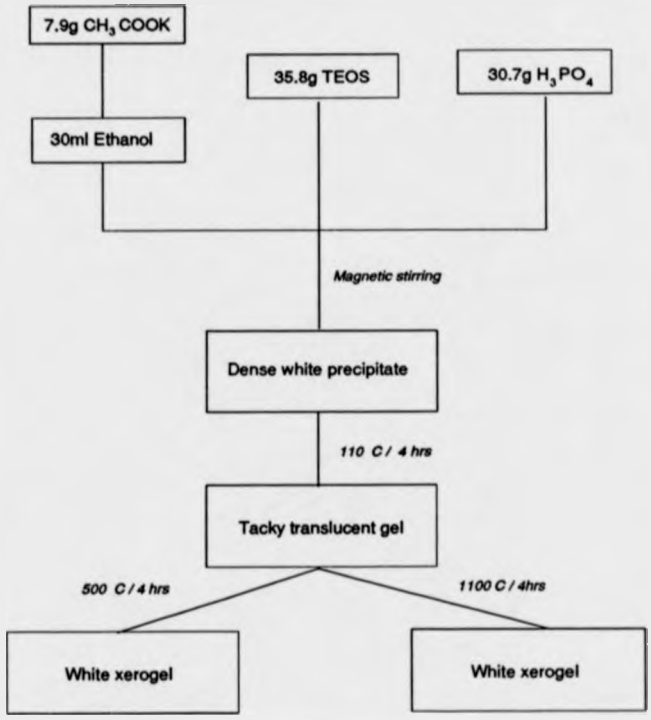

Figure 4.14. A flow diagram to illustrate the preparation route and subsequent heat treatments applied to KSP7SG.

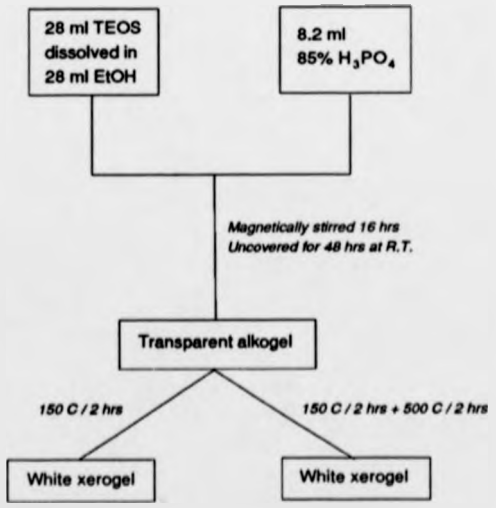

Figure 4.15. A flow diagram to illustrate the preparation route and subsequent heat treatments applicable to sol-gel derived SiP_2O_7.

differential thermal and thermal gravimetric analysis data. All reagents were of analytical grade. Each sample was examined via x-ray diffraction, the corresponding crystal phases are given in tables 4.7 and 4.8.

4.4.3. NUCLEAR MAGNETIC RESONANCE.

4.4.3.1. ^{29}Si MAS NMR.

No paramagnetic ions were added to either sample, therefore the ^{29}Si relaxation times could have been expected to be of the order of tens of minutes to hours. However it was found that the normal acquisition parameters (section 2.3.2.) were sufficient. Spectra recorded with delays between pulses of up to 20 minutes showed no variation in excess of the experimental error in the relative resonant intensities in comparison to a 1 minute delay. Figure 4.16 illustrates this with spectra of sol-gel prepared SiP_2O_7 heated to 500°C recorded using delays of 1 minute and 5 minutes between pulses.

The chemical shifts and widths of the resonances are detailed in tables 4.7 and 4.8 with examples of the ^{29}Si spectra shown in figure 4.16 and 4.17.

4.4.3.2. ^{31}P MAS NMR.

All the ^{31}P spectra were accumulated as per the melt glasses (4.2.3.2) using the standard spectrometer settings (2.3.2.). The chemical shifts and full width at half maximum are given in tables 4.7 and 4.8 with an example spectrum illustrated in figure 4.18.

SAMPLE	HEAT TREATMENT TEMPERATURE	SPECTRAL PARAMETERS						Crystal Phases
		^{1}H Chemical shift (ppm) (± 0.5 ppm)	FWHM (± 1.0 ppm)	^{29}Si Chemical shift (ppm) (± 0.5 ppm)	FWHM (± 1.0 ppm)	^{31}P Chemical shift (ppm) (± 0.5 ppm)	FWHM (± 1.0 ppm)	
KSP7-SG	110 °C	6.4 4.0 2.1 1.2	0.9 n.m. n.m. 0.6	-101.2 -110.9	12.2 10.1	-1.5 -5.4	3.6 3.4	$K_4P_2O_7$
KSP7-SG	+ 500 °C	8.9	0.2	-110 * -213.7 -215.0 -216.6	20.8 2.7 1.5 1.9	-5.0 -16.7 -31.3 -51.0 -53.4 -55.1 -56.8 -58.5 -60.9	1.4 2.5 10.5 2.4 n.m. 0.8 1.9 1.7 1.4	[M] $Si_5P_6O_{25}$ [m] SiP_2O_7
KSP7-SG	+ 1100 °C	8.4	0.5	-209.8 -213.6 -215.5 -218.0 -220.6	2.4 1.8 1.6 1.4 1.8	-31.7 -47.9 -49.6 -53.3 -54.2 -55.2 -59.2 -72.9	19.7 1.5 1.7 3.5 2.0 1.7	[m] $Si_5P_6O_{25}$ [M] SiP_2O_7

* Estimate of shift ± 5 ppm

Table 4.7. Spectral parameters obtained from the MAS NMR investigation of KSP7SG. Where XRD identified more than one crystal phase, the phases are classed as major [M] or minor [m] phases.

SAMPLE	HEAT TREATMENT TEMPERATURE	SPECTRAL PARAMETERS						Crystal Phases
		^{1}H Chemical shift (ppm) (± 0.5 ppm)	FWHM (± 1.0 ppm)	^{29}Si Chemical shift (ppm) (± 0.5 ppm)	FWHM (± 1.0 ppm)	^{31}P Chemical shift (ppm) (± 0.5 ppm)	FWHM (± 1.0 ppm)	
SiP_2O_7	150 °C	8.6 3.9 1.4	0.3 0.2 0.2	-91.4 -102.2 -111.1	8.2 6.2 11.5	0.2	7.3	AMORPHOUS
SiP_2O_7	+ 500 °C	8.4	0.2	-110.4 -118.5 (-211.6) -213.7 (-215.8)	13.6 5.8 3.0 4.7 2.8 } 11.1	-0.6 -44.3	3.2 2.1	$Si_5(PO_4)_4$

Table 4.8. Spectral parameters obtained from the MAS NMR investigation of sol-gel derived SiP_2O_7. Note that the ^{29}Si spectrum of the heated (500°C) xerogel was very noisy and contained an octahedral resonance that exhibited shoulders either side of the central peak. These shoulders may be due to noise or to similar but crystallographically distinct silicon environments. The data in the table reports the actual shifts of these shoulders.

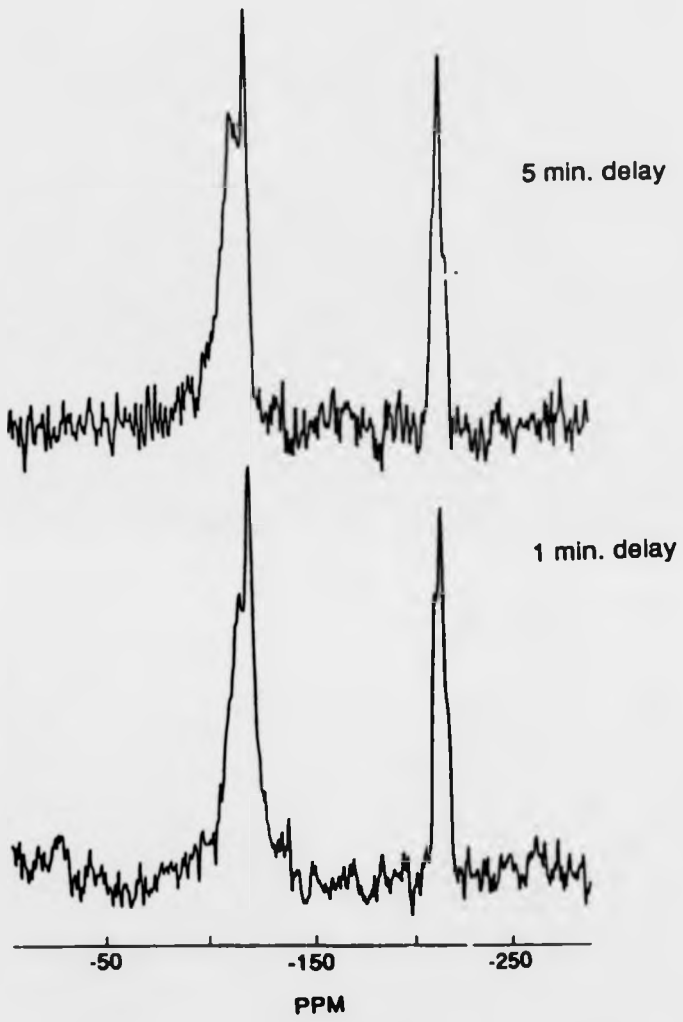

Figure 4.16. Comparison of two ^{29}Si MAS NMR spectra from SiP_2O_7 xerogel recorded with delays of 1 and 5 minutes between pulses. Although the number of sweeps in each accumulation was slightly different, the data processing of each F.I.D. was identical. The $[SiO_6]/Q^4$ ratios are 0.40 and 0.42 respectively.

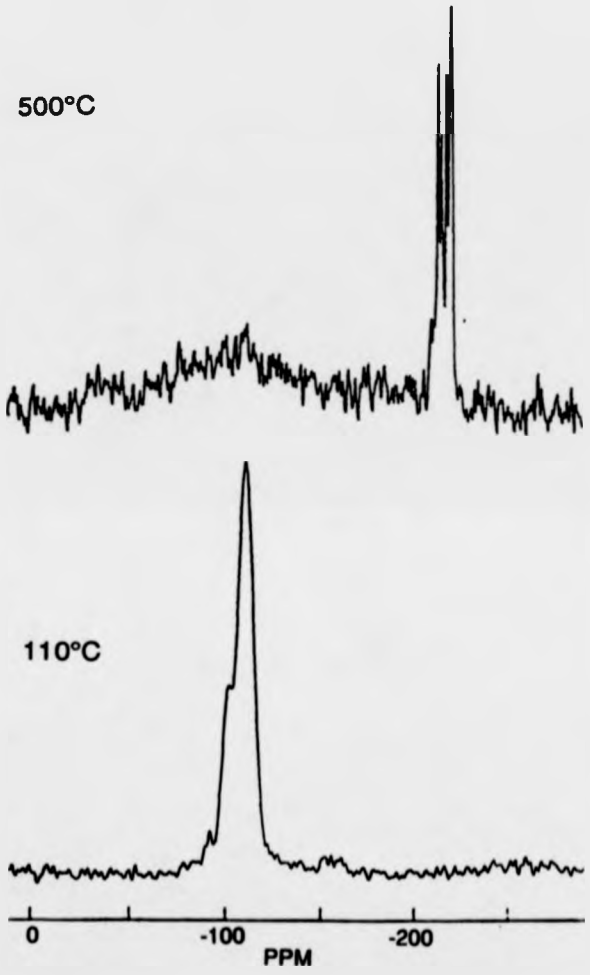

Figure 4.17. *^{29}Si MAS NMR spectra obtained from KSP7SG xerogel after drying at 110°C and subsequent heating to 500°C. Note the lack of octahedral silicon species in the dried sample compared to the virtual non-existance of tetrahedrally coordinated silicon after heating at 500°C.*

4.4.3.3. ^{1}H MAS NMR.

The presence of protons in the form of hydrocarbons, hydroxide, molecular water or otherwise can be established via proton NMR. High resolution proton NMR is, in principle, a very useful technique for the study of protons in inorganic solids. However protons can suffer appreciable broadening due to the strong homonuclear dipolar coupling between each other. There are a number of methods to overcome this problem including multiple pulse line narrowing in addition to magic angle spinning [89] or via isotopic dilution of the protons with deuterium [90]. More recently it has been established that simply spinning at the magic angle at rates in excess of 8kHz can also result in high resolution ^{1}H MAS NMR spectra [91]. This was the technique applied in this study. The spectrometer frequency, pulse length and delay are given in table 2.1. The high speed Doty probe was used with the Si_3N_4 spinners fitted with Vespel caps (section 2.3.2.). Spinning speeds were varied up to approximately 10kHz in order to establish the chemical shifts of the isotropic lines. A selection of the spectra obtained are given in figure 4.19 and the corresponding spectral data is in tables 4.7 and 4.8.

4.4.4. DISCUSSION.

As is readily apparent from the data of tables 4.7 and 4.8 along with figures 4.16 - 19 it does not appear possible to prepare truly amorphous samples, free from organic/water residue, of these two compositions via this route. Even samples that were only dried (i.e. majority of solvent mass removed at temperatures between 110 and 150 °C) contained crystalline phases detected by MAS NMR if not by XRD as well.

Considering KSPSG first, the ^{29}Si MAS NMR spectra of the dried

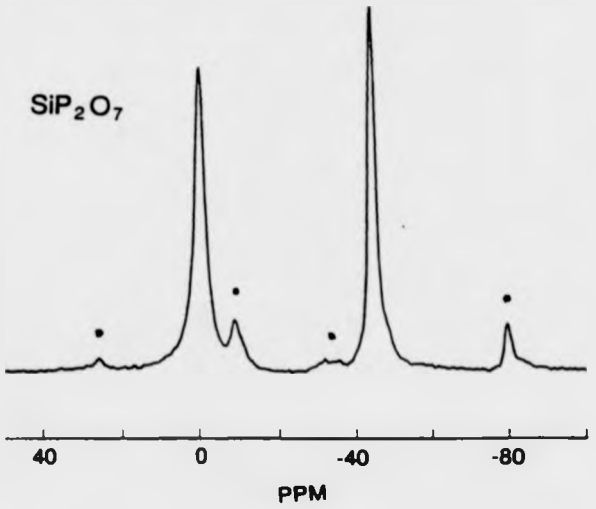

Figure 4.18. The ^{31}P MAS NMR spectrum from SiP_2O_7 xerogel heated at 500°C. The two dominant resonances are the isotropic peaks, the remainder are spinning sidebands, 1 pair with each isotropic line.

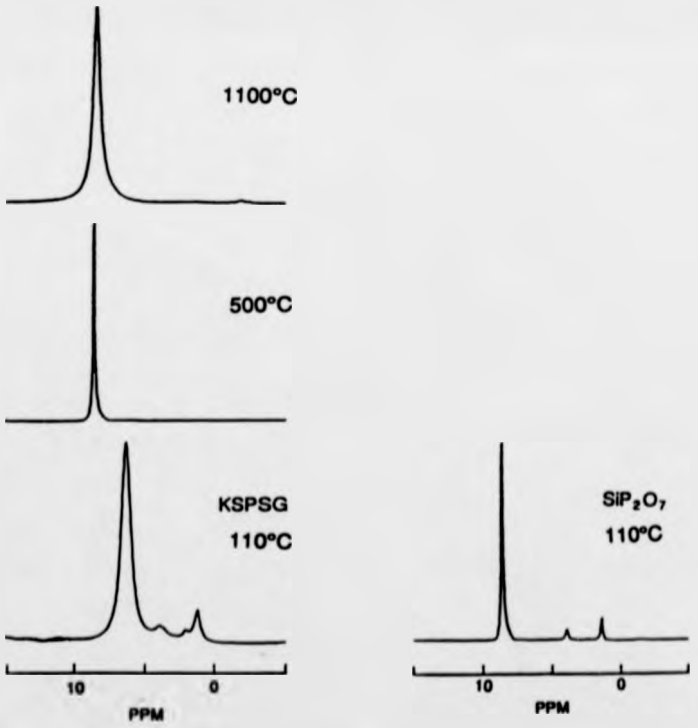

Figure 4.19. A selection of the ^1H MAS NMR spectra recorded. Each spectra consists of 800 accumulated sweeps with the resulting time domain signal processed with no additional broadening.

sample (110°C / 4 hours) contains two resonances. With regard to previous silica sol-gel studies [92-95] it is possible to assign the resonances to Q^4 (-110 ppm) and Q^3-OH (-101 ppm) where one of the four bonds is not with another Si but a hydroxide unit, i.e. $Si(OSi)_3(OH)$. The typical shift of a Q^3 species with associated K^+ cations is in the range -94 to -89 ppm [96], therefore the assignment of the -101 ppm resonance to Q^3-OH is reasonable. However is it possible to detect such species via ^1H MAS NMR ? The corresponding ^1H spectrum contained four resolvable peaks, 6.4, 4.0, 2.1 and 1.2 ppm. Yesinowski and Eckert [91] studied the ^1H isotropic chemical shift in a variety of calcium phosphates and attributed proton shifts around 6 ppm to surface absorbed moisture and shifts between 0.2 and 2.0 ppm to numerous forms of OH species. Freude et al [97] report that ^1H shifts in the range 1.5 to 2.5 ppm arise from OH groups of small acidity, such as SiOH, and proton shifts of 6 to 10 ppm are from hydroxyl groups of higher acidity, e.g. POH. Employing this information the ^1H shifts observed in KSP7-SG heated to 110°C are tentatively assigned as follows. The 6.4 ppm resonance is probably due to some residual water trapped within the xerogel because if the water were absorbed by the sample as a whole it would be expected to be visible in the ^{31}P spectrum in the form of narrow resonances centred around 0 ppm in a similar manner to the melt prepared glasses of 4.2. The remaining three resonances from 4.0 to 1.2 ppm are attributed to hydroxyl ions with varying degrees of acidity dependent upon their immediate environment, less acidic SiOH or more acidic POH. Hence the ^1H MAS NMR spectrum appears to support the assignment of Q^3-OH to the -101 ppm resonance in the ^{29}Si MAS NMR spectrum. The corresponding ^{31}P spectrum contained two resonances, both of which were reasonably broad, > 3ppm, although in terms of amorphous linewidths they are narrow. The shifts themselves are consistent with $K_4P_2O_7$ as reported by Prabhakar, Rao and Rao [85]. This is in accord with the XRD result which indicated $K_4P_2O_7$ as the sole crystal phase detected. Therefore it appears at this stage as though the silicate and phosphate are distinctly separate. The silicate network is well

polymerised with Q^4 and Q^3-OH species, whereas the phosphate network is well ordered and has the majority, if not all, the K^+ ions present in forming a crystalline phase of $K_4P_2O_7$.

Subsequent heating at 500°C produces marked changes in all the resonating nuclei spectra. The ^1H spectrum now contains a single narrow resonance at 8.9 ppm, which is assigned to OH in an acidic species, probably HPO_4 which was reported to have a shift of 8.7 ppm [91]. Consistent with no Q^3-OH species, as suggested by the proton spectrum, the ^{29}Si MAS NMR spectrum also indicates little or no Q^3-OH resonance. Only a broad hump of width greater than 20 ppm and centred on -110 ppm is seen for silicon in a tetrahedral environment. The majority of the silicon is now incorporated in octahedrally coordinated species, with shifts typical of Si^{vi} with phosphorus as the next nearest neighbour, and widths indicative of crystalline ordering. The ^{31}P MAS NMR spectrum is now far more complicated than previously with 9 separate resonances detected. The resonance at -5.0 ppm is the most difficult to assign. It is close to the resonance seen in the dried (110°C) sample but lacks the corresponding doublet at around -2 ppm. Grimmer and Haubenreisser [98] report that chain terminating PO_4 groups in various potassium phosphates have shifts within the range 0 to -5 ppm. Hence this resonance has been attributed to the terminating phosphate species of a metaphosphate chain, probably with potassium cations in the immediate locale. Grimmer and Haubenreisser [98] also state that the shift range for middle groups is between -18 and -22 ppm for potassium phosphates, so the resonance at -16.7 ppm is probably due to interior PO_4 groups of short metaphosphate chains. The third resonance is the broadest, 10.5 ppm FWHM indicating that this environment is probably non-crystalline, and has a shift more typical of long chain metaphosphates, -31.3 ppm. These assignments are consistent with the assignment of the -5 ppm resonance to terminating phosphate chain species. The final six ^{31}P resonances form a sextuplet of lines between -50 and -60 ppm, all of which are sufficiently narrow as to indicate a crystalline

environment. The XRD pattern of this sample contained numerous reflections that were fully indexed to a combination of $Si_5O(PO_4)_6$ as the major phase and cubic SiP_2O_7. Identical crystal phases were observed by Weeding et al [25] upon devitrification of a $SiO_2P_2O_5$ glass. They define the structure of $Si_5O(PO_4)_6$ as composed of isolated octahedral SiO_6 and tetrahedral Si_2O_7 species interconnected by PO_4 species, i.e. $Si(OSi^{iv})(OP)_3$ and $Si(OP)_6$ respectively. SiP_2O_7 has all the silicon octahedrally coordinated. Therefore it would appear that the broad -110 ppm tetrahedral silicon resonance contains contributions from the Si^{iv} in $Si_5O(PO_4)_6$ in addition to some residual amorphous silicate network. The octahedral silicon resonances and the sextuplet of ^{31}P resonances are due to the octahedral silicon species and their connecting phosphate species within the two crystal phases.

The NMR spectral parameters of the sample heated to 1100°C after drying at 110°C is similar to that of the sample heated to 500°C, however the XRD powder pattern indicates that SiP_2O_7 is now the dominant crystal phase and $Si_5O(PO_4)_6$ the minor. The ^{29}Si MAS NMR spectrum now contains very little if any silicon in a tetrahedral coordination, although there is a suggestion of a broad resonance at a shift around -110 ppm which is barely distinguishable above the background noise of the spectrum, figure 4.17. The presence of $Si_5O(PO_4)_6$, as established by XRD, does require some tetrahedral species, but as it is now the minor phase substantial amounts are unlikely. The presence of at least five octahedral silicon lines is indicative that there are at least as many crystallographically distinct environments, which may suggest that there is more than one silicon phosphate polymorph, with six coordinated silicon, present that is undetected by standard powder XRD. Similarly in the ^{31}P MAS NMR spectrum there are now seven distinct resonances in the shift range associated with phosphorus in silicon phosphate materials. Interestingly there is no evidence of any terminating phosphate species, which implies that the metaphosphate species, proclaimed by the broad ^{31}P shift of -31.7 ppm, are in the form of rings as opposed to linear chains. The

^{1}H MAS NMR spectrum is also comparatively unchanged, although there is a definite increase in the width of the resonance. This suggests a distribution in the degree of acidity of the OH groups contributing to this resonance signal [97].

There is a possible problem regarding the mechanism of formation of the two silicon phosphate polymorphs from a material that after drying at 110°C contained no Si-O-P bonding according to the MAS NMR data. However the particle size of the various components of the initial xerogel, $Si(OSi)_4$, $Si(OSi)_3(OH)$, $P(OP)(O....K)_2(OH)$, and the nature of the sol-gel transition would imply that the level of intermixing of these various species was extremely high. Consequently upon subsequent heating to temperatures in excess of 500°C numerous condensation reactions could have occurred which would produce the bonding arrangements observed by both XRD and MAS NMR. For example the condensation of two phosphoric acid species;

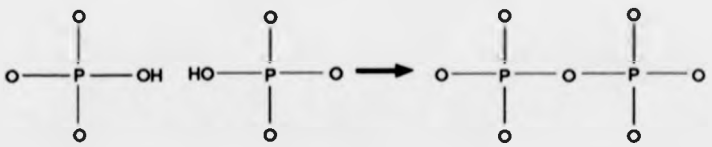

a process which could continue to form the metaphosphate chains and rings. Similarly a comparable condensation reaction could occur between SiOH and POH species to form Si-O-P bonds, where if the silicon species were in close proximity to numerous POH groups then octahedrally coordinated silicon units could be produced. This mechanism is only a hypothetical model as detailed real time NMR experiments, and alternative techniques such as Raman and Infra-Red spectroscopies, would be necessary if the exact route of formation were to be established.

The second sol-gel prepared composition, SiP_2O_7, has been prepared and examined by Szu et al [84] employing the same techniques of MAS

NMR and XRD. They examined the effect of different phosphate precursors on the structure after various heat treatments. They report that the $SiO_2.P_2O_5$ composition was x-ray amorphous and contained no Si-O-P linkages after drying at 60°C. Subsequent heating produced the crystal phase $Si_5O(PO_4)_6$. Interestingly their analysed composition indicated significant loss of phosphorus; nominal SiP_2O_7 was found to be 0.62 SiO_2 - 0.38 P_2O_5 (±2%). Similarly the SiP_2O_7 xerogel prepared for this study was shown by XRD to be amorphous after drying at 150°C. The corresponding ^{29}Si NMR spectra contains three resolvable resonances centred on -91, -102 and -111 ppm assigned to tetrahedral species with 2, 3 and 4 bridging oxygens respectively, the non-bridging oxygens terminating with protons, i.e. Q^2-$(OH)_2$, Q^3-OH and Q^4. The ^{31}P spectrum contains a single resonance at around the shift of the reference shift, and as such is believed to originate from a species similar to that of the phosphoric acid precursor, H_3PO_4. The ^1H MAS NMR spectrum exhibits three resonances, all of which are quite narrow. The 8.6 ppm shift is consistent with hydroxyl bonded to a highly acidic species and is the predominant proton environment in this sample. Hence this resonance is attributed to protons in a hydroxide group bonded to phosphorus, an assignment that tallies with the assignment of the ^{31}P resonance. The two remaining ^1H resonances, 3.9 and 1.4 ppm, can be assigned to OH species bonded to the two silicon species Q^2 and Q^3. Szu et al observed an identical situation with their H_3PO_4 prepared gel, although they did not report any ^1H MAS NMR results [84].

Heating to 500°C produced a crystalline phase detectable by XRD in addition to some residual amorphous phase. The crystalline phase was indexed to $Si_3(PO_4)_4$. This is in contrast to Szu et al [84] who found that their gel partially crystallised to $Si_5O(PO_4)_6$. Unfortunately it is not known whether the $Si_3(PO_4)_4$ phase has silicon in an octahedral or tetrahedral environment. Liebau [99] does not list it amongst his table of compounds containing octahedrally coordinated silicon, nor does Eittel [100]. Indeed the original reference for the powder diffraction pattern

makes no mention of the crystallographic space group [101], nor is $Si_3(PO_4)_4$ listed in the Daresbury crystal structure database [102]. Perison and White [83] also investigated the structure of $SiO_2.P_2O_5$ gels which were heated to form glasses and crystals via XRD, Raman and Infra-Red spectroscopies and found that there to be seemingly contradictory results. Their Raman data was assigned to $Si_3(PO_4)_4$, their XRD patterns suggested a mixture of $Si_3(PO_4)_4$ and SiP_2O_7 and the Infra-Red data was more consistent with polymorphs of SiP_2O_7. Their conclusions were that the Raman spectrum was more sensitive to the major crystalline phase whereas the Infra-Red data is independent of degree of crystallinity, and therefore is slightly more reliable in this case and did indicate "rich changes in structure in the heated silicophosphate gels" [85].

The ^{29}Si NMR spectrum now contained three clearly resolved resonances; -110, -118 and -213 ppm, figure 4.16, with the possibility of shoulders on the octahedral resonance at -211.6 and -215.8 ppm, arising from crystallographically distinct silicon environments or from noise. The relative intensities of the total tetrahedral and octahedral resonance envelopes does not varying significantly with increasing delays between pulses, figure 4.16. The shift of -110 ppm is assigned to a Q^4 species with next nearest neighbours of silicon which due to the width of the resonance is from an amorphous phase. The -118 ppm shift is again Q^4 although with a second coordination sphere containing 2 or more phosphorus atoms. This resonance is appreciably narrower than the -110 ppm resonance and so is believed to originate from a crystalline phase. The third resonance is from silicon in an octahedral environment. Although the total linewidth is similar to that encountered in the Si^{vi} resonances of the amorphous potassium tetrasilicates with > 40 mol% P_2O_5, if there are three convoluted octahedral resonances present then it may be that these resonances are sufficiently narrow as to indicate a crystalline phase. The ^{31}P spectrum contains two resonances; at -0.6 and -44.3 ppm. The resonance at -44 ppm is undoubtedly from those phosphorus atoms

associated with the crystalline silicon phosphate phase detected by XRD as the position is consistent with the ^{31}P shifts reported for these types of material [47]. The -0.6 ppm resonance is likely to be from a compound similar to that of the phosphorus precursor, H_3PO_4, an assignment that would fit well with the ^{1}H resonance at 8.4 ppm suggesting a highly acidic hydroxide species.

It is the lack of a definite knowledge of the silicon coordination state in $Si_3(PO_4)_4$ that hampers the full assignment of the relevant ^{29}Si and ^{31}P NMR resonances and hence an interpretation of the structure. However it is possible to discuss the main alternatives. The first is that the silicon coordination in $Si_3(PO_4)_4$ is totally tetrahedral. Thus the narrow ^{29}Si resonance at -118 ppm arises from this phase with the residual glass phase containing the remaining tetrahedrally coordinated silicon, shift -110 ppm, along with the octahedral species which are in close proximity to the phosphate units of the crystal phase. Alternatively the octahedral silicon resonance may indeed contain 3 separate crystalline resonances which originate from one or more crystal phases that are of insufficient concentration to be detectable by powder XRD. The second possible interpretation is that the crystalline phase $Si_3(PO_4)_4$ actually contains silicon in both tetrahedral and octahedral coordiations in a similar manner to $Si_5O(PO_4)_6$ and wadeite. Thus the tetrahedral resonance at -118 ppm and one or more of the possible octahedral resonances may originate from this phase, which leaves the residual amorphous phase consisting of the tetrahedral silicon with silicon as the next nearest neighbour atom along with some, or no, octahedral silicon species.

With regard to the mechanism of formation of these silicophosphate materials, which. in a similar vein to the potassium phosphosilicate case, evidently contained no Si-O-P bonding after the initial drying, it is believed that the process of condensation/water removal is the most plausible explanation.

Previous attempts to prepare and investigate the structure of SiP_2O_7 via sol-gel [83,84] have been inconsistent, Szu et al [84] report an initially

amorphous xerogel that partially crystallises to $Si_5O(PO_4)_6$ whereas Perison and White [83] report $Si_3(PO_4)_4$ as the main crystalline end product. This study, whilst consistent with the findings of Szu et al [84] at the xerogel stage; x-ray amorphous, no Si-O-P linkages, Q^2-$(OH)_2$, Q^3-(OH), Q^4 and phosphate tetrahedra monomers as the structural species, actually partially crystallised to $Si_3(PO_4)_4$, the phase observed by Perison and White [83]. The most likely reason for this lies in the actual final composition of the heated gel, which is unknown in this case. Szu et al established a significant loss of P_2O_5, 38% from a nominal 50%, after heating, and therefore it is believed that SiP_2O_7-SG is also non-stoichiometric, although how far from a 1:1 ratio of SiO_2:P_2O_5 is uncertain, but contains a concentration more preferential to the crystallisation of $Si_3(PO_4)_4$.

4.4.5. CONCLUSION.

From the information obtained via multinuclear MAS NMR and XRD it does not appear possible to produce perfectly amorphous potassium phosphosilicate or silicophosphate materials free from water or organic residue via this particular sol-gel preparation route. Indeed, it is proposed that the presence of hydroxide species is believed to form an integral part of the condensation reactions that produce the Si-O-P linkages not evident in the dried (110/150°C) xerogels.

From the XRD pattern obtained from the dried KSP7-SG sample and the fact that no amorphous silicate phase with associated non-bridging oxygens can be clearly detected by ^{29}Si MAS NMR in either of the samples heated to 500°C or 1100°C, it appears as though the potassium ions are preferentially associated with the phosphate network, initially in the form of crystalline $K_4P_2O_7$ and subsequently with the residual amorphous phosphate network. Heating to 500°C produced a significant change in structure. Octahedrally coordinated silicon was detected via ^{29}Si MAS NMR and by XRD which indicated the presence of two crystal phases,

$Si_5O(PO_4)_6$ and SiP_2O_7. The remaining protons are in the form of OH which are associated with phosphate units. When heated to 1100°C the tetrahedral silicon environment was practically unobservable via NMR although the continued presence of the $Si_5O(PO_4)_6$, all be it as the minor phase, does contain this arrangement. SiP_2O_7 is now the predominant crystalline phase, although the number of distinct Si^{vi} sites within this phase is uncertain, Tillman et al [67] suggest only a single site, whereas ^{29}Si MAS NMR, which can be more sensitive to site differences than techniques such as XRD, appears to imply up to three distinct environments. ^{31}P MAS NMR also indicates a variety of slightly different phosphate environments with seven resolvable resonances in the range of -50 to -70 ppm along with a broad metaphosphate environment assigned to an amorphous potassium metaphosphate phase.

The sol-gel prepared SiP_2O_7 initially is consistent with the findings of Szu et al [84] where the xerogel is amorphous and contains no interbonding between silicate and phosphate species. However heating to 500°C produced $Si_3(PO_4)_4$ as the main crystalline end product in contrast to $Si_5O(PO_4)_6$. $Si_3(PO_4)_4$ is a phase of unknown structure and may or may not contain octahedrally coordinated silicon. However ^{29}Si MAS NMR has definitely shown the presence of this environment, although it is not definite as to whether this octahedral resonance is a single broad resonance or a combination of three or more narrower lines. If it contains only a single line then it is likely that the octahedral silicon is in a non-crystalline structure, whereas three narrower lines would imply slightly different crystal sites.

4.5. OVERALL CONCLUSION.

Glasses prepared by the fusion of component oxides and carbonates

have been investigated by multinuclear MAS NMR, IRAS and thermal analysis. It has been established that as increasing amounts of P_2O_5 is added to a base glass composition $K_2O.4SiO_2$ the modifier ions are removed from the silicate network to become associated with, initially monomer and dimer phosphate species, and eventually long chain metaphosphates. The onset of Si - O - P bonding has been observed which eventually produces an amorphous "SiP_2O_7-like" structural environment where the silicon is octahedrally coordinated by phosphorus via oxygen for P_2O_5 concentrations above 28 mol%. Increasing the P_2O_5 content increases the proportion of [SiO_6], however it is not the sole contributing factor.

The concentration of octahedral silicon has also been found to be a function of thermal history, or more specifically, the fictive temperature, with the relative proportion of [SiO_6] increasing for increasing T_f. An estimation of the energy required to convert 1 mol of [SiO_4] to [SiO_6] was obtained, 9.98 kJ, the positive value implying that this reaction is exothermic.

The density of the glasses was also found to be dependent upon the amount of P_2O_5, initially decreasing before increasing upon the appearance of octahedrally coordinated silicon. It has also been established that there is a relationship between the density and the relative proportions of tetrahedral and octahedral silicon, which suggests a rising trend towards 2.5 g/cm^{-3} as the proportion of [SiO_6] increases.

A combination of multinuclear MAS NMR and x-ray diffraction was employed in the investigation of a potassium phosphosilicate and silicon phosphate xerogel materials. Apparently it is not possible, via the preparation route taken in this study, to prepare completely amorphous samples free from water or organic residues. Therefore a direct comparison between sol-gel and melt quenched materials is not feasible.

The dried xerogel of KSP7SG contained $K_4P_2O_7$ as a crystal phase with no indication of any Si - O - P bonding from either ^{29}Si or ^{31}P MAS NMR, thus

the potassium ions were preferentially associated with the phosphorus whilst OH species were bonded to the non-bridging oxygens of the Q^3 silicon tetrahedra. Heating the xerogel to 500°C and 1100°C produced crystalline phases of $Si_5O(PO_4)_6$ and SiP_2O_7 both containing silicon in an octahedrally bonded environment which, according to ^{29}Si NMR, was the major silicon coordination. Some residual amorphous phase remained, believed to be a potassium metaphosphate glass.

Similarly the SiP_2O_7 dried xerogel exhibited no evidence of any Si - O - P bonding with the silicate network even more depolymerised with Q^2-$(OH)_2$, Q^3-OH and Q^4 species. Heating this xerogel produced $Si_3(PO_4)_4$ as a crystal phase along with a silica amorphous phase. The coordination state of silicon within $Si_3(PO_4)_4$ has not been reported, however the ^{29}Si MAS NMR spectrum exhibits both tetrahedral and octahedral silicon resonances typical of crystalline environment.

Thus this chapter has established that multinuclear MAS NMR is a technique that can be applied to the study of intermediate structure of phosphosilicate glasses, and the resulting deductions regarding the species present can be applied to the interpretation of the variation in macroscopic properties such as density. It has also established that the formation, and consequently the relative proportion, of octahedrally coordinated silicon is a function of both P_2O_5 content and fictive temperature. Application of the technique to sol-gel derived phosphosilicate materials permits the elucidation of their intermediate range structure and has been found to correlate well with the information obtained from x-ray diffraction.

4.6. REFERENCES.

[1] E. Lippmaa, M. Mägi, A. Samoson, G. Engelhardt & A-R. Grimmer, *J. Am. Ceram. Soc.* 102, 4889, (1980)

[2] J.F. Stebbins, *Nature* 330, 465, (1987)

[3] E. Schneider, J.F. Stebbins & A. Pines, *J. Non-Cryst. Solids* 89, 371, (1987)

[4] C.M. Schramm, B.H.W.S. de Jong & V.E. Parziale, *J. Am. Ceram. Soc.* 106, 4396, (1984)

[5] L.F. Gladden, T.A. Carpenter & S.R. Elliot, *Phil. Mag. B*53, L81, (1986)

[6] A-R. Grimmer, M. Mägi, M. Hahnert, H. Stade, A. Samoson, W. Weiker & E. Lippmaa, *Phys. Chem. Glasses* 25, 105 (1984)

[7] I. Yasui, H. Hasegawa & M. Imoaka, *Phys. Chem. Glasses* 24, 65, (1983)

[8] M. Imoaka, H. Hasegawa & I. Yasui, *Phys. Chem. Glasses* 24, 72, (1983)

[9] J.F. Emerson, P.E. Stallworth & P.J. Bray, *J. Non-Cryst. Solids* 113, 253, (1989)

[10] E.R. Andrew, "Nuclear Magnetic Resonance", Cambridge Univ. Press 1958

[11] C.A. Fyfe, "Solid State NMR for Chemists", CRC Press (1984)

[12] R. Dupree & D. Holland in "Glasses and Glass-Ceramics", ed. M.H. Lewis, Chapman Hall (1989)

[13] S.R. Elliott, *J. Non-Cryst. Solids* 76, 79, (1985)

[14] S.R. Elliott, *J. Non-Cryst. Solids* 123, 149, (1990)

[15] R.J. Kirkpatrick, T. Dunn, S. Schramm, K.A. Smith, R. Oestrike & G. Turner, in "Structure and Bonding of Non-Crystalline Solids", eds. G. Walrafen & A.G. Revesz, (1986)

[16] R.J. Kirkpatrick in "Spectroscopic Methods in Mineralogy and Geology", ed. F.C. Hawthorn, Mineralogical Soc. of America (1988)

[17] P.J. Bray, *J. Non-Cryst. Solids* 95/6, 45, (1987)

[18] P.J. Bray, J.F. Emerson, D. Lee, S.A. Feller, D.L. Bain & D.A. Feil, *J. Non-Cryst. Solids* 129, 240, (1991)

[19] J.F. Stebbins & I. Farnan, *Science* 245, 257, (1989)

[20] P.E. Stallworth & P.J. Bray, *Glass. Sci. Technol.* 4, 77, (1990)

[21] H. Eckert, *Prog. in NMR Spectroscopy* 24, 159, (1992)

[22] S.M. Stishov & S.V. Popova, *Geokhimiya* 10, 837, (1961)

[23] B.D. Santarsiero, X. Xue & M. Kanzaki, *Trans. Am. Crystallogr. Ass.* 1991 to be published

[24] D.K. Swanson & C.T. Prewitt, *Am. Mineral.* 68, 581, (1983)

[25] T.L. Weeding, B.H.W.S. de Jong, W.S. Veeman & B.G. Aitken, *Nature* 318, 352, (1985)

[26] I.N. Chakraborty & R.A. Condrate Snr., *Phys. Chem. Glasses* 26, 68, (1985)

[27] W.H. Zachariasen, *J. Am. Chem. Soc.* 54, 3841, (1932)

[28] C.A. Angell, P. Cheeseman & S. Tamaddon, *Bull. Mineral.* 106, 87, (1983)
[29] L.V. Woodcock, C.A. Angell & P. Cheeseman, *J. Chem. Phys.* 65, 1565, (1976)
[30] T.F. Stoules, *J. Chem. Phys.* 71, 4570, (1979)
[31] J.D. Kubicki & A.C. Lasagna, *Am. Mineral.* 73, 941, (1988)
[32] C.A. Angell, C.A. Scarehorn, C.C. Phifer, R.R. Kidiyala & P.A. Cheeseman, *Phys. Chem Mineral.* 15, 221, (1988)
[33] C.A. Angell, P. Cheeseman & S. Tamaddon, *Science* 218, 885, (1982)
[34] S.M. Ridgen, T.J. Ahrens & E.M. Stolper, *J. Geophys. Res.* 93, 367, (1988)
[35] E. Knittle & R. Jeanloz, *Science* 235, 668, (1987)
[36] G.V. Gibbs, *Am. Mineral.* 67, 421, (1982)
[37] K.L. Geisinger, N. L. Ross & P. McMillan, *Am. Mineral.* 72, 984, (1987)
[38] S.H. Risbud, R.J. Kirkpatrick & A.P. Taglialavore, *J. Am. Ceram. Soc.* 70, C-10, (1987)
[39] P. McMillan & B. Piriou, *J. Non-Cryst. Solids* 53, 279, (1982)
[40] S.K. Sharma, D. Virgo & B.O. Mysen, *Am. Mineral.* 64, 779, (1979)
[41] M.F. Hochella Jr. & G.E. Brown Jr., *Geochim Cosmochim Acta* 49, 1137, (1985)
[42] M.E. Fleet, C.T. Herzberg, G.S. Henderson, E.D. Crozier, M.D. Osborne & C.M. Scarfe, *Geochim. Cosmochim. Acta* 48, 1455, (1984)
[43] E. Ohtani, F. Taulelle & C.A. Angell, *Nature* 314, 78, (1985)
[44] J.E. Dickerson, C.M. Scarfe & P.F. McMillan, *EOS* 70, 487, (1989)
[45] R. Dupree, D. Holland & M.G. Mortuza, *Nature* 328, 416, (1987)
[46] A-R. Grimmer, F. von Lampe, M. Mägi, *Chem. Phys. Lett.* 132, 549, (1986)
[47] I.L. Mudrakovskii, V.M. Mastikhin, V.P. Shmackova & N.S. Kotarenko, *Chem. Phys. Lett.* 120, 424, (1985)
[48] R. Dupree, D. Holland & M.G. Mortuza, *Phys. Chem. Glasses* 29, 18, (1988)
[49] R. Dupree, D. Holland, M.G. Mortuza, J.A. Collins & M.W.G. Lockyer, *J. Non-Cryst. Solids* 112, 111, (1989)
[50] T. Sekiya, N. Mochida, A. Ohtsuka & K. Uchida, *Nippon Seram. Kyokai Gak. Ronbunshi* 96, 571, (1988)
[51] J.F. Stebbins & P.W. McMillan, *Am. Mineral.* 74, 965, (1989)
[52] J.F. Stebbins, *Nature* 351, 638, (1991)
[53] C.T.G. Knight, R.J. Kirkpatrick & E. Oldfield, *J. Non-Cryst. Solids* 116, 140, (1990)
[54] R.R. Ernst, G. Bodenhausen & A. Wokaun, "Principles of NMR in one and two Dimensions", Clarendon Press (1986)
[55] M.G. Mortuza, PhD. Thesis, University of Warwick, 1989
[56] C. Nelson & D. Tallant, *Phys. Chem. Glasses* 25, 31, (1984)
[57] British Standard B.S. 2469:PART 1:1988. Analysis of glass, Part 1. Glasses of the soda-lime-magnesia-silica type. B.S.I. 1988

[58] R.Dupree, D. Holland & D.S. Williams, *J. Non-Cryst. Solids* 81, 185, (1985)
[59] I.L. Mudrakovskii, V.P. Shmakkova & N.S. Kotsarenko, *J. Phys. Chem. Solids* 47, 335 (1986)
[60] L. Griffiths, A. Root, R.K. Harris, K.J. Packer, A.M. Chippendale & F.R. Thomas, *J. Chem. Soc. Dalton Trans.* 1986, p. 2247
[61] R.K. Brow, R.J. Kirkpatrick & G.L. Turner, *J. Non-Cryst. Solids* 116, 39, (1990)
[62] R.K. Brow, R.J. Kirkpatrick & G.L. Turner, *J. Am. Ceram. Soc.* 73, 2293, (1990)
[63] J. Wong, *J. Non-Cryst. Solids* 20, 83, (1976)
[64] S.W. Martin, *Eur. J. Solid State Inorg. Chem.*, 28, 163, (1991)
[65] CRC Handbook of Chemistry and Physics, CRC Press, (1992)
[66] International Critical Tables of Numerical data, Physics, Chemistry & Technology, vol. 1, ed. in chief E.W. Washburn, M^{c}Graw Hill, 1926
[67] Figure calculated from the x-ray density given by E. Tillman, W. Gelbert & W.H. Baur, *J. Solid State Chem.* 7, 69, (1973)
[68] C.T. Moynihan, A.J. Easteal, M.A. DeBolt & J. Tucker, *J. Am. Ceram. Soc.* 59, 12, (1976)
[69] D. Holland, *Bol. Soc. Esp. Ceram. Vid.* 31 - C(3), 65, (1992)
[70] Ebelman, *Ann.* 57, 319, (1846)
[71] H. Schmidt, H. Stolze & A. Kaiser, *J. Non-Cryst. Solids* 63, 1, (1984)
[72] H. Dislich, *Angewandte Chemie. Int. Ed. (Eng)* 10, 365, (1970)
[73] H. Dislich, J. Non-Cryst. Solids, 73, 599, (1985)P.F. James, *J. Non-Cryst. Solids* 100, 93, (1988)
[74] A.E. Roy, *J. Am. Ceram. Soc.* 35, 39, (1952)
[75] J. Zarzycki in "Glass .... Current Issues" NATO ASI Series E-92 ed. A.F. Wright & J. Dupuy, Martinus Nijhoff 1985
[76] J.D. Mackenzie, *J. Non-Cryst. Solids* 48, 1, (1982)
[77] C.J. Brinker & G.W. Scherrer, *J. Non-Cryst. Solids* 70, 301, (1985)
[78] P.F. James, *J. Non_cryst. Solids* 100, 93, (1988)
[79] H. Dislich, *J. Non-Cryst. Solids* 63, 1, (1984)
[80] C.J. Brinker, D.E. Clark & D. R. Ulrich, eds., "Better Ceramics Through Chemistry", Elsevier (1984)
[81] E.A. Hayri & M. Greenblatt, *J. Non-Cryst. Solids* 94, 387, (1987)
[82] J.P. Boilot & P. Colomban, *J. Mater. Sci. Lett.* 4, 22, (1985)
[83] J.B. Perison & W.B. White, *Diff. Defect Data* 53/4, 381, (1987)
[84] S-P. Szu, L.C. Klein & M. Greenblatt, *J. Non-Cryst. Solids* 143, 21, (1992)
[85] S. Prabhakar, K.J. Rao & C.N.R. Rao, *J. Mater. Res.* 6, 592, (1991)
[86] D.C. Douglass, T.M. Duncan, K.L. Walker & R. Csencsits, *J. Appl. Phys.* 58, 197, (1985)
[87] S.G. Kosinski, D.M. Krol, T.M. Duncan, D.C. Douglass, J.B. MacChesney & J.R. Simpson, *J. Non-Cryst. Solids* 105, 45, (1988)
[88] F. Tian, L. Pau, X. Wu & F. Wu, *J. Non-Cryst. Solids* 104, 129, (1988)

[89] B. Gerstein, R.G. Pembleton, R.C. Wilson & L.M. Ryan, *J. Chem. Phys.* 66, 361, (1977)
[90] R. Eckman, *J. Chem. Phys.* 76, 767, (1982)
[91] J.P. Yesinowski & H. Eckert, *J. Am. Chem. Soc.* 109, 6274, (1987)
[92] W.G. Klemper, V.V. Mainz & D.M. Millar, *Mat. Res. Soc. Symp.Proc.* 73, 15, (1986)
[93] C.A. Balfe & S.L. Martinez, *Mat. Res. Soc. Symp. Proc.* 73, 27, (1986)
[94] J.C. Pouxviel, J.P. Boilot, J.C. Beloeil Y J.Y. Lallernad, *J. Non-Cryst. Solids* 89, 345, (1987)
[95] R.H. Glaser, G.L. Wilkes & C.E. Bronniman, *J. Non-Cryst. Solids* 113, 73, (1989)
[96] G. Engelhardt & D. Michel, "High Resolution Solid State NMR of Silicates and Zeolites", Wiley (1987)
[97] D. Freude, M. Hunger & H. Pfeifer, *Chem. Phys. Lett.* 91, 307, (1982)
[98] A-R. Grimmer & H. Haubenreisser, *Chem. Phys. Lett.* 99, 487, (1983)
[99] F. Liebau, "Structural Chemistry of Silicates; Structure, Bonding and Classification", Springer-Verlag 1985
[100] W. Eitel, "Silicate Science, vol. 1; Silicate Structures", Academic Press, 1964
[101] Makart, *Helv. Chim. Acta.* 50, 399, (1967)
[102] Chemical Databank System, Daresbury Laboratory, Warrington, Cheshire.

CHAPTER 5.

Na_2O . CaO . SiO_2 . P_2O_5 SYSTEM.

5.1. INTRODUCTION.

5.1.1. GENERAL INTRODUCTION.

In 1969 Hench and his co-workers at University of Florida came upon a remarkable discovery; a man-made, surface-active material that underwent a chemical bonding to bone [1]. This new type of 'biomaterial' was a soda-lime phosphosilicate glass labelled "Bioglass" [2]. This was the first 'bioactive' material discovered and, not surprisingly, extensive studies have been carried out to detail the exact mechanism that underlies the formation of the glass-tissue interface [3-11]. However little or no investigation of the glass structure has been reported. Therefore this chapter employs ^{29}Si, ^{23}Na and ^{31}P MAS NMR in the examination of the medium range structure of a series of Na_2O . CaO . SiO_2 . P_2O_5 glasses. As Hench has also reported a bioactive glass-ceramic, obtained via a controlled heat treatment of Bioglass 45S5 [1,2], the glasses prepared in this study have been similarly heat treated and the resulting structure examined by MAS NMR and powder x-ray diffraction.

Prior to the development of the Bioglass [2], all materials implanted into living tissue were termed inert, although the use of this term is somewhat misleading. All foreign implanted materials elicit some response from the host tissue and the type of response can be used to categorize the possible implant material; if the implant is toxic then the surrounding tissue dies, if the implant is non-toxic but

soluble (e.g. tricalcium phosphate) then gradually the neighbouring tissue replaces it, or finally, if the implant material is non-toxic and insoluble the host tissue encapsulates the implant generally with fibrous tissue that has no strength at the interface [12]. Bioglass [2] introduced a fourth response, the formation of a strong chemical bond across the tissue/implant interface.

Subsequently a range of surface active biomaterials have been developed including glasses [1,3,4,6,13-16], glass-ceramics [17-20], ceramics [21-23] and composites [24,25].

In the field of surface active glasses and glass-ceramics as of 1984 all materials under investigation were essentially derived from the original Bioglass [2] system with additions of various other oxides and fluorides [12]. That still appears to be the situation today [26] although the number of component oxides and halides has increased. The practical use of glass as an implant material is hampered by its inherent lack of mechanical strength, hence the greatest success has been achieved in fields of reconstructive surgery where strength is not an essential component, e.g. facial and middle ear repair. The low strength of glass can even be of benefit in these applications as it permits the implant to be machined and shaped by the surgeon just prior to implantation whilst in the operating theatre [12,26]. Attempts have been made to coat a variety of metals used in medical prosthesis, stainless steel [27,28], vitallium [29,30], titanium [31] and also high density alumina [32], with surface active glass coatings. The coatings did improve the adhesion of the prosthesis and were predicted [12] to increase the life expectancy of a hip replacement considerably above the 10 or so years obtainable from conventional polymethylmethacrylate adhesives. However precautions are necessary regarding the possibility of diffusion of the substrate components through the glass coating and hence into the surrounding living tissue.

Aside from the use of surface active glasses as enamel coatings for metals, another means of increasing mechanical strength exists; the glass to glass-

ceramic process. Basically this is a transformation from mechanically weak glass into a stronger polycrystalline material via a carefully controlled heat treatment (see section 5.3.1.). Hench and Wilson [12] give details of three particular bioactive glass-ceramics, Ceravital [33,34], A/W ceramic [35] and an unnamed material developed by Vogel et al [36]. Of the three, Ceravital [33] is the nearest in composition to the Bioglass system, although with a lower alkali content [12]. The increased mechanical strength of Ceravital [33] is evident from the method of failure of the implant, under tension catastrophic failure occurred in the bone and not at either the interface or the bulk glass-ceramic. Ceravital [33] has subsequently undergone human testing [37], especially in the field of ossicular reconstruction, where implants have been in situ for up to 5 years without complications and with better results than were attained from allogenic ossicles. Another advantage of Ceravital is the ability to machine using standard operating theatre equipment, although machining takes longer in comparison to simple bioactive glasses.

The bioglass-ceramic developed by Vogel et al [36] consists of mica and hydroxy-apatite crystal phases incorporated in a glass matrix and is both easy to machine and adapt by altering the base composition, enabling even production of a magnetic bioactive material [12].

A/W glass-ceramic has also undergone human testing, most successfully in spinal fusion procedures. It consists of an unknown glass phase matrix with wollastonite and hydroxy-apatite as crystalline fillers [12].

Alternative biomaterials developed to date include dense hydroxyapatite ceramics, which have been successfully applied in dentistry [38-42], as bioactive coatings on sturdier load bearing substrates such as stainless steel [27], in porous forms for facial reconstructive surgery [43,44] and in restoration of the bony components of the middle ear [45].

The field of composites has also undergone investigation. Surface active composites combine the bioactivity of a bioglass with the specific mechanical

properties of the filler. A composite of Bioglass [2] 45S5 and a 316L stainless steel fibre matrix has completed human trials, as an orthopaedic implant, successfully [46].

5.1.2. BIOACTIVITY AND THE BIOGLASS [2] SYSTEM.

Bioactivity is defined as the ability to chemically bond to living tissue [12], but what differentiates a standard soda-lime silicate glass and these bioactive compositions? There are three major differences; the low SiO_2 content (< 60 mol%), and correspondingly, the higher than average alkali/ alkaline earth content and the high $CaO:P_2O_5$ ratio.

The base Bioglass composition is 45S5, a nomenclature explained as [1] 45 weight% SiO_2 with a calcium to phosphorus ratio of 5. Table 5.1, from reference [26] details a variety of materials developed from this base composition. These alterations from 45S5 do affect the bioactive properties, decreasing the $CaO:P_2O_5$ reduces the level of bioactivity, but does provide for other desirable features such as machinability, mechanical strength, lower melting temperatures and

Composition of Bioactive Glasses and Glass-Ceramics (wt%)

Component	45S5 Bioglass®	45S5 4F Bioglass®	45S10S6 Bioglass®	52S4.6 Bioglass®	55S4.3 Bioglass®	KGC Cerabital®	KGS Cerabital®	KGy213 Cerabital®	A/W glass-ceramic	MB glass-ceramic	S45P5
SiO_2	45	45	30	52	55	46.2	46	38	34.2	19–52	45
P_2O_5	6	6	6	6	6				16.3	4–24	7
CaO	24.5	14.7	24.5	21	19.5	20.2	33	31	44.9	9–3	22
$Ca(PO_3)_2$						25.5	16	13.5			
CaF_2		9.8							0.5		
MgO						2.9			4.6	5–15	
MgF_2											
Na_2O	24.5	24.5	24.5	21	19.5	4.8	5	4		3–5	24
K_2O						0.4				3–5	
Al_2O_3								7		12–33	
B_2O_3			15								2
Ta_2O_5/TiO_2								6.5			
Structure	Glass and glass-ceramic	Glass	Glass	Glass		Glass-ceramic	Glass-ceramic	Glass-ceramic	Glass-ceramic	Glass-ceramic	

Table 5.1. The composition of various bioactive glasses and glass-ceramics as given in reference [26]. Note that the concentration of each component is given in wt %.

open gel structure then permits rapid migration of Ca^{2+} and PO_4^{3+} to the interface region which subsequently produces a $CaO-P_2O_5$ rich film on the gel layer which develops into a thicker and denser amorphous layer via the arrival of more ions from the bulk glass absorption of calcium and phosphate ions from the physiological solutions. This stage has been detected after only ten minutes of immersion in a controlled in vitro examination [26]. The final stage involves the crystallization of the amorphous calcium phosphate into a mixed hydroxyl, carbonate and fluoro-apatite layer, the necessary OH^-, CO_3^{2-} and F^- anions again being derived from the host tissue. Laboratory in vitro simulations with the implant surface examined by FTIR indicate that by 1½ hours the P-O vibration is more consistent with crystalline apatite. Concurrently C-O modes are also observed [52]. Around 10 hours subsequent to implantation, the mixed apatite layer is approximately 4 microns thick

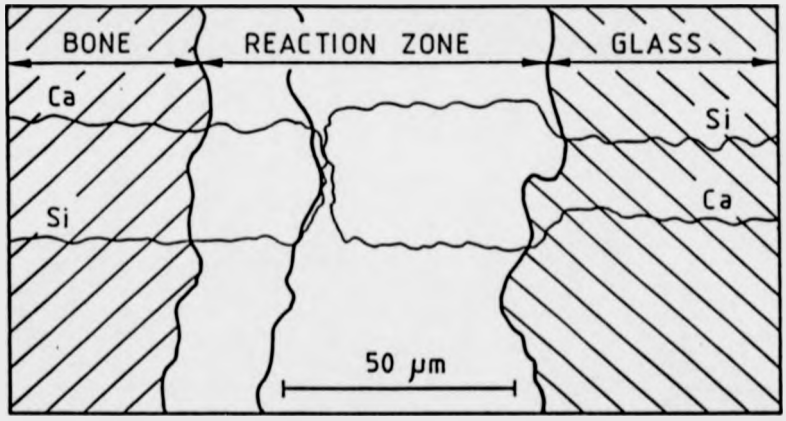

Figure 5.1. An illustration of the 3 stage interface between a bioactive glass and a rabbit tibia 6 weeks after insertion. Concentration profiles of Si and Ca drawn from an SEM micrograph [49]

[53]. Figure 5.1, taken from Karlsson et al [54], illustrates the three stage profile of the tissue-glass interface.

The bioactivity - compositional dependence of glasses within the soda-lime silicate system is illustrated in figure 5.2. Compositions within region A form strong bonds with living tissue, hence the region is known as the bioactive

open gel structure then permits rapid migration of Ca^{2+} and PO_4^{3+} to the interface region which subsequently produces a $CaO-P_2O_5$ rich film on the gel layer which develops into a thicker and denser amorphous layer via the arrival of more ions from the bulk glass absorption of calcium and phosphate ions from the physiological solutions. This stage has been detected after only ten minutes of immersion in a controlled in vitro examination [26]. The final stage involves the crystallization of the amorphous calcium phosphate into a mixed hydroxyl, carbonate and fluoro-apatite layer, the necessary OH^-, CO_3^{2-} and F^- anions again being derived from the host tissue. Laboratory in vitro simulations with the implant surface examined by FTIR indicate that by 1½ hours the P-O vibration is more consistent with crystalline apatite. Concurrently C-O modes are also observed [52]. Around 10 hours subsequent to implantation, the mixed apatite layer is approximately 4 microns thick

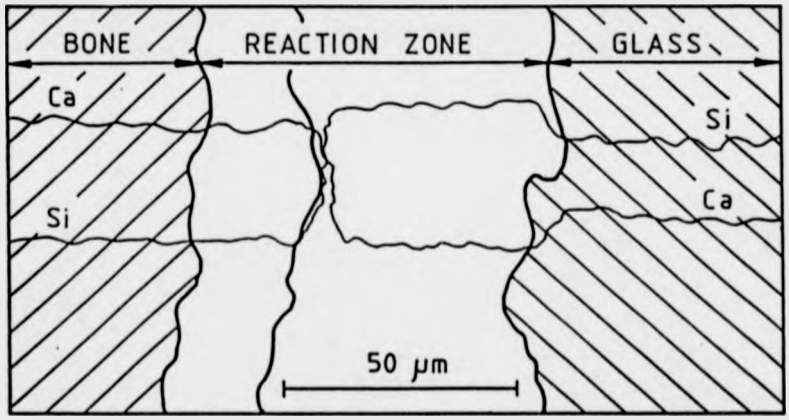

Figure 5.1. An illustration of the 3 stage interface between a bioactive glass and a rabbit tibia 6 weeks after insertion. Concentration profiles of Si and Ca drawn from an SEM micrograph [49]

[53]. Figure 5.1, taken from Karlsson et al [54], illustrates the three stage profile of the tissue-glass interface.

The bioactivity - compositional dependence of glasses within the soda-lime silicate system is illustrated in figure 5.2. Compositions within region A form strong bonds with living tissue, hence the region is known as the bioactive

increased adhesion to substrates. Perhaps, most importantly, controlled crystallization of the bioactive glasses into glass-ceramics produces no detectable reduction in the tissue bonding ability. Certain halides such as CaF_2, substituting for up to 12.5 weight% of CaO, have been introduced as nucleating agents to ensure the crystallization of required phases such as fluroapatite. One important group of oxides does have a distinctly destructive affect upon bioactivity [47-49], transition metal oxides. As little as 3 weight% of oxides such as Ta_2O_3, TiO_2 and ZrO_2 destroys all bone bonding ability. A similar concentration of Sb_2O_3 or Al_2O_3 also has the same adverse effect. However the bioactive glass-ceramic developed by Vogel, which does contain alumina, remains bioactive. This is achieved by the Al_2O_3 being incorporated into the mica crystalline phase and as such it does not interfere with the initial surface reaction kinetics [36]. Andersson et al [50] have more recently shown that up to approximately 1.6 mol% of alumina can be tolerated without destroying the ability to bond to living tissue.

These surface reaction kinetics have been studied most extensively in the 45S5 Bioglass [2] and apparently proceed via 5 stages after implantation [26]. Initially there is an ion exchange between the implant surface and the surrounding physiological environment with Na^+ being replaced by H^+ or H_3O^+. This process is diffusion controlled and is therefore time dependent, proportional to $t^{-1/2}$, with a depletion depth in excess of 0.5 microns within minutes of implantation [26]. The second stage involves the break up of the silicate network to form silanols viz;

$$Si - O - Si + H_2O \text{ -------> } 2\ Si - OH_{aq}$$

This is an interfacial reaction and hence is directly proportional to time. The third stage involves the equilibrium condensation and partial repolymerisation of these silanols to form an SiO_2 rich gel layer at the interface. The formation of this gel layer has been observed after as little as 20 minutes after implantation [51]. The

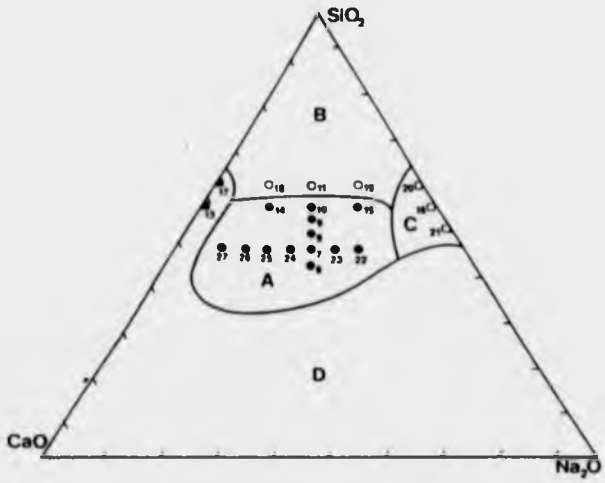

Figure 5.2. Bioglass bonding behaviour represented on a triaxial composition diagram. All compositions contain a constant 6 wt% P_2O_5. Illustration from [9]

bonding boundary. Increasing the SiO_2 content of the glasses, region B, to compositions typical of window or bottle glass destroys the bioactivity, these compositions behave in a similar manner to 'inert' implants in that they elicit encapsulation by fibrous membranes from the host. Compositions within region C are found to be completely resorbable, disappearing completely after 10 to 30 days of implantation. region D is a non-glass forming region due to the very low SiO_2 content. Interestingly, within the region A, the degree of bioactivity decreases as the composition nears the region boundary [26].

5.1.3. SODA - LIME GLASSES.

The majority of glasses encountered in everyday life such as bottles and windows are based upon the soda-lime silicate system. According to Kreidl [55] their development arose from the fact that SiO_2 could be fused more readily after Na_2O was added, however the glass produced was not as durable. With the addition of CaO, the glasses were found to have increased chemical durability. Typical

container glass has a composition near Na_2O . CaO . 6 SiO_2.

The soda lime silicate glass forming region is extensive, covering practically the whole of the ternary triangle for SiO_2 concentrations above 50 mol% [56]. Indeed Rawson [57] notes that small regions of invert glasses can be formed in this system, ostensibly because of the relatively strong Ca - O bond.

The phase diagram, initially established by Morey and Bowen [58] has more recently been adjusted by Shahid and Glasser [59]. Of all the phases that can be formed in this ternary system Na_2O 2CaO 3SiO_2, (equivalent to Na_2SiO_3 . 2$CaSiO_3$), is perhaps the most curious. Moir and Glasser [60] have established that this phase is not of fixed stoichiometry, but varies from 28.5 to 53.5 mol% Na_2SiO_3, with a variety of polymorphic forms, and consequently XRD powder patterns, possible depending upon the exact heat treatment. Phase separation is a possible problem in soda lime silicates as the soda silicate system has a metastable region of liquid immiscibility whereas the calcium silicate binary has a stable region of liquid - in - liquid phase separation. These regions extend into the combined ternary system, a problem that has been studied by Burnett and Douglas [61]. They have stated that the development of any phase separation is very dependent upon composition, but when present is more likely than not to be detectable visibly and is apparently associated with the onset of crystal nucleation.

Structural examination of the soda lime silicate system via MAS NMR seems remarkably rare. Dupree, Holland and Williams [62] have published some ^{29}Si and ^{23}Na MAS NMR results concerning the introduction of CaO into two soda silicate compositions. Where the CaO was consistently added as a direct substitute for Na_2O the ^{29}Si shifts for silicon in Q^3 and Q^4 became progressively more negative, from -90 to -93 ppm and -105 to -108 ppm respectively, as the amount of CaO was increased. The corresponding ^{23}Na peak position was also shifted to the high field from -3 ppm for the Na_2O 4SiO_2 glass to -15 ppm where the ratio of Na_2O to CaO was 2:3. Interestingly substitution of Na_2O by Cs_2O produced

the opposite effect, with the ^{23}Na peak position becoming more positive for increasing concentrations of Cs_2O. The same paper also gives details of another series of glasses of nominal composition $^{x}/_{2}$ Na_2O $^{x}/_{2}$ CaO (100-x)SiO_2. This time the ^{23}Na peak position became less shielded, -13 ppm to -4 ppm, as the total modifier content was raised from 20 to 40 mol%. Previous work on the same nominal composition by Veal et al [63] was reported to show only 80% of the Ca^{2+} behaving as network modifiers, the remainder actually forming linkages within the network. However the ^{29}Si MAS NMR recorded by Dupree et al showed that all the modifier ions produced non-bridging oxygens and that their distribution was best described by the binary model.

5.2. GLASSES.

5.2.1. PREPARATION.

The compositions examined in this study are illustrated in the ternary (Na_2O - CaO - SiO_2) phase diagram of figure 5.3. It should be noted that all compositions also contained P_2O_5 at a constant 6 weight%, around 2.6 to 2.7 mol%. Table 5.2 details the nominal compositions in both weight and mol per cent. In an identical manner to the potassium tetra-silicate system (see chapter 4) 0.05 mol% $MnCO_3$ was added to each batch to facilitate speedier ^{29}Si MAS NMR spectra accumulation. The two tie lines represent two substitutions, CaO for Na_2O and CaO for SiO_2.

50g batches of the correct proportions of analytical grade sodium carbonate, calcium carbonate, sodium dihydrogen orthophosphate and Limoges quartz were dry milled for 16 hours. Melting took place in Pt or Pt/Rh crucibles in order to avoid possible Al_2O_3 contamination. Ultimate melt temperatures were

SAMPLE	Na_2O	CaO	SiO_2	P_2O_5
BG1	47.9 (47.0)	------	49.5 (47.0)	2.7 (6.0)
BG2	37.9 (37.6)	10.5 (9.4)	48.9 (47.0)	2.6 (6.0)
BG3	33.0 (32.9)	15.6 (14.1)	48.7 (47.0)	2.6 (6.0)
BG4	28.2 (28.2)	20.8 (18.8)	48.4 (47.0)	2.6 (6.0)
BG5	23.2 (23.5)	25.8 (23.5)	48.2 (47.0)	2.6 (6.0)
BG6	18.6 (18.8)	30.8 (28.2)	48.0 (47.0)	2.6 (6.0)
BG7	13.9 (14.1)	35.8 (32.9)	47.7 (47.0)	2.6 (6.0)
BG8	9.2 (9.4)	40.7 (37.6)	47.5 (47.0)	2.6 (6.0)
BG9	4.6 (4.7)	45.6 (42.3)	47.3 (47.0)	2.6 (6.0)
BG10	19.0 (18.8)	------	78.4 (75.2)	2.6 (6.0)
BG11	18.8 (18.8)	10.4 (9.4)	68.1 (65.8)	2.6 (6.0)
BG12	18.7 (18.8)	20.7 (18.8)	58.0 (56.4)	2.6 (6.0)
BG13	18.5 (18.8)	40.8 (37.6)	38.1 (37.6)	2.6 (6.0)

Table 5.2. Nominal compositions, in mol%, of the glasses prepared in this system. The weight% equivalent compositions are given in the brackets.

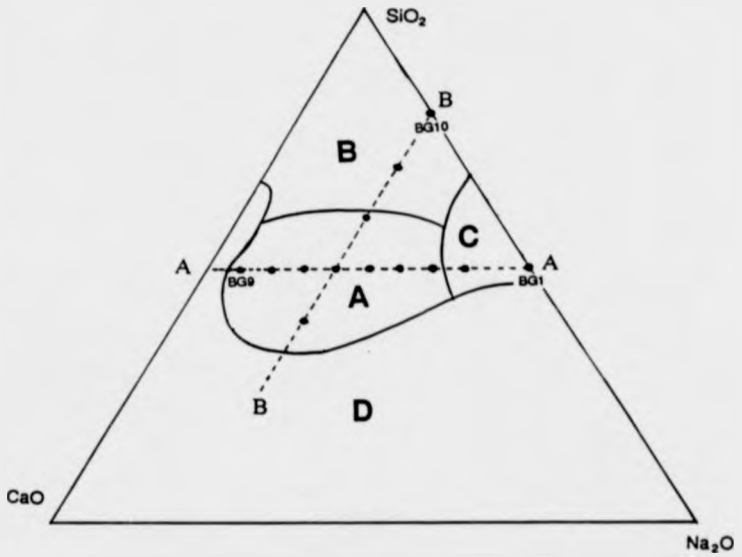

Figure 5.3. Ternary phase diagram (in weight%) illustrating the compositions prepared in this study. Tie line AA represents the first series with Na_2O substituted by CaO and tie line BB the second series where CaO systematically replaces SiO_2. Note that all compositions also contain a constant 6 wt% of P_2O_5.

between 1250 and 1300 °C, with a hold for 1 hour, then the glass was poured into a graphite coated steel mould at room temperature. The glass block was then rapidly transferred to an annealing furnace set to 450 °C and left for 6 hours prior to slow cooling. The annealing stage was incorporated to produce samples as close as possible to those reported by Hench et al [1]. After annealing the samples were examined by XRD (Philips diffractometer, Cu Kα radiation) and stored under vacuum in a desiccator until required.

All samples, except the final compositions of each tie line, BG9 and BG13, were amorphous according to their lack of intense x-ray reflections. The powder patterns obtained from BG9 and BG13 were attributed to α-$CaSiO_3$ and a combination of α - Ca_2SiO_4 and β - $CaSiO_3$ respectively.

5.2.2. CHEMICAL ANALYSIS.

Only one of these compositions has been analysed for composition; BG4. The actual concentration of SiO_2, Na_2O and CaO were determined by wet chemical gravimetric analysis as set out in BS 2649 [64]. The concentration of P_2O_5 was estimated by difference. Table 5.3 compares the nominal and analysed compositions.

	Na_2O	CaO	SiO_2	P_2O_5
NOMINAL (mol%)	28.2	20.8	48.4	2.6
ANALYSED (± 1.0 mol%)	28.0	21.1	47.9	3.0

Table 5.3. Comparison of the nominal and analysed composition of BG4. All figures in mol% only.

As can be seen the actual composition is within experimental error of the nominal composition, hence analysis of the other compositions was considered unnecessary. Therefore all glasses in this study will be discussed in terms of their nominal composition.

5.2.3. THERMAL ANALYSIS.

Differential thermal analysis (section 3.2.1.) was carried out on each composition after annealing to ascertain the glass transition, crystallization and liquidus temperatures. The results are given in the following table 5.4.

The feasibility of these materials being employed as bioactive coatings on metallic substrates would be increased if their coefficient of thermal expansion were near that of the substrate. To this end the linear thermal expansivity

SAMPLE	GLASS TRANSITION TEMPERATURE (°C)	ONSET OF CRYSTALLIZATION (°C)	LIQUIDUS / SOFTENING TEMPERATURE (°C)
BG1	390 ± 3	600 ± 5	680
BG2	455 ± 5	600 ± 4	840
BG3	474 ± 2	635 ± 6	835
BG4	530 ± 2	700 ± 8	1135 / 1180 / 1200
BG5	560 ± 5	700 ± 8	980 / 995
BG6	570 ± 10	700 ± 10	1210 / 1225
BG7	615 ± 5	680 ± 8	1050
BG8	655 ± 2	800 ± 5 / 820 ± 5	1040 / 1070
BG9	695 ± 2	825 ± 10	1040 / 1160
BG10	435 ± 5	700 ±5	950 / 1000
BG11	505 ± 5	630 ± 3 / 670 ± 4	------
BG12	560 ± 10	680 ± 5 / 875 ± 10	------
BG13	500 ± 5	620 / 710 / 900 / 950	1240 / 1260

Table 5.4. A collation of the thermal data obtained via differential thermal analysis of the glasses.

of all the compositions bar BG13 were investigated by vertical dilatometry, (see section 3.2.3). Dilatometric softening points were also measured. Table 5.5 contains the results.

SAMPLE	COEFFICIENT OF THERMAL EXPANSION (ppm) (± 0.5)	DILATOMETRIC SOFTENING POINT (°C) (± 10°C)
BG1	17.4	425
BG2	16.9	465
BG3	15.2	485
BG4	13.4	515
BG5	12.3	535
BG6	12.4	545
BG7	12.0	540
BG8	11.7	550
BG10	11.8	475
BG11	11.7	480
BG12	12.2	580

Table 5.5. Comparison of the thermal expansion and dilatometric softening temperatures of these glasses as determined by vertical dilatometry.

5.2.4. NUCLEAR MAGNETIC RESONANCE.

All spectra were accumulated on the Bruker MSL 360 spectrometer operating under conditions detailed in section 2.3.2, the particular probe employed was the most appropriate to each nucleus.

Table 5.6 (a) and (b) contain the accumulated NMR data, chemical shifts of ^{29}Si and ^{31}P, peak positions of ^{23}Na along with linewidths of all resonances.

5.2.4.1. ^{29}Si MAS NMR.

The MAS spectra were obtained using the Bruker DB low frequency probe. Approximately 0.5g of powdered sample was spun at 3-3½ kHz within 7mm outer diameter zirconia double bearing spinners. Figure 5.4 illustrates the spectra obtained from the compositions along tie line AA and figure 5.5 from tie line BB.

5.2.4.2. ^{23}Na MAS NMR.

The ^{23}Na spectra were recorded in the high spinning speed Doty probe. Approximately 0.3g of powdered sample was spun in silicon nitride spinners with vespel fluted caps. Spectrometer operating parameters are given in section 2.3.2. Examples of the spectra recorded are given in figure 5.6.

5.2.4.3. ^{31}P MAS NMR.

In order to obtain high spinning speeds, in excess of 10 kHz, the Doty probe was used again with the 5mm outer diameter silicon nitride spinners. Spectrometer parameters and other experimental details can be found in section 2.3.2. Examples of the spectra recorded are illustrated in figure 5.7.

(a)

SAMPLE	^{23}Na peak posn (± 2 ppm)	^{23}Na FWHM (± 1 ppm)	^{31}P shift (± 0.2 ppm)	^{31}P FWHM (± 0.2 ppm)	^{29}Si shift (± 0.2 ppm)	^{29}Si FWHM (± 0.2 ppm)
BG1	-8.7	43.0	15.6	4.2	-76.7 -86.3	7.8 9.8
BG2	-9.1	42.2	13.3	7.5	-78.9 -86.1	8.0 9.8
BG3	-8.0	41.5	11.2	7.5	-80.3 ¶	15.6
BG4	-10.6	42.7	9.5	8.1	-81.2 ¶	16.5
BG5	-10.6	43.4	7.7	7.5	-81.6 ¶	15.4
BG6	-9.5	40.6	6.4	7.5	-81.1 ¶	15.2
BG7	-9.1	40.0	4.2	7.5	-82.0 ¶	14.8
BG8	-9.5	38.4	4.7	7.5	-82.7 ¶	16.2
BG9	-3.9	29.9	2.8 -8.4	6.5 n.m.	-83.2 ¶	15.4

(b)

SAMPLE	^{23}Na peak posn (± 2 ppm)	^{23}Na FWHM (± 1 ppm)	^{31}P shift (± 0.2 ppm)	^{31}P FWHM (± 0.2 ppm)	^{29}Si shift (± 0.2 ppm)	^{29}Si FWHM (± 0.2 ppm)
BG10	-15.4	41.8	13.8 2.4	4.7 5.3	-92.2 -106.9	10.3 12.5
BG11	-13.6	38.4	2.7 -2.6	10.5 5.7	-92.1 -104.9	14.2 12.5
BG12	-12.6	39.3	6.2	7.5	-89.0 ¶	14.2
BG6	-9.5	40.6	4.7	7.5	-81.1 ¶	15.2
BG13	-1.7	28.6	1.8 -12.1	8.7 n.m.	-69.3 -78.5 -89.0	9.0 6.9 6.3

Table 5.6. The spectral parameters obtained from the multinuclear MAS NMR investigation of compositions lying along AA (a) and along BB (b). Note that the ^{29}Si shifts labelled ¶ are believed to be composed of two separate Q^2 and Q^3 resonances convoluted together.

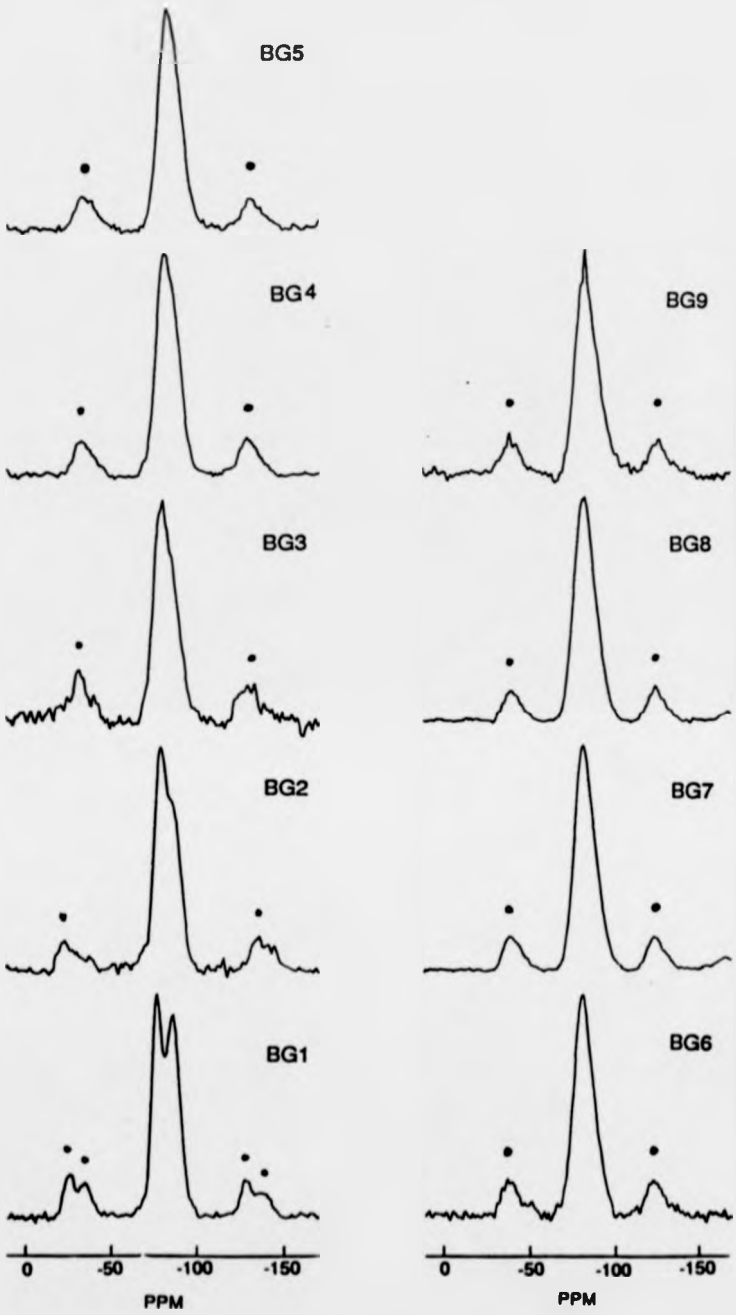

Figure 5.4. The ^{29}Si NMR spectra recorded from compositions lying along AA, corresponding to a progressive substitution of Na_2O by CaO. Each spectrum is composed of approximately 1500 accumulated sweeps, and has 50Hz of exponential broadening.

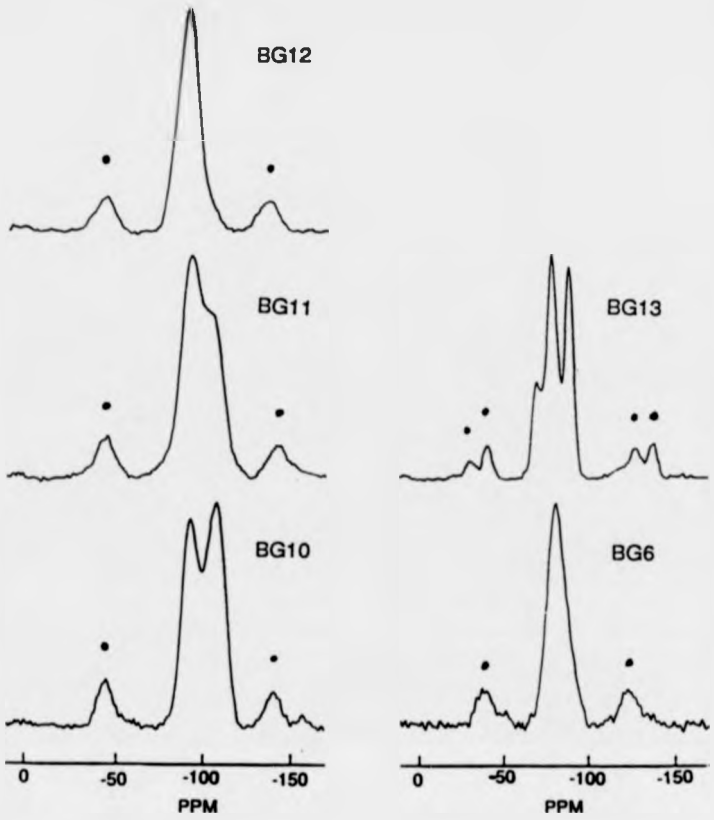

Figure 5.5. The ^{29}Si NMR spectra recorded from compositions lying along BB, corresponding to a progressive substitution of SiO_2 by CaO. Each spectrum was accumulated and processed in an identical manner to the spectra of figure 5.4.

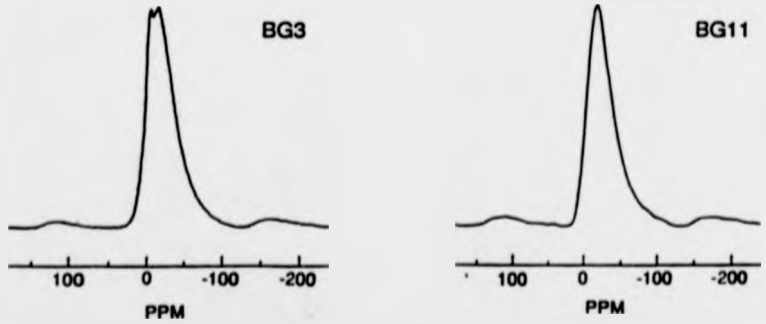

Figure 5.6. An example of ^{23}Na MAS NMR spectra from each of the two tie lines. Each spectrum contains 320 sweeps and is Fourier transformed with no broadening.

Figure 5.7. Examples of ^{31}P MAS NMR spectra from compositions lying along both AA and BB. The number of sweeps in each spectrum is 1600 and 50 Hz of line broadening was applied prior to Fourier transformation.

5.2.5. DISCUSSION.

5.2.5.1. THERMAL ANALYSIS.

The general consensus is that addition of CaO to Na_2O - SiO_2 glasses will provide for greater chemical durability and improved stability. Thus the increase in glass transition temperature throughout the first series of substitutions is not unexpected. Indeed their appears to be a linear relationship between the amount of Na_2O substituted by CaO and the corresponding transition temperature. This is most obviously seen graphically, figure 5.8 plots T_g against the ratio of CaO to total modifier content. From this plot it can be calculated that increasing the ratio by 0.1 will increase the transition temperature by around 33 °C. All the samples were annealed prior to the DTA experiments, however the annealing temperature of 450 °C is significantly lower than the transition temperatures of compositions BG7, BG8 and BG9 so it may be that these final three compositions experienced limited structural strain relaxation during this process. Thus their transition temperatures may be artificially high in comparison to the other compositions. Importantly the

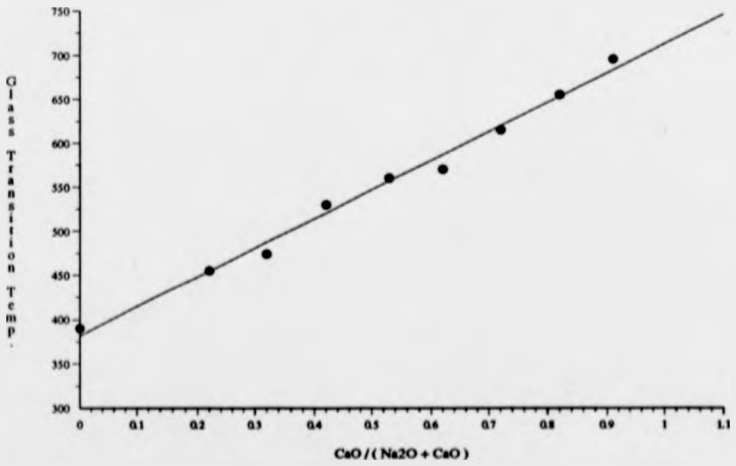

Figure 5.8. A plot of the glass transition temperature against CaO content as a function of total modifier oxide for compositions following AA. Note that errors in estimating T_g are insignificant on this scale.

annealing temperature is at least 150 °C below any crystallization onset temperature recorded by DTA.

The glass transition temperatures of samples BG10 through BG13 show no direct relation between compositional variation and T_g. Obviously this is because the CaO is being included at the expense of SiO_2, hence as the 'stabilising oxide' is added the network former is being removed. This would seem to imply a degree of covalency of the Ca - O - Si bonding.

The thermal coefficient of expansion of glasses BG1 through BG9 are given in table 5.5 along with the dilatomic softening point, which is defined as the temperature at which the thermal expansion is balanced by the viscous flow [65]. The same pattern can be found in relating the linear expansivity with the amount of CaO substituted as was observed with the glass transition temperature. Again this observation goes with the accepted norm, which according to Rawson [57] is a decrease in coefficient of expansion with increasing CaO concentration. The softening point also increases for additions of CaO. The actual measured coefficients indicate that these glasses have good potential, in terms of thermal expansion, as bioactive coatings on metal substrates such as certain stainless steels, certain NiCr alloys and possibly titanium. However other problems such as adhesion to the metal and the possibility of diffusion of substrate material across the substrate-coating interface and through the coating to the tissue-implant interface would need to be satisfactorily overcome.

5.2.5.2. NMR DISCUSSION.

As was stated in section 5.2.2 all compositions will be discussed in terms of their nominal composition.

Considering the CaO substitution for Na_2O tie line first. As the

substitution is in terms of weight %, the molar ratio of modifier ionic charge per silicate tetrahedron is not constant but increases from 1.94 to 2.12 for BG1 to BG9.

The MAS NMR investigation of the Bioglass system as summarised in table 5.6 (a) shows how the ^{29}Si, ^{23}Na and ^{31}P environments alter as tie line AA is followed. In the case of BG1, which contains no CaO, the ^{29}Si spectra, figure 5.4, contains two overlapping resonances centred on -86.3 and -76.7 ppm each with a pair of associated spinning sidebands. As this composition contains such a high concentration of alkali ions, 47.9 mol% Na_2O, it was expected that the silicate network would contain a large number of silicate tetrahedra with one or more non-bridging oxygens. Thus from the shift positions and the data on ^{29}Si shift in relation to connectivity (see figure 2.3) the resonance at -76.7 ppm is assigned to a Q^2 species and the -86.3 ppm resonance to Q^3 species. The corresponding ^{31}P spectrum contains a single resonance with a lineshape consistent with an orthophosphate-like environment. The recorded shift, 15.4 ppm, is close to that of crystalline Na_3PO_4 [66]. Hence it appears that the phosphorus is closely associated with the sodium ions, removing them from their network modifying role in the silicate network. The effect upon the silicate network of the removal of some sodium ions can be estimated by simple calculations based on the molar composition. Namely 2.7 mol% P_2O_5 would require approximately 16.2 mol% of Na^+ to form a charge balanced "Na_3PO_4-like" species. Therefore assuming that the remaining sodium ions are evenly distributed within the silicate framework, the calculation produces a Q^2 to Q^3 ratio of approximately 3:2, which is consistent with the observed ratio of resonance intensity.

Sample BG2 has 10 weight% of Na_2O substituted by CaO which has very apparent effects upon both the ^{31}P and ^{29}Si spectra. The ^{31}P resonance, whilst retaining a lineshape consistent with an orthophosphate structure, has both a less positive shift and a greater full width at half maximum than observed in BG1. The greater width implies that there is a greater range of phosphorus environments than

is found in the sodium only glass and the less positive shift position suggests that calcium ions are also associated with the phosphorus as the reported shifts for $Ca_3(PO_4)_4$ are 0.0 ppm [66] and 3.0 ppm [67]. Indeed this pattern is continued throughout the CaO for Na_2O substitution series, the width remains around 7.5 ppm and the shift progressively becomes less and less positive. Figure 5.9 illustrates the ^{31}P shift trend graphically. This trend of decreasing orthophosphate shift in these glasses is due to the slight difference in electronegativities between Na^+ and Ca^{2+}, 0.9 and 1.0 respectively. Therefore substitution of Ca^{2+} for Na^+ would result in displacement of charge from the oxygen and hence from the P-O bond, consequently increasing the electronic shielding of the phosphorus and producing a more negative chemical shift. Hence it appears that the average phosphorus environment is quite disordered with no real preference in the type of alkali ion that it 'scavenges' from the silicate network.

The effect upon the ^{29}Si spectra is similarly striking but is more difficult to ascribe. The ^{29}Si spectrum of BG2 definitely contains two resonances but the degree of overlap is greater than that observed in BG1, figure 5.4. Computerized

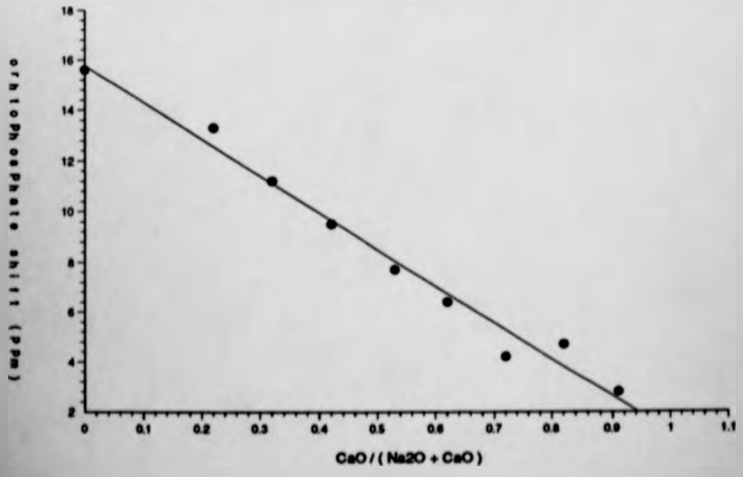

Figure 5.9. A plot of the measured ^{31}P chemical shift against CaO content as a function of total modifier oxide for compositions along AA. Note that errors are insignificant on this scale.

is found in the sodium only glass and the less positive shift position suggests that calcium ions are also associated with the phosphorus as the reported shifts for $Ca_3(PO_4)_4$ are 0.0 ppm [66] and 3.0 ppm [67]. Indeed this pattern is continued throughout the CaO for Na_2O substitution series, the width remains around 7.5 ppm and the shift progressively becomes less and less positive. Figure 5.9 illustrates the ^{31}P shift trend graphically. This trend of decreasing orthophosphate shift in these glasses is due to the slight difference in electronegativities between Na^+ and Ca^{2+}, 0.9 and 1.0 respectively. Therefore substitution of Ca^{2+} for Na^+ would result in displacement of charge from the oxygen and hence from the P-O bond, consequently increasing the electronic shielding of the phosphorus and producing a more negative chemical shift. Hence it appears that the average phosphorus environment is quite disordered with no real preference in the type of alkali ion that it 'scavenges' from the silicate network.

The effect upon the ^{29}Si spectra is similarly striking but is more difficult to ascribe. The ^{29}Si spectrum of BG2 definitely contains two resonances but the degree of overlap is greater than that observed in BG1, figure 5.4. Computerized

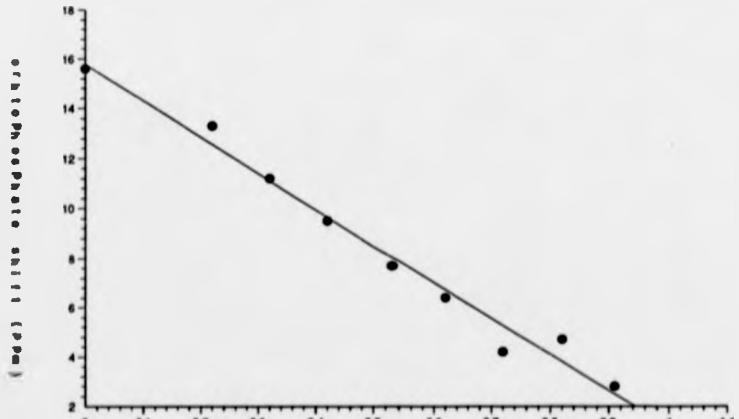

Figure 5.9. A plot of the measured ^{31}P chemical shift against CaO content as a function of total modifier oxide for compositions along AA. Note that errors are insignificant on this scale.

gaussian fitting gives shifts of -86.0 and -78.9 ppm with similar linewidths to the BG1 ^{29}Si resonances. From simple molar compositions it is calculated that there must be a combination of Q^2 and Q^3 species present, even after allowing for the removal of some of the alkali ions by phosphorus. Thus the -86.0 ppm resonance can be assigned to Q^3 species and the -78.9 ppm resonance to Q^2. Engelhardt and Michel [68] quote a table of Q^2 shifts and linewidths of binary alkali and alkali-earth silicate glasses including those of $Na_2O.SiO_2$ [69] and $CaO.SiO_2$ [70]; -76 ppm and -81.5 ppm respectively. They also quote the data of Dupree et al [71] obtained from a 45.0 Na_2O - 55.0 SiO_2 glass composition where their observed Q^3 shift was 86.0 ppm and the Q^2 shift 75.7 ppm. Applying this information to this composition it is proposed that the Q^3 species has predominantly all the non-bridging oxygens neutralized by sodium ions and the Q^2 species has a combination of calcium and the remaining sodium ions associated with its non-bridging oxygens, producing a Q^2 shift in between that reported for $Si(OSi)_2(O...Na)_2$ and $Si(OSi)_2(O...½Ca)_2$.

The ^{29}Si spectrum obtained from BG3 at first sight could be said to contain a single resonance centred on -80.3 ppm. However the molar composition calculations require the presence of at least two Q^n species; both Q^2 and Q^3 if the binary model is followed. Hence it appears that the two separate resonances have now overlapped to such an extent that they are indistinguishable from the MAS spectrum. Indeed computerized gaussian fitting showed a best fit for only a single line, hence it is not possible to estimate the individual Q^2 and Q^3 resonance shifts with any degree of accuracy. However if the reasoning employed in assessing the silicon spectrum of BG2 is sound, then it appears that the calcium ions are again predominantly associated with the Q^2 species, the greater electronegativity of the Ca^{2+} ion shifting the Q^2 position to the high field in comparison to a sodium associated Q^2 shift. It is suggested that the sodium ions are split between both silicon species, but are probably the sole modifiers of the Q^3 units.

The ^{29}Si spectra of glasses BG4 to BG8 all contain a "single" line,

although the shift becomes slightly more negative with each successive CaO - Na_2O substitution, -81.2 ppm for BG4 to -82.7 ppm for BG8. A simple calculation of the Q^2 : Q^3 for BG8 from the molar composition yields approximately 3.3:1, the increase arising from the substitution being carried out in terms of weight % and not mol%. Thus it appears that throughout this series of glasses the Ca^{2+} ions are terminating the non-bridging oxygens of the Q^2 units whereas the Na^+ ions are more and more only associated with the more polymerised silicate species, i.e. the silicate network overall consists of a calcium metasilicate-like environment combined with a predominantly sodium disilicate-like environment. This then raises the question of phase separation. No visible evidence was found to support this, although it is possible that on a microscopic level some glass-in-glass immiscibility may be present.

The final composition studied in this series of substitutions, BG9, was shown by x-ray diffraction to contain α-$CaSiO_3$. This is also evident from the resulting ^{29}Si spectrum which contains a narrow spike atop the typically broad "glass" resonant line. The shift of -83.2 ppm is compatible with what would be expected from such a crystal phase; simple ring α-$Ca_3Si_3O_9$ has a recorded shift of -83.5 ppm [68]. This is then further evidence, although indirect, for the suggestion of a calcium metasilicate-like environment within this series of glasses. This composition also produced the only ^{31}P spectrum that contained a resonance in addition to the orthophosphate line, a small resonance centred on -8.4 ppm. This shift is evidence of a pyrophosphate environment and, with so little sodium present in the composition, probably arises from a calcium pyrophosphate species. The size of the resonance is so small as to make a judgement regarding the periodicity of this phase impossible.

The series of compositions following tie line BB traverses from a high silica content glass, through the bioactive composition range and into a region of non-glass formation, figure 5.3.

As in the previous series of compositions the initial glass, BG10, contains only Na_2O as the modifier oxide. The observed ^{31}P spectrum is quite different to those recorded for samples BG1 to BG9, as it contains two resonances, at 13.8 ppm along with 2.4 ppm which has a pair of associated spinning sidebands. These resonances can be readily assigned to two sodium phosphate type of environments, an orthophosphate-like species at 13.8 ppm and a pyrophosphate-like species at 2.4 ppm. The ^{29}Si MAS spectrum also contains two separate resonances with shifts of -92.2 ppm and -106.9 ppm. From the shift positions these can be readily assigned to silicon atoms with 3 and 4 bridging oxygens respectively. The single pair of spinning sidebands are a consequence of the anisotropic bonding arrangement of the Q^3 unit. The Q^4 species is completely isotropic and so has no spinning sidebands. The ^{23}Na spectrum has a single broad resonance typical of the previous compositions, the width of approximately 40 ppm a consequence of the large electric field gradient experienced by the sodium nuclei. The actual peak position is however slightly more negative than those found in samples BG1 through BG9.

BG11 has 10 weight% of SiO_2 substituted by CaO and it is therefore expected that the resulting silicate network would be less polymerised than in BG10. This is born out by the resulting ^{29}Si spectrum which shows two overlapping resonances, chemical shifts of -92.1 and -104.9 ppm assigned to Q^3 and Q^4 respectively, although the relative intensity of the isotropic Q^4 resonance has diminished appreciably. Computerized fitting of this resonance yields a Q^3:Q^4 of approximately 5:2. The ^{31}P MAS NMR spectrum obtained from BG11, like BG10, also contains two resonances; 2.7 and -2.6 ppm. From the spectrum illustrated in figure 5.7 it can be seen that there are a pair of spinning sidebands present. These are associated with the narrow resonance centred on -2.6 ppm, and the large spread of sidebands is indicative of a large chemical shift anisotropy. This large anisotropy coupled with the recorded shift suggest a pyrophosphate type environment with the

charge neutralizing cation probably being sodium. The second and much broader resonance at 2.7 ppm is most likely from phosphorus in an orthophosphate environment. Here the metal cation is predominantly calcium as $Ca_3(PO_4)_2$ has reported shifts in the range 3.0 to 0.0 ppm [66,67]. The width of this resonance indicates that this particular species has a greater range of environments than the pyro species.

The appearance of pyrophosphate species in addition to the isolated orthophosphate in these two compositions, BG10 and BG11, is puzzling, although it has been reported previously in sodium and potassium disilicates containing 1 to 5 mol% P_2O_5 [68]. Dupree et al [68] found that the pyrophosphate environment was not formed in lithium disilicate compositions and so concluded that steric hinderance impeded the formation of completely isolated orthophosphate species in the sodium and potassium glasses. Both BG10 and BG11 contain sufficient concentrations of metallic cation to enable the charge neutralization of all the phosphorus ions if they were all in an orthophosphate configuration, however it appears as though there is some preference for a degree of P - O - P bonding, especially in BG10 where the pyro- species is the main environment. The concentrations of P_2O_5 are low such that, in purely statistical terms, the probability of two phosphorus nuclei being next nearest neighbours is extremely unlikely. Therefore it seems increasing likely that there is some micro-fine structural phase separation into phosphorus rich and phosphorus poor regions. The ^{29}Si spectra of these compositions itself gives no indication of large scale phase separation, although this in itself is not conclusive. The ^{23}Na spectra are similarly unhelpful in this matter, the resonance from BG11 has a peak position which is slightly less negative and less broad than from BG10.

The ^{31}P MAS NMR spectrum from BG12 contains only a single resonance centred on 6.2 ppm. A pair of spinning sidebands are also present, but are close to the isotropic line, thus the overall envelope is quite small. This is consistent

with a small degree of chemical shift anisotropy and is typical of phosphorus in an orthophosphate environment. The shift of 6.2 ppm is between the shifts of Na_3PO_4 and $Ca_3(PO_4)_2$, and as in the first series of glasses in this system, it appears as though both types of modifier ion are associated with the orthophosphate unit. As the phosphorus is removing alkali from the bulk silicate network in a simple manner the degree of polymerization of the silicate network can be estimated simply from the molar composition. After deducting the necessary modifier to ensure neutrality of the orthophosphate species, the remainder can be assumed to create non bridging oxygens within the silicate network. This yielded a silicate framework essentially composed of Q^3 with only around 6% or so of Q^2 according to a binary model distribution. The actual ^{29}Si MAS NMR spectrum fits this prediction extremely well. The resonant lineshape is symmetric and the shift of -89.0 ppm is typical of silicon-oxygen tetrahedra with one non bridging oxygen. The ^{23}Na resonance has a peak position less negative than that recorded for BG11, although the width is similar.

The following composition in this substitution of CaO for SiO_2 is identical to BG6, the MAS NMR spectra of which were discussed in the previous section. Suffice to mention that the ^{29}Si spectrum appears to show just a single resonance of shift -81.1 ppm, accordant with Q^2. However compositional calculations decree that a combination of Q^2 and Q^3 species in the ratio 2.7:1 be present. Therefore it is suggested that the ^{29}Si spectrum actually consists of two convoluted resonances; a Q^3 structural unit probably associated with Na^+ along with Q^2 where the main modifying cation is Ca^{2+}. The ^{31}P spectrum is assigned to an orthophosphate species with a combination of modifier ions similar to that of BG12 which produced a chemical shift of 6.2 ppm. The pattern of a less negative ^{23}Na peak position as the amount of CaO increases continues for this composition. The peak position recorded was -9.5 ppm, although the width of the resonance was again around 40 ppm.

The final composition, BG13, lies well outside the nominal glass

forming region, figure 5.3, and as expected did not produce a glass. The crystal phases present were analysed by powder x-ray diffraction and were found to be α - Ca_2SiO_4 and β - $CaSiO_3$. Evidence from the ^{29}Si NMR spectrum seems to confirm this assignment; three resonances are present at -69.3, -78.5 and -89.0 ppm, the latter two with associated spinning sidebands, whilst the reported shifts for these compounds are -70.3 and -89.0 ppm [70]. The remaining resonance is believed to originate from a glass phase with an average connectivity of a Q^2 network. There is also likely to be additional contributions from this, or other, amorphous phase in the resonance lineshapes attributed to the two crystal phases because of their rather large widths. In the same manner as BG9, the final composition of the first series of substitutions, the ^{23}Na peak position of -1.7 ppm is the least shielded of the series and the linewidth is reduced to less than 30 ppm. The narrower width indicates a smaller electric field gradient experienced by the sodium nuclei. The ^{31}P MAS NMR spectrum contains two separate resonances, which are believed to originate from phosphorus in ortho- and pyro- arrangements with predominantly calcium cations responsible for charge neutralization. The width of these lines suggests that the phosphorus is not in a crystalline phase but contained within the glass region.

5.2.6. SUMMARY.

MAS NMR has shown that for both compositions with no CaO, BG1 and BG10, the distribution of non-bridging oxygens in the silicate network follows the binary model. The P_2O_5 present in these compositions increases the relative amount of the higher Q^n species via the removal of sodium ions from the network to form "Na_3PO_4 - like" structural units.

Replacing some Na_2O with CaO produces a more negative ^{31}P shift, a trend that continues as the amount of substituting CaO increases. This has been

interpreted as indicating that the phosphorus shows no preference for the type of cation it removes from the silicate network. The actual position of the ^{31}P resonance, lying between that quoted for sodium and calcium orthophosphates, depends upon the actual ratio of Na_2O to CaO for each composition. The corresponding ^{29}Si resonances from Q^2 and Q^3 species begin to converge as the Na_2O is substituted until 15 wt% has been replaced by CaO, whereupon only a single silicon resonance appears to be present. However it is believed that two separate resonances are present but that they completely overlap. This can be explained by preferential association of the calcium ions with the non-bridging oxygens of the Q^2 species and the sodium ions with the Q^3 species, where the higher electronegativity of Ca^{2+} shifting the Q^2 resonance to the high field with respect to sodium associated Q^2 resonances. Information from the sodium NMR is limited, the large peak widths, around 40 ppm, indicating a large effective field gradient across the average sodium nuclei. Consequently the overall intermediate structure of compositions along AA consists of a combination of environments similar to calcium meta-silicate, sodium disilicate and mixed sodium/calcium orthophosphate. The presence of $CaSiO_3$ as a crystal phase in BG9 indirectly supports this hypothesis. The thermal stability of these compositions also increases as the concentration of CaO increases; increasing the CaO:Na_2O by 0.1 increased T_g by approximately 33°C.

The series of glasses along BB exhibit a more depolymerised silicate network as the substitution of CaO for SiO_2 proceeds, from a combination of Q^4 and Q^3 to Q^3 alone and then Q^3 and Q^2 as detailed in table 5.7. This is expected because the major network forming oxide is being systematically replaced by a modifier oxide. In regard of the ^{31}P MAS NMR data from BG10, which contains no CaO, two resonances are observed and assigned to species similar to sodium ortho- and pyrophospahte. BG11 also exhibits two ^{31}P resonances. Exactly why two phosphorus environments are present in these compositions is uncertain. Statistically the occurrence of P - O - P bonding is unlikely, so it may be that there is some micro

SAMPLE	CaO/SiO_2 (mol%)	Relative Amounts of Q^n Species Present			
		Q^4	Q^3	Q^2	Q^1
BG10	0	0.49	0.51		
BG11	0.15	0.32	0.68		
BG12	0.36		1.00		
BG6	0.64		0.30 [2]	0.70 [2]	
BG13 [1]	1.07		0.37	0.50	0.13

[1] BG13 contained α-Ca_2SiO_4 and β-$CaSiO_4$ as crystal phases.

[2] ^{29}Si NMR spectrum contained only one line, believed to be a convoluted envelope of seperate Q^3 and Q^2 resonances. Relative amounts estimated from the nominal composition assuming a binary distribution for the non-bridging oxygens.

Table 5.7. A table to illustrate the increasing depolymerisation of the silicate network as the substitution of CaO for SiO_2, tieline BB, proceeds.

phase seperation within the glases. The ^{31}P spectra of BG12 and BG6 show an orthophosphate environment with a mix of charge neutralizing cations as seen in the AA series. Interestingly the ^{23}Na peak position shows a trend of less negative shift for increasing concentrations of CaO.

5.3. GLASS-CERAMICS.

5.3.1. THE GLASS TO GLASS - CERAMIC PROCESS.

The clearest and most exact definition of a glass-ceramic is that given by McMillan [65]. " Glass-ceramics are polycrystalline solids prepared by the controlled crystallization of a glass." The conversion process from glass to glass-ceramic requires a deliberate heat treatment regime designed specifically to the final crystal phase(s) required and the initial glass composition.

There are a variety of reasons why this process maybe preferable to traditional sintering of ceramic powders, notably the high density and complex

shapes that can be achieved. The molten glass can be formed into numerous complex shapes via rolling, pressing, casting or blowing and the subsequent heat treatment, which involves little shrinkage or deformation, produces the glass-ceramic. The final morphology of a glass-ceramic tends to be randomly orientated fine grained crystals embedded in a a residual glass matrix, but importantly contains no voids and close to 100% density. Other advantages over traditional ceramics include a high degree of uniformity and reproducibility of physical properties; translucency, coefficient of thermal expansion matching, high mechanical strength and electrical insulation.

Crystallization is the process undergone when a disordered liquid structure transforms into the regular periodic lattice characteristic of crystals. It is however not an instantaneous process but develops from nucleation sites which are usually small embryo crystallites (a process known as homogeneous nucleation), or foreign inclusions (heterogeneous nucleation) onto which more material deposits forming larger and larger crystalline regions. The formation of these embryonic crystals is a result of statistical fluctuations in atomic arrangement producing regions of longer range atomic regularity than the host liquid/glass phase. They exist in equilibrium with the host material but need to achieve a critical minimum size before they can be considered actual nucleation sites. This critical size is given by the empirical relation below.

$$r^* = 2\,\Delta f_s / \Delta f_v$$

where r^* is the critical radius and Δf_s and Δf_v are the change in free energy associated with the surface area and unit free volume resulting from the transformation from one phase to the other. In pure thermodynamic terms, once below the liquidus temperature, these embryos can form although not at a detectable rate . However once the crystals commence to nucleate they grow both easily and

rapidly [72].

When considering glasses heated to temperatures above their annealing point but below their liquidus any nucleation that occurs will initially commence at the surface or interfaces with foreign bodies. Even internal crystallization is normally the result of nucleation via insoluble foreign particles, and the controlled crystallization process, necessary for successful glass-ceramic formation, is easiest achieved via nucleating agents or seed crystals [74].

A far more detailed examination of the realm of glass-ceramic manufacture and application can be found in the text by McMillan [65].

5.3.2. GLASS - CERAMIC PREPARATION.

As briefly explained in 5.2.1 the production of a glass-ceramic requires a two stage heat treatment. Initial nucleation is normally achieved by heating at around 500 - 700°C whereupon small regions of crystalline periodicity of the order of tens to hundreds of Å in size develop. A subsequent increase in temperature enables the the desired crystal phases to grow from these nuclei (seed) crystals. The ultimate size and volume fraction of these crystals is dependent upon the period of time the material is held at this increased temperature.

Hench has reported [1] a heat treatment profile for the complete crystallization of the Bioglass [2] 45S5. It contains two nucleation and growth stages. The temperature/time plot of the heat treatment is given in figure 5.10.

For completeness this profile was followed in this study. Small sections of glass were cut from the annealed glass blocks by diamond saw, washed ultrasonically in acetone, dried and then heated on a Pt dish in a muffle furnace programmed to follow the heat treatment outlined in figure 5.10. The glass-ceramics were then powdered in an agate mortar and pestle and the resulting crystal phases

and structures examined by XRD and MAS NMR.

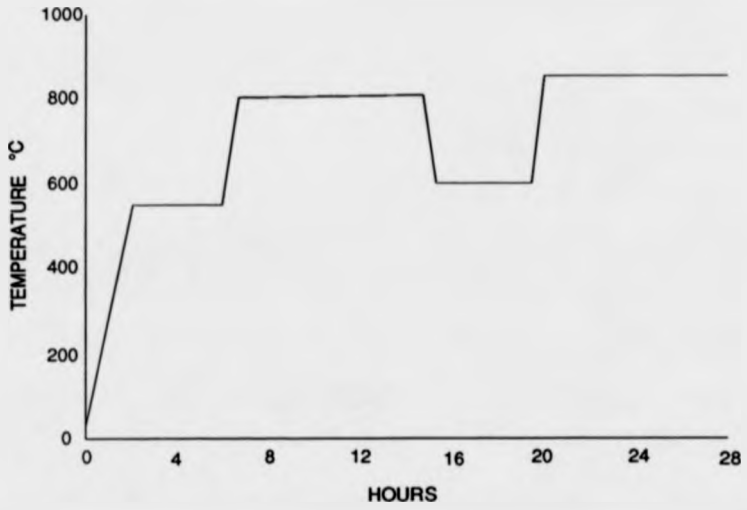

Figure 5.10. The nucleation and crystallization heat treatment described by Hench et al [1] for the production of fully crystallized Bioglass [2] glass-ceramics. This profile was followed in the preparation of the glass-ceramics investigated in this study.

5.3.3. EXPERIMENTAL.

The Bruker spectrometer operating conditions for the various nuclei are the same as detailed in sections 5.2.4.1-3. The sweep width of particular accumulations was adjusted in order that the full free induction decay signal was accrued.

Powder x-ray diffraction patterns of all the glass-ceramics were accumulated on a Philips moving arm goniometer fitted with a Cu source. Section 3.2.4 contains the experimental details.

5.3.4. RESULTS

Table 5.8 (a) and (b) details the crystal phases assigned to the powder

x-ray patterns obtained from the various glass-ceramics along with the MAS NMR data. Figure 5.11 illustrates the powder pattern obtained from BG5 and, for comparison, the reported pattern of Bioglass [2] 45S5 glass-ceramic [1]. The ^{29}Si spectra of the glass-ceramics prepared from glasses along AA are shown in figure 5.12. A selection of some of the corresponding ^{31}P MAS NMR spectra, figure 5.13, and ^{23}Na MAS NMR spectra, figure 5.14, are also given.

Figure 5.15 illustrates the ^{29}Si MAS NMR spectra from the glass-ceramics along BB and figures 5.16 and 5.17 contain examples of their corresponding ^{31}P and ^{23}Na spectra.

5.3.5. DISCUSSION.

With two separate techniques employed in this structural evaluation of the Bioglass glass-ceramics it should be a straightforward exercise to correlate the two sets of data and determine the changes in structure brought about by the heat treatment process. It is perhaps pertinent to restate that XRD is a technique that requires a reasonably large region of atomic regularity to be of significant use whereas MAS NMR is nuclei specific and probes the immediate and intermediate atomic arrangement of the resonating nucleus.

According to the powder x-ray pattern of the heat treated sample of BG1, labelled BGC1, two sodium silicate crystal phases are present; Na_2SiO_3 and the α polymorph of $Na_2Si_2O_5$. The accepted ^{29}Si MAS NMR shifts for these phases are -76.8 and -94.4 ppm respectively [70], and indeed the silicon spectrum of BGC1, figure 5.12, does contain narrow resonances centred on -76.7 and -94.3 ppm. Therefore upon first impression there is excellent agreement between the two techniques. However the ^{29}Si spectrum contained additional resonances, one being due to the residual glass phase matrix that is centred around -83 ±4 ppm which may

SAMPLE	CRYSTAL PHASES (via XRD)	^{23}Na peak posn (± 2 ppm)	^{23}Na FWHM (± 1 ppm)	^{31}P shift (± 0.2 ppm)	^{31}P FWHM (± 0.2 ppm)	^{29}Si shift (± 0.2 ppm)	^{29}Si FWHM (± 0.2 ppm)
BGC1	Na_2SiO_3 [a] α - $Na_2Si_2O_5$ [b]	15.2 13.4 7.3 -8.3	9.9 n.m. n.m.	13.9 11.2	2.1 n.m.	-76.7 [a] -83.5 * -90.5 -94.3 [b]	4.2 n.m. 5.7 4.0
BGC2	$Na_2CaSi_3O_8$ [e]	13.1 -5.1	10.8 34.3	13.9	2.3	-77.3 -87.4 [e]	8.4 6.6
BGC3	$Na_2CaSi_3O_8$ [e]	13.6 -4.8	10.4 25.9	13.9	2.8	-76.1 -87.2 [e]	9.8 7.2
BGC4	$Na_2CaSi_3O_8$ [e] $Na_2Ca_2Si_3O_9$ [d]	13.1 -6.4	10.6 25.2	13.0 2.3	5.7 1.0	-90.8 [e]/[d] -98.7	6.3 12.0
BGC5	$Na_2CaSi_3O_8$ [e]	11.7 -11.8	13.4 23.4	5.6 2.4	4.8 1.1	-89.0 [e] -97.2	5.9 14.7
BGC6	$Na_2CaSi_3O_8$ [e]	12.4 -10.3	11.3 25.8	5.8 2.4	5.0 1.2	-90.1 [e] -97.8	5.7 15.7
BGC7	$Na_2CaSi_3O_8$ [e] $Na_2Ca_3Si_6O_{16}$ [c]	12.0	33.1	4.8 2.9	5.9 1.9	-84.4 -88.6 [c] -89.1 [e]	5.6 3.2 3.1
BGC8	$Na_2CaSi_3O_8$ [e] $CaSiO_3$ [f]	11.8	31.7	4.2 3.1	1.7 4.2	-84.0 -88.3 [e] -90.0 [f]	10.0 3.1 4.2
BGC9	$CaSiO_3$ [f] α - $CaSiO_3$ [g]	-8.8	17.1	4.9 3.0 -8.0 -19.6	5.8 1.8 1.7 3.0	-83.5 [g] -88.5 [f] -91.7	2.6 4.5 n.m.

*Estimated shift ± 4 ppm.

Table 5.8 (a). The spectral parameters of the glass-ceramic materials prepared via the controlled heat treatment of glasses along AA. The superscripts alongside the XRD identified crystal phases and the ^{29}Si chemical shifts indicate which particular shift is assigned to which particular phase.

SAMPLE	CRYSTAL PHASES (via XRD)	^{23}Na peak posn (± 2 ppm)	^{23}Na FWHM (± 1 ppm)	^{31}P shift (0.2 ppm)	^{31}P FWHM (0.2 ppm)	^{29}Si shift (0.2 ppm)	^{29}Si FWHM (0.2 ppm)
BGC10	SiO_2 [a] (Tridymite)	0.8	20.6	14.0	1.1	-90.7	13.2
		-15.7	26.0	15.8	n.m.	-112.0 [a]	4.3
				2.8	4.3		
BGC11	SiO_2 [b] (Cristobalite)	-9.5	23.5	2.3	0.9	-90.4	15.8
						-108.5 [b]	7.2
BGC12	$Na_2Ca_3Si_6O_{16}$ [c]	-11.8	19.2	2.4	1.0	-84.9	4.5
	$Na_4Ca_8Si_3O_{20}$ [d]	-4.0	n.m.	2.5	9.2	-88.2 [c][d][e]	5.2
		11.7	n.m.	14.2	8.6	-92.4	7.6
						-101.0	14.0
BGC6	$Na_2CaSi_3O_8$ [e]	12.4	11.3	2.4	1.2	-90.1 [e]	5.5
		-10.3	25.8	5.8	4.2	-97.8	15.7
						-101.0	17.8

Table 5.8 (b). The spectral parameters obtained from the glass-ceramics prepared via the controlled heat treatment of glasses along BB. Note that the superscripts alongside the XRD identified crystal phases and the ^{29}Si NMR shifts indicate which particular shift is assigned to which particular phase.

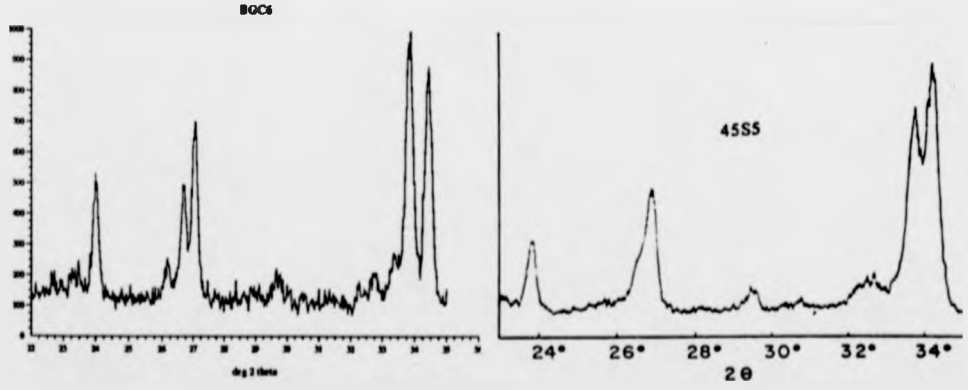

Figure 5.11. A comparison of the XRD pattern obtained from BGC5 and that reported by Hench et al [1] for the glass-ceramic obtained from the heat treated Bioglass 45S5 [2].

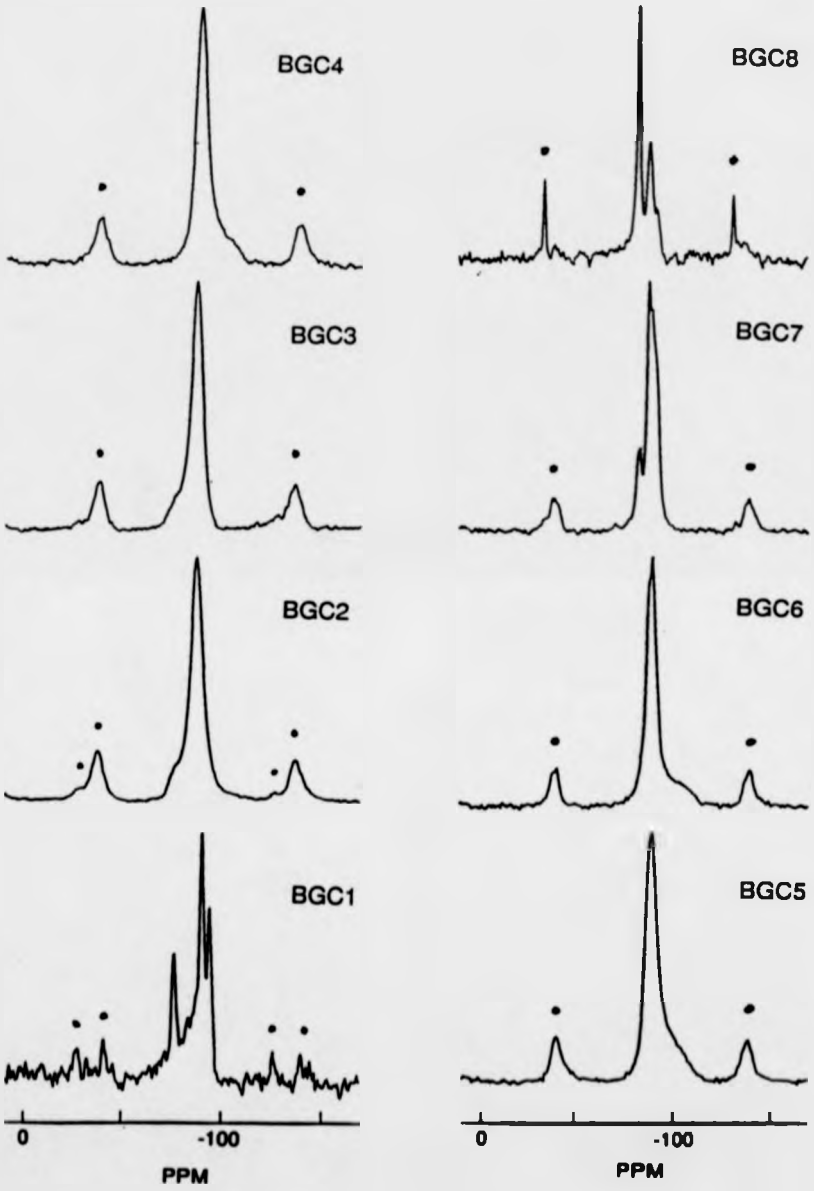

Figure 5.12. The ^{29}Si MAS NMR spectra from glass-ceramic compositions lying along AA. All the spectra bar BGC1 are composed of 1200 sweeps with 50 Hz of exponential broadening. BGC1 contains only 624 sweeps and has 100Hz of broadening.

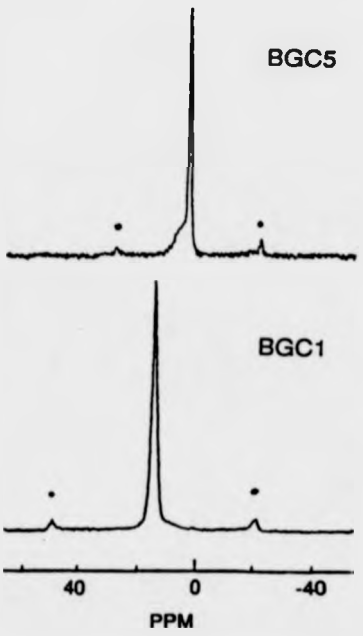

Figure 5.13. Two examples of the ^{31}P MAS NMR spectra from glass-ceramic compositions lying along AA.

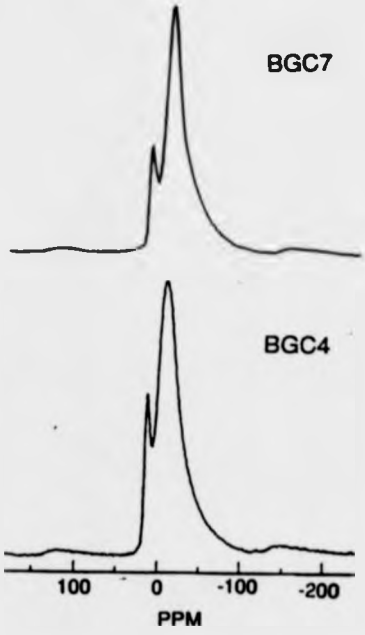

Figure 5.14. Similarly two examples of the ^{23}Na spectra recorded from compositions lying along AA.

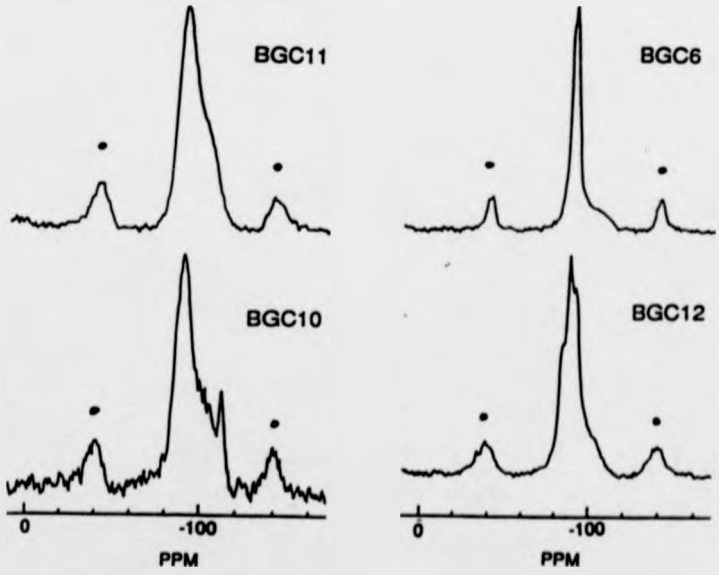

Figure 5.15. The ^{29}Si MAS NMR spectra of glass-ceramic compositions lying along BB. Each spectra contains 50Hz of exponential line broadening.

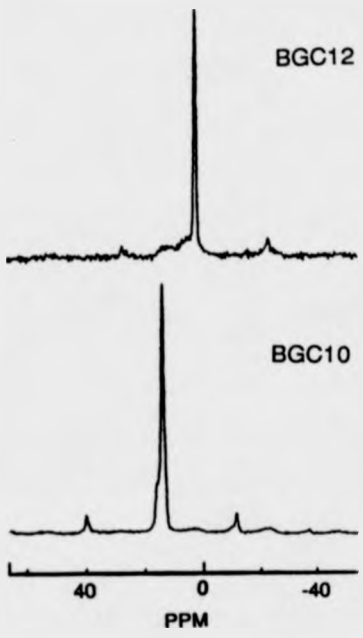

Figure 5.16. Two of the ^{31}P MAS NMR spectra recorded from glass-ceramics lying along compositional tie line BB. Each spectrum has no line broadening prior to Fourier transformation.

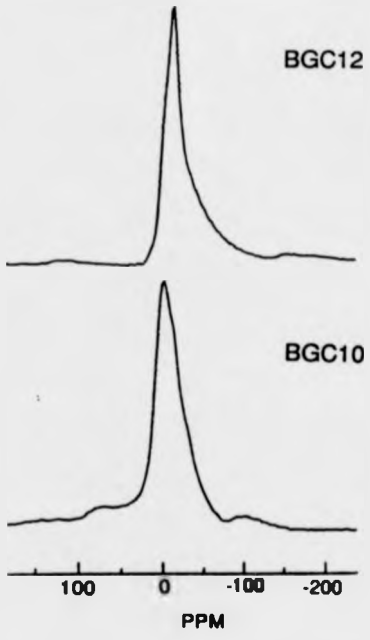

Figure 5.17. Two of the ^{23}Na MAS NMR spectra recorded from compositions lying along BB. 50Hz of line broadening has been applied.

contain a combination of Q^2 and Q^3 units. The fourth and final detected resonance, -90.5 ppm, is so narrow, 5.7 ppm FWHM, that the resonating nuclei must be in a very ordered local structure. The shift position is consistent with a Q^3 structure, the same arrangement as found in α - Na_2SiO_5 of which six separate polymorphs are known to exist [75]. Of these polymorphs the δ structure has a ^{29}Si shift closest to that observed in BGC1 at -90.0 ppm [76]. This polymorph was not detected by XRD however. The width of this resonance does suggest some degree of non-uniformity and it maybe that the local ordering of the silicon atoms is essentially that of the delta phase but the atomic arrangement becomes significantly distorted outside the third coordination sphere, rendering the coherent diffraction of x-rays impossible. The corresponding ^{31}P spectrum, figure 5.13, shows a very narrow resonance, typical of an orthophosphate, atop a small broad resonance. The shift of the narrow

resonance, 13.9 ppm, is identical to that recorded from pure crystalline Na_3PO_4 [66,77], although this crystal phase was not detected by XRD. This is most likely because of the low concentration. The small broad resonance indicates that some of the phosphorus remains in the glassy matrix, although with some Na^+ in close attendance. In the ^{23}Na spectrum of BGC1 four separate peaks can be resolved, two very sharp neighbouring resonances at 15.2 and 13.4 ppm, a slightly more broad peak around 7.3 ppm and broad peak typical of an amorphous state at -8.3 ppm. It is believed that the two very sharp resonances originate from sodium in the two sodium silicate crystal phases detected by both XRD and ^{29}Si NMR. Following the ^{31}P spectrum which showed the presence of Na_3PO_4, the resonance peak at 7.3 ppm is assigned to this structure, whilst the broad glassy ^{23}Na peak appears to confirm that the residual glassy matrix contains sodium, phosphorus and silicon oxides.

The introduction of CaO at the expense of Na_2O in BGC2 yields a different crystal phase as detected by XRD; $Na_2CaSi_3O_8$. The nucleation and growth of crystal phases within the soda lime silicates is a complicated area as there exist a number of different compounds that could possibly be formed from glasses with compositions away from the known crystal stoichiometries. Indeed certain phases such as $Na_2Ca_2Si_3O_9$ are not phases of fixed stoichiometry but can vary over quite a large composition range [60]. The process of assigning the powder XRD reflections of these Bioglass glass-ceramics is complicated by the fact that the numerous stoichiometric powder patterns vary only slightly [78] as the scattering factors of the component elements are similar. In spite of this the XRD pattern from BGC2 has been definitely assigned to $Na_2CaSi_3O_8$. The ^{29}Si NMR spectrum contains two convoluted resonances, one corresponding to a Q^2 glass phase and another narrower peak at -87.4 ppm. No NMR data on $Na_2CaSi_3O_8$ has been reported but it is assumed that this resonance arises from silicon nuclei in this compound. The ^{31}P spectrum is practically identical to that from BGC1 showing the presence of a sodium orthophosphate crystal phase along with a similar amorphous species.

The ^{23}Na spectrum also contains two resonances, a new narrow peak at 13.1 ppm which is believed to originate from the $Na_2CaSi_3O_8$ phase along with a broader, 34.3 ppm FWHM, glassy peak with a position of -5.1 ppm. Hence this glass-ceramic has $Na_2CaSi_3O_8$ crystals dispersed in glass matrix containing sodium, phosphorus and silicon oxides along with a small quantity of crystalline sodium orthophosphate. It is not certain if all the calcium ions are incorporated into the crystal phases or some remain within the matrix.

The same crystal phase was detected in BGC3, and consequently both the ^{29}Si and ^{31}P spectra are practically identical to those from BGC2. There is some difference in the ^{23}Na spectrum where the crystalline resonance peak at 13 ppm is more clearly defined. The peak position of the sodium within the glassy phase remains around -5 ppm but the width of the resonance is reduced. This possibly indicates a reduced effective electric field gradient being experienced by the average sodium nucleus, although as this composition does contain less Na_2O than BGC2, the distribution of different sodium environments will be tighter.

The XRD pattern from BGC4 has been attributed to a combination of $Na_2CaSi_3O_8$ and $Na_2Ca_2Si_3O_9$. The corresponding ^{29}Si spectrum shows some changes in comparison to the previous samples. The narrow crystalline resonance, composed of the silicon resonances from each crystal phase, has become slightly more shielded by approximately 3 ppm, and the remaining amorphous resonance is now more typical of a more polymerized network, i.e. has a shift close to -100 ppm. This shift could indicate some Q^4 species appearing or possibly some Q^3 with phosphorus as a next nearest neighbour. The ^{31}P spectrum contains two resonances. The main peak is from an orthophosphate structure but in comparison to the previous samples this resonance has shifted to the high field and the linewidth has increased. This suggests an increase in the distribution of orthophosphate sites due to the incorporation of Ca^{2+} ions in addition to Na^+. The second resonance is a lot sharper, due a more regular atomic arrangement. From the shift position this

resonance can be attributed to regions of sodium pyrophosphate crystals, which, it is assumed, are of such a low concentration as to be undetectable via XRD. The ^{23}Na spectrum obtained from BGC4, figure 5.14, is very close to that obtained from BGC3 and provides no direct evidence of sodium nuclei in a sodium pyrophosphate crystal region. However it may be that the ^{23}Na peak position for the pyrophosphate is not too dissimilar to that from the orthophosphate. The broad sodium resonance has remained unchanged with a peak position of 13.1 ppm and a width of 25.2 ppm. Hence it appears that in this composition the residual glass matrix does contain some CaO, whilst the crystal phases are $Na_2CaSi_3O_8$, $Na_2Ca_2Si_3O_9$ and a small concentration of $Na_4P_2O_7$.

The XRD pattern from BGC5, figure 5.11, shows a return to the single crystal phase of $Na_2CaSi_3O_8$. Comparison with the reported XRD pattern of Hench et al [1] is very good, although the relative intensity of the two peaks around $2\Theta = 34°$ is reversed in BGC5. The pattern from BGC5 also shows better resolution of all the reflections. Interestingly Hench does not specify the crystal phase present in his material and only reports the pattern. It is therefore assumed, neglecting the difference in intensity between the two pairs of reflections around $2\Theta = 34°$ that the phase producing the pattern in Hench's paper is also $Na_2CaSi_3O_8$. The ^{29}Si spectrum of BGC5, figure 5.12, again consists of the relatively narrow resonance from silicon in the $Na_2CaSi_3O_8$ crystals along with a separate highly polymerized amorphous silicate network. Meanwhile the ^{31}P MAS spectrum shows no presence of a purely sodium orthophosphate environment but the crystalline species is now sodium pyrophosphate. A broad resonance does remain however but the shift is now around 5.6 ppm which implies a mix of charge balancing metal cations in a similar manner to the glass. The ^{23}Na MAS spectrum shows little change from that recorded from the previous composition, a peak at 11.7 ppm attributed to the sodium pyrophosphate species and the wider peak at -11.8 ppm again thought to arise from sodium in a glass phase.

In the case of BGC6 the XRD pattern and the ^{29}Si MAS NMR spectrum are in accordance with the previous samples that contain $Na_2CaSi_3O_8$. The ^{23}Na and ^{31}P spectra show no difference from those obtained from BGC5. These compositions, which lie near the centre of the bone bonding region, both contain crystal phases of $Na_2CaSi_3O_8$ and sodium pyrophosphate dispersed in a glass matrix that contains all the constituent oxides.

The composition of BGC7 has a definite excess of Ca^{2+} over Na^+ and this is apparent from the change in the XRD powder pattern which now contains reflections from $Na_2CaSi_3O_8$ and $Na_2Ca_3Si_6O_{16}$. Interestingly there is no sign of any sharp crystalline resonances in the ^{23}Na NMR spectrum, figure 5.14, which contains a single broad line, 33.1 ppm, with the peak position of 12.0 ppm. This is a change from the spectrum obtained from the glass, the resonance is now narrower and the peak position is appreciably different. A peak position of 12.0 ppm is not too dissimilar to the ^{23}Na resonances attributed to the $Na_2CaSi_3O_8$ phase previously and it maybe that the sodium environment in $Na_2Ca_3Si_6O_{16}$ is not very different. However the additional calcium ions in the locality may increase the field gradient around the sodium nucleus so increasing the linewidth. Of the three resonant lines observed in the ^{29}Si spectrum the resonance at -88.6 ppm is assigned to the $Na_2CaSi_3O_8$ crystal phase, silicons in the residual glass phase producing the slightly broader line at 84.4 ppm, and consequently the final resonance at -89.1 ppm is believed to be due to the $Na_2Ca_3Si_6O_{16}$ phase. The relative intensities of the three resonances compare favourably with the estimated volume fractions determined from the powder XRD pattern. The ^{31}P spectrum contains two resonances, in the same manner as BGC6, a residual glassy environment at 4.8 ppm with a mix of metal ions and a narrower line at 2.9 ppm probably due to some crystalline regions of calcium orthophosphate.

The ^{23}Na spectrum from BGC8 is almost indistinguishable from that of BGC7, a broad line with peak position near 12 ppm and no sharp peaks. The peak

position is therefore still close to that believed to be from the $Na_2CaSi_3O_8$ phase, which according to the XRD pattern is still present. An additional phase identified by XRD is that of $CaSiO_3$. Using this information it is possible to make assignments for the three separate ^{29}Si resonances detected; -89.5 ppm from the $Na_2CaSi_3O_8$ phase, -88.3 ppm from the calcium silicate and the remaining glass phase producing the peak centred on -84.0 ppm. The ^{31}P MAS spectrum now shows the narrow resonance centred on 4.2 ppm, whereas the broader resonance is at 3.1ppm.

The small concentration of sodium ions in BGC9 is readily apparent from the two crystal phases detected by XRD; two forms of calcium silicate. There is some change in the sodium environment as deduced from the ^{23}Na spectrum, the peak position is more negative and the width has decreased by a factor of almost two. It maybe that this reduction in width is due to the majority of the calcium ions being contained within the crystal phases. The ^{31}P spectrum shows that the majority of the phosphorus has remained in the glassy state with a mix of metal cations in the second coordination shell. Two crystalline sites are also resolvable, at 3.0 ppm probably from calcium orthophosphate and at -8.0 ppm from calcium pyrophosphate units. The corresponding ^{29}Si MAS NMR spectrum, figure 5.12, contains two easily identifiable resonances, -83.5 and -88.5 ppm, with a third visible as a shoulder on the high field side of the -88.5 ppm line. Now XRD has identified the calcium silicate phases as α–$CaSiO_3$ (J.C.P.D.S # 31-300) and $CaSiO_3$ (27-1064). However according to Engelhardt and Michel [70] the shifts for synthetic pseudowollastonite (α-$Ca_3Si_3O_9$) and β-wollastonite (β-$Ca_3Si_3O_9$) are -83.5 and -89.0 ppm respectively where in each compound the silicon sites are indistinguishable. Therefore it seems impossible to determine from these techniques alone exactly how many '$CaSiO_3$ - units' compose these chains or rings other than to say that the ^{29}Si shifts are so near as to suggest 3 membered rings for α form and 3 member chains for the β form. The residual glass matrix is believed to be responsible for the shoulder.

It is pertinent to point out that, although the crystal phase $Na_2CaSi_3O_8$ has been definitely assigned to the XRD patterns from compositions BGC2 through to BGC8, the corresponding ^{29}Si MAS NMR shifts that are attributed to this phase are not constant but fall within the range -87 to -90 ppm. This is quite a large shift range for a single crystalline composition, and as no published NMR data exists for this phase, the assignments would appear tentative and made only to correlate the NMR and XRD data. However, as well as the variation in the ^{29}Si chemical shift, there is deviation in the recorded XRD powder patterns from the published XRD reflection intensities. Indeed the recorded powder pattern that gave the best match to the published relative intensities for the reflections was obtained from BGC7, which had a shift of -88.6 ppm assigned to this phase. As this shift lies at the centre of the range of shifts that have been attributed to $Na_2CaSi_3O_8$ it seems reasonable to believe that stoichiometric $Na_2CaSi_3O_8$ has a ^{29}Si chemical shift of -86.5 ppm and that the corresponding variation of ± 1.5 ppm in the shift and in the relative intensities of certain reflections is due to small departures from the ideal stoichiometry.

The resulting structures of the second series of glasses that were heat treated as per Hench et al [1] were also investigated by the same combination of XRD and MAS NMR. Table 5.8 (b) presents the information obtained.

BGC10 was found by XRD to contain a single crystal phase after the heating, tridymite which is a silica polymorph. This is substantiated by the appearance of a resonance in the ^{29}Si MAS NMR spectra at -112.0 ppm, figure 5.15. This shift is consistent with the major peak in the reported ^{29}Si NMR spectrum of tridymite [79] where the dominant line is at -111 ppm with overlapping lines within the range -109.3 to -114.0 ppm. The presence of those other lines in the spectrum from BGC10 is not readily apparent due to the low S/N ratio. The remaining silicons are in a glassy environment with an average of 1 non bridging oxgen per SiO_4 tetrahedron, i.e. Q^3. The ^{31}P spectrum, figure 5.16, contains three resonances, a

small broad resonance at 15.8 ppm atop which is a very narrow line at 14.0 ppm and finally a broad peak at 2.8 ppm. The first two convoluted resonances are assigned to amorphous and crystalline forms of sodium orthophosphate and the third to phosphorus in an amorphous phase with local symmetry akin to sodium pyrophosphate. Similarly the ^{23}Na spectrum, figure 5.17, indicates a change in the resonating nuclei environment even though it is undetected by XRD. Two resonances can be resolved although the overall envelope is still very broad. Computerized Gaussian fitting gives the peak positions as 0.8 and -15.7 ppm, the latter being the same as in the pre heat treated sample.

Another polymorph of SiO_2 is present in BGC11. The ^{29}Si NMR spectrum initially looks little different from that of the glass with a combination of Q^3 and Q^4 resonances. However there is a definite shoulder at -108.5 ppm, a shift consistent with cristobalite, which was detected by x-ray diffraction. Slight changes are seen in the ^{23}Na spectrum after heat treatment. No sharp resonances are observed, but the peak position has moved to the low field suggesting less shielding of the sodium nuclei, and the overall width has diminished. Interestingly it appears as though all the phosphorus is contained in crystalline sites according to the ^{31}P spectrum. The only resonance present is at 2.3 ppm consistent with calcium orthophosphate. This phase was not detected by XRD because of its low concentration. Therefore it appears as though all the sodium ions remain as network modifiers within the residual glass phase and take no part in any crystalline phase.

The XRD powder pattern obtained from BGC12 was fully assigned to a combination of $Na_2Ca_3Si_6O_{16}$ and $Na_4Ca_8Si_5O_{20}$. The ^{31}P spectrum, figure 5.16, shows the presence of two amorphous phosphorus sites one corresponding to an environment similar to sodium orthophosphate and the other similar to calcium orthophosphate. The dominating feature within the spectrum is a very narrow resonance at 2.4 ppm which is due to crystalline calcium orthophosphate. The ^{23}Na spectrum, figure 5.16, shows a broad resonance, although narrower than the pre-heat

treated sample, with a peak position of -11.8 ppm with a small shoulder at 11.7 ppm. This positive shift is in a similar position to resonances recorded from the first series of heat treated Bioglasses which contained $Na_2CaSi_3O_8$, therefore it is believed that the peak at 11.7 ppm corresponds to either or both of the soda-lime silicate crystal phases. It may be that some sodium ions remain within the residual glass phase. The ^{29}Si MAS NMR spectrum contains three sharp resonances along with a broad background resonance from the residual glass phase. This glass phase resonance is centred around -100 ppm suggesting a highly polymerised network. Hence if there remain any of either metal cations within this phase their concentration must be quite small. Of the 'crystalline' peaks it is not possible to ascribe convincingly either resonance to one specific crystal phase. As there are three sharp peaks it may be that one of these phases has two non-equivalent silicon sites, or another phase is present which went undetected by XRD.

The final composition heat treated in this series is the same composition as BGC6. The crystal phase detected by XRD was $Na_2CaSi_3O_8$. Consequently the two resonances present in the ^{29}Si spectrum were assigned to this phase and the residual glass. Similarly one of the two separate ^{23}Na NMR resonances was assigned to the $Na_2CaSi_3O_8$ phase, 12.4 ppm peak position, the other to sodium ions still contained within the glass. The ^{31}P spectrum also contained two resonances, one from a site, crystalline in nature, similar to $Ca_3(PO_4)_2$ at 2.4 ppm and the other from another orthophosphate environment with a mixture of neutralising cations but amorphous.

5.3.6. SUMMARY.

For the glass-ceramics prepared from compositions lying along AA the structural information discussed previously can be summarised in a tabular form, table 5.9.

SAMPLE	CRYSTAL PHASES DETECTED BY XRD AND MAS NMR	OTHER CRYSTAL PHASES SUGGESTED BY MAS NMR	REMAINING AMORPHOUS SILICATE NETWORK
BGC1	Na_2SiO_3 α-$Na_2Si_2O_5$	Na_3PO_4 δ-$Na_2Si_2O_5$	Q^2 + Q^3
BGC2	$Na_2CaSi_3O_8$	Na_3PO_4	Q^2
BGC3	$Na_2CaSi_3O_8$	Na_3PO_4	Q^2
BGC4	$Na_2CaSi_3O_8$ $Na_2Ca_2Si_3O_9$	$Na_4P_2O_7$	Q^3 + Q^4
BGC5	$Na_2CaSi_3O_8$	$Na_4P_2O_7$	Q^3
BGC6	$Na_2CaSi_3O_8$	$Na_4P_2O_7$	Q^3
BGC7	$Na_2CaSi_3O_8$ $Na_2Ca_3Si_6O_{16}$	$Ca_3(PO_4)_2$	Q^2 + Q^3
BGC8	$Na_2CaSi_3O_8$ $CaSiO_3$	$Ca_3(PO_4)_2$	Q^2 + Q^3
BGC9	$CaSiO_3$ α-$CaSiO_3$	$Ca_3(PO_4)_2$ $Ca_2P_2O_7$	Q^3

Table 5.9. A summary of the conclusions reached regarding the intermediate structure of the series of glass-ceramics prepared from glasses lying along tie line AA.

Neglecting the two extremes of AA, BGC1 and BGC9, the major crystal phase found in all other glass-ceramics was $Na_2CaSi_3O_8$. This phase also appears to be the major phase in Hench's Bioglass [2] 45S5 glass-ceramic. Although not actually identified, the published powder X-ray diffraction pattern [1] is very similar to that observed in these glass-ceramics, see figure 5.11. It is also noticable in these compositions that the remaining glass matrix appears to still contain an appreciable concentration of modifying cations.

Table 5.10 summarises the MAS NMR and XRD data obtained from the glass-ceramics with compositions following BB. Interestingly the major crystal phases of both BGC10 and BGC11 are purely SiO_2 polymorphs, although minor orthophosphate phases are detected by ^{31}P MAS NMR.

SAMPLE	CRYSTAL PHASES DETECTED BY XRD AND MAS NMR	OTHER CRYSTAL PHASES SUGGESTED BY MAS NMR	REMAINING AMORPHOUS SILICATE NETWORK
BGC10	TRIDYMITE	Na_3PO_4	Q^3
BGC11	CRISTOBALITE	$Ca_3(PO_4)_2$	Q^3
BGC12	$Na_2Ca_3Si_6O_{16}$ $Na_4Ca_8Si_5O_{20}$	$Na_4P_2O_7$	Q^3 + Q^4
BGC6	$Na_2CaSi_3O_8$	$Na_4P_2O_7$	Q^2 + Q^3

Table 5.10. A summary of the main structural species found by XRD and MAS NMR in the glass-ceramics prepared from glasses along BB.

5.4. CONCLUSION.

The substitution of CaO for Na_2O in the series of glasses along tie line AA has shown some interesting results. The ^{29}Si MAS NMR spectrum of the initial composition, BG1, contained resonances from two tetrahedrally coordinated silicon species; Q^2 and Q^3. Substitution of 10 mol% Na_2O with CaO produced a visible convergence of these two ^{29}Si resonances, a convergence that continued with subsequent substitutions until, for BG3, the resulting ^{29}Si spectrum contained what appeared to be a single resonance. However from simple stoichiometric considerations the degree of depolymerisation of the silicate network should remain consistent, i.e. continued presence of both Q^2 and Q^3 species. Hence the ^{29}Si spectra of compositions BG3 to BG9 have been interpreted as consisting of two convoluted resonances assigned to these two $[SiO_4]$ species, with the convergence due to the preferential association of the Ca^{2+} ions with the Q^2 species and the Na^+ ions with the Q^3 species. Thus it is concluded that these compositions consist of a mix of two amorphous silicate environments similar to calcium metasilicate and sodium disilicate. The addition of CaO also affects the small amount of phosphorus present in the glasses. The ^{31}P MAS NMR resonances show a decreasing shift for increased

concentrations of CaO from a "Na_3PO_4 - like" structure to a shift more consistent with a "$Ca_3(PO_4)_2$ - like" structure. Intermediate compositions have a ^{31}P shift implying a mixed "$Na_3PO_4/Ca_3(PO_4)_2$- like" structure with the relative concentration of each of these orthophosphare species determined by the relative Na_2O:CaO. The appearance of CaO also affects the thermal stability of the glasses as determined from the glass transition temperature; increasing the amount of CaO at the expense of Na_2O raises T_g in a linear fashion with an increase of approximately 33°C each time the relative concentration of CaO as a function of total modifier oxide content is increased by 0.1.

This chapter has illustrated the effectivenes of employing multinuclear MAS NMR along with another technique, XRD, in the elucidation of intermediate range glass structure.

Compositions along tie line BB have progressive substitution of SiO_2 by CaO. Consequently the silicate network in the glasses becomes more depolymerised as the substitution proceeds. The main point of interest is the presence of two phosphorus environments in samples BG10 and BG11. Simple stoichiometric considerations would suggest that the presence of relatively large concentrations of pyrophosphate species would be very unlikely due to the low P_2O_5 concentration. However both these compositions contain ^{31}P resonances consistent with pyrophosphate environments. Hence it may be possible that some microfine phase separation has occurred.

As these glasses are multicomponent in nature it is not necessarily unusual that after a controlled devitrification treatment, the resulting glass-ceramics would be multiphase. Interestingly all compositions, whether along AA or BB, that fell within the so-called "bioactive" region of the triaxial phase diagram, figure 5.2, contained $Na_2CaSi_3O_8$ as the major crystalline phase. This is believed to be the same crystal phase present in the Bioglass [2] 45S5 glass-ceramic [1]. Certain phases, notably the various crystalline phosphates, were below the detection level of powder

XRD, but were detectable via MAS NMR. This illustrates the effectiveness of employing multinuclear MAS NMR alongside another technique; XRD, in the elucidation of the major and minor crystal phases and of the remaining glass matrix in glass-ceramic materials.

5.5. GLASS STRUCTURE AND BIOACTIVITY.

Since the structure of certain glasses, both within and outside the 'Bioactive' region of figure 5.1, have been investigated, the question of whether or not it is possible to relate the intermediate glass structure to the potential for bone bonding arises. This section attempts to provide an answer to this question, however, these thoughts are rather speculative in nature.

The series of glasses following tie line AA traverses from the 'Dissolution' region, BG1 and BG2, into the 'Bioactive' region, BG3 to BG9, and the MAS NMR results have shown some difference in their structure. BG1 contains no CaO and consequently is composed of structural species similar to sodium meta and disilicate, which are highly soluble. Substitution of 10 mol% Na_2O by CaO produced a convergence of the two separate ^{29}Si MAS NMR resonances due to Q^2 and Q^3, however the highly soluble sodium disilicate structure remained predominant. Further additons of CaO produced glasses that were 'bioactive' according to the phase diagram, figure 5.2, with an intermediate structure composed of a combination of sodium disilicate and calcium metasilicate species. The presence of the latter species controls the dissolution of the former. The interface between an implanted bioactive glass and the surrounding physiological environment has been shown to consist of three stages, figure 5.1, where an calcium phosphate layer is found on top of a silica gel which is formed at the glass surface. Hence it is suggested that the silica gel layer is formed via a process of restricted dissolution of

the sodium disilicate species, followed by condensation of the hydroxy silicate ligand complexes to form the silica gel. Thus the calcium, and phosphate, ions can then diffuse through the gel layer to form, initially, an amorphous calcium phosphate layer. Similarly the compositions lying along tie line BB initially have a structure comparable to that of sodium tetrasilicate, which is of low solubility and consequently, an inert biomaterial. By BG12, which lies near the boundary of the 'bioactive' region and is consequently has a lower degree of bioactivity than compositions nearer the centre of region A [1,9], the glass structure appears to be composed of a mix of calcium and sodium disilicates. The sodium dislicate species are obviously able to undergo a similar dissolution/condensation process to form the gel layer, whereas the greater difficulty of calcium ion diffusion from the calcium disilicate species slows the rate of formation of the calcium phosphate formation.

Hence if this supposition is valid then it is possible to determine from a structural assesment of a glass whether the composition will be 'bioactive'.

5.6. REFERENCES.

[1] L.L. Hench, T.K. Greenlee, R.J. Splinter & W.C. Allen, *J. Biomed. Res. Symp.* 2, 117, (1971)

[2] Bioglass is a registered trademark of the University of Florida, Gainesville, FL, U.S.A.

[3] O.H. Andersson, K.H. Karlsson & K. Kangasniemi, *J. Non-Cryst. Solids* 119, 290, (1990)

[4] J. Christoffersen, M.R. Christoffersen, W. Kiblczyc & F.A. Andersen, *J. Crsytal Growth* 94, 767, (1989)

[5] A.E. Clark Jr., C.G. Pantano & L.L. Hench, *J. Am. Ceram. Soc.* 59, 37, (1976)

[6] Y. Ebisawa, T. Kokubo, K. Ohura & T. Yamamuro, *J. Mat. Sci.: Materials in Medicine* 1, 239, (1990)

[7] U.M. Gross, J. Brandes, V. Strunz, I. Bab & J. Sela, *J. Biomed. Mat. Res.* 15, 291, (1981)

[8] U. Gross, in "C.R.C. Critical Reviews in Biocompatability" vol. 4 p. 155, CRC Press 1988

[9] L.L. Hench & A.E. Clark Jr., in "Biocompatabilty of Orthopedic Implants" vol. 2, ed. D.F. Williams, CRC Press, 1982

[10] P. Li & F. Zhang, *J. Non-Cryst. Solids* 119, 112, (1990)

[11] M. Ogino & L.L. Hench, *J. Non-Cryst. Solids* 38/9, 673, (1980)

[12] L.L. Hench & J. Wilson, *Science* 226, 630, (1984)

[13] J. Wilson, G.H. Pigott, F.J. Schoen & L.L. Hench, *J. Biomed. Mater. Res.* 15, 805, (1981)

[14] T. Fujiu, M. Ogino, K. Kariya & I. Ichimura, *J. Non-Cryst. Solids* 58, 417, (1983)

[15] A. Krajewski, A. Ravaglioli, A. Bertoluzza, P. Monti, M.A. Battaglia, A. Pizzoferrato, R. Olmi & A. Moroni, *Biomaterials* 9, 528, (1988)

[16] F. Pernot, J. Zarzycki, P. Baldet & P. Rabischong, in "Clinical Applications of Biomaterials" ed. A.C. Lee, Wiley, 1982

[17] F-H. Lin & M-H. Hon, *J. Crystal Growth*, 94, 357, (1988)

[18] W. Vogel & W. Höland, *J. Non-Cryst. Solids* 123, 349, (1990)

[19] T. Kokubo, S. Ito, S. Sakka & T. Yamamura, *J. Mater. Sci.* 21, 536, (1986)

[20] T. Nakamura, T. Yamamura, S. Higashi, T. Kokubo & S. Ito, *J. Biomed. Mater. Res.* 19, 685, (1985)

[21] F-H. Lin & M-H. Hon, *J. Mater. Sci.* 23, 4295, (1988)

[22] C. Lavernia & J.M. Schoening, *Ceramic Bull.* 70, 95, (1991)

[23] M. Jarcho, *Clin. Orthop. Relat. Res.* 157, 259 (1981)

[24] P. Ducheyne, *J. Biomed. Mater. Res.* 19, 273, (1985)

[25] T.B. Troczynski & P.B. Nicholson, *J. Amer. Ceram. Soc.* 73, 164, (1990)

[26] L.L. Hench, *J. Am. Ceram. Soc.* 74, 1487, (1991)

[27] P. Ducheyne et al, *J. Biomed. Mater. Res. Symp.* 14, 225, (1980)

[28] N. Inoue et al, *J. Jpn. Orthod. Soc.* 40, 291, (1981)

[29] Vitallium is the trade name for a vanadium/titanium/aluminium alloy.
[30] J. B. Grey, M.E. Steen, G.J. King & J.M. Waldron, *J. Dent. Res.* 83. 311, (1983)
[31] P. Ducheyne & K.E. Healy, *J. Biomed. Mater. Res.* 22, 1137, (1988)
[32] J.R. Smith, *Am. J. Orthod.* 76, 618, (1979)
[33] Ceravital is a trademark of E. Lietz, Watzler, Germany
[34] U.M. Gross & V. Strunz, *J. Biomed. Mater. Res.* 2, 46, (1978)
[35] T. Kokubo, in "Biomaterials 84, Transactions of 2nd World Congress on Biomaterials", ed. J.M. Anderson, p. 351, Soc. for Biomaterials, Washington D.C., 1984
[36] W. Holland, K. Naumann, W. Vogel & J. Gummel, *Wiss. Z. Freidrich Schiller Univ. Jena, Math. Naturwiss Reihe* 32, 571, (1983)
[37] M. Bunte & V. Strunz, *J. Maxillofacial Surg.* 5, 303, (1977)
[38] H. Dennissan, Thesis, Free Univ. Amsterdam, 1979
[39] C. de Putter, K. de Grost, P.A.E. Sillevissmit, in "Clinical Applications of Biomaterials", ed. A.J.C. Lee, T. Albrektsson & P-I. Branemark, p. 237, Wiley, 1982
[40] M. Ogiso, *J. Dent. Res.* 60A, 419, (1981)
[41] C. de Putter, K. Grost, P.A.E. Sillevissmit & J.M. van der Zel, *Trans. Soc. Biomater.* 6, 27, (1987)
[42] M. Jarcho, *J. Mater. Sci.* 11, 2027, (1976)
[43] J.M. Kent, J.H. Quinn, M.F. Zide & M. Jarcho, Abstracts of the 2nd Southern Biomedical Engineering Conference, San Antonio, TX, 1983
[44] A.N. Cranin, in "Biomaterials 84, Transactions of 2nd World Congress on Biomaterials", ed. J.M. Anderson, Soc. for Biomaterials, Washington D.C., 1984
[45] J.J. Grote,"Biomaterials in Otology", Nijhoff, The Hague, 1984
[46] P. Ducheyne & L.L. Hench, in "Biomaterials 82", ed. G.D. Winter, D. Gibbons & H. Plenk, Wiley, 1982
[47] U.M. Gross & V. Strunz, in "Clinical Applications of Biomaterials", ed. A.J.C. Lee, T. Albrektsson & P-I. Branemark, p. 278, Wiley, 1982
[48] U.M. Gross & V. Strunz, *J. Biomed. Mater. Res.* 19, 251, (1976)
[49] O.H. Andersson, K.H. Karlsson, K. Kangesniemi & A. Yli-Urpo, *Glastech. Ber.* 61, 300, (1988)
[50] O.H. Andesson, G. Liu, K.H. Karlsson, L. Niemi, J. Mettinen & J. Juhanoja, *J. Mater. Sci.: Materials in Medicine* 1, 219, (1990)
[51] C.Y. Kim, A.E. Clark Jr. & L.L. Hench, *J. Non-Cryst. Solids* 113, 195, (1989)
[52] R.F. Le Geros, G. Bone & R. Le Geros, *Calcif. Tissue Res.* 26, 111, (1978)
[53] M. Ogino, F. Ohuchi & L.L. Hench, *J. Am. Ceram. Soc.* 59, 37, (1976)
[54] K.H. Karlsson, K. Fröberg & T. Ringbom, *J. Non-Cryst. Solids* 112, 69, (1989)
[55] N.J. Kreidl, in "Glass Science & Technology" vol. 1 Glass Forming

Systems, eds. D.R. Uhlmann & N.J. Kreidl, Academic Press, 1983
[56] J. Hlavác, " The Technology of Glasses and Ceramics", Elsevier, 1983
[57] H. Rawson, "Inorganic Glass Forming Systems", book..
[58] G.W. Morey & N.L. Bowen, *J. Soc. Glass Technol.* 9, 272, (1925)
[59] K.A. Shahid & F.P. Glasser, *Phys. Chem. Glasses* 12, 50, (1971)
[60] G.K. Moir & F. P. Glasser, *Phys. Chem. Glass* 15, 6, (1974)
[61] D.G. Burnett & R.W. Douglas, *Phys. Chem. Glasses* 11, 125, (1970)
[62] R. Dupree, D. Holland & D.S. Williams, *J. Phys. (Paris)* 46, C8-119, (1985)
[63] B.W. Veal, D.J. Lam, A.P. Paulikas & W.Y. Ching, *J. Non-Cryst. Solds* 49, 309, (1982)
[64] British Standard BS 2649:PART 1:1988. Analysis of glass, Part 1. Glasses of the soda-lime-magnesia-silica type. B.S.I. 1988
[65] P.W. McMillan, "Glass-Ceramics", Academic Press, 1979
[66] I.L. Mudrakovskii, V.P. Shmakkova & N.S. Kotsarenko, *J. Phys. Chem. Solids* 47, 335, (1986)
[67] G.L. Turner, K.A. Smith, R.J. Kirkpatrick & E. Oldfield, *J. Magn. Reson.* 70, 408, (1986)
[68] R.Dupree, D. Holland & M.G. Mortuza, Phys. Chem. Glasses 29, 18, (1988)
[69] G. Engelhardt & D. Michel, "High Resolution Solid State NMR of Silicates and Zeolites", Wiley, 1987
[70] A-R. Grimmer, M. Mägi, M. Hahnert, H. Stade, A. Samoson, W. Wieker & E. Lippmaa, *Phys. Chem. Glasses* 25, 105, (1984)
[71] J.B. Murdoch, J.F. Stebbins & I.S.E. Carmichael, *Am. Mineral.* 70, 332, (1985)
[72] R. Dupree, D. Holland, P.W. McMillan & R.F. Pettifer, *J. Non-Cryst. Solds* 68, 399, (1984)
[73] G. Tammarin, "State of Aggregation", VNR, 1925
[74] G.H. Beale, "Advances in Nucleation and Crystallization in Glasses", American Ceramic Soc. 1971
[75] J. Williamson & P.F. Glasser, *Phys. Chem. Glasses* 7, 127, (1966)
[76] M.G. Mortuza, PhD Thesis, University of Warwick, 1989
[77] S. Prabhakar, K.J. Rao & C.N.R. Rao, *J. Mater. Res.* 6, 592, (1991)
[78] J.C.P.D.S. Powder Diffraction File, J.C.P.D.S. 1984
[79] J.V. Smith, C.S. Blakewell & G.L. Hovis, *Nature (London)* 309, 140, (1984)

CHAPTER 6

$PbO . P_2O_5 . Al_2O_3$ SYSTEM.

6.1. INTRODUCTION.

Particular problems are encountered when attempting an investigation of phosphate glasses, namely the volatility of P_2O_5 at elevated temperatures and their high reactivity especially with water; vitreous and crystalline polymorphs of P_2O_5 deliquesce extremely rapidly if exposed to atmospheric water vapour. These problems are particularly acute in ultraphosphates where the ratio of network modifier to former is less than unity. Hence, even though P_2O_5 was noted by Zachariasen [1] as one of the four classic glass forming oxides, phosphate glasses were mainly considered mere laboratory curiosities with few technical applications [2] and so the number of studies concerned with their structure and properties has been rather limited. However even with their limiting chemical durability phosphate glasses are recently finding more applications, especially in the technology of high expansion, low temperature, glass to metal sealants [3] (where the addition of aluminium oxide and other metal oxides has increased their resistance to aqueous attack in particular [4]), as well as fast ionic conductors [5,6] and novel laser and non-linear optical materials [7-9]. Thus in these fields any relation between the composition and the glass structure will be of benefit to those attempting to design glasses with particular properties such as thermal coefficient of expansion matching.

CHAPTER 6

$PbO . P_2O_5 . Al_2O_3$ SYSTEM.

6.1. INTRODUCTION.

Particular problems are encountered when attempting an investigation of phosphate glasses, namely the volatility of P_2O_5 at elevated temperatures and their high reactivity especially with water; vitreous and crystalline polymorphs of P_2O_5 deliquesce extremely rapidly if exposed to atmospheric water vapour. These problems are particularly acute in ultraphosphates where the ratio of network modifier to former is less than unity. Hence, even though P_2O_5 was noted by Zachariasen [1] as one of the four classic glass forming oxides, phosphate glasses were mainly considered mere laboratory curiosities with few technical applications [2] and so the number of studies concerned with their structure and properties has been rather limited. However even with their limiting chemical durability phosphate glasses are recently finding more applications, especially in the technology of high expansion, low temperature, glass to metal sealants [3] (where the addition of aluminium oxide and other metal oxides has increased their resistance to aqueous attack in particular [4]), as well as fast ionic conductors [5,6] and novel laser and non-linear optical materials [7-9]. Thus in these fields any relation between the composition and the glass structure will be of benefit to those attempting to design glasses with particular properties such as thermal coefficient of expansion matching.

6.1.1 VITREOUS P_2O_5.

Generally phosphorus has a valency of 5 in glasses, forming tetrahedral basic structural units with fourfold coordination like silicon, achieved via the double bonding of one of the surrounding oxygen atoms, see figure 6.1.

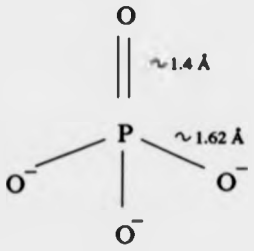

Figure 6.1. A schematic representation of a PO_4 tetrahedron. The single P - O bonds are sigma bonds whereas the P = O bond is a hybridized pi-sigma type. Typical bond lengths according to [13] are also shown.

This only leaves a maximum of three possible bridging oxygens and so is in this way more comparable to vitreous B_2O_3 where 3 corners are shared but in a trigonal planar arrangement. The higher ratio of oxygen atoms for P_2O_5 (1: 2.5) than for SiO_2 (1:2) enables phosphate glasses to dissolve certain elements and oxides that are either insoluble or poorly soluble in silicate melts, e.g. platinum [10], hence it is probably more practical to melt high P_2O_5 glasses in Al_2O_3 crucibles.

Apparently Galeener et al [11,12] carried out the first significant structural study of vitreous P_2O_5. Employing Raman spectroscopy they confirmed that v-P_2O_5 did indeed form a continuous three dimensional network via the sharing of 3 of the tetrahedral corner oxygens with the fourth doubly bonded to the phosphorus atom. According to Martin [13], Kordes et al [14] proposed the same structural arrangement for v-P_2O_5 simply by correlating known crystalline polymorph structures to the Zachariasen 'postulates' [1]. Grimmer and Wolf [15]

reported a ^{31}P MAS NMR spectrum obtained from glassy P_2O_5; a single isotropic line with spinning sidebands indicative of an axially symmetric environment. The position of the isotropic peak was -55 ppm. No other spectroscopically based structural examinations of pure v-P_2O_5 have been found in the literature, although a brief mention was made of some neutron diffraction data [13] that predicts a short P=O bond length with longer P-O bonds but gave no information concerning the intermediate ordering of the glass.

6.1.2. BINARY PHOSPHATE SYSTEMS (R_2O - P_2O_5 / RO - P_2O_5).

Addition of monovalent alkali metal oxides to P_2O_5 is similar in certain respects to the R_2O - SiO_2 situation; the extra oxygen atoms introducing non-bridging oxygens into the structure whilst the cation is believed to be in the locality to ensure full charge neutrality. Clearly, however there is a difference from SiO_2 in that pure P_2O_5 already contains one non-bridging oxygen per tetrahedron. However even though the 'mechanism' of incorporating the modifier atoms is similar, the effect upon the strength of the glass structure and consequently the melting point is the opposite. Kreidl states that the addition of modifier to P_2O_5 increases the melting point suggesting a strengthened structure [16]. However identical problems to those found with v-P_2O_5 are encountered concerning glass preparation and hygroscopicity for compositions with less than 30 mol% modifier content, and consequently few studies have been reported under this compositional limit [13]. Above this figure both the preparation and handling is appreciably eased, however a degree of hygroscopicity still exists.

Models for the formation of non-bridging oxygens upon modifier addition are similar to those proposed for simple alkali silicate glasses. Assuming that the P=O bond remained unaffected by the modifier addition Kordes et al [14]

predicted a simple direct relation between the concentration of alkali ions and the number of non-bridging oxygens produced. This has been validated by such techniques as NMR and it is now known that the depolymerisation of phosphate glasses by alkali addition occurs via the break-up of the P-O σ bonds with the P=O bond remaining [13].

As in terms of basic structural units there is some correlation between R_2O - P_2O_5 and R_2O - SiO_2 systems it is possible to employ a Q^n unit notational system such as that developed for silicate glasses [17]. In this case though, n again corresponds to the number of non-bridging oxygens but lies between 3 and 0. This can be seen schematically in figure 6.2. Van Wazer [18] developed his "reorganization theory" along the same lines where the configuration of phosphorus and oxygen could be visualized in terms of isolated orthophosphate units and end, middle and branching units which include the associated modifier ion regardless of whether R^+ is bonded to an oxygen or is completely ionised. Similarly the formation of these structural species passes from Q^3 to Q^2 to Q^1 to Q^0 as the ratio of modifier to phosphate passes from 0 to 1 to 2 and finally 3, although any type of structural unit may react with others to form alternative units, i.e. two meta units can transform into one end unit and one branching unit.

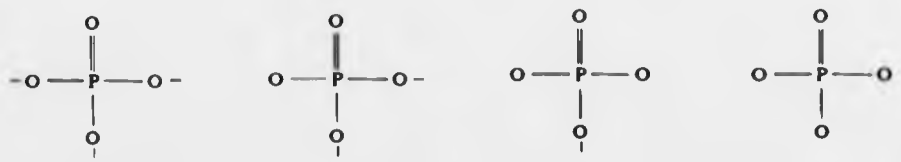

Figure 6.2. A schemetic representationof the 4 Q^n structural species. The non-bridging oxygens have an associated negative charge which is compensated for by a local cation.

Subsequently the reverse reaction could occur and hence there is a

series of equilibrium reactions, each with an equilibrium constant.

$$2\ Q^2 \xrightleftharpoons{K_1} Q^1 + Q^3$$

$$2\ Q^1 \xrightleftharpoons{K_2} Q^0 + Q^2$$

and in general

$$2\ Q^0 \xrightleftharpoons{K_3} 2\ Q^1 + R_2O_{(unreacted)}$$

The reactions giving rise to each successive Q^n species are controlled by their respective equilibrium constants. The first extreme of completely ionised metal cations would strongly favour the left hand side of these equations such that both K_1 and K_2 are almost zero and K_3 is zero. This produces a structural species distribution similar to that predicted by the constrained (binary) model of silicate Q^n units where only two particular Q^n species are present in any one composition (see section 1.2.1.). Conversely for an almost completely covalent R-O bond Van Wazer predicts K_2 and K_1 to be approximately 0.33. Not surprisingly the structural unit distribution in this case resembles that of the statistical model of silicates (section 1.2.1.) where Q^3, Q^2, Q^1 and Q^0 appear simultaneously for any concentration of modifier oxide.

Depolymerisation of the phosphate network can also occur due to the presence of residual water originating from the chemical precursors, mainly those used for a P_2O_5 source; $(NH_4)_2HPO_4$ or $NH_4H_2PO_4$. Gray et al [19] and Brow et al [20] have established that all or most of any water present is in the form of -OH and not H_2O and therefore acts as a network modifier, so increasing the effective alkali

content of the glass.

This leads to the question of both qualitative and quantitative determination of the Q^n types present in any particular composition and, as in the case of silicates, MAS NMR is the preferred technique employed here. The ^{31}P nucleus is particularly well suited to intermediate structural elucidation via NMR as, not only is it practically 100% abundant, but has a nuclear spin of ½ so avoiding the problems associated with quadrupolar broadening. One hindrance in quantitative ^{31}P MAS NMR is that the chemical shift anisotropies for phosphorus Q^3 , Q^1 and especially Q^2 can be quite large so producing intense and numerous associated spinning sidebands [2] in MAS experiments. This can be overcome if the spectra are accumulated at a high spin speed (> 10kHz), and with a wide frequency sweep width. The isotropic shift ranges and powder patterns obtained from each of the Q^n species have been well established [2,21-23] and are indicated in figure 6.3. As was demonstrated in ^{29}Si MAS NMR [24] higher degrees of network polymerisation result in increased shielding and hence more negative chemical shifts.

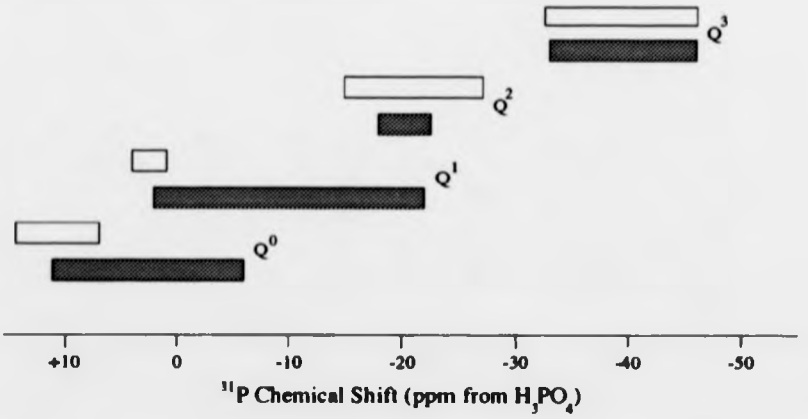

Figure 6.3. The reported shift ranges for crystalline phosphates with differing tetrahedral arrangements (white ranges from Brow et al [20] and the general ^{31}P shift ranges (shaded) as reported by Martin [13]).

Although P_2O_5 easily forms binary glasses with monovalent alkali

metals and bivalent alkali earth metals acting as network modifiers certain other bivalent metals, Mg, Be, Zn and Cd, are believed to be incorporated more directly into the structural network [10]. To this end there is some question as to the exact role that PbO would play when added to P_2O_5. In the case of lead silicate glasses it is possible to achieve "invert' glass compositions where, according to stoichiometry, it should not be possible to stabilise a continuous silicate network, i.e. PbO content up to 70 mol% [25]. Hence it would appear that, at this high concentration, lead is acting as a bridging matrix between isolated SiO_4 tetrahedra. Further conclusions reached by this study show that the role which PbO plays within the glass structure is composition dependent: Below 30 mol%, PbO can be considered a typical network modifier producing non-bridging oxygens in a manner consistent with the binary model. From 30 to 65 mol% the ^{29}Si MAS NMR spectra suggest that the distribution of the silicate Q^n species is more consistent with the statistical model and that some Si-O-Pb bonding maybe occurring with PbO perhaps acting more like an intermediate glass former. However Volf [10] states that in phosphate glasses lead acts solely as a modifier and separate published infra-red spectra appear to confirm this statement [26] for PbO concentrations of less than 33 mol%. A ^{31}P MAS NMR study of a higher PbO content glass, 60 PbO - 40 P_2O_5, contained two resonances at -9.9 and -23.7 ppm which were assigned to lead acting as both an intermediate and modifier oxide simultaneously. The two ^{31}P signals were claimed to come from P bonded to PbO_4 tetrahedra within the phosphate network and P where ionic Pb^{2+} sites are associated with [PO_4] non bridging oxygens [27].

6.1.3 BINARY PHOSPHATE SYSTEMS (Al_2O_3 - P_2O_5).

Addition of alumina (Al_2O_3) to high phosphate glasses has long been known to improve chemical (i.e. water) durability [28]. However the structural role

undertaken by the aluminium ion is somewhat open to question. Chakraborty and Paul [26] propose that when Al_2O_3 is added to glasses in the K_2O - P_2O_5 system that "... initially Al_2O_3 reacts with K_2O and when all the K_2O is consumed, Al_2O_3 starts reacting with P_2O_5 forming cristobalite-type of structural groups". This would require the breaking of the P=O bond in order to form the SiO_2 isostructure $AlPO_4$. Similar conclusions regarding the formation of $AlPO_4$ in phosphate glasses with alumina added were reached by Tallant and Nelson [29] and Yifen et al [21]. Structural data obtained from ^{27}Al NMR experiments on crystalline alkali aluminophosphates contradicts this by indicating a preference for aluminium in an octahedral coordination as opposed to the tetrahedral arrangement found in $AlPO_4$ [22]. Subsequently Brow et al [30] suggested that the increase in chemical durability obtained from Al_2O_3 addition to alkali phosphates arose because of cross-linking of phosphate chains , $(PO_3)_n^{n-}$, by an $Al(OP)_6$ network. For Al_2O_3 concentrations around 12.5 mol% changes are evident in the structure with the aluminium coordination switching to a tetrahedral arrangement. For higher alumina contents, the phosphate structures will be bonded to multiple Al polyhedra, and so a preference is shown for both $Al(OP)_4$ and $Al(PO)_5$ which have a more regular arrangement of P-O-Al bonds than the octahedral species. [30]

Therefore it is the proposal of this part of the study to determine the intermediate structure of certain compositions in the PbO - Al_2O_3 - P_2O_5 system via ^{27}Al and ^{31}P MAS NMR and ascertain the role played in that structure by both the aluminium and lead ions.

6.2. GLASS PREPARATION.

All samples in this system were prepared [31] via two preparation

routes ; (i) direct melting of mixed powder reagents and (ii), melting of lead and aluminium source compounds previously dissolved/reacted with phosphoric acid.

For direct melting the required mass of hydrated aluminium phosphate, red lead oxide and ammonium dihydrogen orthophosphate were tumble milled for two hours, heated in an alumina crucible to 3-400°C and held for 2 hours to evolve any water and ammonia. Subsequently the temperature was raised until a clear melt was obtained and the sample then splat cooled by quenching between two graphite coated steel plates at room temperature. Fowler [31] did not provide information relating to the ultimate melt temperature.

As the nominal molar concentration of P_2O_5 decreased it was noted that sample preparation by this route became impractical, so a new method was employed. Correct masses of aluminium nitrate and red lead oxide were added to a magnetically stirred alumina crucible containing the necessary volume of concentrated (85%) phosphoric acid. After approximately one hour the magnetic follower was removed and the crucible transferred to a furnace at 200°C for two hours. As before the temperature was then increased until a clear pourable melt was obtained whereupon the melt was splat cooled as above. Again no data is available concerning the final melt temperature.

Because of the high P_2O_5 content in these compositions all samples were kept under vacuum in a desiccator until required for NMR or compositional analysis. Each sample, apart from LAP2 and LAP3, was shown to be amorphous by x-ray diffraction at least to the limit of the equipment; < 5% crystalline. Powder XRD patterns of LAP 2 and 3 contained a single low intensity peak of width 0.8° 2θ centred on 26.7 ° 2θ.

Table 6.1 gives both the nominal and analysed composition of each glass as well as the relevant route of preparation.

	NOMINAL (MOL%)			ANALYSED (MOL%)		
SAMPLE	PbO	Al_2O_3	P_2O_5	PbO	Al_2O_3	P_2O_5
LAP1	30	---	70	30.2	1.8	68.0
LAP2†*	28	2	70			
LAP3†*	25	5	70	26.4	6.5	67.1
LAP4	20	10	70	18.2	11.4	70.4
LAP5	10	20	70	7.7	20.7	71.6
LAP6	30	10	60	27.2	12.0	60.8
LAP7†	49	---	51	46.6	1.0	52.4
LAP8	50	---	50	47.6	1.1	51.3
LAP9†	46	11.5	42.5			
LAP10†	57.5	---	42.5	55.3	1.0	43.7

† Prepared by phosphoric acid method.

* Approximately 5 volume % crystalline $Al(PO_3)_3$.

Table 6.1. Nominal and analysed compositions of the lead alumino-phosphate glasses prepared for study in this chapter.

6.3 WET CHEMICAL ANALYSIS.

The final concentration of lead oxide and aluminium oxide in these glasses was determined via wet chemical analysis following the procedure outlined by method 1.8, "Rapid determination of PbO and Al_2O_3 in full lead crystal glasses", in the British Glass Industry Research Analysis handbook [32]. Essentially the procedure involves decomposition of a known mass of sample using hydrofluoric/ perchloric acids, with lead and aluminium oxides complexed by ethylene di-nitrilo tetra acetic acid (EDTA). The resulting solution is then back titrated with zinc acetate solution and ammonium fluoride, using xylenol orange as an indicator, to determine values for the PbO and Al_2O_3 concentrations. Subsequently the P_2O_5 content was calculated by difference. The analysed compositions are given alongside the nominal in table 6.1.

6.4 NUCLEAR MAGNETIC RESONANCE.

6.4.1 ^{31}P MAS NMR.

The ^{31}P spectra of all compositions were acquired on the Bruker MSL 360 spectrometer operating under the conditions given in table 2.1. The probe employed was the Doty Scientific 360 MHz double bearing probe (see section 2.3.2). The samples were powdered with an agate pestle and mortar and carefully packed into the 5mm double bearing diameter spinners under nitrogen. Where multiple lines were present in a spectrum the sample spinning speed was varied such that the isotropic peaks could be determined.

Figure 6.4 illustrates the phosphorus spectra acquired from these samples. The best computerized fit for the asymmetric meta-phosphate peaks centred around -24 and -25ppm respectively was achieved for a combination of two gaussians. Similar expanded plots around the same shift range of the remaining compositions showed lines that were not as significantly asymetric and were best fitted by single gaussians. Therefore it is suggested that these compositions either contain no phosphate units with 3 bridging oxygens or so few as to unresolvable by this technique. The full chemical shift data is given in table 6.2. Note that, as in the potassium phospho-silicate system, the ^{31}P MAS NMR spectra appear complicated due to the abundance of spinning sidebands associated with the isotropic lines and 'water absorption' peaks, present as narrow resonances either side of 0 ppm. However in each spectrum the isotropic peak was determined and is clearly labelled.

6.4.2. ^{27}Al MAS NMR.

The ^{27}Al NMR spectra were also recorded on the MSL 360

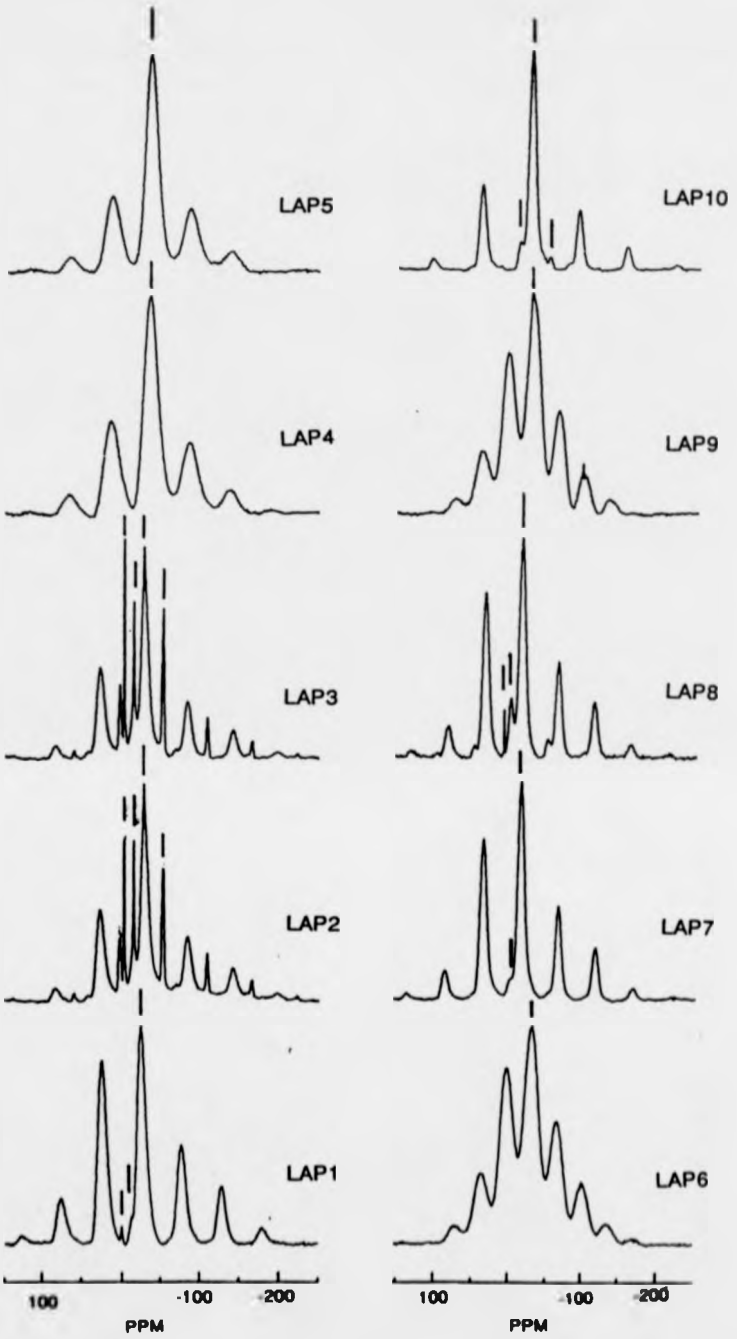

Figure 6.4. The ^{31}P MAS NMR spectra recorded in this study. The isotropic lines are denoted and the remaining peaks are spinning sidebands. Each spectrum is composed of 400 accumulations with exponential broadening equivalent to 50Hz applied to each time domain signal prior to Fourier transformation.

SAMPLE	^{31}P Chemical shift (ppm) (± 0.5 ppm)	FWHM (± 1.0 ppm)	Relative Area (± 0.1)	^{27}Al Peak posn. (ppm) (± 1.0 ppm)	FWHM (± 1.0 ppm)	Relative Area (± 0.1)
LAP1	0.6	2.0	0.01	-10.7	8.1	1.00
	-11.9	n.m.	0.01			
	-23.8	13.6	} 0.97			
	-41‡	10.2				
LAP2	-2.2	1.8	0.06	-18.6	4.7	1.00
	-14.8	2.1	0.04			
	-28.4	11.5	0.72			
	-53.9	3.9	0.17			
LAP3	-2.2	2.0	0.05	-18.7	4.6	1.00
	-14.8	2.2	0.08			
	-28.6	11.4	0.71			
	-53.8	4.2	0.16			
LAP4	-35.9	22.0	1.00	37.9	21.0	0.17
				8.8	20.2	0.3
				-14.1	17.7	0.53
LAP5	-34.8	21.8	1.00	38.1	18.8	0.25
				10.8	18.2	0.30
				-14.1	17.6	0.45
LAP6	-31.2	24.9	1.00	39.6	16.8	0.23
				10.6	14.7	0.24
				-12.0	16.1	0.53
LAP7	-5.3	6.0	0.04	-11.1	12.3	1.00
	-18.4	11.6	0.96			
LAP8	5.9	1.7	0.01	-10.2	11.7	1.00
	-3.3	6.3	0.10			
	-18.7	10.5	0.89			
LAP9	-30.1	12.1	1.00	40.9	21.1	0.33
				11.2	15.3	0.27
				-11.8	16.4	0.39
LAP10	-11.9	5.4	0.04	-10.2	8.3	1.00
	-25.5	12.2	0.94			
	-50.1	5.2	0.02			

‡ Estimated ± 2 ppm.

Table 6.2. The deduced spectral parameters from the ^{31}P and ^{27}Al MAS NMR investigations of the lead alumino-phosphate glasses prepared in this study.

spectrometer although with an in house probe based around a Doty rotor assembly. Typical spinning speed was approximately 10 KHz. The accumulated spectra are given in figure 6.6 with the peak positions and full widths at half height detailed in table 6.2.

Table 2.1 details the relevant reference materials and the standard acquisition parameters employed in the study of this nucleus.

6.5. DISCUSSION.

As was stated previously the majority of these compositions are ultraphosphates with PbO contents less than 30 mol%. Hence there is a problem regarding absorption of atmospheric moisture. In an attempt to reduce the effect all samples were prepared immediately prior to spectral accumulation whenever possible by being powdered and packed into spinners under a dry nitrogen atmosphere within a glove box. However certain ^{31}P MAS NMR spectra do exhibit resonances consistent with moisture-powder surface reaction products. These resonances tend to be very sharp and around the reference standard shift of 0 ppm. The remaining ^{31}P resonances can generally be quite easily assigned to PO_4 tetrahedra in various degrees of polymerization; i.e. with 1 non-bridging oxygen (Q^3) or 2 non-bridging oxygen atoms (Q^2). Giffiths et al [33] found, in the case of crystalline sodium phosphates, that the longer the metaphosphate (Q^2) chains became, the more negative was the ^{31}P shift observed and it would seem likely that this finding may hold for phosphate glasses although the random intermediate structure may muddy the waters a little in this respect. As illustrated by figure 6.3 there is a shift region around -30 ppm that lies between the reported shift ranges of framework and chain phosphates and so care is required when assigning peaks with this approximate shift to being solely due to network or chain species.

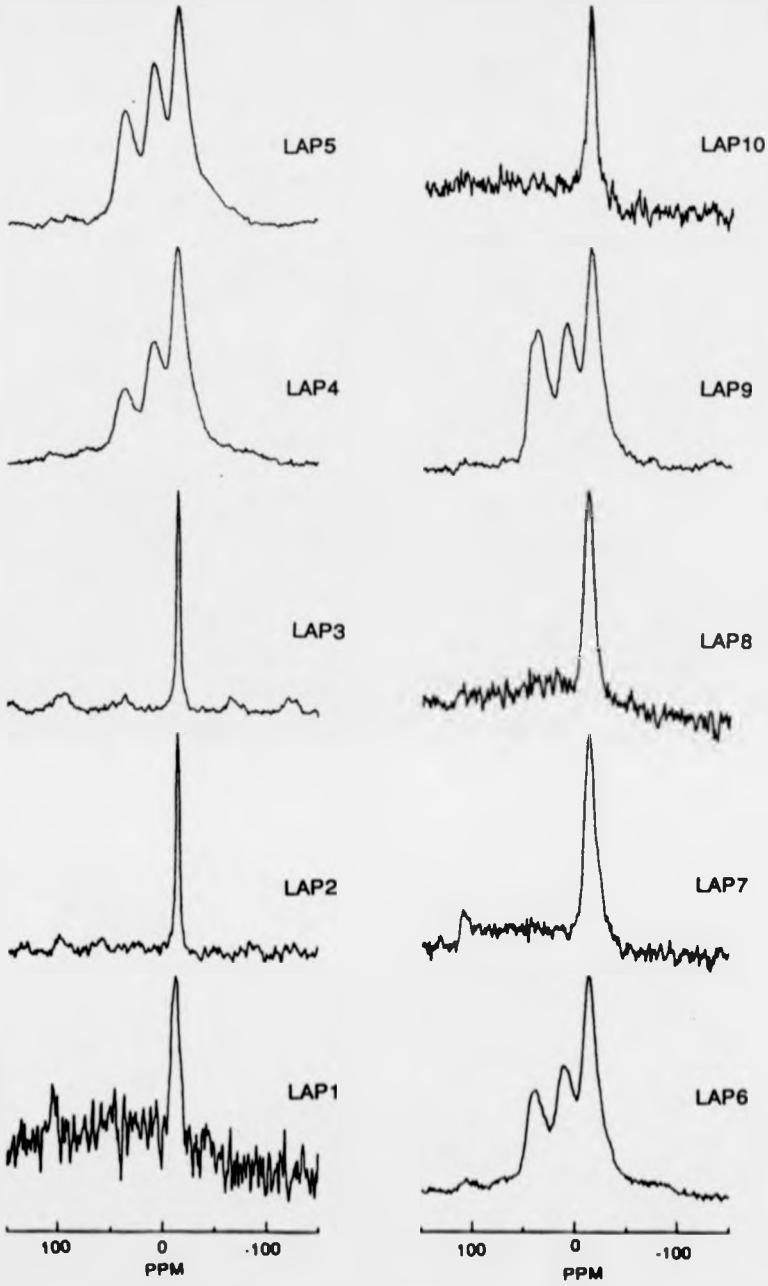

Figure 6.6. The ^{27}Al MAS NMR spectra recorded in this study. Typical spinning speeds are in excess of 10kHz. Each spectrum consists of 800 sweeps with 100Hz exponential broadening applied prior to Fourier transformation.

The ^{31}P resonances found in the accumulated LAP1 spectra centred on 0.6 and -11.9 ppm are believed to be simply the result of limited exposure to the atmosphere because of their exceptionally narrow lineshape, and so yield no structural information. At first glance the spectra appear to contain a single metaphosphate resonance, along with associated spinning sidebands, centred on -23.8 ppm. An expanded plot of the isotropic peak is definitely assymetric, suggesting another resonance is present. Computerised gaussian fitting of two resonances achieved a good fit to the data indicating a second resonance was present with a shift of approximately -40 ppm. The relative amount of this second resonance is somewhat imprecise but is somewhere between 2 to 5 % of the total phosphorus atoms. The shift position is indicative of Q^3 units, framework PO_4 tetrahedra.

The ^{27}Al spectrum of LAP1 is solely due to 'impurity' aluminium leached from the crucible during sample melting. A peak position of -10.7 ppm can only originate from aluminium in an octahedral environment. However the position is not sufficiently negative to be due to $Al(OP)_6$, which has a shift around -19 ppm, and is too negative to be from $Al(OAl)_6$, approximately 8 to 0 ppm. Hence it may be that some of the second coordination sphere atoms are phosphorus and the remainder aluminium, although with such a low Al_2O_3 content (1.8 mol%) any Al-O-Al linkages would be statistically unlikely unless phase separation has occurred, a possibility that cannot be entirely excluded. It may also be possible that this shift suggests some lead atoms as next nearest neighbours to octahedral aluminium along with phosphorus and possibly aluminium. Pb has an electronegativity similar to that of silicon and, following similar reasoning to that in chapter 3 where a ^{27}Al peak at -13 ppm was attributed to $Al(OP)_x(OSi)_y$ units where (x+y=6), the present Al position of -10.7 ppm could result from an arrangement like $Al(OP)_i(OAl)_j(OPb)_k$ with $i + j + k = 6$. The width of the resonance is not especially large for a nucleus that experiences quadrupolar broadening, hence the aluminium nuclei are not encountering a large electric field gradient. This suggests

that the bond arrangement of the aluminium octahedra is reasonably symmetric.

LAP2 and LAP3 exhibit very similar ^{31}P and ^{27}Al MAS NMR spectra. As for LAP1 the sharp ^{31}P resonances around 0 and -12 ppm are due to moisture exposure, or, as these samples were prepared with H_3PO_4 acid, some residual water within the glass. Data published by Grimmer and Wolf suggest $P(O)(OH)_3$ has a shift around 0 ppm and $P(O)O^-(OH)_2$ around -13 ppm [15]. As no data is available concerning the final melt temperature achieved in their preparation it is not possible to say for certain just how unlikely this idea of residual OH units from water is. The peaks are certainly more intense than in LAP1. The isotropic peaks at -28.4 and -28.6 ppm for LAP2 and LAP3 respectively appear symmetric and so are assigned to metaphosphate Q^2 units with the slightly more negative shift in comparison to that recorded for LAP1 suggesting chains of longer length [33]. There is an additional ^{31}P resonance in these spectra that is relatively narrow and has 2 pairs of spinning sidebands with an isotropic shift of -53 ppm. The ^{27}Al spectra also contain a resonance with a much narrower linewidth than is normally experienced in glasses, 4.7 ppm. This would imply a crystalline environment. According to Mudrakovski et al [34] the ^{31}P shift for $Al(PO_3)_3$ is -51.8 ppm and, although there is no information published on the ^{27}Al peak position for the same compound, the observed aluminium position of -19 ppm is what would be expected from octahedral aluminium with 6 phosphorus atoms as next nearest neighbours. This in itself is consistent with the crystal structure of $Al(PO_3)_3$ as detailed by Wyckoff [35]. Thus the MAS NMR data confirms the x-ray diffraction powder pattern which was within experimental error of that quoted for the major powder pattern line of crystalline $Al(PO_3)_3$; J.C.P.D.S. # 15-364, d-spacing 3.34 equivalent to 26.7° 2θ for Cu Kα radiation [36]. It also confirms that as a technique MAS NMR is more sensitive to low concentrations of crystallites or crystalline phases than XRD. As MAS NMR only probes the intermediate bonding arrangement, up to 3 nnn shells, the MAS spectra may show crystallites of only a few polyhedra in size,

physical dimensions of around 10Å which would be lost to x-ray diffraction [37].

LAP4 was shown to be completely x-ray amorphous and the ^{31}P and ^{27}Al NMR linewidths reflect this. Indeed the isotropic phosphorus linewidth is now 20 ppm in comparison to 14 ppm recorded for LAP1. This increase reflects a greater distribution in bond lengths and angles of the Q^2 units as well as a possible increase in the range of n in $(PO_3)_n^{n-}$, i.e. a variety of different metaphosphate chain lengths. Unlike LAP1 the peak in LAP4 appears relatively symmetric such that computer fitting of two Guassians was a more unreliable fit than a single gaussian. The shift of this peak, -35.9 ppm, however is more negative than those reported for purely metaphosphate Q^2 species [13,20] and is into the range of Q^3 framework PO_4 tetrahedra. Complete repolymerization of the phosphate network is unlikely however since there is still a reasonable concentration of Pb^{2+} ions (18.2 mol%) not all of which could be offset by the Al^{3+} ions fulfilling a network intermediate role of non bridging oxygen removal. Hence it is believed that this peak is due mainly to metaphosphate (Q^2) chains of considerable length, although some contribution from a degree of undetectable but convoluted Q^3 resonances maybe present. Unfortunately no real grasp can be obtained as to the exact number of Q^2 units composing these chains/rings, but Griffiths et al [33] quote a shift of -23 ppm for crystalline $Na_8P_8O_{24}.6H_2O$. In purely schematic terms the longer the metaphosphate chain the greater the number of P nuclei that have P in the second, fourth etc coordination sphere, hence the greater the effective shielding and so a more negative shift.

The ^{27}Al MAS spectrum of LAP4 is quite distinctive as it contains three peaks, 37.9, 8.8 and -14.1 ppm. The former and latter result from tetrahedral and octahedral aluminium respectively; the four coordinated species surrounded by phosphorus as the next nearest neighbour, the six coordinated species probably incorporating a mix of phosphorus and aluminium or lead atoms as in LAP1 although with an average increase in the mean number of second coordination

sphere phosphorus yielding the slightly more negative peak position. The third peak, at 8.8 ppm, is more difficult to assign. $Al[OAl]_6$ has a position around 5 to 0 ppm [24] in glasses and from 1 to 12 ppm in amorphous alumina films [38], whereas $Al[OP]_5$ is reported to be around 10 to 14 ppm [39]. Again Al-O-Al bonding arrangements would statistically necessitate some phase separation into alumina rich regions and with no evidence to the contrary this cannot be ruled out. It may also be possible that this peak arises from 5 or 6 coordinated aluminium with a mix of second coordination sphere elements, but not from an additional tetrahedral environment which would be unlikely to produce such a peak position. Similar arguments regarding the structural assignments can be made for both LAP5 and LAP6 which exhibit similar ^{31}P and ^{27}Al shifts and peak positions to those recorded for LAP4.

LAP7 and LAP8 were approximately the same nominal composition, LAP7 prepared via the H_3PO_4 route and LAP8 via the more usual melt technique. Their analysed compositions are correspondingly not too dissimilar and, as shown in table 6.2, their resulting ^{31}P and ^{27}Al MAS NMR results are within experimental error of each other. Noticeably the width of the ^{31}P peaks is less than LAP4,5 and 6, thus the distribution of chain lengths appears to have shrunk.These are the first compositions in this study where the total PbO concentration is above 30 mol% and the possibility of intermediate-like oxide activity arises. The two ^{31}P shifts observed in each composition, around -5 and -19 ppm, are not too dissimilar to those reported for 60 PbO - 40 P_2O_5 [27] at -9 and -24 ppm which were attributed to two different phosphorus environments; one having incorporated corner sharing $[PbO_4]$ tetrahedra into the glass network the other from $[PO_4]$ - Pb^{2+} ionic sites. Of the two samples LAP7 has the higher lead to phosphorus ratio, 1:2.25 in comparison to LAP8, 2.16. and this is manifest in the slightly smaller amount of the orthophosphate resonance. Hence it can be postulated that further increases in lead content above that in LAP8 will increase this ionic environment. The similarity also extends to the ^{27}Al MAS

NMR spectra which show the presence of a single resonance around -11 ppm with a fullwidth at half maximum of 12ppm. As stated earlier this position is consistent with aluminium in an octahedral environment however the shift is not sufficiently negative to arise from six phosphorus atoms as the next nearest neighbours. Hence it is believed that the average aluminium second coordination sphere is a mixture of phosphorus, lead and possibly other aluminium atoms.

The ^{31}P spectrum of LAP9 contains a single resonance at -30.1 ppm with spinning sidebands. Similar to LAP4,5 and 6 this shift is slightly more negative than the accepted upper limit for Q^2 chain/ring structures, but, as previously, is believed to arise predominantly from Q^2 units with perhaps some Q^3 convoluted into the overall envelope. Likewise with the other compositions in this series that have Al_2O_3 concentrations greater than a trace impurity level, the ^{27}Al spectrum has resonances attributed to 4,5 and 6 coordinated aluminium.

LAP10 however exhibits three separate resonances in its ^{31}P spectrum. The dominant shift is centred on -25.5 ppm and has 3 visible pairs of spinning sidebands. This accounts for over 90 % of the resonating phosphorus atoms and is at the upper end of the metaphosphate (Q^2) shift range [20] suggesting chains of rather long length. Unfortunately there is no accurate method of determining the number of Q^2 units that comprise these chains. The larger of the two remaining resonances is centred on -11.9 ppm and has a single pair of resolvable sidebands. This shift is indicative of a pyrophosphate (Q^1) species. The smallest of the resonances is at -50.1 ppm and again has one pair of associated spinning sidebands. This shift position is significantly more negative than that quoted for network (Q^3) phosphate [13,20] in figure 6.3 although the paper from Prabakar et al [27] contains a diagram attributing a ^{31}P NMR shift of approximately -52 ppm to crystalline $Al(PO_3)_3$. Thus it would appear that LAP10 contains a phosphorus environment resembling this structure, however the absence of any XRD reflection along with the width of the resonance is such that the regular crystal arrangement is lacking.

Perhaps the best method of comparison for these compositions is to analyse the relationship between the actual metaphosphate shift position and the structural parameter G, where G is the ratio of lead to phosphorus and aluminium atoms, i.e.

$$G = [Pb] / ([P] + [Al])$$

Neglecting the samples where no analysed composition information is available along with the samples which were shown to be partially crystalline yields the data shown in figure 6.7.

The three compositions included which contain only a trace amount of aluminium can be fitted to a straight line separate to the line fitting to the compositions containing deliberate Al_2O_3 addition of approximately 10 mol%. As only the metaphosphate shift is plotted in this figure we are essentially looking at the

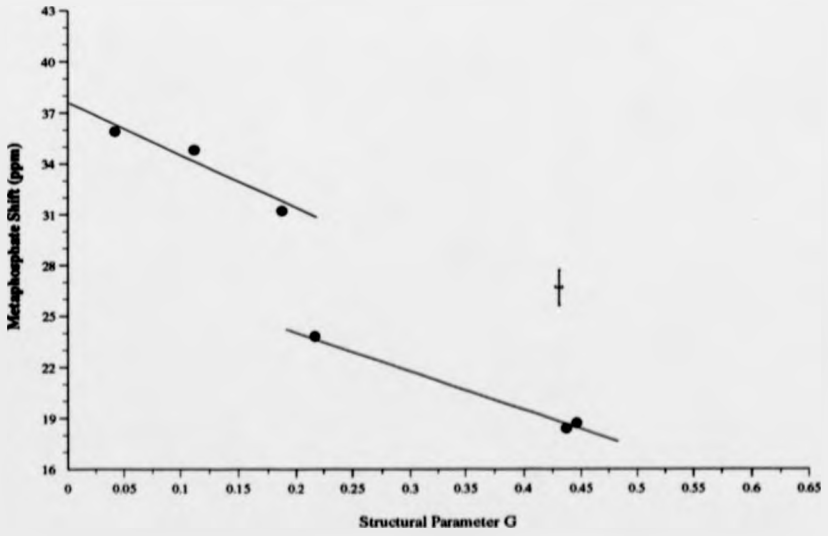

Figure 6.7. A plot of the metaphosphate species shift against the defined structural parameter G. The average error of each point is also plotted.

main 3-d network forming structure in these glasses.

As previously stated these shifts are more negative than reported Q^2 shift ranges, therefore if the assumption that these resonances are from metaphosphate species is valid then the P nuclei must be experiencing a highly shielded environment. A consequence of these long chains is an increase in the width of the isotropic line. This would arise because of small but significant variations in the shielding experienced by each phosphorus in the chain from directly linked phosphate species numbering between 1 and $^n/_2$ for chains consisting of n members.

If this is a true representation of the phosphate network then how are these long Q^2 structures stabilised ? One common factor is all these samples contain aluminium in three different coordinations, could this be an important factor in terms of stabilisation ?

Addition of Al_2O_3 to Na_2O - P_2O_5 glasses [30] has shown that initially octahedral aluminium is the preferred orientation with 6 n.n.n. phosphorus atoms. For Al_2O_3 additions approaching 14.3 mol% they observe a preference for lower coordinations; 4 and 5. This observation was discussed in terms of a simple valence neutrality model where the valence unit value for each aluminium coordination is the result of valence number divided by the coordination number. Hence Al^{vi} has 0.5 vu, Al^{v} 0.6 vu and Al^{iv} 0.75 vu. Thus in any Al - O - P bonds the phosphorus must supply the remaining valence units to ensure a neutral oxygen atom, i.e. 1.5 vu for Al^{vi} , 1.4 vu for Al^{v} and 1.25 vu for Al^{iv}. Underbonding of the oxygen can be accommodated however either by distributing the remaining charge among the neighbouring P - O bonds (bridging or non-bridging), or by the local presence of modifier ions. There is a functional limit on the degree of oxygen underbonding that can be sustained, and hence there is a limit on the amount of high coordination aluminium. This fits with the results obtained in this study where the relative amount of tetrahedral aluminium increases for increasing Al_2O_3

concentration. A very simple schematic representation of this model is presented below.

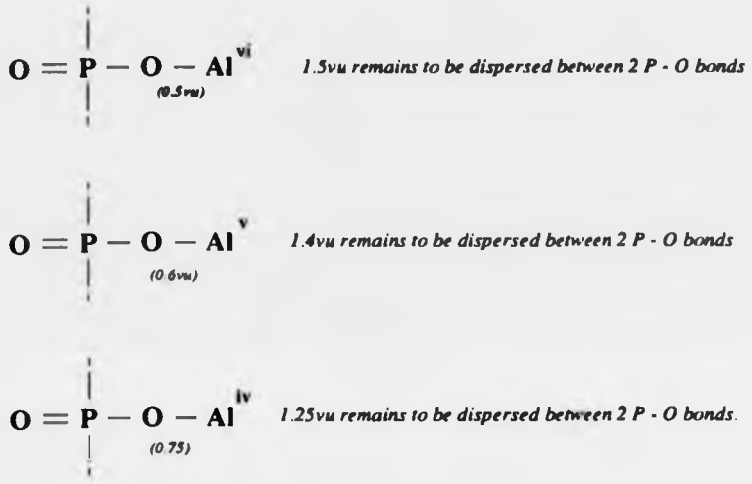

Figure 6.8. A schematic illustration of the underbonding described by the valence unit model proposed by Brow et al [30].

Intuitively then as the vu figure of the aluminium approaches 1 the burden upon phosphorus is reduced, and so it is postulated that the occurrence of 5 and 4 coordinated aluminium species stabilises the extensive metaphosphate chains. Simple calculations indicate that there are insufficient modifier ions in LAP5 to stabilise the underbonding required by a completely octahedral aluminium network. Although stoichiometrically there are the necessary modifier ions in LAP4 and LAP6 to balance the octahedral underbonding, the concentration of lead oxide implies that lead maybe performing the dual role of intermediate and or modifier.

Returning to figure 6.8 the compositions containing Al_2O_3 as an

impurity can also be fitted to a separate straight line. These compositions also have PbO around the concentration where lead may show intermediate-like behaviour. The ^{31}P metaphosphate shifts are consistent with the accepted range [13,20], and as would be expected from the compositional differences the higher P_2O_5 glass, LAP1, has a network of longer chains. The width of the isotropic peaks are also similar, approximately 11 ppm. However in both LAP7 and LAP8 there are ^{31}P resonances suggesting lead is bonded to phosphorus in two different manners, one predominantly covalent in nature, around -3 to -5 ppm, and the other predominantly ionic arrangement consistent with modifier-like behaviour. This dual lead role is not readily apparent from the spectra of LAP1 and so it is not possible, solely from these compositions, to fix a lower compositional limit above which lead commences to act as an intermediate and form a part of the glass network, but it certainly appears to for concentrations above 46.6 mol%.

6.6. CONCLUSION.

The glasses prepared from the PbO - Al_2O_3 - P_2O_5 system have shown some interesting results. Compositions that contain > 10 mol% Al_2O_3 have been shown via ^{27}Al MAS NMR to contain aluminium in 3 different coordinations; 4, 5 and 6, with a variety of next nearest neighbours. It appears that this multiple coordination stabilises longer metaphosphate chains then previously recorded although this is purely a deduction from the highly negative ^{31}P MAS NMR chemical shift. It is not possible to ascertain how many $(PO_3)_n^{n-}$ units compose these chains. To determine 'n' would probably require chromatography.

It has also been determined that phosphate glasses with > 46.6 mol% PbO, and possibly nearer 30 mol%, contain (PbO_4) tetrahedra within the network in an apparent intermediate-like role similar to the situation in silicate glasses [25].

This study has shown again that MAS NMR is a valuable technique in determining small amounts of crystal phases within a 'nominal' glass which are barely or undetectable by x-ray diffraction [15].

6. 7. REFERENCES.

[1] W.H. Zachariasen, *J. Am. Chem. Soc.* 54, 3841, (1932)

[2] H. Eckert, *Prog. in NMR Spectroscopy* 24, 159, (1992)

[3] J.A. Wilder, *J. Non-Cryst. Solids* 38/9, 879, (1980)

[4] J.A. Wilder & J.E. Shelby, *J. Am. Ceram. Soc.* 67, 438, (1984)

[5] T. Minami, Y. Takuma & M. Tanaka, *J. Electrochem. Soc.* 124, 1659, (1977)

[6] J.P. Malugami, A. Wasniewski, M. Doreau & G. Robert, *Mater. Res. Bull.*, 13, 427, (1978)

[7] D. Ehrt, C. Fuchs & W Vogel, *Silikattechnik* 35, 6, (1984)

[8] R.K. Sandwich, R.J. Scheller & K.H. Mader, *S.P.I.E.* 171, 161, (1979)

[9] W.K. Tredway & S.H. Risbud, in "Non-Oxide Technical & Engineering Ceramics", ed. S. Hampshire, p.203, Elsevier (1987)

[10] P. Volf, "Technical Glasses", Pitman & Sons (1961)

[11] F. Galeener & J. Mikkelsen, *Solid State Comm.*, 30, 505, (1979)

[12] F. Galeener, J. Mikkelsen, R.H. Geils & W. Mosby, *J. Appl. Phys. Letts.*, 32, 34, (1978)

[13] S.W. Martin, *Eur. J. Solid State Inorg. Chem.*, 28, 163, (1991)

[14] E. Kordes, Z. *Anorg. Allgem. Chem.*, 1939, 241 & *Z. Physik Chem.*, 50, 194, (1941)

[15] A.R. Grimmer & G.U. Wolf, *Eur. J. Solid State Inorg. Chem.*, 28, 221, (1991)

[16] N.J. Kriedl, in "Glass Science & Technology" vol. I, ed. D. Uhlmann & N.J. Kriedl, Academic Press (1989)

[17] E. Lippmaa, M. Magi, A Samoson, G. Engelhardt & A. Grimmer, *J. Am. Ceram. Soc.*, 102, 4889, (1980)

[18] J. Van Vazer, "Phosphorus and it's Compounds", vol. I & II, Interscience New York (1951)

[19] P. Gray & I. Klein, *Glass Tech.* 24, 202, (1983)

[20] R.K. Brow, R.J. Kirkpatrick & G. Turner, *J. Non-Cryst. Solids* 116, 39, (1990)

[21] J. Yifen, C. Dehua, C. Xiangsheng, B. Beiya & H. Xihuai, *J. Non-Cryst. Solids* 80, 147, (1986)

[22] D. Muller, I. Grunze, E. Hallas & G. Ladwig, *Z. Anorg. Allgem. Chem.* 500, 80, (1983)

[23] C.S. Blackwell & R.L. Patton, *J. Phys. Chem.* 88, 6135, (1984)

[24] R. Dupree & D. Holland, in "Glasses and Glass-ceramics", ed. M.H. Lewis, Chapman & Hall, London, 1989

[25] R. Dupree, N. Ford & D. Holland, *Physics Chem. Glasses* 28, 78, (1987)

[26] S. Chakraborty & A. Paul, *Jnl. Mat. Sci. Letts.* 8, 1358, (1989)

[27] S. Prabhakar, K.J. Rao & C.N.R. Rao, *Chem. Phys. Letts.* 139, 96, (1987)

[28] N.J. Kreidl & W.A. Weyl, *J. Am. Ceram. Soc.* 24, 372, (1941)

[29] D.R. Tallant & C. Nelson, *Phys. Chem. Glasses* 27, 75, (1986)

[30] R.K. Brow, R.J. Kirkpatrick & G.L. Turner, *J. Am. Ceram. Soc.* 73, 2293, (1990)

[31] The samples examined in this chapter were prepared by Mr. Rex Fowler as a part of his final year project for the degree of BSc Physics at the University of Warwick 1991.

[32] Methods of analysis for glasses, part1, method 1.8 from The British Glass Industry Research Association, Northumberland Road, Sheffield, U.K.

[33] L. Griffiths, A. Root, R.K. Harris, K.J. Packer, A.M. Chippendale & F.R. Thomas, *J. Chem Soc. - Dalton Trans.* 1986, p. 2247

[34] I.L. Mudrakovskii, V.P. Shmakkova & N.S. Kotsarenko, *J. Phys. Chem. of Solids* 47, 335 (1988)

[35] R.N.G. Wychoff, "Crystal Structures", Wiley, (1964)

[36] J.C.P.D.S. Powder Diffraction File, J.C.P.D.S. 1984

[37] R. Dupree, *Topical Issues in Glass* 1, 11, (1993)

[38] R. Dupree, I. Farnan, A.J. Forty, S. El-Mashri & L. Bottyan, *J. Phys.* 46, C8 - 113 (1985)

[39] B.C. Bunker, R.J. Kirkpatrick, R.K. Brow, C. Nelson & G.L. Turner, *J. Am. Ceram. Soc.* 74, 1430, (1991)

CHAPTER 7.

CONCLUDING REMARKS.

7.1. GENERAL CONCLUSIONS.

This study has involved the application of multinuclear Magic Angle Spinning nuclear magnetic resonance to the investigation of the intermediate range structure of three distinct and different glass systems, two essentially silicate based and the other phosphate based. Since summaries and conclusions drawn from the MAS NMR investigations have already been provided in each of the experimental chapters, the purpose of this section is mainly to discuss some overall conclusions regarding multinuclear MAS NMR and its applicability to the structure determination of completely or partially amorphous inorganic materials.

To date, actual calculation of the chemical shift of a particular nucleus in a specific bonding arrangement is not possible. Deduction of the surrounding environment therefore remains, in essence, a 'fingerprint' technique where the experimentally observed shift is compared to the shift of the nucleus in a material where the structure has been previously determined by alternative techniques. In terms of ^{29}Si MAS NMR of glasses and glass-ceramics the experimental shifts are compared with those obtained from various crystalline silicates whose structures have been established by XRD. Hence from the shift position it is possible to ascertain the coordination state, either tetra, penta or octahedral, as well as the number of the Si - O bonds that are either bridging or non-bridging. It is also feasible to make some statements regarding the atom type of the next nearest neighbour, although with glasses in particular, where the NMR

resonance linewidths can be rather large, this tends to be of the form of an estimate of their number rather than a specific figure. For example in chapter 4, a ^{29}Si chemical shift of -117 ppm, which undoubtedly arises from silicon in a tetrahedral coordination, indicates 'some' phosphorus in the second coordination sphere because the shift is significantly downfield from that expected of $Si(OSi)_4$. However it is not possible to say exactly how many Si - O - P linkages are present. Indeed silicon NMR suffers appreciably from two problems, the low relative abundance of the ^{29}Si isotope and its often exceptionally long relaxation times. Isotopic enrichment is the most obvious solution to the low abundance problem and, although this is very expensive, the results can be extraordinary, for example, the observation by Stebbins of approximately 0.1% of total silicon being five coordinated in a $K_2Si_4O_9$ glass [1]. The problem of long relaxation times is more readily overcome by limited doping of the glass by paramagnetic impurites which act as 'energy sinks' for the resonating nuclei.

Other nuclei investigated in this study include ^{23}Na, ^{27}Al and ^{31}P. Of these both sodium and aluminium suffer appreciably from broad resonant linewidths because of their quadrupolar moments which makes structural assignments even more inconclusive than is the case for silicon. Phosphorus on the other hand is a nucleus ideally suited for the MAS NMR investigation of glass structure as it is practically 100% ^{31}P and has a spin of ½, and so it is a surprise to have found so little investigation of the structure of phosphate glasses whether by MAS NMR or by other spectroscopic or diffraction based techniques.

Overall it has been seen that, although multinuclear MAS NMR is as a technique well suited to the study of amorphous materials, any technique employed in isolation will only provide a limited amount of information. Far better would be to employ MAS NMR as one of a series of complementary techniques, possibly encompassing neutron scattering, Raman and infra-red spectroscopies as well as thermal techniques as this work has shown the thermal history of a glass does have

an effect upon the resulting structure. It must also be emphasised that the final chemical composition of the glass be accurately established prior to any attempt to execute any credible structural interpretation of the experimental data. This work has also shown that multinuclear MAS NMR and XRD can be employed to good effect when attempting to elucidate the various crystalline and amorphous phases formed in glass-ceramics without resorting to electron microscopy and energy dispersive analysis of x-rays. Without doubt, MAS NMR as a tool for physicists, chemists and materials scientist, will continue to be of increasing use with further advancements in both spectrometer hardware, software and pulse programs.

7.2. SUGGESTIONS FOR FURTHER STUDY.

With regard to octahedrally coordinated silicon in glasses this study has illustrated that the presence and concentration of this structural species has an effect upon the density, it would be of interest to establish if any other macroscopic physical properties show a similar dependance or variation. It would also be of interest to look at higher coordination states of aluminium in glasses, and their effect on physical properties.

Thermal history undoubtedly affects the resulting glass structure and, although there are technical limitations at present, it may be of interest to attempt to investigate structural changes occuring in a material in situ, i.e. within a high field magnet enclosed in a heated NMR probe.

The interesting finding of the Bioglass [2] system was the apparent specific association of a particular modifier species with a particular Q-type. This undoubted requires further investigation, perhaps initially via high resolution electron microscopy so as to establish if some phase separation has occurred. If this should prove inconclusive then perhaps complementary neutron diffraction and ^{29}Si MAS NMR studies would be useful, or even a two dimensional NMR experimental

similar to that described by Kirkpatrick et al [3] to determine possible connectivity between the different Q-types.

Phosphate glasses are particularly under investigated, and so any study would be welcome. One experiment in particular that may be of interest would be apply the spin-echo double-resonance method of van Eck [4] to the aluminophosphate and phosphosilicate glasses, similar to those of chapters 4 and 6, to establish connectivity between different resonating species and the spatial distribution of similar species.

7.3. REFERENCES.

[1] J.F. Stebbins, *Nature* 351, 638, (1991)

[2] Bioglass is a registered trade mark of the University of Florida, Gainesville, FL, U.S.A.

[3] C.T.G. Knight, R.J. Kirkpatrick & E. Oldfield, *J. Non-Cryst. Solids* 116, 140, (1990)

[4] E.R.H. van Eck, R. Janssen, W.E.J.R. Maas & W.S. Veeman, *Chem. Phys. Lett.* 174, 428, (1990)